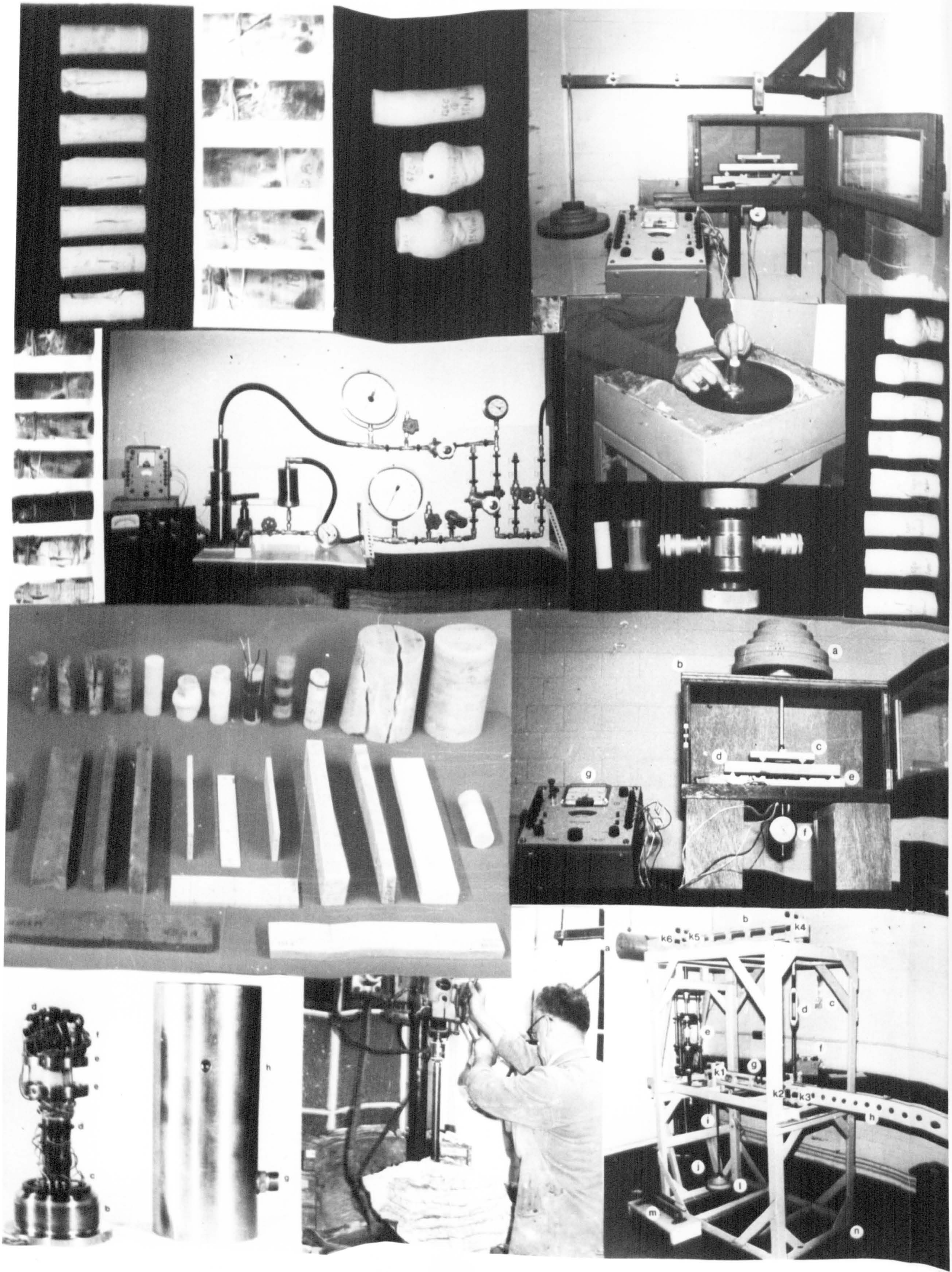
a
b
c
d
e
f
g
k1
k2
k3
k4
k5
k6
h
i
l
m
n

THE TIME DEPENDENT BEHAVIOUR OF SOME EVAPORITE ROCKS

by

Mohammed Ayoub Sabry Elizzi
(B.Sc., M.Sc.)

May 1976

A thesis submitted to the University
of Sheffield for the Degree of
Doctor of Philosophy

To

Ali, Maysa and Omar

Acknowledgements

The author wishes to express his sincere gratitude to his supervisor, Dr. F.T. Williams, senior lecturer, for his guidance, assistance, useful discussion and for the loan of reference materials.

He also wishes to thank the Government of Iraq and Calouste Gulbenkian Foundation for their financial support.

Professor H.T. Hanna, the head of the Department of Civil and Structural Engineering is also to be thanked for his assistance in many ways.

Thanks are also extended to the following people:

Mr. Hufdhi Bahia for his valuable friendship and useful discussion.

All the staff of the Department of Civil and Structural Engineering workshop, in particular, Mrs. D. Hutson, Mr. E.R. Barwell and Mr. J.W. Strafford, for their continuous help.

Mrs. A. Firth for her accurate typing.

Finally, the author wishes to express his deep thanks and appreciation to his wife Raja'a for her continuous encouragement and support.

Note

Extracts from this thesis were published or accepted for publication under the following headings:

1. "Bending creep tests in gypsum", Journal of the Iraq Engineers Soc., 1975, accepted for publication.
2. "The determination of time dependent behaviour of rock under triaxial loading", Dept. of Civil and Structural Eng., Univ. of Sheffield, Research report No.66, July, 1975.
3. "An apparatus for the determination of time dependent behaviour of rock under triaxial loading", Int.Jour. Rock Mech. Min. Sci. and Geomech. Abstr., accepted for publication.
4. "A study of the creep properties of gypsum rock under triaxial loading" Dept. of Civil and Structural Eng., Univ. of Sheffield, Research report No.72, Jan. 1976.

SUMMARY

In practical circumstances the bulk of the rock material beneath a foundation, in the surrounding regions of an excavation, or inside mine pillars is in fact triaxially loaded over long time periods. It was felt that studying the creep phenomena of some evaporite rocks under a triaxial system of loading could add valuable information to the limited knowledge available on rock behaviour in such conditions. Gypsum and anhydrite were initially chosen as suitable evaporite rocks for carrying out this work.

An apparatus has been designed and constructed to enable experiments to be carried out on the chosen rocks. The axial strain of the deformed rock specimen was measured on the rock specimen inside the pressure cell. Triaxial compression creep tests were carried out at 10, 20 and 30 N/mm^2 confining pressure. Bending and uniaxial compression creep tests were also performed on the chosen rocks. Instantaneous strengths of gypsum and anhydrite under the given systems of loading were found and various percentages of the instantaneous strengths were applied in the creep tests. All short term and creep tests were carried out at room temperature.

It was found that the creep behaviour of the tested rocks obeyed the following equations:

$$\Sigma = A + B \log t \quad \text{and/or}$$

$$\Sigma = Ct^n$$

The effect of varying axial stress, confining pressure and differential stress on the creep behaviour of the tested rocks was observed and studied. A method for determining the

safe creep stress, at any confining pressure, was suggested depending on the creep data available.

CONTENTS

CHAPTER 3

CHAPTER 4

CHAPTER 5

CHAPTER 6

CHAPTER 7

CHAPTER 8

LIST OF FIGURES

LIST OF TABLES

Chapter 1

INTRODUCTION

Chapter 1

INTRODUCTION

1-1 General Introduction:

In rock mechanics problems in the fields of mining and civil engineering, the design process is generally concerned with the failure of rock material. The influence of high temperature, presence of solutions, confining pressure, etc. have well known effects on the failure properties of rock. Only some of these factors will be effectively applicable to any given rock structure situation, but such structures can hardly be unaffected by the influence of time. The consideration of time-dependent behaviour of rocks indicates that rock failure may occur in a mine or under a foundation even when the rocks are subjected to loads well below their normally short term rated strengths.

Schwartz[77] studied the movements of the roof and floor rocks in road ways in French Coal mines and has demonstrated that the convergence of the roof and floor depends on time. Hofer[36] in Germany reported that the expansion of pillars in potash mines due to the mass of the overlying beds also depends on time. Denkhaus[18] studied the problem of rock bursts in South Africa and reported that rock bursts following after blasting due to time effects. Reynolds and Gloyna[71] have made creep measurements in salt mines in the U.S.A. They reported that creep rate decreases as the age of a tunnel increases. Potts[66] carried out creep tests in the laboratory and at the Meadow bank Rock Salt Mine, Cheshire. He reported that the existing old pillars are creeping at nearly constant rate. (His work will be dealt with later in this thesis).

Hence, from the foregoing investigations and other field observations it is evident that crushing of pillars in room and pillar workings, closure of salt workings if left undisturbed for a long time, convergence of roof and floor in coal mine gate roads, widening of junctions on road ways, sagging and settling of the strata behind a long wall faces in coal mines, settlement of foundations, delay of rock bursts after blasting, etc. suggest that they are time-dependent or ''creep" processes.

Thus, time-dependent phenomena or "creep" in rocks is clearly important to civil and mining engineers. It is not only important for the question of the time factor, it is also important for questions of stress, for differences of stress distribution must occur if we compare slow or fast advance rates in tunnels and workings. A knowledge of creep properties offers important information to clarify the effects of the time factor in the behaviour of the excavations, it also gives a fair picture of the movements of the rock masses surrounding an excavation prior to fracture. Particularly in rock subject to large creep strains a knowledge of its creep properties is essential in determining the time during which a temporary excavation may be safely used. Creep studies provide information about fracture possibilities well in advance of that event, even at stress levels well below the normally regarded instantaneous strength of the rock, the only condition being that the second stage of creep has been reached and the load is to act for sufficiently long time. Obviously, then, an understanding of creep behaviour of rocks would be used in mine design, i.e. mine layout, sizes of galleries and supporting pillars and in an estimation of the useful

life of mine structures. It also would be of help in the development of strata support and control temperatures.

Creep of metals is a familiar property to engineers; in steels it normally occurs at high temperatures. It has also been observed in polymers, glass, ceramics, concrete, mineral crystals and rocks. Most of the research work on creep has been carried out on metals. The research of creep in rocks is still in its earlier stages. However, all investigators in this field have found that the creep of rock is affected by number of factors, such as the:-

1. Applied stress: value and method of application.
2. Temperature of specimen.
3. Structure of rock specimen: mineral orientation, porosity and permeability, composition, etc.
4. Confining pressure.
5. Presence of solutions.

In the research work described here, the effect of applied stress and confining pressure on the creep characteristics of some evaporite rocks namely, gypsum and anhydrite at room temperature was studied, and a new apparatus was designed for use in this investigation.

In chapter 2 a brief discussion about the principles of creep in general is given. The general structure and physical properties of rocks are mentioned in chapter 3, while the evaporite rocks and especially gypsum and anhydrite are studied in more details in chapter 4. A brief review of previous published work on creep in general and on rocks in particular are dealt with in chapter 5. The experimental work, including short term and creep tests in bending, uniaxial and triaxial compression,

the results obtained and their discussion are given in the remaining chapters of the thesis. Full details of the new apparatus for experimental study of deformation and creep of rocks subjected to triaxial compression stresses, including the design, materials used and calibration are given in chapter 8.

1-2 Stress Conditions and Design Requirements:

Stresses applied to the rock in the earth crust or in any rock structure may have a wide variety of forces, and in many cases it is extremely difficult to assess at the design stage the exact nature of a stress field in a rock structure, especially when the rock mass is in a fractured state. However, it is possible to recognise that in a large number of rock structure problems the following states of loading are of importance:

1. Bending (tension).

2. Uniaxial compression.

3. Triaxial compression.

It was therefore decided to study the creep properties of the chosen rock materials under the influence of various percentages of their instantaneous strengths in the above systems of loading.

The major requirements of any testing machine used for creep investigations are the following:

1. The known required stresses applied to the specimen must be kept constant for the whole period of the test without affects arising from outside mechanical or electrical disturbances.

2. The measuring devices, both the stress and the deformation, must be accurate, sensitive and capable to measure very small variations.

3. The deformation measuring devices must be stable, free from drift and be unaffected by environmental changes or by immersion in hydraulic oil, even at high pressures (in the case of triaxial test), for the whole period of the creep test.

1-3 The Aim of This Research

The aim of this work is of two parts. Firstly, to design and construct a complete apparatus for studying the deformation and creep of rock under triaxial compression. Secondly, to carry out triaxial creep tests using the mentioned apparatus on some evaporite rocks namely, gypsum and anhydrite. Bending and uniaxial compression creep tests also were carried out on the same rocks in order to provide supporting evidence of the properties of the materials and in the case of the uniaxial compression, as a basis of comparison with the triaxial results.

1-4 Practical Significance of the Work:

It is hoped that the information obtained on the creep behaviour of the rocks tested may be of use in mines in which these materials form the strata of the workings.

Knowledge of creep of materials under confinement is limited. The results obtained are thus an addition to knowledge in this field of study.

Movements of evaporite rocks in the earth's crust and the geological structures so produced may perhaps be better understood with additional knowledge of the creep properties of these materials. In this respect the extension of the work to oil reservoir cap rocks should result in information of use in petroleum engineering.

The experimental work has provided a practical base for

future work on rock testing and for the design of more powerful test equipment in which higher confining pressures can be used.

1-5 Summary of the Research Programme:

Short term loading tests were carried out on both the chosen rocks to find their instantaneous strengths in bending, uniaxial and triaxial compression.

In the triaxial compression tests, three levels of confining pressure were used namely, 10, 20 and 30 N/mm^2.

The creep tests were then carried out at various percentages of the instantaneous strength of each rock obtained, using the same system of loading as that used in the corresponding short term tests. An exception was that the creep triaxial tests of anhydrite were carried out at 10 N/mm^2 confining pressure only due to the limitations in the time available.

All compressive tests were carried out on rock specimens cut from rock mass so that the major stress was applied perpendicular to the rock bedding. Fig. (6-3) gives illustrations of specimens with respect to rock bedding.

All the short term and creep tests were carried out at room temperature.

Chapter 2

THE PRINCIPLES OF CREEP

Chapter 2

THE PRINCIPLES OF CREEP

2-1 Definition of Creep:

Creep may be defined as the continuous increase in deformation of material under constant or decreasing differential stress. It may be exhibited in the elastic range, where the creep strain may be completely, or very nearly, recovered on removal of stress, or in the plastic range, where the creep deformation is permanent. In the plastic range an elastic component also exists but in a small amount by comparison.

2-2 The Typical Creep Curve:

It was found that the time-dependent strain, or creep, curves of materials, including rocks, under stress are generally similar. These curves can be represented by what may be refered to as the typical creep curve. This comprises, Fig. (2-1), of the following four parts:

1. Instantaneous elastic deformation.
2. Primary creep (delayed elastic flow).
3. Secondary creep (steady-state flow).
4. Tertiary creep (rupture flow).

2-2.1 Instantaneous Elastic Deformation:

This deformation is not due to any time effect, it is the deformation of the specimen which occurs during the loading operation and its magnitude varies with the applied stress. It is represented by the part (OA) of the creep curve. In this stage the body follows Hooke's Law of deformation i.e. the deformation is elastic and recoverable if the applied stress is removed.

2-2.2 Primary Creep:

This stage of creep is represented by the part (AB) of the typical curve. It is also known by other terms such as transient creep, delayed elastic flow, elastic creep etc. The rate of deformation in this stage decreases with time, see part (ab) of the curve shown in Fig. (2-2). The deformation at this stage is mostly recoverable if the applied stress is removed, i.e. at any time (T_e) in the period AB, of the typical curve, if the specimen is unloaded there is first an instantaneous elastic recovery (EF) followed by time-elastic recovery, represented by the curve (FG) at a rate which is generally less than the creep rate of (AB). The reduction of creep rate at the primary stage is thought to result from the gradual closure of any pore spaces or small discontinuities in the material.

The primary stage of creep is important from the point of view of engineering design. Estimation of permissible stresses with reference to allowable dimensional tolerance in service can be made from the deformation - time curve and preference may well be given to designs involving values of stress which will not cause creep beyond the primary stage during the expected life of the structure.

2-2.3 Secondary Creep:

If the decreasing creep rate in the primary stage does not vanish, then a stage of secondary creep starts. This is sometimes called steady-state creep, pseudoviscous flow, minimum creep, plastic flow, etc. This stage is represented by the part (BC) of the typical curve. The rate of creep in this phase is constant and determined by the slope $S_o = \frac{\Delta\epsilon}{\Delta t}$ of the creep curve in the secondary period, see part (bc) of the curve in Fig.(2-2).

In the secondary stage of creep in crystalline materials the movement of the crystals on either side of the slip planes is relatively organized and the crystals with preferred orientation generally align themselves in the direction of the plane of movements after the grain edges have been rounded off[94]. The creep strain in this stage is irrecoverable, i.e. if the specimen at point (H) of the typical curve in the period of secondary creep is unloaded the strain curve will follow the path (HIJ) with a permanent deformation. The secondary creep stage represents from the engineer's point of view, a period in the creep history of a material when its ultimate failure may become relatively imminent.

2-2.4 Tertiary Creep:

This stage of creep is represented by the last part of the typical creep curve (CD). The rate of strain increases in this stage leading to rupture of the specimen, see part (cd) of Fig. (2-2). This stage is also known as plastic flow, accelerating creep, rupture creep, elastic fatigue, stress corrosion, etc. In this stage of creep the strain rate accelerates with time because of the formation of line cracks, eventually lowering the load carrying area of the specimen[63]. Another explanation suggested for the rupture is that the grain boundaries gradually break up because of excessive heating under continuous straining[10].

An understanding of deformation and fracture of rocks in the tertiary creep phase possibly help in understanding the rock behaviour and fracture immediately prior to earthquakes and in mine rock bursts.

2-3 Rheological Behaviour of Rocks:

The time-dependent behaviour of different materials may be classified on the basis of observed reactions in the form of a series of rheological models. Such an approach may be justified by comparing the actual time dependent properties of the real material with an idealized rheological element. The models consist of one or combination of more of the simple elements: spring (elastic element), dash pot (viscous element) and frictional contact (plastic element). A number of these models will be described in the following sections.

2-3.1 Elastic Deformation:

Any material that behaves in perfectly elastic manner is called a Hookean substance. The relation between its uniaxial stress (σ) and strain (ε) follows the equation.

$$E = \frac{\sigma}{\varepsilon} \qquad (2\text{-}1)$$

where E is the modulus of elasticity (Young's modulus) which is a constant of the material. The spring is a mechanical model for such material. Fig.(2-3) shows the model (spring) and the graphical representation of stress-strain relationship which is a straight line passing through the origin with a slope equal to (E).

2-3.2 Viscous Deformation:

The model of this behaviour is a dash-pot, see Fig.(4-2). Any material exhibiting purely viscous properties is known as Newtonian substance. The relation between the stress (σ) and the strain rate (ε') with respect to the time follows the equation:

$$\sigma = \eta\varepsilon' \qquad (2\text{-}2)$$

where η is a constant of the material known as its viscosity.

If the stress applied (σ) kept constant at (σ_o) then Eq. (2-2) will be $\frac{d\varepsilon}{dt} = \frac{\sigma_o}{\eta}$ and by integration

$$\varepsilon = \frac{\sigma_o t}{\eta} \qquad (2\text{-}3)$$

It can be seen from Eq.(2-3) that the strain increases linearly with time, see Fig. (2-4b).

2-3.3 Plastic Deformation:

This may be represented by friction contact, Fig. (2-5). The material will not deform if the applied stress (σ) is less than (σ_o) and will deform permanently if $\sigma = \sigma_o$. Also, the material in this case will not support a stress greater than (σ_o). The stress-strain relationship, shown in Fig. (2-5b) must, therefore, be a straight line parallel to the strain axis at stress equals to (σ_o). This value is called the yield stress.

2-3.4 Viscoelastic Deformation - Maxwell Unit:

A simple combination of elements which shows viscoelastic behaviour can be represented by the Maxwell unit. This unit is composed of a dash-pot (viscous element) in series with a spring (elastic element) as shown in Fig.(2-6). Assume, ($\varepsilon_\eta, \sigma_\eta$) and ($\varepsilon_E, \sigma_E$) are the strain and the stress in the dash-pot and the spring respectively, then from Fig.(2-6)

$$\sigma = \sigma_\eta = \sigma_E \qquad (2\text{-}4)$$

$$\varepsilon = \varepsilon_\eta + \varepsilon_E \qquad (2\text{-}5)$$

Differentiating Eq.(2-5) with respect to time gives

$$\varepsilon' = \varepsilon'_\eta + \varepsilon'_E \qquad (2\text{-}6)$$

Substituting Eqs. (2-1) and (2-2) in Eq.(2-6) gives the following stress-strain relationship

$$\varepsilon' = \frac{\sigma}{\eta} + \frac{\sigma'}{E} \qquad (2\text{-}7)$$

Assume a constant stress (σ_o) is applied at time equal to

zero. As the stress is constant therefore $\sigma' = 0$. From equation (2-7) where $\sigma' = 0$ and $\sigma = \sigma_o$ then $\varepsilon' = \frac{\sigma_o}{\eta}$

By integration of the above equation

$$\varepsilon = \frac{\sigma_o t}{\eta} + K \qquad (2\text{-}8)$$

Where K is the constant of integration and equal to the elastic strain ε_o ($\Leftarrow \frac{\sigma_o}{E}$) that occurs when the stress is applied at t = O. Equation (2-8) can be rewritten in the form:

$$\varepsilon = \frac{\sigma_o t}{\eta} + \frac{\sigma_o}{E} \qquad (2\text{-}9)$$

when $\varepsilon = 0$ then $\frac{\sigma_o t}{\eta} = -\frac{\sigma_o}{E}$

or $t = -\frac{\eta}{E}$ = constant

Thus different values of σ_o will give different straight lines on the strain-time plane, all of which emanate from a single point (A) on the time axis given by $t = -\frac{\eta}{E}$ as illustrated in Fig.(2-6b).

Equation (2-9) represents steady state creep (secondary stage) but does not include transient creep (primary stage).

If the strain is kept constant at a value equal to (ε_o) then $\varepsilon' = 0$. Eq. (2-7) will be $\frac{\sigma'}{\sigma} = -\frac{E}{\eta}$

which on integration gives:

$$\sigma = \sigma_o \left[\exp(-\frac{Et}{\eta})\right] \qquad (2\text{-}10)$$

where (σ_o) is the stress at t = O necessary to produce the strain (ε_o). Eq. (2-10) represents stress relaxation from its initial value under conditions of zero creep rate.

2-3.5 Firmo-Viscous Deformation - Kelvin Unit:

This behaviour can be represented by a spring and a dash-pot in parallel which is called Kelvin or Voigt unit, as illustrated

in Fig. (2-7). For this unit the following conditions will apply

$$\sigma = \sigma_\eta + \sigma_E \tag{2-11}$$

$$\epsilon = \epsilon_\eta = \epsilon_E \tag{2-12}$$

Substituting Eqs. (2-1) and (2-2) in eq. (2-11)

$$\sigma = E\epsilon + \eta\epsilon' \tag{2-13}$$

Assume that a constant stress σ_o is applied to the unit at t = O, when ϵ = O. Then integration of Eq. (2-13) leads to

$$\epsilon = \frac{\sigma_o}{E} \left[1 - \exp\left(-\frac{Et}{\eta}\right)\right] \tag{2-14}$$

Equation (2-14) shows that the strain ϵ = O when the time t = O and equal to $\frac{\sigma_o}{E}$ after an infinite time.

This behaviour represents primary creep but does not include secondary creep stage.

If the unit is deformed to some value of strain ϵ_o and then the stress is removed. Eq. (2-13) becomes

$$E\epsilon = -\eta\epsilon' \quad \text{or}$$

$$\frac{\epsilon'}{\epsilon} = -\frac{E}{\eta}$$

which on integration gives

$$\epsilon = \epsilon_o \left[\exp\left(-\frac{Et}{\eta}\right)\right] \tag{2-15}$$

Thus the strain relaxes under zero stress, but will take infinite time before the strain completely vanishes.

2-3.6 Elastoplastic Deformation - St. Venant Unit:

The material which shows an elastoplastic property is known as St. Venant substance whose behaviour can be represented by a spring in series with a friction contact as shown in Fig. (2-8). This material is perfrectly elastic for stress less than σ_o (yield stress), i.e. it follows Eq. (2-1) and is perfectly

plastic at stress equal to σ_o, see section (2-3.3).

2-3.7 Bingham Unit:

The St. Venant Unit (section (2-3.6) has no restriction on its deformation once the yield stress is exceeded. Bingham removed this disadvantage in his unit, Fig. (2-10), which consists of a dash-pot, a frictional weight and a spring in a series. This unit gives a reasonable representation of the deformation of a material having a yield point. When the applied stress is less than a certain value σ_o(yield stress) the body deforms elastically, i.e. follows Eq. (2-1), and for greater stress deforms with steadily increasing strain.

If a constant stress σ is applied at t = 0 then

(a) For $\sigma < \sigma_o$

$$\varepsilon = \frac{\sigma}{E} \qquad (2\text{-}16)$$

(b) For $\sigma \geq \sigma_o$

$$\varepsilon = \frac{(\sigma - \sigma_o)t}{\eta} + \frac{\sigma}{E} \qquad (2\text{-}17)$$

2-3.8 Burger's Model:

Behaviour of real materials is more complex than to be represented by one of the previously described units. Many investigators have suggested how different models may be built up from combinations of the above units.

One of the more useful complex models is the M-V or Burger's model which consists of Maxwell unit in series with Kelvin-Voigt unit as shown in Fig. (2-9a). This model may, nearly, represent the creep phenomenon, i.e. the spring, E_1 in Maxwell unit represents the instantaneous elastic deformation, the Kelvin-Voigt unit represents the primary creep stage or the delayed elastic deformation. The component of secondary creep, or psuedo-viscous

deformation, is contributed by the dash-pot η_1 of the Maxwell unit.

If a constant stress σ_o is applied to the model at t = 0, the total strain in the model will be

$$\varepsilon = \varepsilon_K + \varepsilon_M \qquad (2\text{-}18)$$

where ε_K = deformation of Kelvin unit as given by Eq.(2-14) and ε_M = deformation of Maxwell unit as given by Eq. (2-9) substituting the values of ε_K and ε_M in Eq. (2-18) gives

$$\varepsilon = \frac{\sigma_o}{E_2}\left[1 - \exp\left(-\frac{E_2 t}{\eta_2}\right)\right] + \left(\frac{\sigma_o t}{\eta_1} + \frac{\sigma_o}{E_1}\right) \qquad (2\text{-}19)$$

If Eq. (2-19) represents the creep behaviour of some rock under constant stress σ_o, then the term $\frac{\sigma_o}{E_1}$ represents the instantaneous deformation while the exponential term

$\frac{\sigma_o}{E_2}\left[1 - \exp(-\frac{E_2 t}{\eta_2})\right]$ represents the recoverable primary creep. The steady-state deformation which is irrecoverable is represented by the term $\frac{\sigma_o t}{\eta_1}$. Fig. (2-9b) shows the strain-time relationship in Burger's model.

Obert and Duvall[56] mentioned that Burger's model may closely represent the creep properties in some rocks when subjected to sudden constant uniaxial or triaxial loading. This representation requires suitable choice of the four constants, E_1, E_2, η_1 and η_2.

In time-dependent studies, many investigators such as Hardy[31] on rocks, Afrouz and Harvey[2] on rocks within the soft to medium strength range, Lee and Markwick (see Reiner[70]) on bituminous road materials and others have indicated that the creep behaviour of the material follows, or nearly follows, the behaviour of Burger's model.

2-3.9 B-V Model:

In applying Burger's model to the creep behaviour there is one important defect which is when a constant stress is applied to the model and after the delayed elastic deformation due to Kelvin unit (E_2, η_2) Fig.(2-9) is complete, the model would continue to deform at a uniform rate indefinitely due to the Maxwell dash-pot (η_1), even if the applied load is extremely small. A modified model which consists of a Voigt unit in series with Bingham unit as shown in Fig. (2-11) has been suggested. This is known as B-V model. In this model the spring E_1 represents the instantaneous deformation, while the Voigt-Kelvin (η_2, E_2) represents the delayed elastic deformation.

Before the pseudo-viscous deformation by the dash-pot (η_1) takes place the frictional resistance of the weight (W) must be overcome. The stress necessary to overcome the frictional resistance, as in Bingham unit, represents the yield strength of the material. This resistance, in B-V model, represents the long term strength of the solid. In a series of creep experiments on beams of Pennant and Wolstanton Sandstones in simple bending, Price[69] indicated that the data obtained followed the behaviour of B-V model reasonably well.

In order to decide which, if either, models, Burger's or B-V, will represent the creep behaviour of a certain rock, it is necessary to obtain creep data of that rock at different stress levels. From the data a curve of rate of secondary creep versus stress is plotted, this curve then must be compared with a similar relationship of the two models as shown in Figs.(2-9c) and (2-11b) for Burger's and B-V models respectively.

2-4 Practical Use of Rheological Models

The practical purpose of rheological models lies in the field of long term prediction of material behaviour. Frequently, the long term deformation at low stress levels are required when the time available for testing may be two or more orders of magnitude less.

In these circumstances "accelerated tests" involving higher stresses than design values can be fitted to a model which - when a good fit is possible - may then be used to predict the required long term behaviour. For this purpose some investigators, see Attewell[6], have assembled models far more complex than the Burger's or B-V models, There is little purpose in describing these in detail as they generally refer to particular material under investigation.

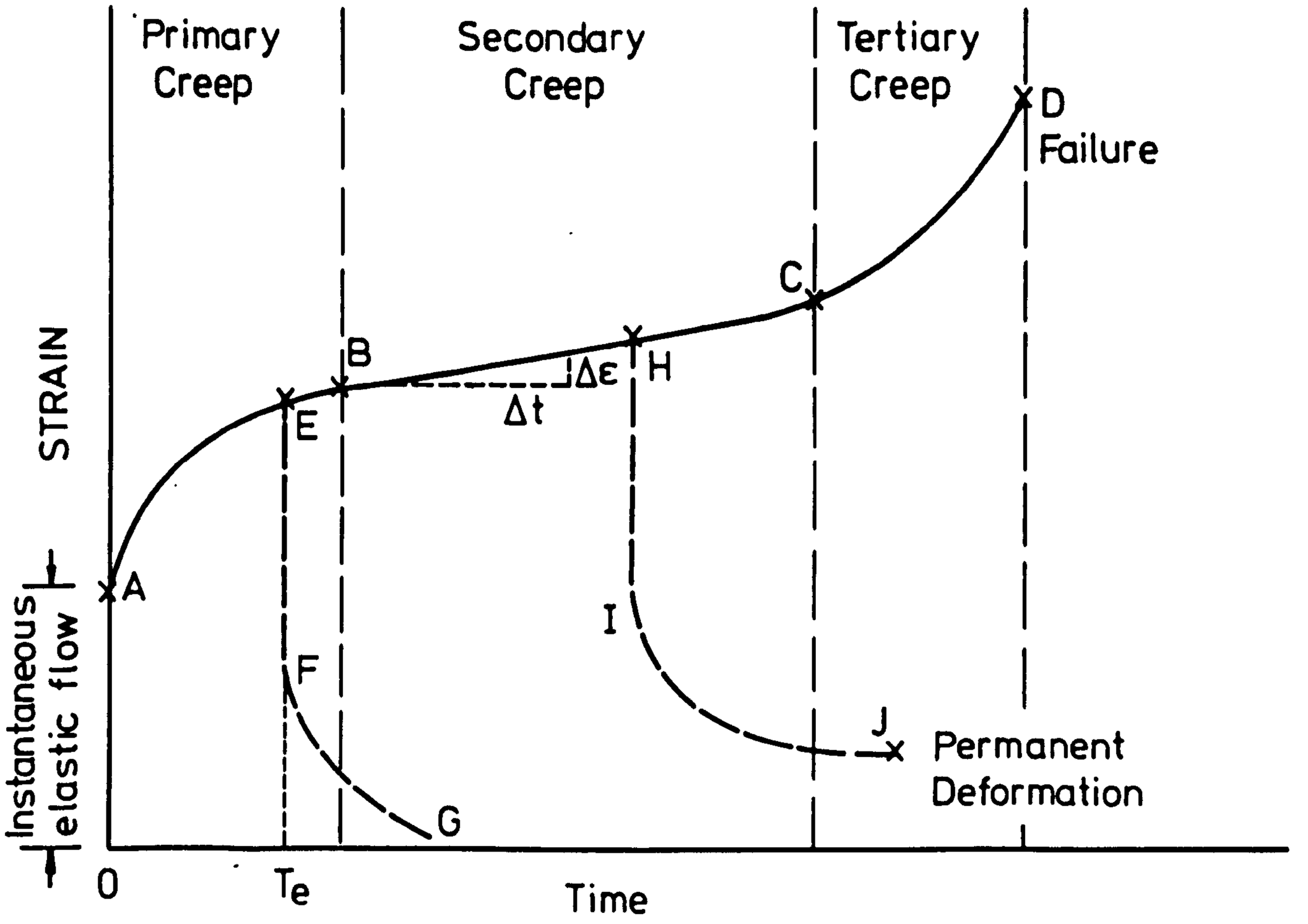

FIG. 2-1 TYPICAL CREEP CURVE

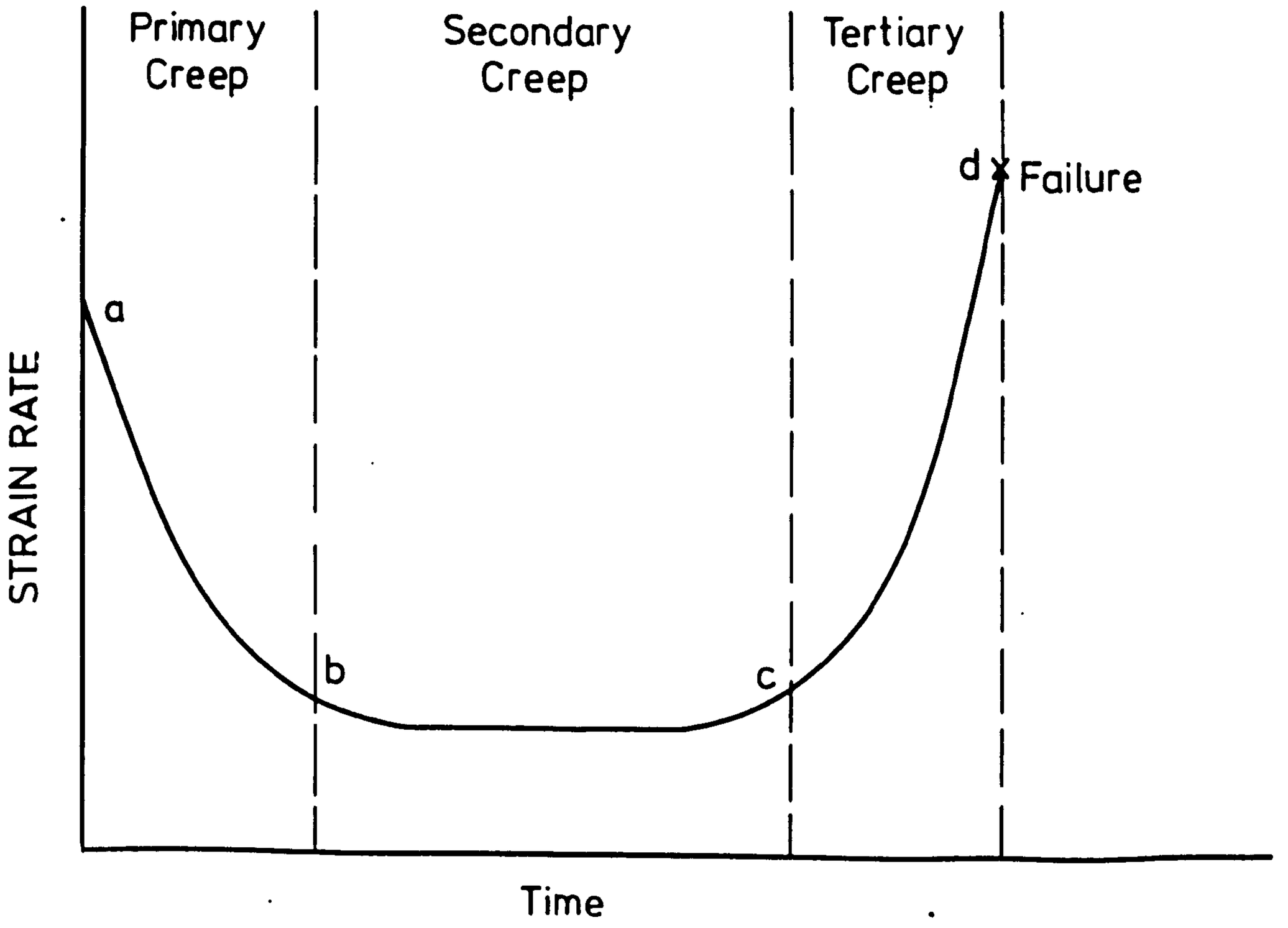

FIG. 2-2 STRAIN RATE VERSUS TIME

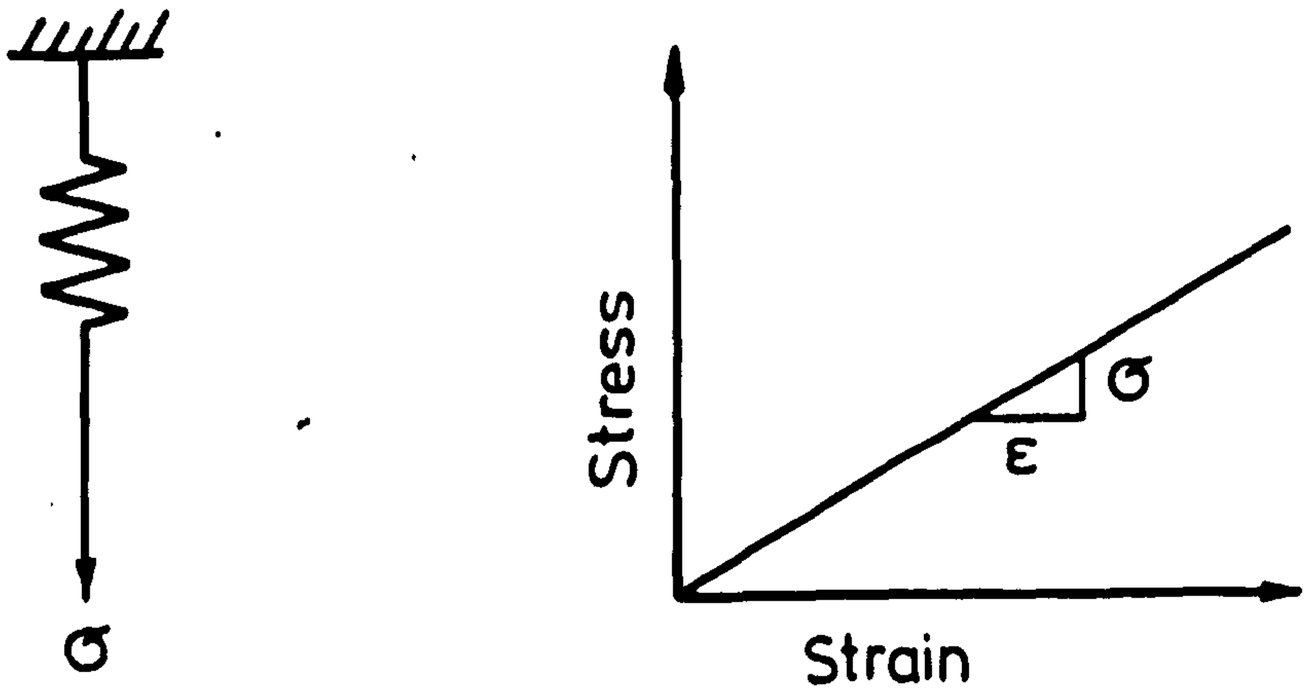

(a) (b)

FIG. 2-3 ELASTIC DEFORMATION (HOOKEAN SUBSTANCE)
(a) Model (Spring) (b) Stress-strain curve

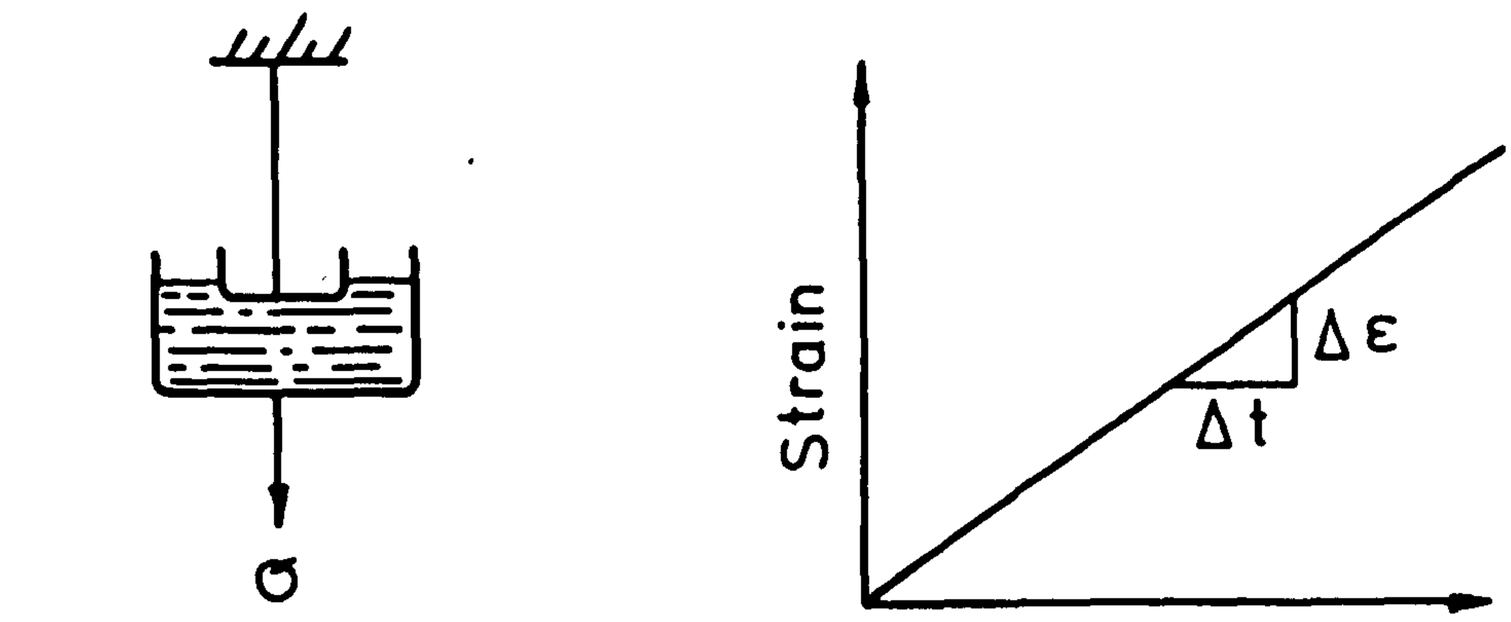

(a) (b)

FIG. 2-4 VISCOUS DEFORMATION (NEWTONIAN SUBSTANCE)
(a) Model (Dash pot)
(b) Strain-time relation at constant stress

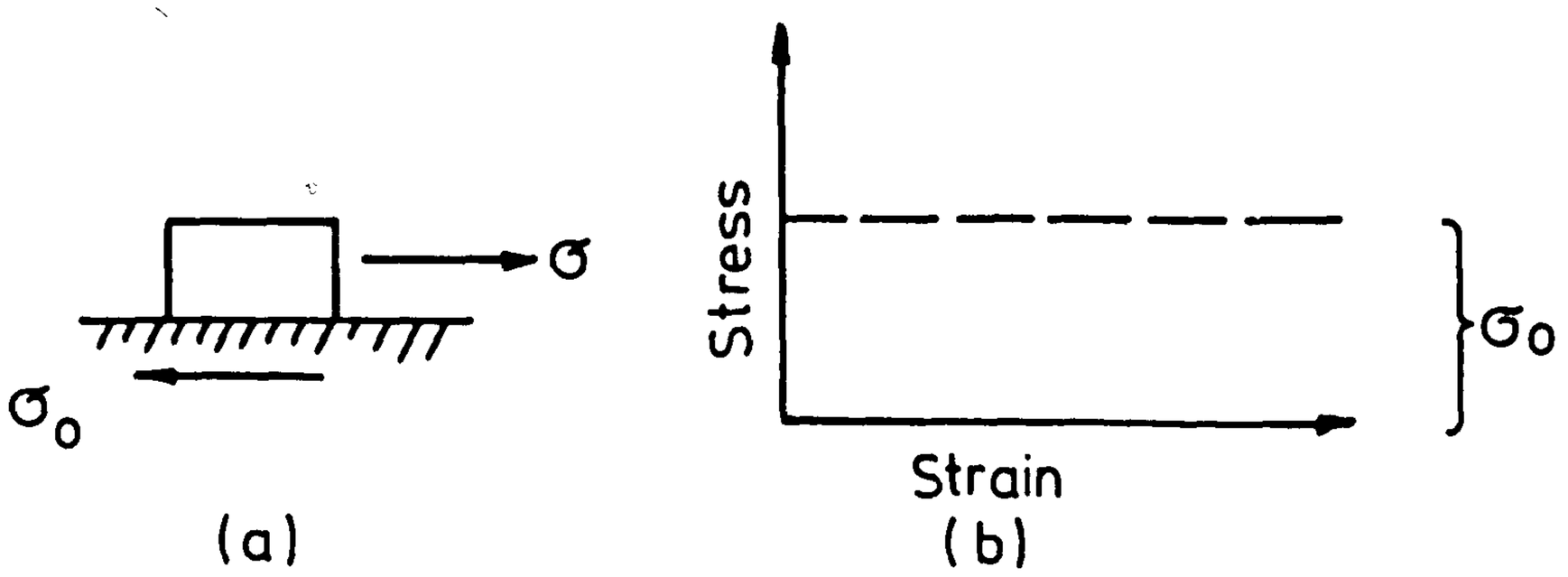

(a) (b)

FIG. 2-5 PLASTIC DEFORMATION (FRICTION CONTACT)
(a) Model (Friction contact)
(b) Stress-Strain curve

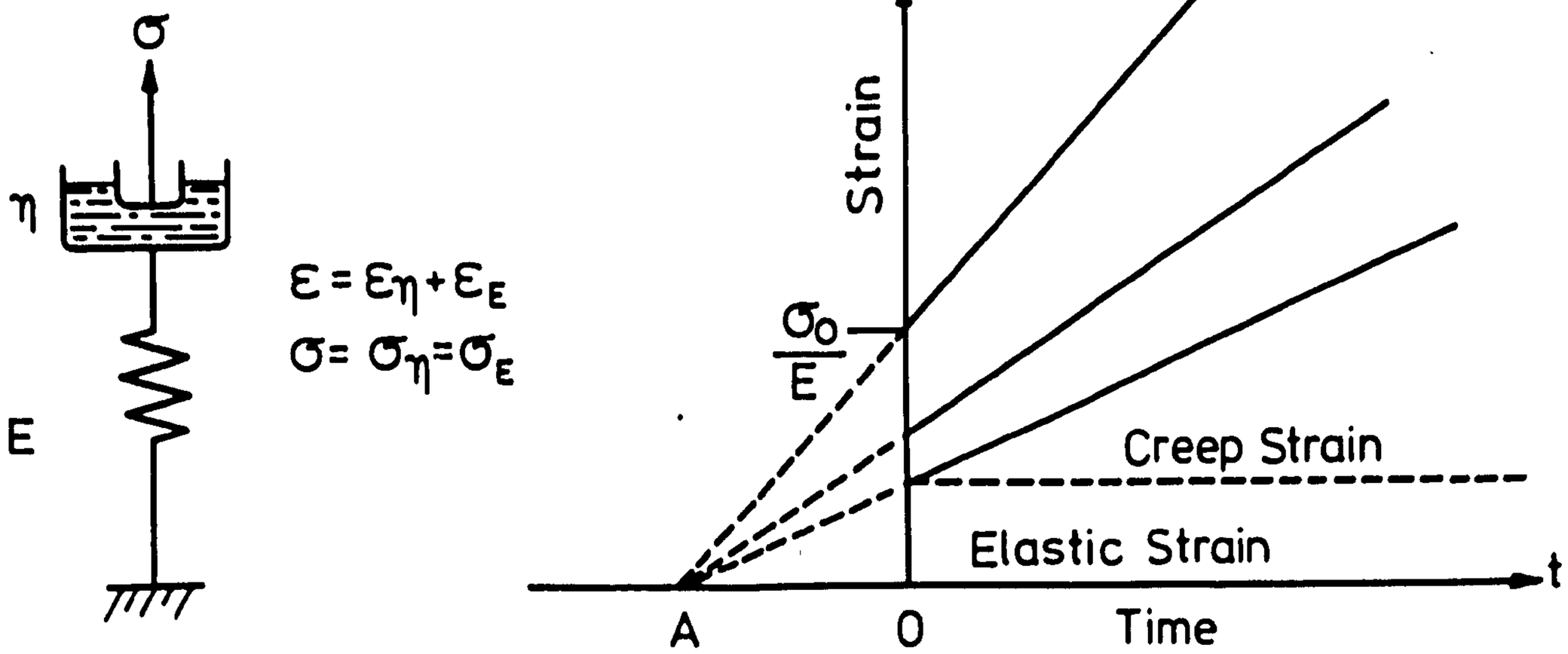

FIG. 2-6 MAXWELL UNIT

(a) Model (b) Strain-time curve at constant σ_0

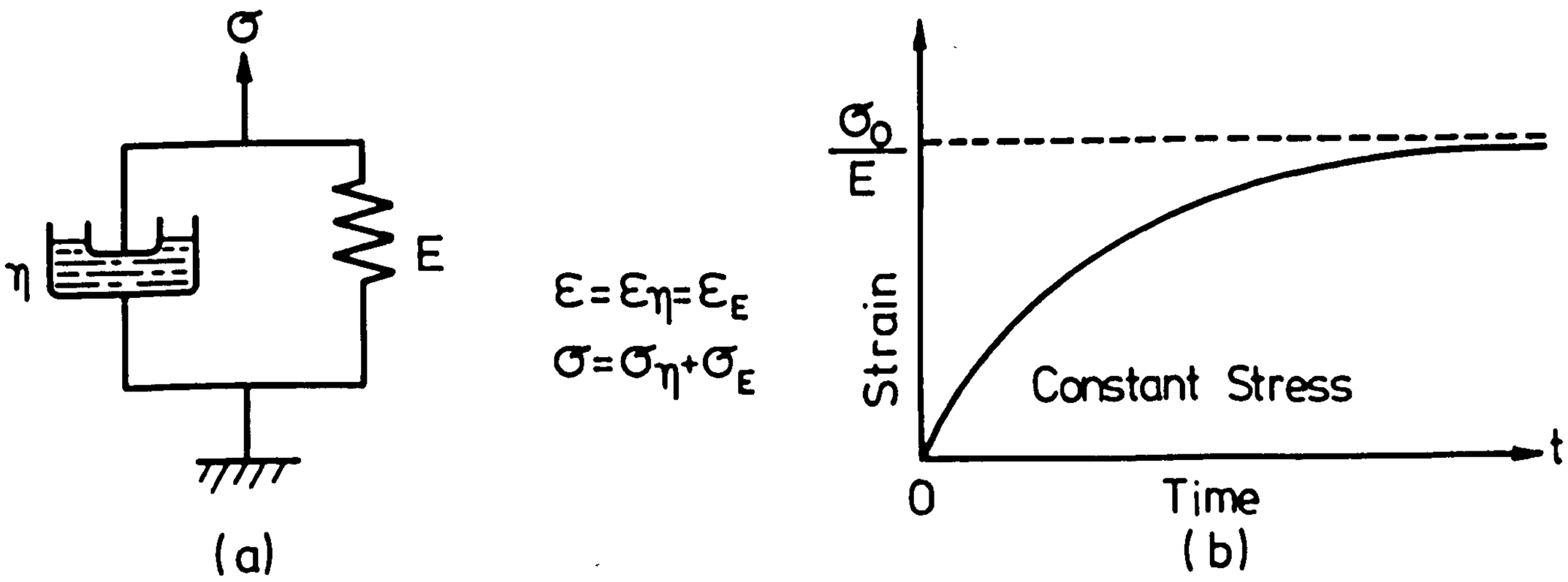

FIG. 2-7 KELVIN OR VOIGT UNIT

(a) Model (b) Strain-time curve at constant stressed

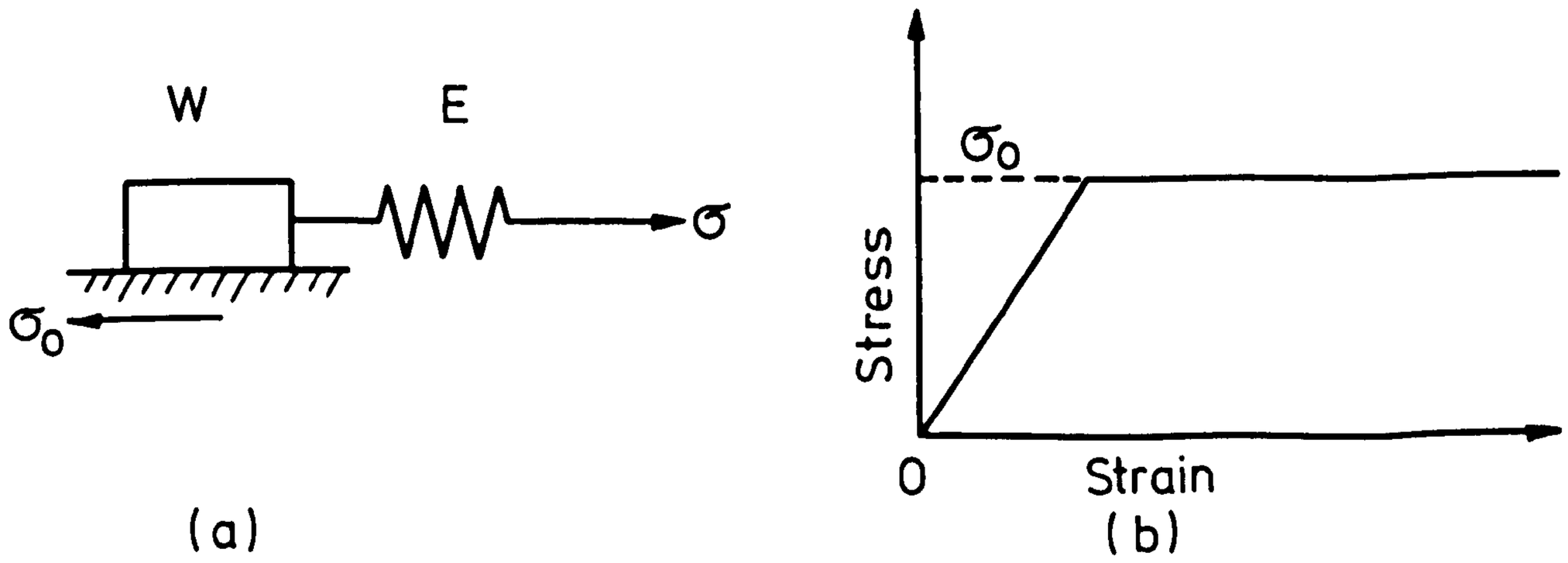

FIG. 2-8 ST. VENANT UNIT

(a) Model (b) Stress-strain curve

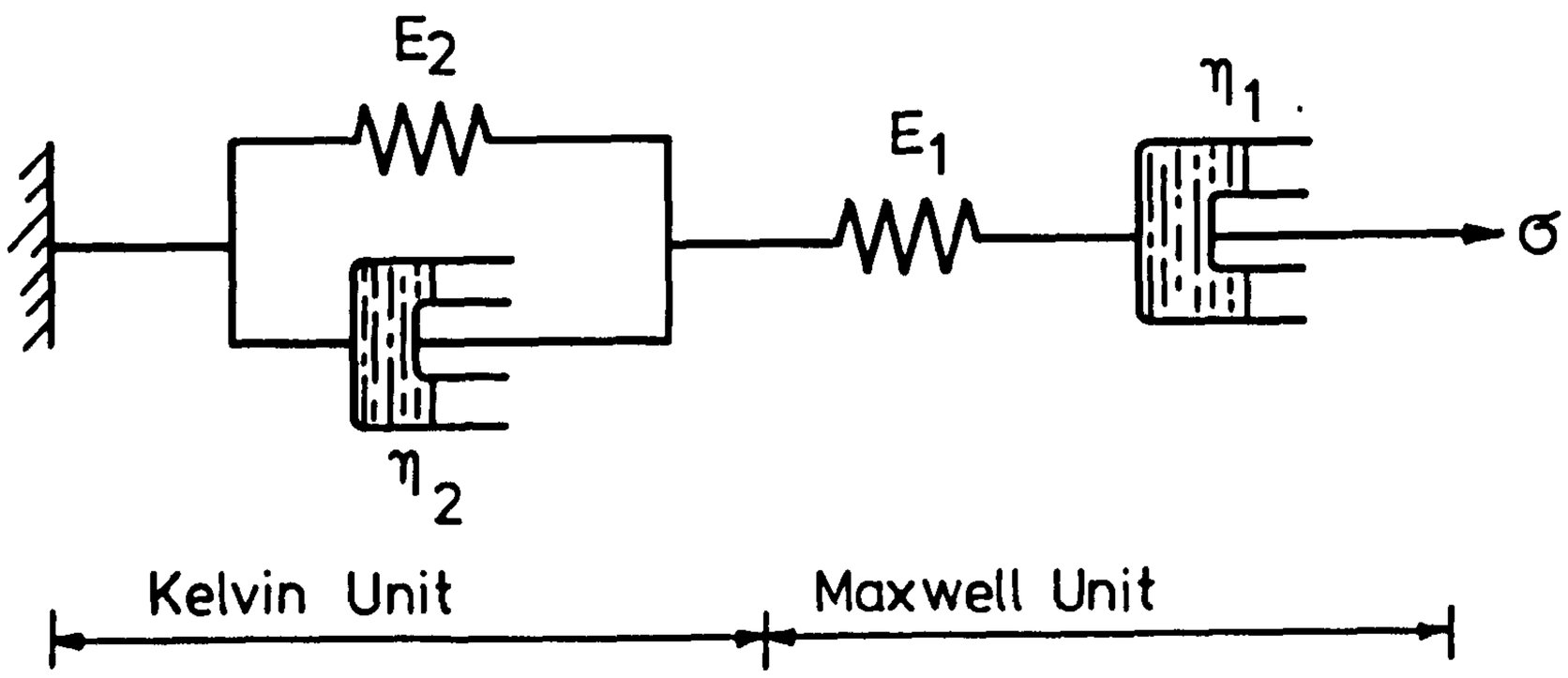

(a) Model

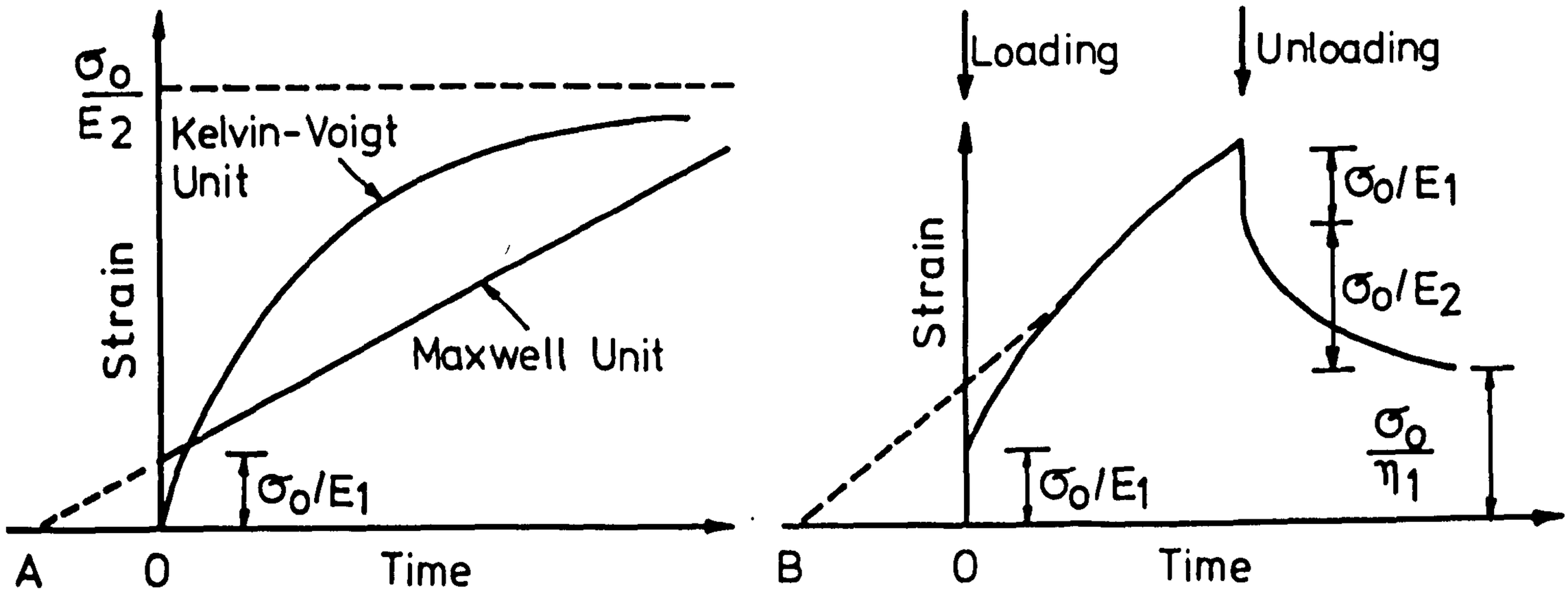

(b) Strain-time relationship

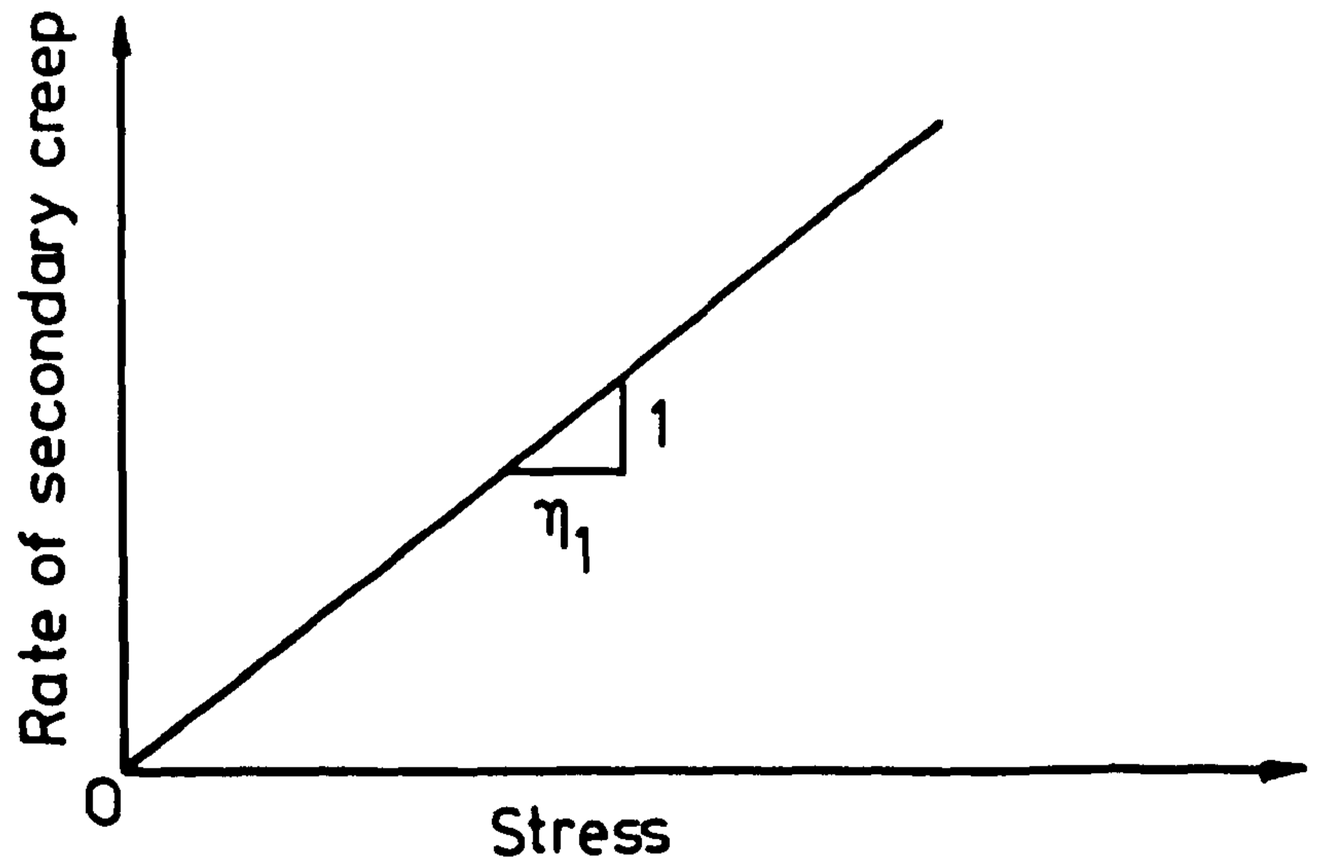

(c) Rate of secondary creep versus stress

FIG. 2-9 BURGER'S MODEL

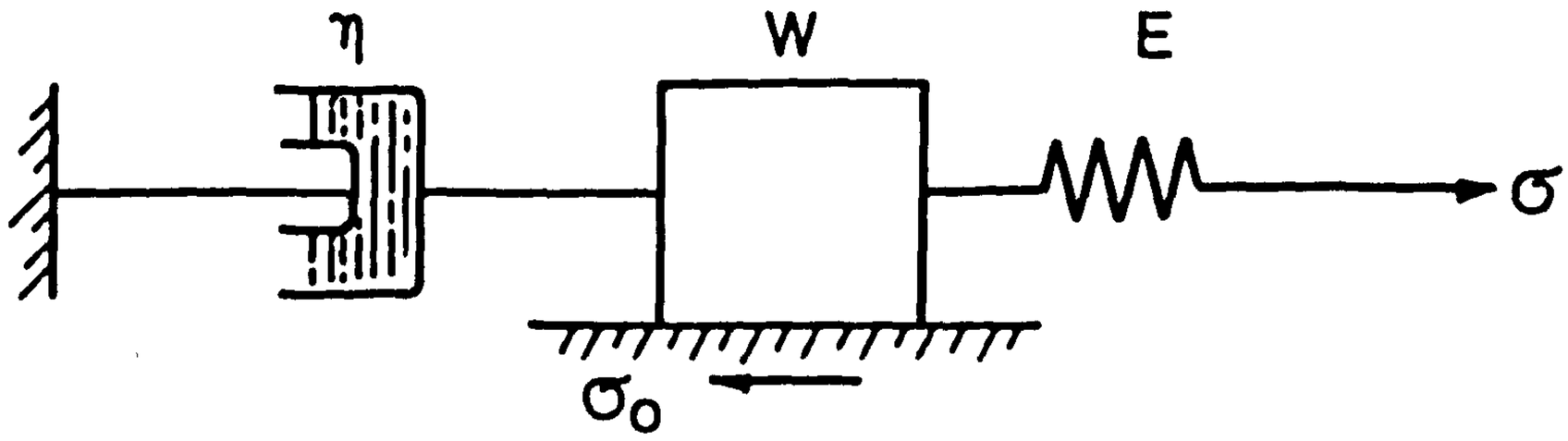

FIG.2-10 BINGHAM UNIT

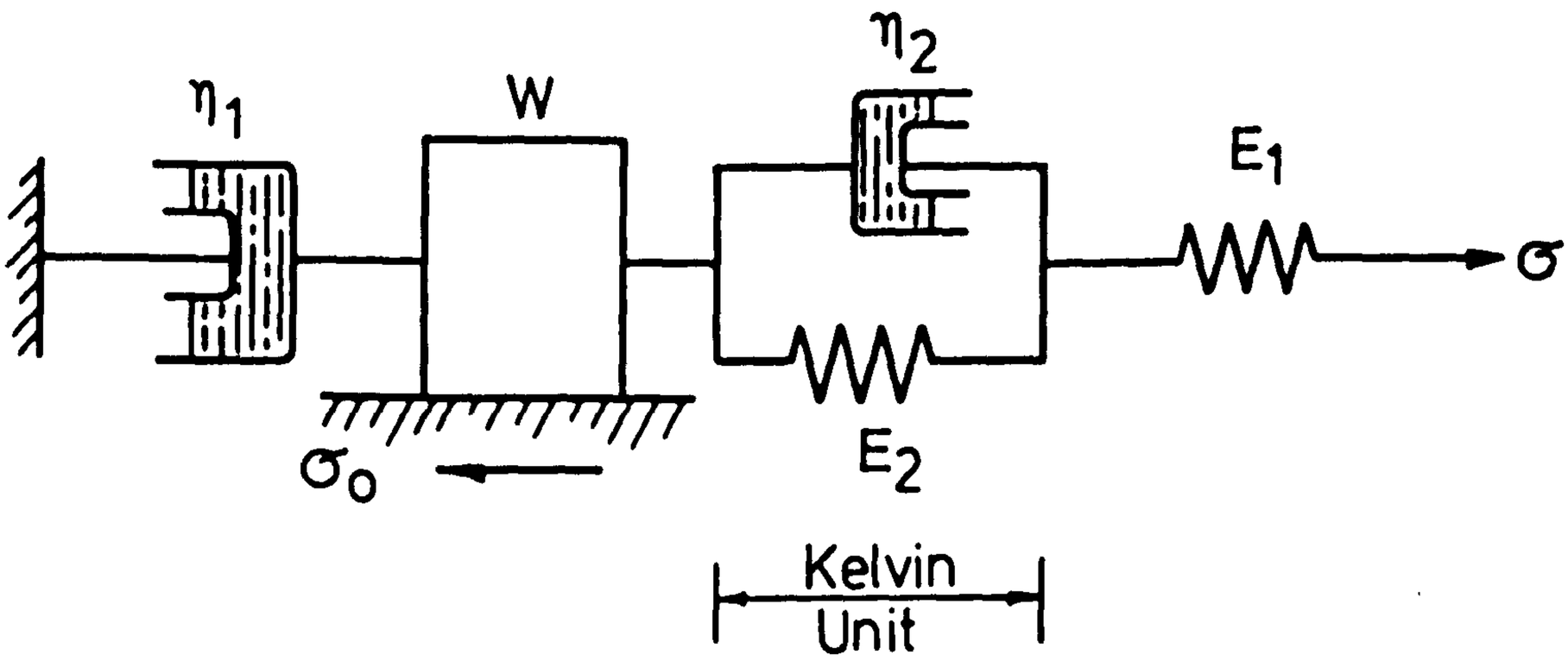

(a) Model

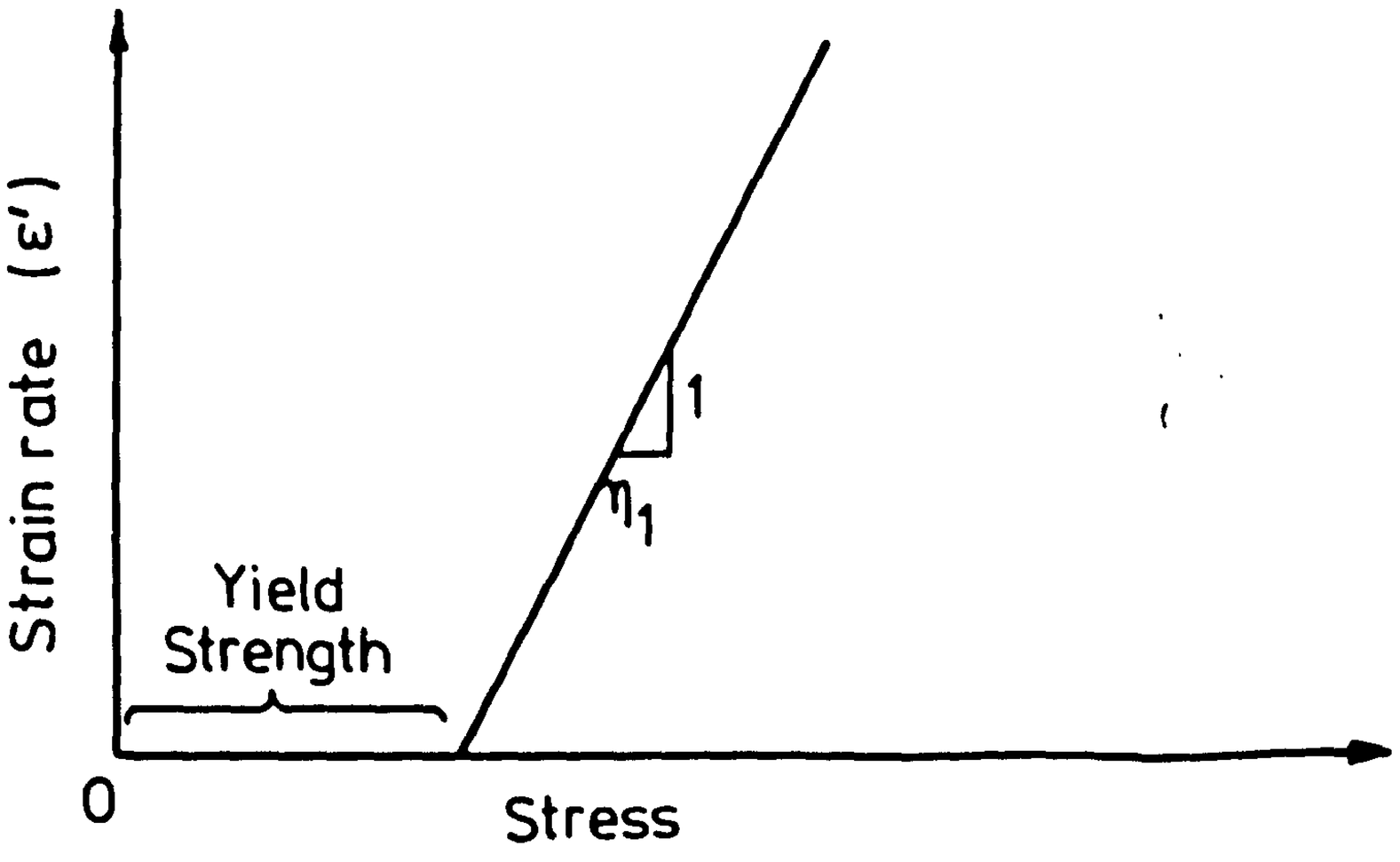

(b) Secondary creep rate versus stress

FIG. 2-11 B-V MODEL

Chapter 3

SOME PHYSICAL STRUCTURE AND MECHANICAL PROPERTIES OF ROCKS

Chapter 3

SOME PHYSICAL STRUCTURE AND MECHANICAL PROPERTIES OF ROCKS.

3-1 Porosity

Among the important properties of rocks is their porosity, which may be defined as the ratio, usually expressed as a percentage, of the volume of the pore space to the total volume of the rock:

$$n = \frac{V_v}{V_s+V_v} \times 100 = \frac{e}{1+e} \times 100 \qquad (3\text{-}1)$$

where:

n : porosity, percent

V_v : Volume of pore space or Voids volume

V_s : Volume of solid rock.

e : void ratio $= \frac{V_v}{V_s}$

Porosity in rocks varies from as much as 30% in the case of sandstones and limestones to less than 0.5% in some igneous and metamorphic rocks. The difference in the magnitude of the porosities of various rocks arises from the difference in their mode of formation and their physical structure.

In the case of igneous rocks a slowly cooling magma will render a relatively non-porous rock, whereas a rapidly cooling lava particularly associated with escaping gases will yield a porous rock. Metamorphic rocks have been formed by recrystallisation due to heat and pressure, and possibly by the invasion of hot magmatic solutions (as has been suggested, for example, in the case of granites). In general, however, the small degree of porosity in igneous and metamorphic rocks is probably due to misfit between the mineral crystals composing the rocks arising from differences in thermal, elastic and plastic properties

between different minerals or between different directions in a given mineral crystal. Such misfits may result in inter- or intracrystalline cracks because of the inherent brittleness of most mineral crystals, and these cracks may very well be the main source of porosity in these rocks. Sandstones and limestones have been formed by the cementing together of roughly equiaxial particles (sand grains and fossil organisms respectively) after the sedimentation process, so their porosity will depend largely on the amount of cementing materials present and the size and packing of the granular constituents. Therefore, it is not difficult to see that such rocks could have a high degree of porosity. Shales, which in general have a relatively low porosity, have been formed by the coagulation of sub-microscopic colloidal clay particles, and depend for their cohesion on the surface forces between the clay particles. During the process of consolidation of the shale, water is squeezed out from between the clay particles, and the particles, which are plate-like in shape, tend to become aligned with their planes roughly parallel, giving rise to the familiar shaley parting. This also means, however, that the porosity of consolidated shales will be relatively low as compared with bodies formed from particles which are more nearly isometric.

Evaporites, (such as gypsum and anhydrite) have been formed by deposition from solution, during the evaporation of shallow seas. They may have some degree of intercrystalline porosity because of the solvent water, but since the crystals concerned deform plastically at fairly low stresses, much of this porosity can be eliminated by consolidation. Jones[42] found that the average porosity of Sherburn gypsum (used in the experimental

work) is 0.88%. It should be noted that a porous material is not necessarily permeable, e.g. sandstones and gravels are commonly both porous and permeable, since they allow water to pass through, but clay is porous but impermeable, since it will not allow water to pass through. Many investigators such as Price, 1960; Kowalski, 1966; and Smorodinov et al, 1970, see Vutukuri[84], indicated that compressive strength of rocks decreases with increase in porosity. Ryshkewitch[76] and Duckworth[20] suggested the following relationship between strength of ceramic and its porosity

$$\sigma = \sigma_o \exp(-CP) \qquad (3\text{-}2)$$

where: σ = strength of porous body; σ_o = strength of non-porous body of the same material; P = frictional porosity; and C = constant. One of the reasons for decreasing strength with increasing porosity is that if a rock has internal space its cohesion, molecular or mechanical, will obviously be affected by the amount of remaining internal contact between its constituent fractions. This will be less in the case of a highly porous rock and this will be reflected in the strength of the rock.

3-2 Anisotropy

A body is said to be anisotropic if its physical properties are unequal when measured in different directions. The extent to which a rock is anisotropic is a function of its type and mode of formation. Generally speaking, since many rocks have a preferred particle and crystal orientation, they are anisotropic and would be expected to react differently to forces in different directions. Most igneous rocks have a dense, interlocking fabric with only slight directional differences in physical properties (almost isotropic), with the exception of many surface flow rocks

and near surface intrusives and of some deep-seated intrusives, such as gneissic granites, which show flow structure at the periphery of the intrusion. Metamorphic rocks are the most striking with respect to anisotropy due to the alignment of the mineral crystals during the formation process as the result of recrystallization under stress. Some sedimentary rocks such as shale, sandstone and some limestones are laminated and therefore show considerable anisotropy. Other sedimentary and evaporite rocks such as rocksalt, gypsum, anhydrite and many limestones show only slight anisotropy. Anisotropy is difficult to study particularly as regards it effect on fracture and plastic deformation.

Donath[19] carried out experimental triaxial compressive tests on group of Martinsburg slate specimens prepared so that the cleavage plane varied in 15 degree increments from 0 to 90 degrees, from the direction of the major applied compressive stress. He found that the maximum shear strength was 9400 psi while the minimum was 600 psi. Other investigators found that in some sedimentary and foliated rocks, the tensile and flexural strengths are generally lower in the direction perpendicular to the bedding or foliation than in directions parallel to this.

3-3 Homogeneity

A rock is considered as homogeneous if the size and shape of grains or crystals are evenly distributed through the rock mass. From this definition it should be noted that depending on the grain or crystal size, homogeneity must be defined with reference to the volume of the body considered. A rock which may be fairly homogeneous in mass may be completely heterogeneous when a hand sample is considered. It is essential to distinguish

between the isotropy and homogeneity. Isotropy, as defined previously, is a property regarding the stress-strain and strength behaviour at a given point. Whereas a homogeneous body has stress-strain properties whatever they may be are the same at all points. As mentioned above, homogeneity is largely dependent upon scale and it would be possible to describe a finely grained massive rock as homogeneous, whereas a piece of large-grained rock with limited dimensions must be considered heterogeneous.

3-4 Stress:

Stress or intensity of loading is the total force transmitted per unit of area. It is usually estimated by the following general equation:

$$\sigma = \frac{P}{A} \qquad (3\text{-}4)$$

where:

σ : The stress, force per unit area.

P : Total load in units of force

A : The area of the body normal to the direction of the applied load (P) and over which load is distributed, in area units.

There are two main types of stresses:

(a) Direct or normal stress:

1. tensile stress.

2. compressive stress.

(b) Shear stress which exists between two parts of a body in contact, when the two parts exert equal and opposite forces on each other laterally in the direction of a tangent to their surface of contact.

In uniaxial loading (compression or tension), the axial stress is calculated by

$$\sigma = \frac{P}{A} \qquad (3\text{-}5)$$

Whereas in triaxial loading, the normal stress and the shear stress on the plane of failure are calculated by:

$$\sigma_n = \frac{\sigma_1+\sigma_3}{2} + \frac{\sigma_1-\sigma_3}{2} \cos 2\theta \qquad (3\text{-}6)$$

$$\tau_s = \frac{\sigma_1-\sigma_3}{2} \sin 2\theta \qquad (3\text{-}7)$$

where:

σ_n : the normal stress on the plane of fracture

τ_s : the shear stress on the plane of fracture

σ_1 : the major axial stress

σ_3 : the minor horizontal (confining) stress

θ : the angle between the plane of fracture and the minor stress.

3-5 Strain:

When external forces are applied to a body there is a change of shape, and normally volume, and the body is said to be strained. The main types of strain are:

(a) Longitudinal strain, ε, sometimes is called axial strain (tensile or compressive)

$$\varepsilon = \frac{\text{elongation or contraction}}{\text{original length}}$$

(b) Shear strain, γ, which is defined as the angular change in a right angle

$$\gamma = \frac{\text{deflection in direction of shear force}}{\text{distance between shear forces.}}$$

(c) Volumetric strain = $\frac{\text{change of volume}}{\text{original volume}}$.

Strain is a dimensionless ratio, sometimes is given as a percentage of the original dimension, i.e. strain x 10^2. In this research the author deals with the longitudinal strain only which is measured in microstrain, strain x 10^6 or percentage.

3-6 Modulus of Elasticity:

It is also known as Young's Modulus which is the ratio of the stress in a body to the resulting strain produced in the stress direction. Young's modulus is constant for every material within its elastic range, i.e., where Hooke's Law is obeyed.

Rocks in general are not homogeneous, anisotropic materials and the stress-strain curves are not linear. Thus, the modulus of elasticity of rock material is not constant through the whole range of the stress-strain. Therefore, various moduli of elasticity may be given for each rock depending upon the value of stress applied and whether the stress is increasing or decreasing. There are four methods of measuring modulus of elasticity which are useful for comparative purposes, see Fig. (3-1).

3-6.1 Initial Tangent Modulus, E_i:

It is the slope of the tangent to the stress-strain curve at the origin. $E_i = \tan \theta_1$.

3-6.2 Secant Modulus, E_s:

This is the slope of the straight line joining the origin and any chosen point (D) on the stress-strain curve, usually quoted at stress equals 50% of the compressive strength of the rock. $E_s = \tan \theta_2$.

3-6.3 Tangent Modulus, E_t:

It is the slope of the stress-strain curve at specified stress (σ_c). $E_t = \tan \theta_3$.

3-6.4 Chord Modulus, E_c:

This is the slope of the straight line joining any two chosen points on the stress-strain curve. For example, the two points A and B in Fig.(3-1).

$$E_c = \tan \theta_4.$$

In this research the moduli of elasticity of the tested rocks are evaluated by making use of the instantaneous strains and their corresponding stresses, at various confining pressures, applied during the creep tests.

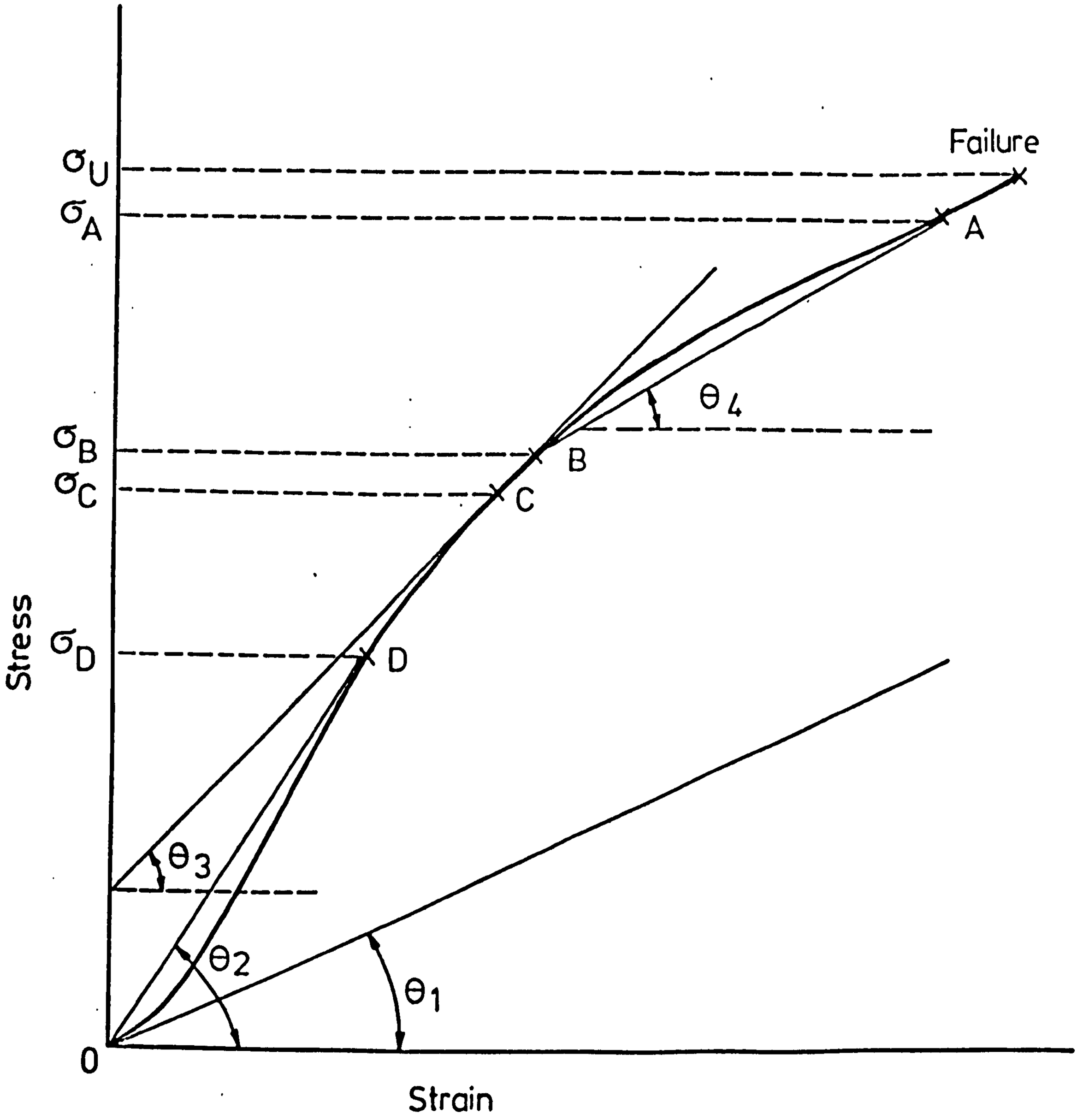

FIG. 3-1 STRESS-STRAIN CURVE OF ROCK.

VARIOUS MODULI OF ELASTICITY

$\tan\theta_1$ = Initial tangent modulus, E_i

$\tan\theta_2$ = Secant modulus, E_s, at point D

$\tan\theta_3$ = Tangent modulus, E_t, at point C

$\tan\theta_4$ = Chord modulus, E_c, between points A and B

Chapter 4

THE EVAPORITE ROCKS

Chapter 4

THE EVAPORITE ROCKS

4-1 General:

The evaporite rocks are non-clastic sedimentary rocks resulting from the evaporation of saline watér. Most evaporites are derived from bodies of sea water. There are two views as to the origin of thick beds of evaporites:

(a) The first suggests formation in a sabkha environment. Sabkha is an Arabic term which refers to the broad, salt-crusted, supra-tidal surfaces or coastal flats bordering lagoonal or inner oceanic shelf regions. An essential feature of the sabkha is that it is only flooded occasionally. Coastal sabkha consists of carbonate sediments. Salt water is drawn into the pores of the sediment and evaporation from the sabkha surface causes concentration of the seawater solution. Seawater also sinks into the sediments during the infrequent flooding of the area. Gypsum is extensively depositied together with some primary anhydrite. Rock salt forms as a superficial crust, most of which is removed by the periodical flooding. However, some is carried down into the sabkha sediments and may ultimately crystallise there.

(b) The second suggests formation by evaporation of isolated seawater. The Dead Sea in Jordan is a well-known example. Evaporites begin to form when seawater is concentrated to about 50%, or slightly less, of its original volume.

The deposits are formed in the reverse order of their solubilities, i.e. the least soluble at the base while the most soluble at the top. A typical evaporite sequence from the top to the bottom is as follows:

(a) Potash and magnesium salts, (sylvite, KCl; carnallite, KCl. $MgCl_2$..$6H_2O$; Kieserite, $MgSO_4$. H_2O; etc).

(b) Rock salt layer.

(c) Gypsum or anhydrite layer.

(d) Dolomitic limestone layer.

Because of the high solubility of layers (a) and (b), it commonly happens that these layers are re-dissolved during the next invasion by the sea. If, however, a layer of impervious sediment is deposited above the evaporite sequence, the highly soluble layers may be preserved. In this way several sequences may be deposited in a rhythmic fashion. Major evaporite fields of considerable economic importance occur at Dead Sea, Jordan; Trucial Coast of Arabia, Abu-Dhabi; Stassfurt, Germany; Cheshire, North Yorkshire and South Durham, U.K.; Arizona, New Mexico and California, U.S.A.; Salzburg, Austria; Chile and elsewhere.

Gypsum and anhydrite were chosen for use in this research. Brief details will be given about each of these in the following sections.

4-2 Gypsum

Gypsum is a chemical compound of 46.5% SO_3, 32.6% CaO, and 20.9% H_2O.

It is known as Hydrous Calcium Sulphate and represented by the chemical formula $CaSO_4.2H_2O$. Gypsum is the most common natural sulphate. It occurs in several forms, each characterized by its own textural identity. The massive, fine-grained, translucent variety is called alabaster; fibrous, silky varieties, often occurring as veins, are known as satin spar; well-formed, crystalline, clear varieties are named sclenite; white, earthy opaque, more massive types are called gypsum rocks. Gypsum is formed by

the evaporation of seawater in shallow inland seas at temperature conditions below 25° C; above this temperature the anhydrous form, anhydrite, is deposited. It is also formed by the decomposition of pyrite (FeS_2) in the presence of calcium carbonate. Gypsum is frequently formed by the hydration of anhydrite in the presence of water under low external pressure (at the maximum average depth of 100 to 150 m). In this alternation of anhydrite to gypsum there is a volume increase of about 30% which involves numerous and complex local disturbances in the mode of occurrence of the gypsiferous strata. The majority of huge gypsum deposits in the world have been formed in this way.

Gypsum has considerable variation in colour, but pinks, reds, yellows and whites are most common. The tints and colours sometimes found in gypsum are due to the presence of iron. Presence of organic matter or disseminated clay gives rise to a pale grey colour.

Gypsum is a soft rock of Mohs hardness equal to 1.5 to 2 (can be scratched by the finger nail) and specific gravity of 2.32. It has a monoclinic crystal system.

Sedimentary gypsum deposits are found all over the world in strata of different geological ages. In commercial deposits, for example, it is found in west and north of Iraq; Yorkshire, Netherfield, etc. in Britain; New York, Arizona, etc. in U.S.A.; Western Urals, Bashkiria, etc. in U.S.S.R.; Germany; Rumania; etc.

Gypsum is used for the production of plaster of Paris, uncalcined (natural) gypsum is used as a retarder in Portland cement. It is, sometimes, used instead of bricks, in the construction of walls and partions in the building industry.

The gypsum which was used in this research is from the British Gypsum Co. mine at Sherburn in Elmet, North Yorkshire, U.K. Its average composition was (91.5%) gypsum, (5.5%) anhydrite, (2.7%) Carbonate and (0.3%) clay. The workings of the mine lie at a depth of about (50) meters below ground surface.

4-3 Anhydrite

Anhydrite is anhydrous calcium sulphate and represented by the chemical symbol $CaSO_4$. Its chemical composition is 41.2% CaO and 58.8% SO_3. Anhydrite occurs in much the same manner as gypsum and is often associated with it but is not nearly so common. It occurs in huge masses in thick sedimentary strata. The hydration of anhydrite is common in nature and reacts according to the following equation:

$$CaSO_4 + 2H_2O \rightleftarrows CaSO_4.2H_2O$$

Anhydrite Water Gypsum

This type of reaction results in a change of volume about 30%. It can be seen that great forces of disruption will consequently be involved in this reaction. It is quite probable that the thick anhydrite strate in gypsiferous regions have derived from the dehydration of original gypsum strata caused by the pressure of the overlying rocks.

Anhydrite is harder and heavier than gypsum, its Mohs hardness (3) to (3.5) and specific gravity (2.8) to (2.9). It is white when pure, often found blue, grey, sometimes tinged red in colour. Anhydrite crystallizes as tabular orthorhombic crystals, which break up into rectangular fragments, owing to the presence of three perfect cleavages.

Anhydrite is used chiefly in the production of binding materials (cements). Dense cryptocrystalline varieties are also

used for ornamental purposes. It is also used as a source of sulphur in manufacture of sulphuric acid.

Anhydrite is found in many areas, such as, West and West North regions of Iraq; Wieliczka in Poland; Billingham in U.K.; Stassfurt, Prussia; Texas, New Mexico in U.S.A.; Gorky regions, Urals in U.S.S.R. and elsewhere.

The anhydrite which was used in this research was from the ICI mine at Billingham, U.K. The average analysis of the rock was (90%) calcium sulphate; (5%) limestone and dolmite; (3%) silica; and (2%) of alumina, ferric oxide and traces of potash and soda. The workings of the anhydrite mine lie at depths varying from 130 meters to 280 meters below OD.

Chapter 5

BRIEF REVIEW OF PREVIOUS PUBLISHED WORK ON CREEP

Chapter 5

BRIEF REVIEW OF PREVIOUS WORK ON CREEP

5-1 Creep of Metals:

It is the field of metals where research on the creep phenomenon has made the most significant progress. For somewhat over 140 years it has been known that metals exhibit creep deformation under load. From the beginning of the 20th century the subject of creep in metals has assumed ever increasing importance due to the enormous industrial progress of man and the consequent vast use of metal. During recent years there has been a rapid rise in the working temperatures of steam boilers, in high speed aircraft, missiles, rockets, nuclear reactors and in other directions where high temperatures are expected. The low (freezing) temperature effect on creep is equally important from the point of view of design of refrigeration equipment and to prove the working ability of materials in Arctic Regions. The present advances of space exploration and interplanetary travel has necessitated the development of very high speed rockets. The abnormally high temperature produced due to frictional resistances in the atmosphere and within the engines render these vehicles susceptible to high rates of metal flow and possible failure.

Hundreds of papers have been published on various aspects of creep in this field. Only some of the investigators work will be summarized here.

Phillips[62] (1905) carried out tensile creep tests on copper, platinum, silver, gold, iron and steel wires. He indicated that the creep follows the logarithm law of the form:

$$x = a + b \log t \qquad (5\text{-}1)$$

where x is the stretch; t is the time; a and b are constants for a particular pull. Andrade[3] (1914) carried out tensile creep tests on several metal wires, such as lead, tin, iron, copper, etc. at various temperatures. He reported that the creep characteristic of all the single metals he studied at a constant temperature follows the equation:

$$L = L_o(1 + \beta t^{1/3}) \text{ exp. } kt \qquad (5\text{-}2)$$

where L is the length of the wire at time t; L_o represents the immediate length on loading; t is the time after loading; β and k are constants. On various steel bars Dickenson[17] (1922) carried out two series of tensile creep tests:

(a) Specimens being subjected to constant load and constant temperature.

(b) Specimens being subjected to constant load and uniformly rising temperature.

He plotted several curves of temperature of specimen versus time required to produce a certain extension or rupture. He did not introduce any equation but he reported that up to temperature 400°C all the steel, he tested, extended alike. He also indicated that as the temperature increases the time required for a specimen to extend to a certain value under a constant load decreases. Weaver[88] (1937) carried out creep tests on steel at constant stress and temperature. His long-time creep tests extended over various periods of time from 1000 hr to 5 years. He reported that the creep rate for steels at constant stress and elevated temperature at any time equals to the sum of (a) the strain hardening (plastic action) rate which varies inversely

with time and (b) an asymptotic constant creep rate (viscous - flow rate).

The fact that any equation designed to fit a creep curve cannot apply over the whole experimental range is illustrated by the behaviour of many metals at low temperature. Wyatt[95] (1953) tested polycrystalline copper over the range 77-443°K and found that at the lower temperatures a logarithmic relationship held, but at higher temperature the strain is greater at a given time than predicted by the logarithmic equation. He proposed the following equation:

$$\varepsilon = A \log t + Bt^n + Ct \qquad (5\text{-}3)$$

where ε is the creep strain; t is the time; A, B and C are constants and $n \simeq \frac{1}{3}$.

Further information and details of creep in metals is contained in work and papers by, Kennedy[44], Honeycombe[38], Nadia[53] Penny and Marriott[60], Conway[13] and others.

5-2 Creep of Non-Metallic Brittle Solids

5-2.1 Creep of Mineral Materials:

Creep of mineral materials has been dealt with in detail by Murrell and Misra[51]. A brief account of some of the important observations of creep in various artificial mineral materials namely concrete and cement mortar, ceramics and glass will now be outlined.

5-2.1.1 Creep of Concrete and Cement Mortar:

Since the time when concrete has been used in structural members, the significance of the creep properties of plain, reinforced and prestressed concrete members has been investigated. In 1934 Davis[16] and others were among the first who carried

out creep tests on plain concrete cylinders. Ross[74] (1937) suggested the following equation should be used for creep in concrete:

$$C = \frac{t}{A+Bt} \qquad (5-4)$$

where C is the creep strain in deflection; t is the time after loading; A and B are constants. Equation (5-4) may be expressed in the form $\frac{t}{C} = A + Bt$ which represents a straight line equation of $\frac{t}{C}$ versus t, which, if plotted, has a slope of B and an intercept on the $\frac{t}{C}$ axis of A. He indicated that several factors affect the creep in concrete among which are: stress, water-cement ratio, humidity, age of concrete at time of loading, size of specimen, class of cement, mineral character of the aggregate, aggregate-cement ratio, temperature, etc. Washa[85] (1947) carried out creep tests on reinforced concrete thin slabs which were subjected to sustained loads for 5 years. He indicated that the importance of the plastic flow problem in thin reinforced concrete slabs is forcibly emphasized by large increase in deflections and strains that were obtained over a 5 year period. He observed that the plastic deformation increased rapidly as the ratio of span length to depth of slab (L/D) increased, so he suggested that design specifications should provide proper restrictions regarding the maximum value of this ratio. Later on Washa and Fluck[86,87] (1952-1956) investigated the effect of compression reinforcement on the plastic flow of both simple and continuous ordinary concrete beams. They found that such reinforcement had a significant effect on the creep deflection and compressive strain of the beams. It was also shown that the creep deflection at 2.5 years in test beams of span/depth ratio (L/D) of 70 was 4 to 6 times that of beams with L/D ratio of 20. Ross[75] (1958)

made observations on elasticity, creep and shrinkage of concrete. He indicated that two equations can be used to represent the creep in concrete, the first is the Kelvin-Voigt equation (see equation 2-14 of section 2-3.5), the second is the following

$$\varepsilon = \varepsilon_c + \sigma \left(\frac{t}{A+Bt}\right) \qquad (5\text{-}5)$$

where A and B are constants. He indicated that creep strain due to a constant sustained stress on concrete at diminishing rate for several years may amount to several times the initial elestic strain. He said that it is the loss of interstitial water by evaporation which causes shrinkage and movement of interstitial water under stress causes at least some of the creep. Neville[54] (1959) has shown that creep in concrete is not associated with any loss of water from mortar but is probably related to its internal movement. He speculates that it might be voids in the cement paste which are responsible both for its strength and high creep. Ibrahim[40] in (1972) fitted creep data obtained from his experiments on early strength light-weight aggregate (solite) concrete in the equation (5-4) which was suggested by Ross. Ibrahim carried out bending creep tests on concrete beams subjected to four-point dead load for various periods of time up to 400 days.

Williams[89] (1973) carried out uniaxial creep tests on cylindrical concrete specimens 300 mm long by 150 mm diameter of two different mixes. The specimens were loaded uniaxially by means of compressed gas/hydraulic creep rigs designed and constructed at Sheffield University. The longitudinal deformation of the specimens was measured by four Demec gauges of 20 mm nominal length. He indicated that the data obtained fitted the

following equation which was suggested by Jones (U.S. Bureau of Reclamation, Engineering Monograph No.29, 1961).

$$\frac{1}{E_c} = \frac{1}{E'} + f(K)\log_e (t+1) \qquad (5\text{-}6)$$

where

$\frac{1}{E_c}$ = Unit strain of concrete per unit stress.

$\frac{1}{E'}$ = Instantaneous unit strain per unit stress.

K = Age of concrete at the time of application of load, day.

t = Loading duration, day.

All the experiments were carried out at room temperature.

Glucklich and Amar[29] (1972) carried out creep experiments on mortar specimens. They studied the volumetric creep of specimens subjected to triaxial compression. Three types of aggreage were used. Each specimen was 150 mm high by 75 mm diameter and contained a specially designed dilatometer that was embedded during casting. This was used as an internal volume change measuring device. The displacement of pressurized liquid within which the specimen was to be immersed indicated the external volume change. They indicated that, from the data obtained, the dilatometer measurements are fairly useless. They reported that the instantaneous bulk modulus was found to be independent of the load. They also indicated that all instantaneous strains were recoverable, whereas the time-strain was almost entirely non-recoverable.

5-2.1.2 Creep of Ceramics and Refractories:

In ceramic and refractories appreciable creep occurs only at elevated temperatures, in general it does not seem to occur

at temperatures below about 1000° C.

Stravrolakis and Norton[80] (1950) carried out torsion creep tests on alumina and zirconia at temperatures up to 1500° C. They indicated that alumina can be safely used above 1500° C with no fear of complete slumping and consequent loss of shape; however, creep will take place at 1300° C and above. Zirconia must be used with caution, however, above 1200° C for, although it does not fail readily, it deforms easily under conditions of load. The twist strain was measured by spherical sapphire mirrors cemented to the specimen at the ends of the gauge length in order to focus the light from lamps on a special calibrated screen. The difference in level of the images produced is proportional to the twist. Wygant[96] (1951) observed transient (primary) creep of dense pure magnesia at temperatures less than 1100° C above of which steady- state (secondary) creep was observed. At 1300° C and 2400 psi, a tertiary or accelerating creep leading to fracture occurred in cast magnesia. Two equations for creep rate were derived which are:

(a) For cast magnesia:

$$\log \gamma' = 2.5 \log \tau_{max} - \frac{23380}{T} - 3.16 \qquad (5\text{-}7)$$

(b) For hydrostatically pressed magnesia:

$$\log \gamma' = 3.5 \log \tau_{max} - \frac{23200}{T} - 0.80 \qquad (5\text{-}8)$$

where γ' = strain rate

τ_{max} = shear stress at the surface of the specimen in torsion

T = temperature

Torsion creep tests were carried out on all specimens and the concave sapphire mirrors technique was used in measuring the twist. Folweirler[24] (1961) carried out bending creep tests on

0.1 x 0.15 x 2 inches of pore-free polycrystalline aluminium oxide beams using the three-point loading system at temperatures between 1400° C and 1800° C. He indicated that the creep rate follows the following equation:

$$\varepsilon' = \frac{10\sigma D\Omega_o}{KTR^2} \qquad (5\text{-}9)$$

where ε' is the strain rate; σ, stress; D, diffusion coefficient; Ω_o, atomic volume of oxygen; K, Boltzmans constant; T, absolute temperature; and R, grain radius. Passmore and others[58] (1966) investigated the creep properties of dense polycrystalline Magnesium oxide (MgO) in bending using four-point dead load system at temperatures between 1380° and 1800° K. The deflection of the beam specimen was measured by LVDT. Stresses of 1000 to 5000 psi were used in this investigation. The effect of temperature, stress and grain size on the creep rate was studied and they introduced an equation similar to Eq.(5-9) with replacement of the number 10 before $\sigma D\Omega_o$ by 20.

Terwilliger and others[81] (1970) carried out bending creep tests on Polycrystalline MgO and MgO-Fe_2O_3. The specimens were tested in four-point dead-load experiments which were conducted at temperatures between 1000° and 1400° C and at stresses between 50 and 550 Kg/cm^2. Each specimen had a rectangular cross-section of 3.80 mm long by 1.90 mm wide. Steady-state (secondary) creep was never achieved in this investigation. The authors indicated that the creep rate decreased continuously with time as described by

$$\varepsilon' = \frac{C_1}{(t+C_2)^P} \qquad (5\text{-}10)$$

where C_1, C_2 and P, although they can be calculated empirically,

have a physical basis in a theory which is based on viscous creep and simultaneous grain growth.

5-2.1.3 Creep of Glass:

Glass behaves as an elastic solid or as viscous material according to the temperature and time scale of observations. Transient creep is observed in glasses at room temperature.

Phillips[62] (1905) carried out tensile creep tests on glass fibres. He reported that the creep stretch can be represented by the equation:

$$x = a + b \log t \qquad (5\text{-}11)$$

where x is the stretch; t is the time; a and b are constants.

Griggs[27] (1939) observed creep in glass specimens subjected to uniaxial compression at temperatures from 160° to 260°C. He reported that the deformation of the glass followed the logarithm equation of the form:

$$S = A + B \log t + Ct \qquad (5\text{-}12)$$

where S is the deformation; t is the time and A,B, and C are constants.

From the above equation it can be seen that Griggs observed both the primary and the secondary stages of creep.

Murgatroyd and Sykes[52] (1947) studied extensively the delayed elastic effect in three silicate glasses, namely, vitrous silica, sheet glass and Wembley (X-8) glass which are widely different in their chemical composition. They carried out torsion tests on glass rods at room temperature. They came to a conclusion that the strain-time relationship at room temperature in these glasses shows that they consist of an elastic framework containing inclusions of materials having a wide range of viscosities. They insisted that the continuous framework is demanded

by the experimental results because the glasses continually return to the original shape after deflection without the assistance of external forces. In bending creep tests on the same materials they reported that the delayed strain had a considerable effect on the breaking strength of each of the glasses tested.

5-2.2 Creep of Rocks:

Although there is a general lack of data on the creep of rocks, it is not the aim of this thesis to give full details of all the published works on this subject. In the following pages a brief review of some of the investigations in this field, particularly on creep of rocks under triaxial compression, will be given.

Michelson[48] (1917-1920) carried out torsion creep tests on many materials including limestone, marble, calcite etc. He suggested an empirical formula for the torsional strain at room temperature of the form:

$$S = A + B\,(1 - \exp(-\alpha t^{\frac{1}{2}})) + Ct^{n} \qquad (5\text{-}13)$$

where S = twist strain; A,B,α, C and n are arbitrary constants, and t = time in minutes. It was found that the average value of n for fifteen substances to be 0.35. The term A in equation (5-13) being the elastic deformation is recoverable.

The term "$B(1 - \exp(-\alpha t^{\frac{1}{2}}))$" has been called "elastic-viscous displacement" by Michelson which he found to be recoverable with time. He called the term "Ct^{n}" the "viscous displacement". This is not recoverable.

Phillips[61] (1932-1948) carried out bending creep tests on shale and uniaxial compression creep tests on siltstone. He observed the longitudinal and lateral creep strain in the

compression tests. He indicated that the lateral creep strain is greater than the longitudinal, and also he mentioned that wet specimens under identical conditions exhibit more creep than dry rock specimens. He, however, did not make a detailed study of the creep behaviour of rocks and did not attempt to derive a creep equation.

Griggs[26,27,28] (1936,1939,1940) conducted, for the first time, a systematic study of time-dependent deformation in geologic materials. He made a detailed study of the effects of various parameters on the creep of rocks, namely effect of stress, temperature, confining pressure, structure of the material and presence of various solutions. He used Solenhofen limestone, shale, talc, glass, alabaster and single crystals of calcite and halite in his compression loaded creep tests. His work has, in fact, laid the foundation of the ideas of the creep behaviour of rocks. He found that the creep of rocks is affected by the parameters mentioned previously. He suggested the following equations to represent his results:

(a) For creep under load:

$$S = A + B \log t + Ct \qquad (5\text{-}14)$$

(b) For recovery on unloading:

$$S = A' + B \log t \qquad (5\text{-}15)$$

where S is the total deformation; t is the time; A,A', B and C are constants, depending on the test conditions and material under investigation. Griggs called the term "B logt" in Eq.(5-14) the "elastic flow". It represents the primary creep, see section (2-2.2), and is recoverable with time. The strain represented by the term "Ct" was called by Griggs the "pseudo-viscous flow" which is not recoverable, and represents the secondary stage of

creep, see section (2-2.3). He mentioned that the foregoing equations do not describe the relation adequately for short-time intervals, since the logarithmic term approaches minus infinity as the time approaches zero. Similarly, the logarithmic term approaches infinity as time approaches infinity. He used Jeffreys[41] method in calculating the equivalent viscosity of solids for the pseudo-viscous flow and suggested the following equation:

$$\eta = \frac{P}{3S'} \tag{5-16}$$

where η is the equivalent viscosity; P the compressive stress and S' is the constant rate of strain with respect to time.

Griggs[27,28] observed secondary creep in boric anhydrite glass at 243° C and found that the creep curve follows equation (5-14). He also carried out uniaxial creep tests on dry alabaster specimens for 6 days after which they were surrounded by distilled water, while the load was maintained constant. Griggs reported that the creep rate immediately increases very greatly. He also observed secondary creep in Solenhofen limestone subjected to 10,000 atmospheres confining pressure and found a level of differential stress at which steady-state creep occurred.

It can be seen from Griggs experiments that secondary creep only took place when he heated the material (boric anhydrite glass), surrounded the specimen with water (alabaster), or subjected the samples to high confining pressure as in the case of Solenhofen limestone. It seems to suggest that rocks in brittle condition, i.e. at room temperature and atmospheric pressure, will generally fracture before creep has proceeded far. The

confining pressure raises the differential stress at which failure occurs, in other words the ability to deform permanently before failure increases with increasing confining pressure. This is supported by the results of Handin and Hager[30] and others who studied the effect of confining pressure on strength and ductility of sedimentary rocks, and is also confirmed by the triaxial test results of this research, see chapters (6) and (9).

Evans and Wood[22] (1937) carried out compression creep tests on granite, marble and slate. They observed both longitudinal and transverse creep. They reported that the creep rate in both directions depends upon stress. They also indicated that the transverse creep rate increased more rapidly with stress than the axial creep rate, particularly in the case of laminated rocks stressed parallel to the planes of lamination. They also observed creep in sandstone and concrete subjected to torsion.

Lomnitz[46] (1956) conducted torsion creep and recovery tests on granodiorite and gabbro specimens at room temperature and atmospheric pressure. He suggested an empirical equation to fit his results:

$$\varepsilon = \frac{\sigma}{\mu} \left[1 + q \ln (1+at)\right] \qquad (5\text{-}17)$$

where ε is the total shear strain in radians; σ is the constant shear stress; μ is the rigidity modulus; t is the time in seconds and q and a are constants. Lomnitz observed transient creep and recovery in all the experiments except in one case of creep of granodiorite where he observed secondary and tertiary creep leading to fracture along helical surfaces characteristic of fracture of brittle materials in torsion. He mentioned that his equation is valid for only small constant torque not greater than (0.05% μ).

Denkhas[18] (1958) investigating the problems of rock bursts in deep mining in the Witwatersrand Goldfields in South Africa reported that the loads thrown on to abutments result in elastic and/or plastic deformation of the rock with time. Rock bursts, whether they are extradosal or intradosal (in fracture zone), are influenced by creep and elastic after effects of the rock. He thinks that elastic creep deformation is more responsible for rock bursts than plastic creep deformation, because the latter deformation may cause gradual release of abutment stress concentrations and hence diminish the danger of rock bursts. The mines of Central Witwatersrand where the majority of severe rock bursts occur are in hard brittle quartizite. Rock-bursts are, however, almost unknown on the far East Rand where the foot-wall of the reef consists of plastic deformable shale. The favourable influence of the plastic deformability on the susceptibility to rock bursts he thinks, is due to dissipation of part of the elastic strain energy stored by means of local internal flow.

Kendall[43] (1958) studied the creep behaviour of Solenhofen limestone, rock-salt and cement mortar under uniaxial and triaxial compression. The maximum confining pressures that Kendall used were: 15000 psi for Solenhofen limestone, 1000 psi for cement mortar and 2000 psi for rock-salt. He reported that the logarithmic creep equation of the form:

$$\varepsilon = A + B \log t + Ct^n \qquad (5\text{-}18)$$

fitted his data closely. He also indicated that the modulus of elasticity for the limestone and cement remains essentially constant and independent of both the confining pressure and the

history of the stress-strain application, where the rate of loading was held constant. He observed only transient creep in the specimens when they were loaded below their fundamental strength, whereas for specimens loaded at stresses greater than that, the transient creep again was observed, followed by rapidly increasing deformation until complete failure occurred.

Robertson[72] (1960) carried out triaxial creep tests on Solenhofen limestone, Danby marble, Rutland White marble and calcite. The cylindrical specimens were jacketed with rubber tubing and surrounded by kerosene. The axial load was increased by increments during the creep tests. After an increase of loading, which takes about 10 seconds, a creep test of 1000 to 10000 seconds duration was performed; at the end of the creep test, kerosene was bled off to maintain a nearly constant confining pressure. All tests were made at room temperature. The confining pressures were from 290 to 4150 bars under differential stresses of 1400 to 8400 bars. Robertson observed only transient creep and suggested the following two equations to fit his data.

$$\varepsilon' = K\, t^{-1} \tag{5-19}$$

$$t\,\varepsilon' = K_1 \sigma_D - K_2 \tag{5-20}$$

where ε' is the creep rate; t is the time in seconds; σ_D is the differential stress in bars and K, K_1 and K_2 are constants. He indicated that an increase of confining pressure from 1000 to 2000 bars causes a 100-fold decrease in transient creep rate per unit stress difference in Solenhofen limestone.

Misra[49] (1962) studied the creep property in various rocks under uniaxial compression, torsion and simple bending modes of loading. He studied the effect of stress, temperature and solutions on the creep behaviour of rocks. He reported that the

creep strain increases as the temperature or/and the stress increases. He tried to fit his results in both logarithmic and power equations of creep of the forms:

$$\varepsilon = A + \log t + Ct \qquad (5\text{-}21)$$

$$\varepsilon = A + Bt^n \qquad (5\text{-}22)$$

The temperature range he was confined to was 300°-700° C which was far below the melting points of the rocks. He reported that the presence of solutions increases the creep rate in bending tests and also lowers the strength of the rocks. He proposed the following relationship between creep rate and the applied stress:

$$\varepsilon' = B\sigma^n \qquad (5\text{-}23)$$

where ε' is the creep rate, σ is the applied stress and B and n are constants.

Heard[33] (1963) studied the effect of temperature, stress, confining pressure and the orientation of specimens with respect to foliation on the creep behaviour of Yule marble subjected to triaxial extension. He used 0.35 inch diameter by 0.70 inch high specimens jacketed by copper tubes. He developed a creep apparatus for constant strain-rate tests up to 5 kb confining pressure and 500°C at strain rates from 0.4 to 3 x 10^{-8} per second. He reported that most of the Yule marble specimens (oriented parallel, at 45° and normal to the foliation) were extended 10 percent at temperatures from 25° to 500° C, at 5kb confining pressure. He mentioned that at 25° C only a slight decrease in strength occurred with decreasing strain rate, whereas at 500° C strengths at 10 percent strain were decreased 80 percent from the fastest (0.25 second duration) to the slowest (35 days) tests. He also observed that strong strain hardening, characteristic in tests

at the lower temperatures and higher strain rates, changes gradually to steady state flow as strain rates are decreased or temperatures increased. He tried to fit his results into an equation proposed by Eyring for steady state flow based on a diffusion mechanism to explain creep behaviour in metals at high temperatures. In this the activation energies for creep are equal to those for self-diffusion, which produces a relationship of the form:

$$\varepsilon' = A \exp\left(-\frac{E}{RT}\right) \times \sinh\left(\frac{\sigma}{B}\right) \qquad (5\text{-}24)$$

where ε' is the strain rate, σ is the differential stress applied to the specimen, E is the empirically measured activation energy for self diffusion, R is the gas constant, T is the absolute temperature and A and B are constants. Heard found different values for A, E and B for different orientations to foliation, namely normal, parallel and at 45^{o}. Heard indicated that extrapolation on the basis of the above equation and his results can be performed to determine the strength of the Yule marble subjected to a geologic strain rate of 3×10^{-14} per second.

Potts[66] (1964) carried out an intensive investigation on the rock salt of Meadowbank Mine at Winsford, Cheshire, U.K. both in the laboratory and underground in the mine itself. His underground investigation and the laboratory study of the physical properties of the rock salt was an attempt to predict the rock behaviour in the mine pillars and workings for a long time after their initial formation and as a guide for mine design not only for rock salt mines but for other materials. In the laboratory he studied the effect of specimen size, width/height (W/D) ratio and the shape of the specimen on the uniaxial compressive strength

of the rock salt. He also studied the creep behaviour of the material for short and long laboratory periods under uniaxial and simple bending modes of loading. He reported that as W/D ratio increases the compressive strength of rock salt increases rapidly, and for a given cross-sectional area as the parameter/ area ratio increases the strength decreases. He also observed the bending creep rate increased rapidly as the humidity increased. In his underground investigation he extensively used the bore-hole extensometers and hydraulic stressmeters. Detailed inform-ation of the extensometer, hydraulic stressmeter, hydraulic modulus meter, bolt load cell, etc. for underground measurements and techniques is given by Potts[64,65a,65b,67]. He measured the stress and both the lateral and vertical strain in some pillars during and after their formation. In consideration of both the laboratory and underground measurements he presented two methods for use in mine design. The first is the time-safe strength concept which indicates that a given pillar will support a given load indefinitely. He gave a graphical method to deter-mine the time-safe strength. The second concept is the time-safe strain method which suggests that a pillar will support a given load for a defined period of time. In both suggested methods the laboratory creep results of rock salt specimens were used as essential parameters.

Price[69] (1964) carried out bending creep tests on beams of Pennant and Wolstanton sandstones in a simple apparatus. He reported that there was a linear relationship between the rate of creep strain in the secondary stage of creep and the applied stress. He plotted this linear relationship for each type of

the rock tested and determined graphically their long term strengths, these being defined as the value of stress at which the secondary creep rate is zero, i.e. when the straight line of the stress versus the secondary creep rate intersects the stress axis. He also reported that the creep behaviour in bending of the mentioned sandstones in a good agreement with the behaviour of the B-V rheological model, see section (2-3.9). He found that the long term strengths of Pennant sandstone and Wolstanton sandstone were 20 and 60 per cent of their instantaneout strengths, respectively.

Comte[11] (1965) carried out triaxial creep tests on artificial rock salt specimens of 1.25 inch long by 0.5 in diameter. He studied the effect of temperature (from room temperature up to 300°C), confining pressure up to 1000 bar and the grain size in the range 0.10 to 0.15 mm for all specimens (except for two specimens where the sizes were 0.55 and 0.63 mm) on the creep behaviour of the rock salt. He reported that the creep law which best fitted his data was a power equation of the form:

$$\varepsilon = A + Bt^n \qquad (5\text{-}25)$$

where ε is the deformation, t is the time in minutes and A, B and n are constant with n a positive number less than one. He indicated that an increase in temperature and/or increase in differential stress increases the creep rate, whereas on the other hand an increase in grain size or increase in confining pressure particularly at elevated temperature decreases the creep rate somewhat. He determined the activation energy for creep in rock salt at atmospheric pressure and at temperatures ranging from 29° to 300° C. He found that this increases with temperature from

12500 cal/mol at 29° C to 30000 cal/mol at 300° C.

Hedley[34] (1965) studied the deformation and failure properties of rock salt and potash. He carried out short term and creep tests under uniaxial compression of both rocks. Triaxial creep tests were carried out on potash only. He used various width/height ratios in the experiments. He presented the results in the form of time-safe stress and time-safe strain, see Potts[66]. He reported that the creep rate of rock salt and potash did not decrease to zero even in a long term creep test. For this reason he stated that the time-safe stress concept is not applicable in this case and suggested the time-safe strain method be used in mines extracting potash. He indicated that a power equation of the form:

$$\varepsilon_1 = A\, t^n \qquad (5\text{-}26)$$

gave the best agreement with his results for the primary creep stage, whereas the secondary creep curve followed the equation:

$$\varepsilon_2 = Ct + B \qquad (5\text{-}27)$$

where ε_1 and ε_2 are the creep strain in the primary and secondary stages, respectively, A and n are constants, C is the constant strain rate, B is the intercept on creep strain axis and t is the time. He indicated that the constant creep rate C can be found by using the following power equation:

$$C = \alpha\sigma^{\beta} \qquad (5\text{-}28)$$

where σ is the applied stress, and α and β are constants.

Buzdar[10] (1968) studied the creep phenomenon in some sedimentary rocks with special reference to potash. Most of his work in the field of creep was on uniaxial compression, only one potash specimen was tested, for creep study, under 4500 psi confining pressure and a differential stresses of 4200 to 6300 psi.

He used various height/width ratios. He reported that an increase in confining pressure decreases the creep rate whereas an increase in height/width ratio increases the creep rate. He has not tried to fit his data in any creep equation or suggested any function. He was mainly concerned with the qualitative analysis of creep behaviour of laboratory specimens obtained from potash borehole cores. He tried to explore the possibility of using the laboratory creep study of evaporite specimens as an equivalent material in laboratory investigations, before any mine development was started. All the short term and creep experiments were carried out at a constant temperature of 92°F with a relative humidity of 50-52%.

Patchet[59] (1970) conducted several short term and creep tests both in laboratory and in situ on evaporite rocks under uniaxial and triaxial compression modes of loading. For the uniaxial creep tests he used a hydraulic rig and several spring rigs, described by Hedley[34], whereas for triaxial creep tests he used a triaxial cell designed by Buzdar[10];some of his conclusions on the creep behaviour of rocks tested are summarized here:

1. For each diameter/height ratio there is a critical stress above which the rock creeps vary rapidly to failure and below which the rock creeps much more slowly and no failure is expected whatever the period of loading.
2. The creep rate of a specimen is dependent on the differential stress applied to the specimen and is independent of the magnitude of either the axial or lateral stresses.

3. The secondary creep rate of small specimens is highly influenced by changes in humidity.
4. Laboratory and 'in situ' creep behaviour of Cheshire rock salt can be correlated, provided that the triaxial creep behaviour of the material is taken into account.
5. The stress on a pillar cannot exceed a critical value for the material which is dependent on the triaxial creep behaviour of the material.
6. The triaxial behaviour of the rock material is the most important factor in determining the behaviour of pillars both in compression and in time.

Hofer and Knoll[37] (1971) studied the creep behaviour of carnallite subjected to uniaxial compression and tried to extrapolate their results and conclusions to practical application in mines. They also tried to derive the creep equations from the latest findings of solid-state physics on deformation behaviour of polycrystalline materials. They said that treatment of creep deformation in this way is more useful and is an improvement on the use of rheological models. From the large number of specimens tested they came to the following conclusions:

(a) For low stress and temperature, the creep data follows the logarithmic law.
(b) For higher stress and temperature, the creep processes take place according to a power law.
(c) For very high stress, which approaches the ultimate stress of the material, the creep deformation according to the power law quickly increases.

They carried out several creep tests on various ratios of specimen height to specimen diameter under different stress levels. They determined the stresses at which the transition from the logarithmic creep equation to the power function has taken place. They plotted a curve for the above stresses versus the slenderness ratio (height/diameter) which represents a boundary curve below which only logarithmic creep without fracture and above which creep according to power law with creep fracture takes place after a more or less longer period of time. They considered this curve as a true boundary curve of the limiting creep stress.

King[45] (1973) carried out creep experiments in model pillars of Saskatchewan potash in an attempt to predict the creep behaviour of the pillars in the mine. He used two different diameter to height ratios of pillar model specimens namely 4 and 8. He used a nitrogen/hydraulic pressure system to apply the uniaxial load to the specimens in a controlled temperature chamber which maintained a constant temperature in the range 80^{o} to $140^{o}F$. He mentioned that the creep strain followed the simple power law of the form:

$$\varepsilon = At^{n} \qquad (5\text{-}29)$$

where ε is the vertical strain, t is the time in hours and A and n are constants with $0 < n < 1$. He compared his results with data obtained by another investigator working on a creep of pillars in the same mine and reported that the creep tests on model pillars can yield information of practical application to the design of pillars underground. In particular, the influence on creep behaviour of the increase in temperature associated with mining at greater depths can be studied by this means with some confidence.

Afrouz and Harvey[2] (1974) carried out creep tests on various rocks both in the Laboratory and in-situ. The Laboratory tests were conducted at room temperature and atmospheric pressure, on dry and saturated rocks exhibiting uniaxial compressive strengths within the soft to medium strength range, whereas the in-situ measurements of creep deformation were carried out on the underclay along the floor of a mine roadway (Britannia Colliery, S.Wales). They chose several empirical creep equations and analysed them on the light of their laboratory data by using a computer program. They reported that close similarity was achieved between laboratory and in-situ time-dependent behaviour, enhancing the possibility of predicting, within reason, the in-situ creep of the rocks used. They also indicated that the air-dried soft to medium strength rocks behave in an elasto-plastic manner, i.e. very close to the Burger's Model, see section (2-3.8) equation (2-17), whereas the saturated soft rocks generally followed the equation:

$$\varepsilon = A + Bt^{c} + Dt^{e} \qquad (5\text{-}30)$$

They found that introduction of water to air-dried coal and underclay increases their overall creep rates three and eight-fold, respectively. On the other hand, the presence of clay bands in the saturated underclay further increased the creep five fold.

In a paper published in (1975) Singh[79] mentioned that in his creep work on Sicilian marble specimens subjected to uniaxial compression, both the axial and the lateral creep curves exhibited the three stages of the general creep curve. He carried out the creep tests by using a gas/hydraulic system and a loading frame at 76°F room temperature. He reported that the steady

state creep rate increased with the increase of stress. He also mentioned that the creep rate in the lateral direction was found far greater than in the axial direction. He fitted his data in a power law of creep of the form:

$$\varepsilon = a\, t^{b} \qquad (5\text{-}31)$$

where ε is the strain, t is the time in minutes and a and b are constants. He indicated that the mode of fracture of most specimens in the creep rig was similar to the mode observed during the uniaxial short term compression tests.

Williams and Elizzi[91,92] (1975-1976) published reports on creep of gypsum under triaxial compression loading. They used the same apparatus described in this thesis, chapter 8, and indicated that the creep behaviour of gypsum under triaxial compression in most cases followed the power law mentioned in equation (5-31).

Chapter 6

BENDING, UNIAXIAL AND TRIAXIAL COMPRESSION TESTS

Chapter 6

BENDING, UNIAXIAL AND TRIAXIAL COMPRESSION TESTS

In order to provide a base from which to decide the loading stresses to be used in the creep tests it was necessary to determine the strength of the materials to be studied under conditions of short term loading, refered to as instantaneous strengths. It was also necessary to perform these tests in a manner such that the stresses applied were in all ways similar to the stress application used in the creep tests. Short term tests in bending, uniaxial and triaxial compressive modes were therefore performed.

In this chapter a brief discussion of each test will be given including apparatus, size and preparation of specimen, test procedure and measurements of stresses and strains.

6-1 Bending Test

6-1.1 Introduction

For mining and civil engineers, the tensile strength of rock is one of its most fundamental properties. Most of the difficulties of uniaxial tension test in rock materials are in the preparation of specimens, in gripping them and in preventing eccentricity in loading. The bending test is one of the indirect tests which have been used in finding the tensile strength of the rock. The main advantages of the bending test are that the test itself is very simple compared to other indirect tests, and in the four point loading of a beam a state of pure tension is set up in the material in the zone where failure takes place.

Moreover, knowledge of the behaviour of rock in bending is of considerable practical importance, because the failure of

strata in mines and excavations often takes place under conditions of bending.

6-1.2 Apparatus:

In order to achieve pure bending moments in the specimen tested, the apparatus Fig.(6-1) was designed to apply four-point loading. The specimen beam is supported at two bottom knife-edges (K_3) and (K_4) 200 mm apart and loaded at two top knife-edges (K_1) and (K_2) 100 mm apart. The top and bottom knife edges are symmetrically interposed about the centre of the beam. The load was applied through a steel ball (c) placed in a hemispherical recess at the centre of component (E) whose underside knife edge (K_5) lies exactly at the centre of the upper steel bar (A).

A 0.002 mm dial gauge (D) was clamped to the lower steel bar (B) to measure the deflection at the centre of the specimen.

A 10 ton Clockhouse Loading Machine was used for applying the load. The machine is motor operated gear-driven and has two ranges of 1000 lbs and 20000 lbs. The rate of loading can be varied by choice of the gears.

Load applied (for the range of 1000 lb) was measured by a proving ring which has 0.002 mm dial gauge, the sensitivity of which is 2.882 N (0.648 lb) per division. The four-point loading system used has the following important advantages:

1. This type of loading creates a zone of zero shearing forces between the loading points, K_1 and K_2, which gives maximum pure uniform bending moment in the zone, see Fig.(6-2).

2. The positioning of the knife-edges gives complete stability within the apparatus during testing.

3. A bending arm of 100 mm between the two points of loading, K_1 and K_2, is provided to measure the deflection at its centre, and the locality of fracture is likely to be situated away from the points of application of load.

6-1.3 Specimen Size and Preparation:

Rectangular 140 mm long by 40 mm wide by 6 mm thick beams of gypsum supported on knife edges 100 mm apart were first tried. It was found that this thickness was not suitable because there were crystals in the gypsum whose diameters were larger than the thickness of the beam, therefore some of these crystals extended from top to bottom of the specimen, so producing a weak section across the beam at which failure occurred below the normal strength of the material. On the other hand, during the preparation of the specimen, namely cutting and grinding, it was found that surface hardening occurred at the faces of the specimen, see Datta[15], therefore, the thinner the beam the greater the effect of this phenomenon on indicated strength.

Other sizes namely 240 mm by 40 mm by 12 mm and 240 mm by 40 mm by 20 mm were found more suitable for the test. Most of the experiments in this research were carried out on 240 mm by 40 mm by 20 mm, nominal size, specimens for both gypsum and anhydrite.

The beams were cut from blocks of rock by diamond cutting equipment to the nominal size approximately, the faces of the beam were treated by grinding machines to bring them true (up to 0.01 mm difference in width and thickness along the beam), then the actual dimensions were measured by micrometer to the nearest 0.01 mm. Cutting and grinding the beams involve wetting of the rock with water. The beams were then left for 15 days to be air

dried, oven drying not being recommended in the case of gypsum due to the possibility that some of the material may be changed into anhydrite due to the loss of water of hydration.

Most of the beams were cut parallel to the bedding, i.e. the line of applying the load during the test is perpendicular to the bedding [type (1) figure (6-3)]. A few beams of types (2) and (3) were tested for comparison. Williams and Elizzi[90] used gypsum type (2) in their creep investigation.

6-1.4 Test Procedure:

In order to determine the instantaneous strength of the rock in bending it was necessary to find the strains at the lower and the upper surfaces of the beam besides the deflection and the applied bending moment, the reason for this will be discussed later. Two electrical resistance strain gauges were bonded at the centre of each the upper and the lower surfaces of the beam (using the same procedure as will be described in section 7-2.1.2 later) to measure the strains at the centre of the outer fibres of the beam. Then the beam was placed in the test apparatus and the load was applied gradually from the Clockhouse loading machine up to failure of the specimen. The ultimate load and the strain at the lower and the upper surfaces of the beam were recorded.

6-1.5 Stress Measurement:

Using the four-point system of loading in the bending test produces a complex concentration of stress near the knife edges. Fortunately, such stress concentrations remain limited to a distance, from the inside knife edges (K_1) and (K_2) toward the centre of the beam, of less than one-half the thickness of the beam[21]. Therefore, a length of about 80 mm between the inside knife edges is available for strain measurements.

The general equation for finding the maximum tensile stress from bending test, which is

$$\sigma_t = \frac{M}{Z} \qquad (6\text{-}1)$$

depends upon the applicability of the following assumptions:

1. Plane sections of the beam before bending will remain plane after bending.
2. The stress distribution is linear across the bent beam and directly proportional to the distance from the neutral axis.
3. Strain varies linearly with stress up to failure.
4. The stress-strain relationship is the same both in tension and compression and the neutral axis is located at the middle of the beam.

For rocks the stress-strain behaviour is not the same in tension and compression and the neutral axis of the beam is thus not located at the middle of it. Therefore, assumption number 4 is not applicable and hence using equation (6-1) gives incorrect results. The author used the modified equation suggested by Duckworth (see Vutukuri[84]) in finding the stresses in bending which is:

$$\sigma_t = \frac{3M(\varepsilon_t + \varepsilon_c)}{bd^2\,\varepsilon_t} \qquad (6\text{-}2)$$

where σ_t : tensile strength at the lower surface of the beam, N/mm^2

M : applied bending moment, N-mm

ε_t : tensile bending strain of the outer lower fibre

ε_c : compressive bending strain of the outer upper fibre

b : width of the beam, mm

d : height of the beam, mm.

Several specimens of gypsum and anhydrite were tested, the mean value of bending stresses of each rock were calculated. Tables (6-1) and (6-2) give the ultimate bending stresses, mean values, and standard deviations for gypsum and anhydrite, respectively.

Table (6-1)

Bending tests on gypsum beams,

L = 240 mm, b = 40 mm, d = 20 mm.

Specimen No.	Tensile stress at bottom surface N/mm^2	Mean stress N/mm^2	Standard deviation
20G 23	15.41		
20G 3	15.84		
20G 7	13.96		
20G 8	14.37	15.07	1.020
20G 9	16.40		
20G 11	15.18		
20G 15	15.89		
20G 16	13.52		

Table (6-2)

Bending tests on anhydrite beams,

L = 240 mm, b = 40 mm, d = 20 mm.

Specimen No.	Tensile stress at bottom surface N/mm^2	Mean stress N/mm^2	Standard deviation
20A 3	20.46		
20A 4	16.80		
20A 9	15.94		
20A 11	17.64	17.73	1.693
20A 12	16.80		
20A 17	18.42		
20A 20	16.42		
20A 21	19.97		

6-2 Uniaxial Compression Test

6-2.1 Introduction

The optimum design of rock structures or excavations in rock requires knowledge of the strength and deformation characteristics of the rock. Many investigators have studied the effect of various factors such as stress, confining pressure, temperature, time, rate of loading, size and shape of specimen, the structure of the rock material and etc. on the strength and deformation properties of rock. In the following pages brief discussion and results will be given on gypsum and anhydrite specimens subjected to uniaxial compression and loaded up to failure, taking into consideration the factors mentioned above. These results will be used in this work as a basis for the study of the creep characteristics of the rocks under uniaxial compressional load. Because of the structure of the rock material,

i.e. the type of grains or fundamental units, cementing material, hemogeneity, etc. two specimens of the same material, and same dimensions, tested under the same conditions may have different compressive strengths. For this reason several specimens were tested and the mean value of strength was found.

6-2.2 Specimen size and preparation

In an A.S.T.M. publication, Newman and Lachance[55] reached the firm conclusion that the length to the diameter ratio of rock core should be ≥ 2.5, while Hawkes and Mellor[32] mentioned that practical experience shows that values up to L/D = 4 are safe. It was decided in this research to use 75 mm long by 25 mm diameter cores which give L/D = 3. Strain was measured within the middle third of the specimen where a near uniform strain and stress distribution are expected.

The specimens were prepared as follows:

A block of rock was fixed to the bench of a drilling machine in a direction so that drilling the cores was perpendicular to the bedding of rock, see Fig.(6-4) and type (1) of Fig.(6-3). Several 25 mm diameter cores were then obtained by using thin-walled water-flushed diamond coring drills. To get the approximate core length required (75 mm) and flat parallel end faces at right angles to the core axis, which is essential for uniform end contact in loading, the faces were initially trimmed by a Cut-rock machine using a diamond saw. Finally, the two ends of the specimen were finished on a grinding and lapping machine, see Fig.(6-5). Two grades of carborundum (400 and 800 mesh) were used on the lapping wheel as abrasive. In this operation the specimen was placed in a close fitting steel tube with flat flange to produce smooth parallel end faces which are at right

angles to the longitudinal specimen axis. Failing to get square smooth end faces will lead to minute differences in height between the sides of the specimen as it stands between the platens of the testing machine, which gives non-uniform loading on the specimen, and consequently stress concentrations which cause the specimen to fail at a compressive stress below its true ultimate compressive strength. Finally, the specimens were washed and left to be air dried at room temperature for 20 days. The actual dimensions of each specimen were measured by micrometer to the nearest 0.01 mm.

6-2.3 Apparatus and Test Procedure:

The specimens were tested by means of a hydraulically driven Avery 100 ton Universal Testing Machine capable of applying loads on five different ranges, namely, 50, 100, 200, 500 and 1000 KN at any selected constant rate. The rate of loading used in the tests was 25 $N/mm^2/min$ (≈ 60 psi/sec.). This rate of loading was selected depending on the following recommendations:

In the U.S. Bur. of Mines publication, Obert and others[57] recommended that the rate of loading should not exceed 100 psi/sec. A.S.T.M. C 170-50 (Reapproved 1970)[4] recommended the same limit. In A.S.T.M. publication E 111-61 (Reapproved 1972)[5] it was stated: "The speed of testing shall be low enough to make negligible the thermal effects of adiabatic expansion or contraction, and high enough to make creep negligible."

The specimens, which were prepared as described in section (6-2.2), were tested in the compression machine using a spherical seating underneath the specimen to ensure that full contact between the sample ends and the smooth steel plates above and beneath the specimen.

6-2.4 Stress Measurement:

The load applied to the specimen by the Avery Compression Machine can be read directly from an indicator rotating on a calibrated chart. The stress was found by using the general equation:

$$\sigma = \frac{P}{A_s} \qquad (6\text{-}3)$$

where

σ : uniaxial compressive stress, N/mm^2

P : Applied load, N.

A_s : Cross-sectional area of the specimen, mm^2.

Several specimens were tested; the mean values of the ultimate stresses are given in tables (6-3) and (6-4) for gypsum and anhydrite, respectively. Full data of the results are given in tables (A6-1), (A6-2) and (A6-3) in Appendix (A) at the end of this thesis. Then the fractured specimens were photographed as shown in figures (6-6) and (6-7).

6-3 Triaxial Compression Test

6-3.1 Introduction

In civil and mining engineering design of rock structures, it is important to know the conditions under which fracture or flow occurs in rocks. Knowledge of the strength and deformation characteristics of the material aid in the design of more economical and safer structures. Adams and Nicholson[1] were the first who attempted to determine the strength of rock under natural conditions. They used a steel jacket to apply the confining pressure to the rock cylinder specimens in a triaxial compression test. The defects in this method will be considered later in chapter (8).

Von Karman[83] in (1911) was the first who used a liquid to transmit the confining pressure to a jacketed cylindrical rock specimen. Since that time numerous investigators have worked in the field of triaxial testing. Most of the workers on triaxial testing have used impermeable membrances as jackets for their rock specimens to prevent them from direct contact with the surrounding oil. Most investigators have represented their data by means of Mohr's stress circles and rupture envelop. Also most of them agree that the strength of rock increases with the increase of confining pressure.

6-3.2 Apparatus:

The triaxial apparatus and techniques for making these tests have been fully described by Murrell[50] and are briefly reviewed in the following pages for the convenience of the reader.

The design is based on the Von Karman[83] (1911) principle, i.e. the confining pressure was transmitted to the rock cylinder specimens through a surrounding fluid. Thus, the relationship between two of the principle stresses will be $\sigma_2 = \sigma_3$ = confining pressure, the third one, σ_1, being variable. The apparatus consists of two parts, Fig.(6-8). The first part is a triaxial cell, Fig.(6-9), which can be used up to 400 N/mm^2 (60000 psi) confining pressure.

The upper anvil, through which the axial load is applied to the rock specimen, has a spherical seating to ensure that the platens are in full contact with the ends of the specimen. The second part is the hydraulic power pack to provide the required confining pressure at constant value. An electrically driven pump was used to maintain a constant confining pressure that was controlled by means of a needle and relief valves to a maximum

of 9000 psi (≈60 N/mm^2). Fig.(6-10) shows the hydraulic circuit for the whole apparatus. The maximum confining pressure required for this research was 35 N/mm^2, therefore, there was no need to use the pressure intensifier which was designed to increase the confining pressure beyond the pump capacity.

6-3.2.1 Calibration of the Apparatus:

New o-rings were used as an oil seal between the ram and the cell, so it was necessary to re-calibrate the apparatus to find the friction force between the ram and the oil seal; the following test was carried out. The cell was filled in oil and placed in the testing machine; the confining pressure was raised to a pre-determined value and kept constant. The load required to push the ram into the pressure cell against this confining pressure is equal to the upward force acting on the ram due to the known confining pressure plus the friction force. Knowing both the force pushing the ram into the pressure cell and the force due to the confining pressure, the friction force was calculated at that level of confining pressure. This test was repeated with various confining pressures. Fig.(6-11) shows the relation between the friction force and confining pressure.

6-3.3 Specimen Size and Preparation:

The rock specimens were prepared using the same procedure described in section (6-2.2) and the same sizes were used (75 mm long by 25 mm dia.). To prevent direct contact between the specimen and the oil in the cell P.V.C. jackets 0.9 mm thick were used. Powdered talc was used as a lubricant inserting each specimen into the jacket. The jacket extended beyond the specimen ends of the anvils to provide the necessary oil seal.

6-3.4 Test Procedure:

The jacketed specimen was placed in the pressure cell. The cell then was filled with oil making sure that all air was displaced. The confining pressure was then raised to the required value and the force on the ram from the testing machine was raised at a constant rate of loading equals to 25 $N/mm^2/min$ until fracture occurred or plastic deformation has taken place. Then the axial load was reduced to zero followed by the confining pressure. The cell air vent was then opened and the oil pumped out of the cell. Finally, the cell was opened to remove the specimen, the P.V.C. jacket was taken off and the specimens were photographed showing the fracture and/or plastic flow, see figures (6-12) and (6-13). Several tests were carried out at each level of confining pressure. The axial load at fracture or plastic flow and the load immediately after failure were recorded for each specimen. The angle of fracture was also measured.

6-3.5 Stress Measurement:

The two minor stresses (σ_2 and σ_3) are equal to the confining pressure in the cell which can be read on the pressure gauge connected thereto.

The axial load can be calculated using the following equation:

$$P = F_m - (F_d + F_f) \qquad (6\text{-}4)$$

where:

P : the actual axial load applied on the specimen, N

F_m : the axial load applied on the ram of the cell which can be read directly on the testing machine dial, N.

F_d : upward force due to the effect of the confining pressure acting on the difference between the cross-sectional areas of the ram and the specimen, N.

F_f : the friction force between the ram and the oil seal at that value of confining pressure which can be determined from Fig.(6-11), N.

The normal and shear stresses immediately after fracture in all tests were calculated by Mohr's equations

$$\sigma_n = \frac{Z + \sigma_3}{2} + \frac{Z - \sigma_3}{2} \cos 2\Theta \qquad (6\text{-}5)$$

$$\tau_s = \frac{Z - \sigma_3}{2} \sin 2\Theta \qquad (6\text{-}6)$$

where:

σ_n : Normal stress on fracture surface immediately after fracture, N/mm^2.

τ_s : Shear stress on fracture surface immediately after fracture, N/mm^2

Z : Axial stress immediately after fracture, N/mm^2.

σ_3 : Confining pressure, N/mm^2.

Θ : Measured angle of fracture which is the angle between the plane of failure and the minor principle stress.

The values of τ_s and σ_n are plotted on Mohr's envelope graphs, figures (6-14) and (6-15) for both gypsum and anhydrite respectively, and they are shown as dotted straight lines.

The maximum shear, $\tau_m = \frac{\sigma_1 - \sigma_3}{2}$, the mean pressure $P_m = \frac{\sigma_1 + \sigma_2 + \sigma_3}{3}$, and the maximum axial strain were also calculated for each rock. Tables (6-3) and (6-4) give summary data of the triaxial tests, while full data is given in tables (A6-4) and (A6-5), Appendix A.

Table (6-3)

Triaxial tests results of gypsum

No. of specimens tested	$\sigma_2 = \sigma_3$ (N/mm^2)	Mean σ_1 (N/mm^2)	Mean z (N/mm^2)	Mean angle of fracture. (deg).			σ_n (N/mm^2)	τ_s (N/mm^2)	$\sigma_{m'} = \frac{\sigma_1+\sigma_3}{2}$ (N/mm^2)	$\tau_{m'} = \frac{\sigma_1-\sigma_3}{2}$ (N/mm^2)	$P_{m'} = \frac{\sigma_1+\sigma_2+\sigma_3}{3}$ (N/mm^2)	Strain %
				Θ	Θ_M	Θ_G						
8	0	57.46	0	72	62.5	60	-	-	28.73	28.73	19.13	0.22
3	5	73.97	42.20	60	60.5	58.5	14.30	16.11	39.49	34.49	27.99	0.54
5	10	92.07	58.79	58	58	56.7	23.71	21.96	51.04	41.04	37.36	0.86
3	15	102.51	79.03	55.7	57	55.9	35.35	29.78	58.76	43.76	44.17	1.02
5	20	114.58	102.57	57.5	56.5	55.3	43.87	37.41	67.29	47.29	51.53	1.18
3	25	128.37	113.31	53.5	56	54.7	56.27	42.22	76.69	51.69	59.46	1.38
6	30	136.44	129.20	53	54	53.7	65.96	47.67	83.22	53.22	65.48	1.50
3	35	147.80	146.26	-	54.5	53	-	-	91.40	56.40	72.60	1.63

Table (6-4)

Triaxial tests results of anhydrite

No. of specimens tested	$\sigma_2 = \sigma_3$ (N/mm^2)	Mean σ_1 (N/mm^2)	Mean Z (N/mm^2)	Mean angle of fracture. (deg).			σ_n (N/mm^2)	τ_s (N/mm^2)	$\sigma_{m'} = \frac{\sigma_1+\sigma_3}{2}$ (N/mm^2)	$\tau_{m'} = \frac{\sigma_1-\sigma_3}{2}$ (N/mm^2)	$P_m = \frac{\sigma_1+\sigma_2+\sigma_3}{3}$ (N/mm^2)	Strain %
				θ	θ_M	θ_G						
8	0	101.25	0	75	68.5	60	-	-	50.62	50.62	33.75	0.08
2	5	131.50	28.85	66	66	59.2	8.82	8.76	68.25	63.25	47.17	0.27
3	10	164.60	65.87	65.5	64	58.2	19.61	20.79	87.30	77.30	61.51	0.52
2	15	186.52	102.11	63	63.5	57.7	32.95	35.28	100.76	85.76	72.17	0.76
3	20	200.51	125.10	63	62	57.1	41.65	42.57	110.26	90.26	80.17	0.95
2	25	224.31	164.33	62.5	62.5	56.8	54.68	57.13	124.66	99.66	91.44	1.14
3	30	236.63	198.16	60	61.5	56.3	72.04	72.81	133.32	103.32	98.88	1.23
2	35	251.11	218.32	60	61.5	56.1	79.33	76.78	143.06	108.06	107.04	1.36

The angle θ_M in the previous tables are determined by Mhor's theory for each rock, while θ_G is the angle of fracture calculated by Griffith equation,

$$\cos 2\theta = - \frac{\sigma_1 - \sigma_3}{\sigma_1 + \sigma_3} . \qquad (6\text{-}7)$$

The strength pressure curves, of maximum shear (τ_m) versus the mean pressure (P_m) were plotted in Fig.(6-16), while curves of maximum strain as a function of mean pressure were also constructed in Fig.(6-17).

It was found that the ultimate strength and the maximum strain of each rock increase with increasing the confining pressure, see figures (6-18), (6-19) and (6-20). Finally, the relation between the maximum normal stress, $\sigma_m = \frac{\sigma_1+\sigma_3}{2}$, and the maximum shear stress, $\tau_m = \frac{\sigma_1-\sigma_3}{2}$, for each rock is plotted in Fig. (6-21). All the mentioned results, tables and graphs will be discussed later in chapter (9).

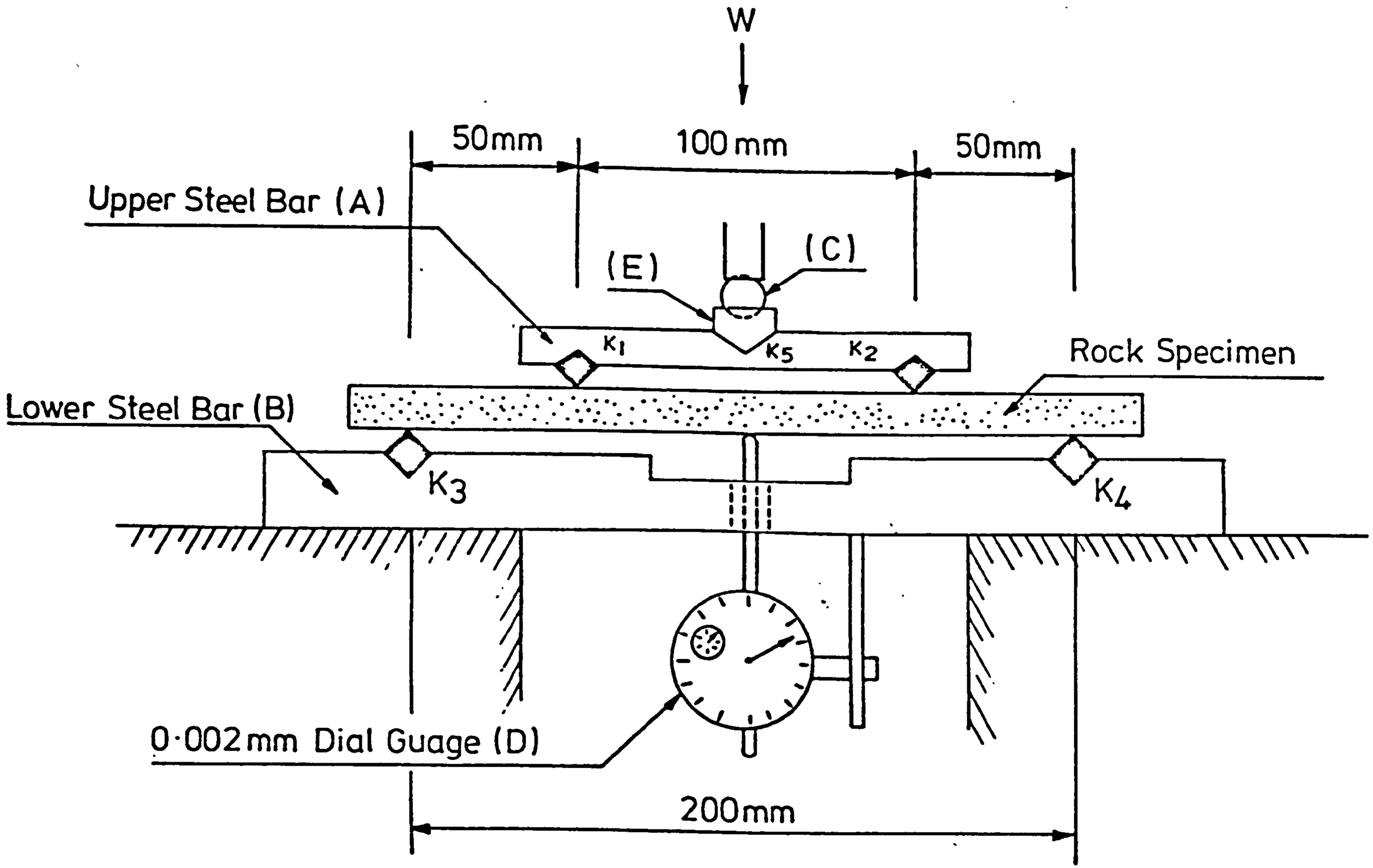

FIG. 6-1 ELEVATION OF BENDING APPARATUS

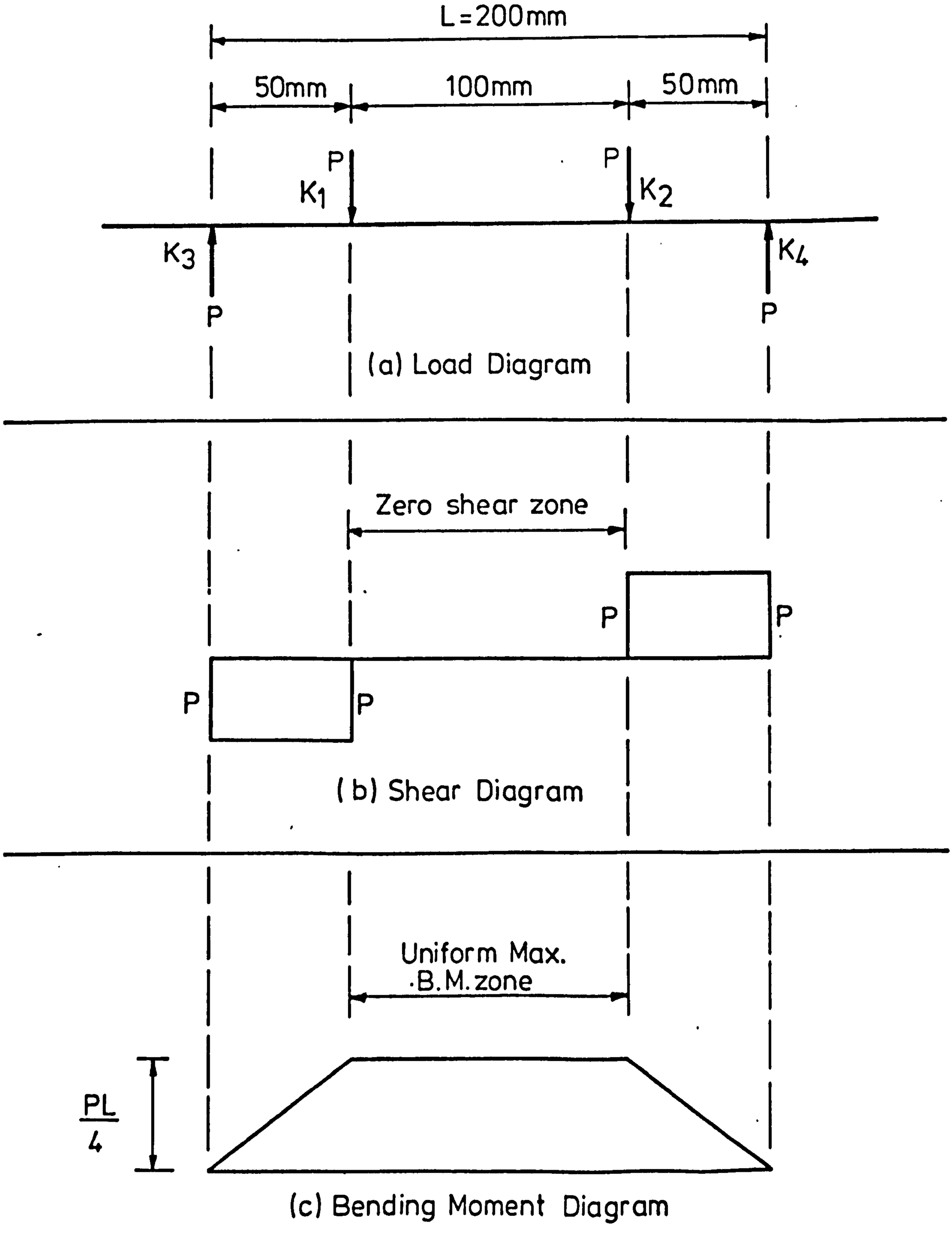

FIG. 6-2 BENDING MOMENT AND SHEAR DIAGRAMS FOR FOUR-POINT LOADING SYSTEM

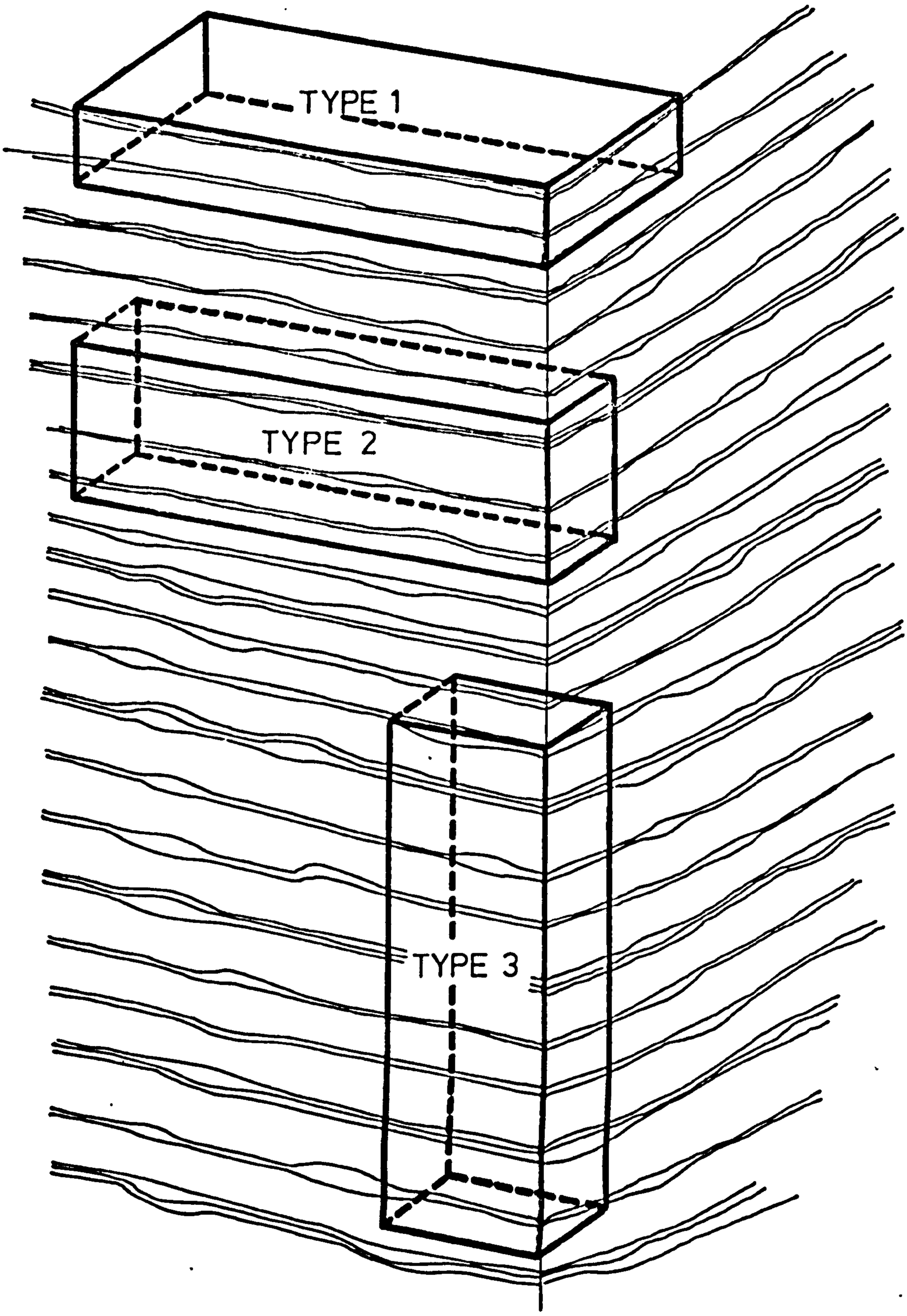

FIG. 6-3 SCHEMATIC DIAGRAM OF ROCK BEDDING

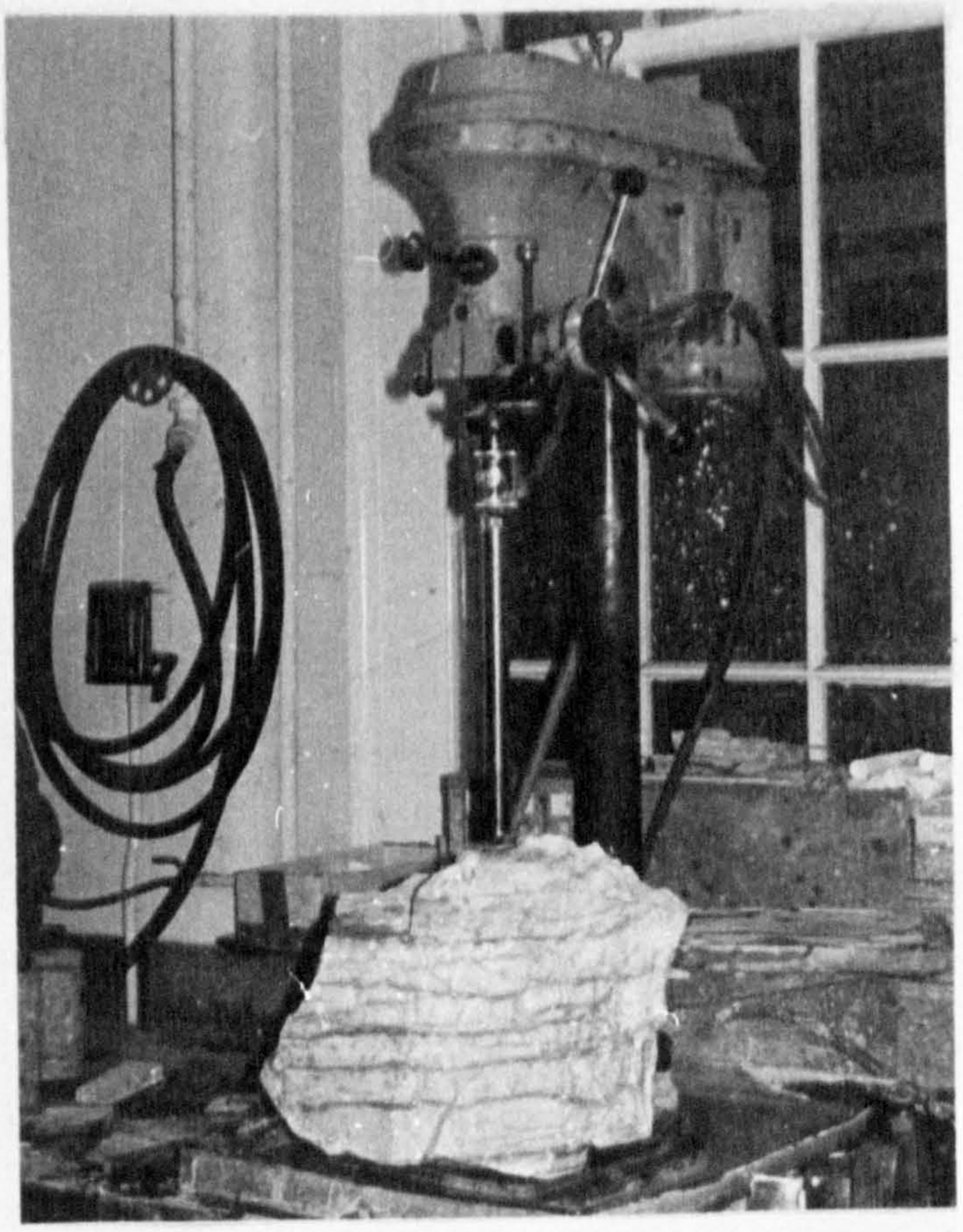

FIG. 6-4 BLOCK OF GYPSUM ON THE DRILLING MACHINE BENCH

FIG. 6-5 TREATMENT OF SPECIMEN ON THE LAPPING MACHINE

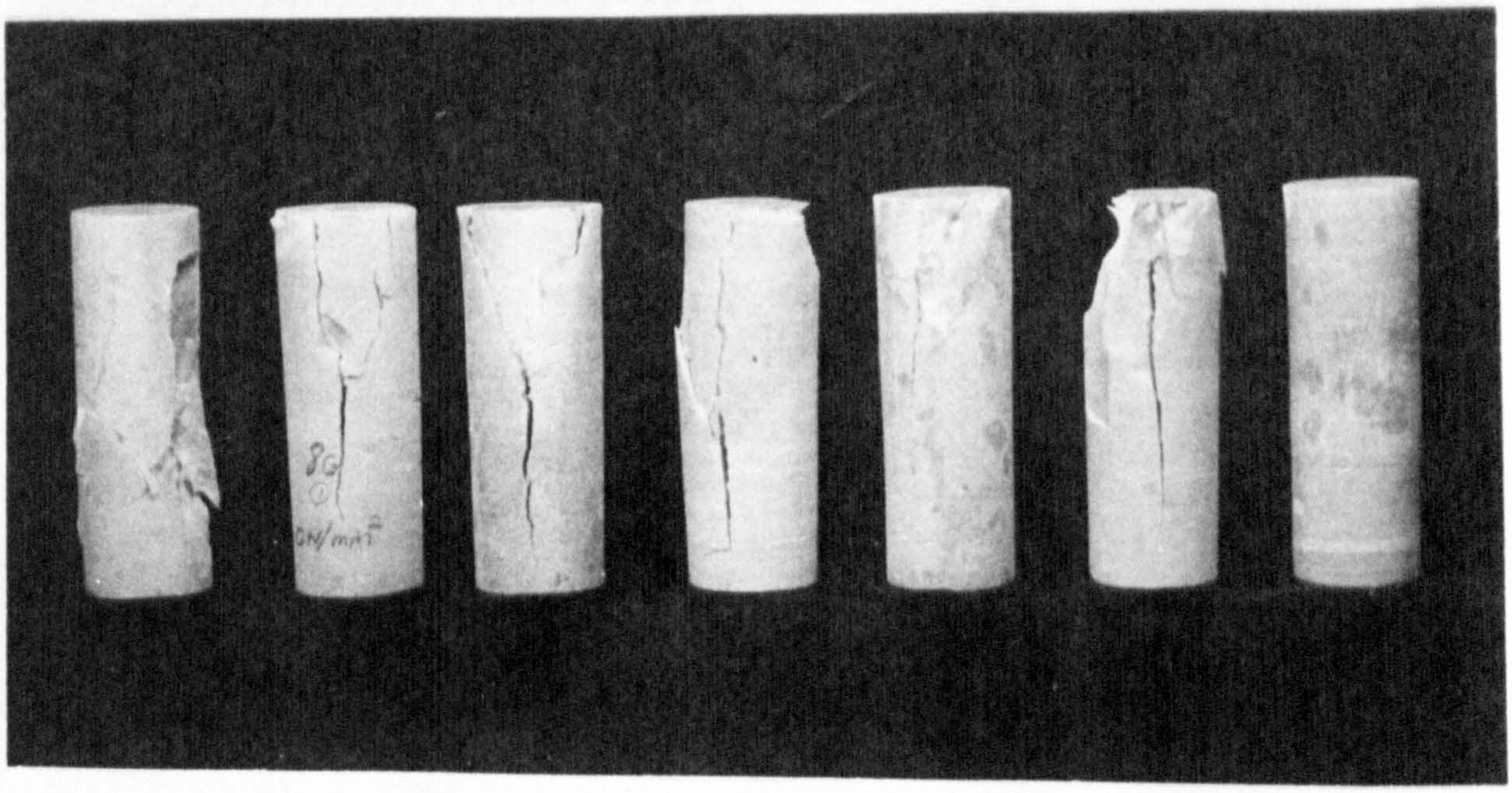

FIG. 6-6 GYPSUM SPECIMENS FRACTURED AT UNIAXIAL COMPRESSION TESTS

FIG. 6-7 ANHYDRITE SPECIMENS FRACTURED AT UNIAXIAL COMPRESSION TESTS

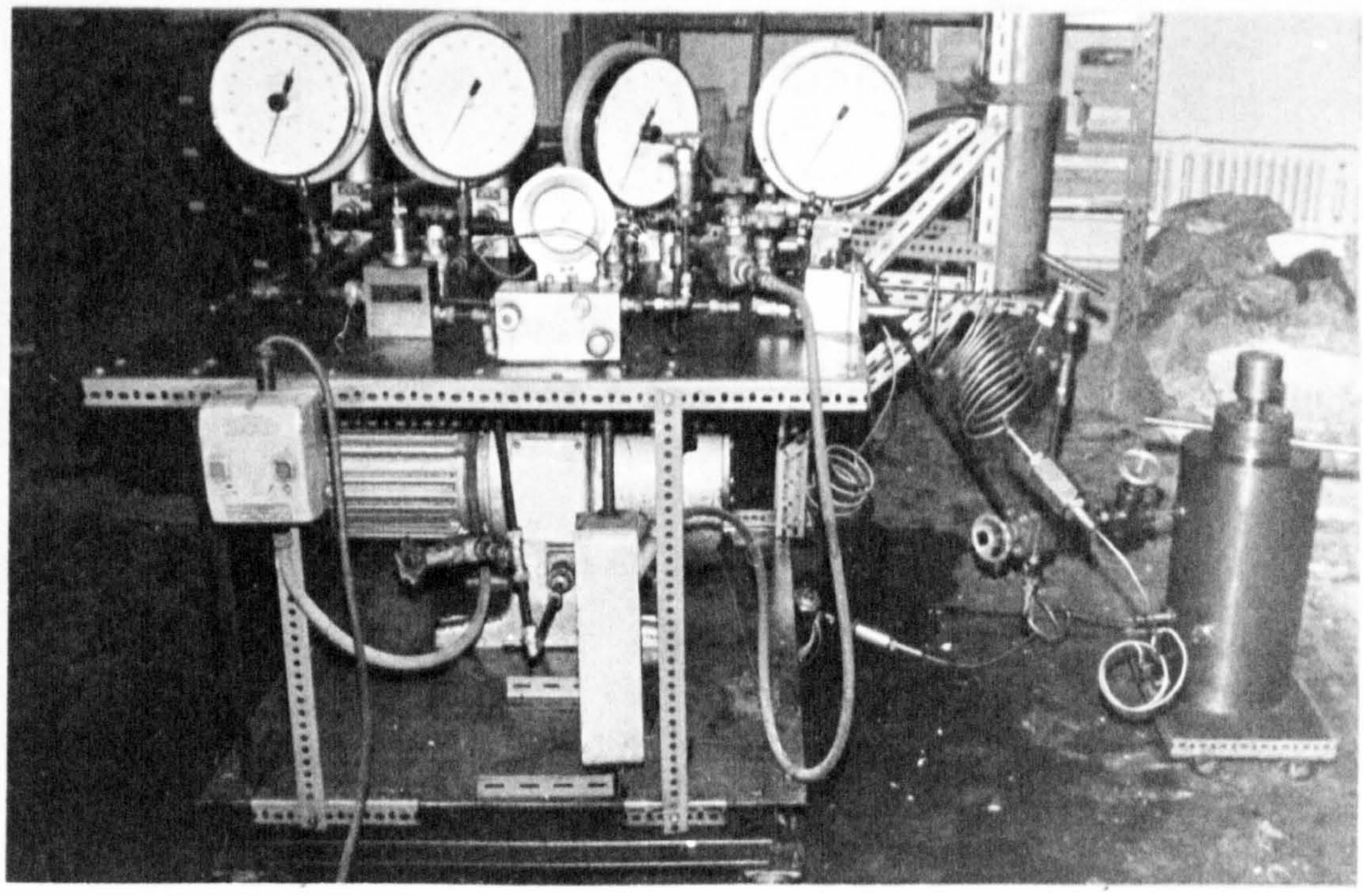

FIG. 6-8 TRIAXIAL TESTING APPARATUS

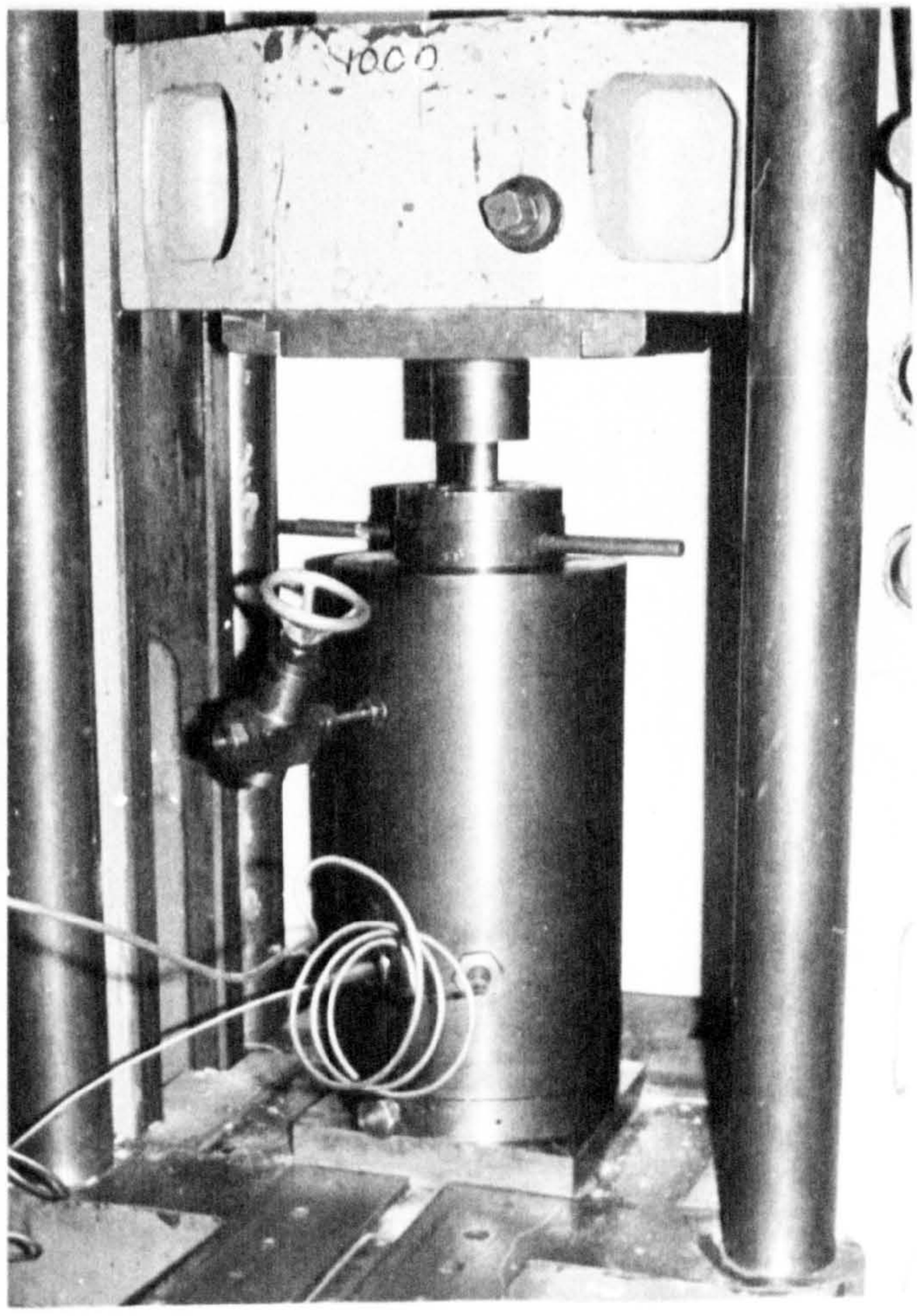

FIG. 6-9 TRIAXIAL TESTING CELL

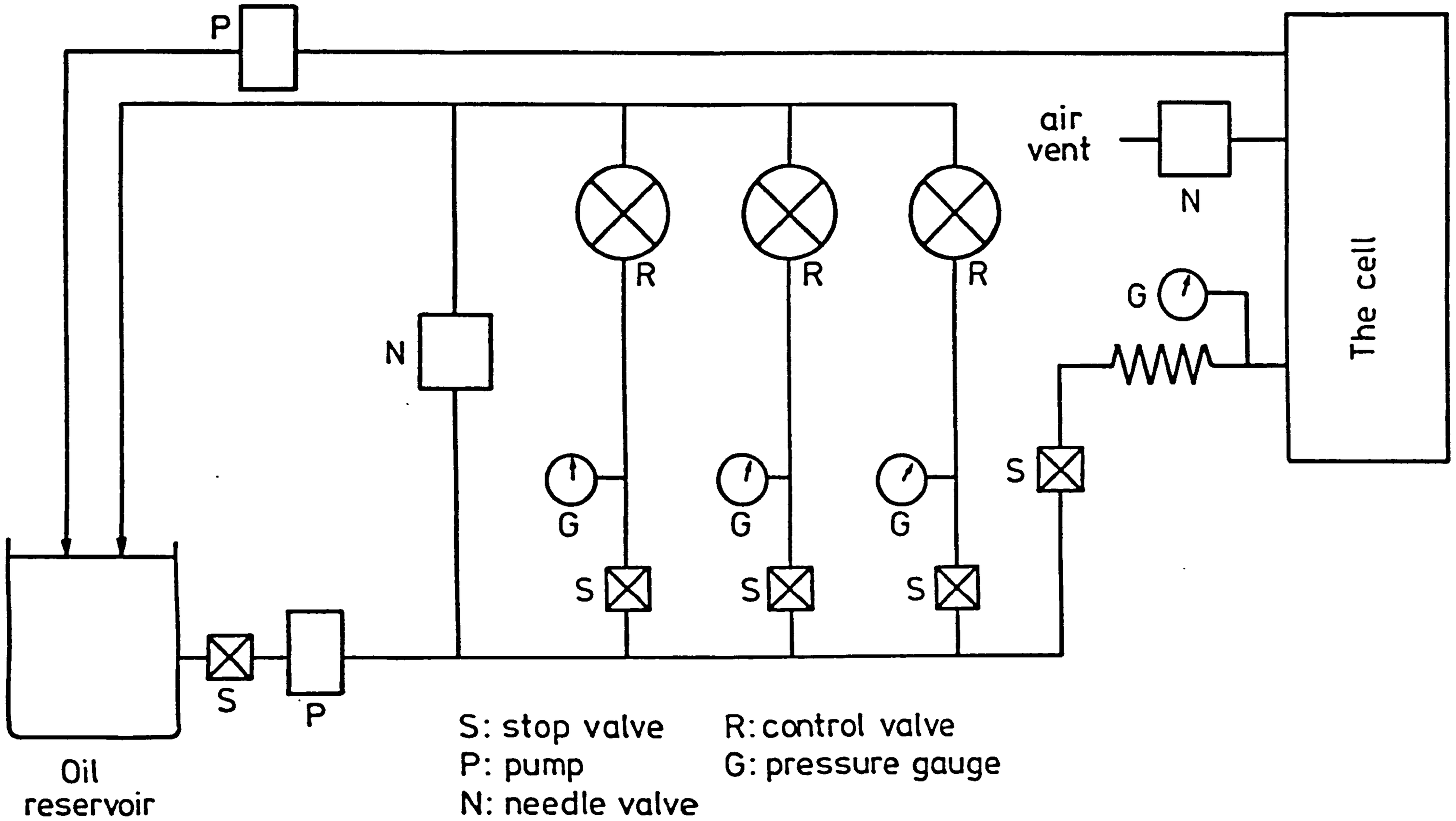

FIG. 6-10 THE HYDRAULIC CIRCUIT OF THE TRIAXIAL APPARATUS

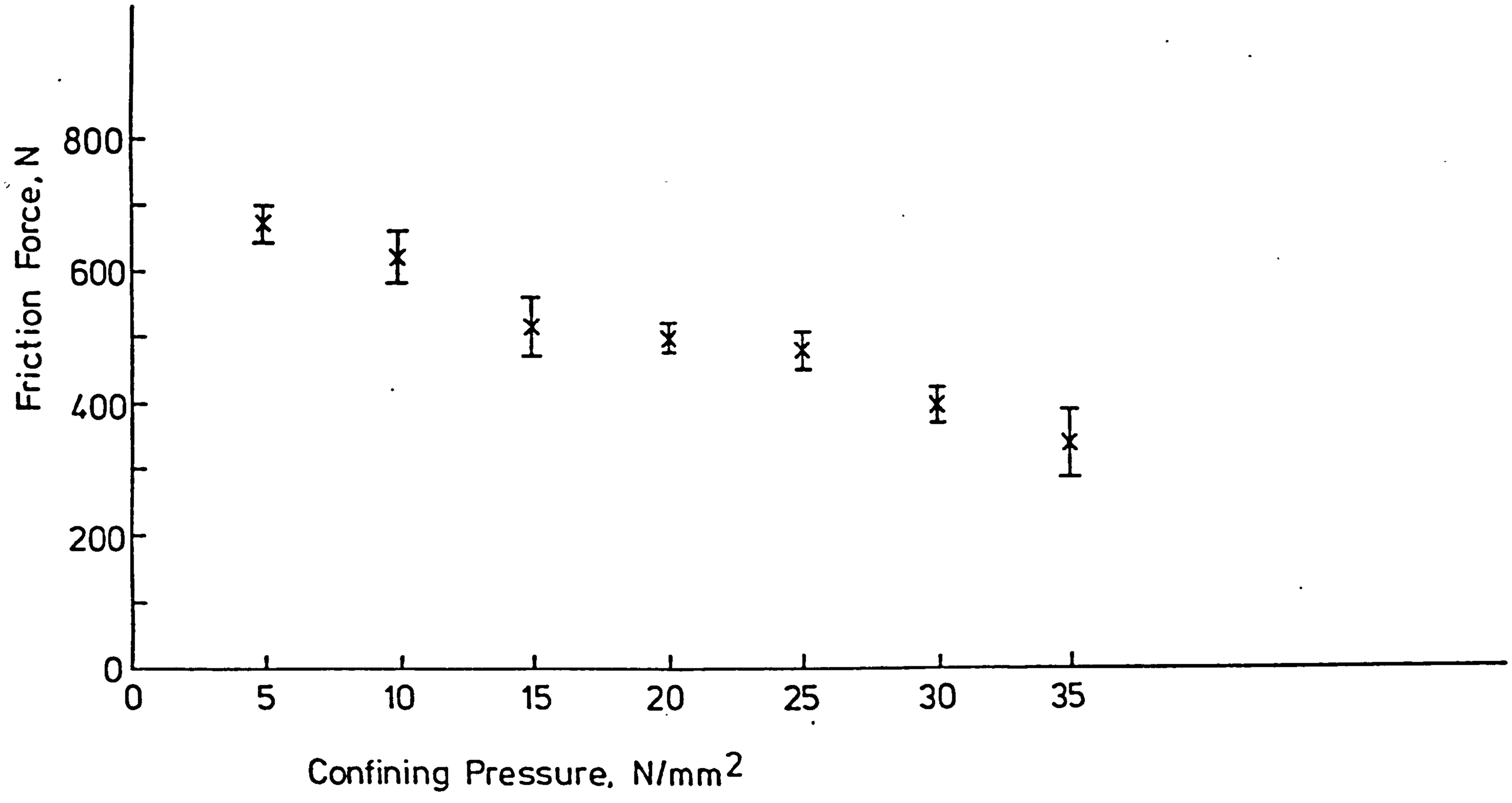

FIG. 6-11 FRICTION FORCE FOR MURREL TRIAXIAL CELL AT VARIOUS CONFINING PRESSURES

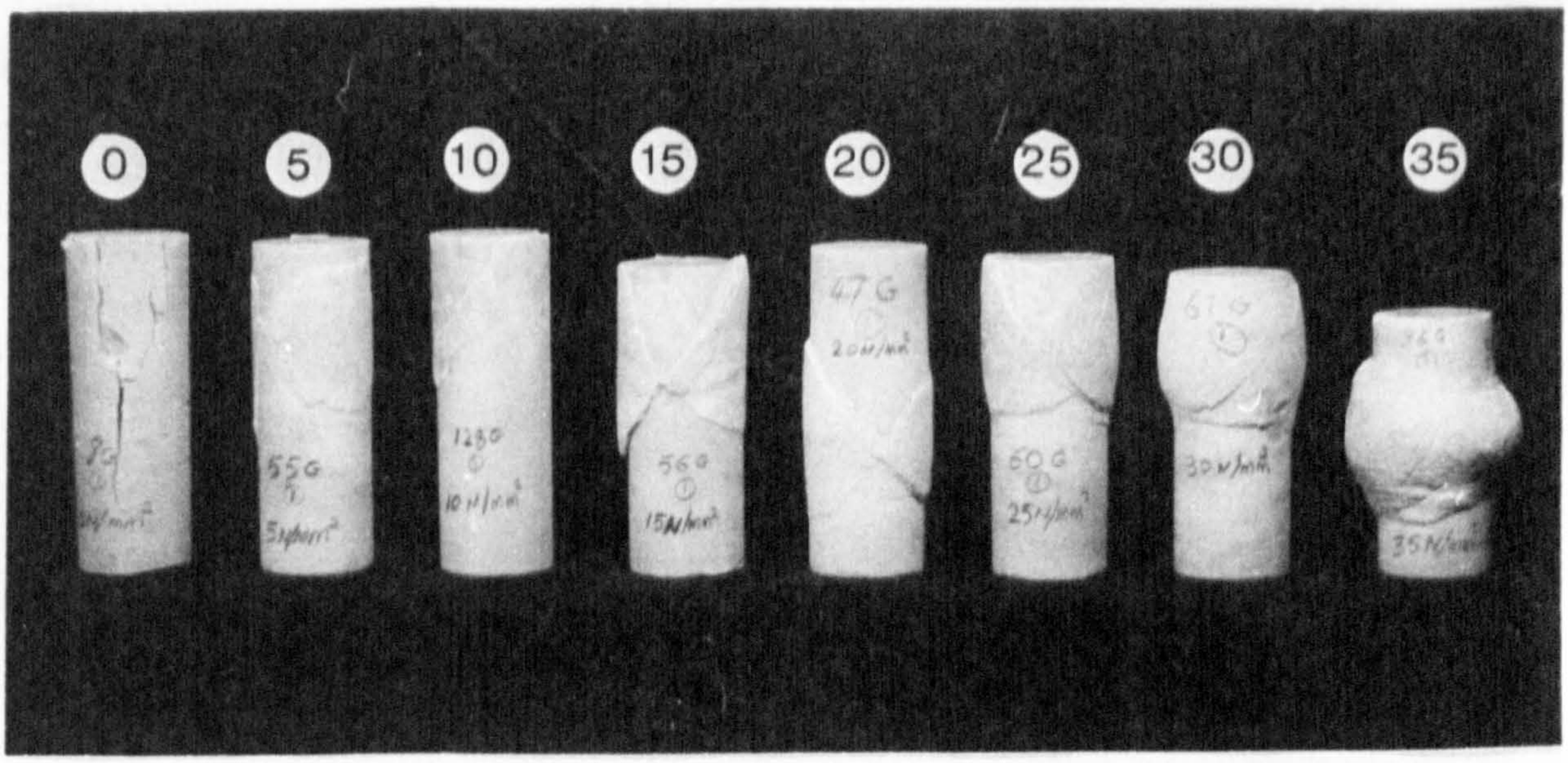

FIG. 6-12 GYPSUM SPECIMENS FRACTURED AND DEFORMED PLASTICALLY AT VARIOUS CONFINING PRESSURES IN N/mm^2

The number above each specimen represents the confining pressure in N/mm^2

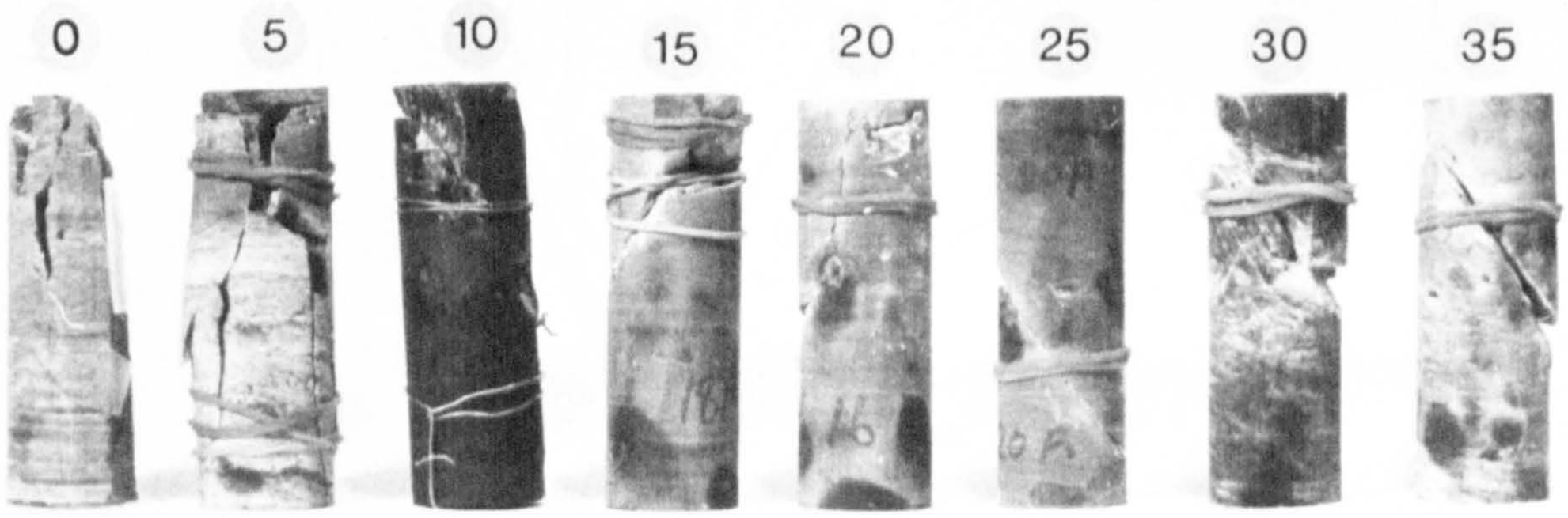

FIG. 6-13 ANHYDRITE SPECIMENS FRACTURED AT VARIOUS CONFINING PRESSURES IN N/mm^2

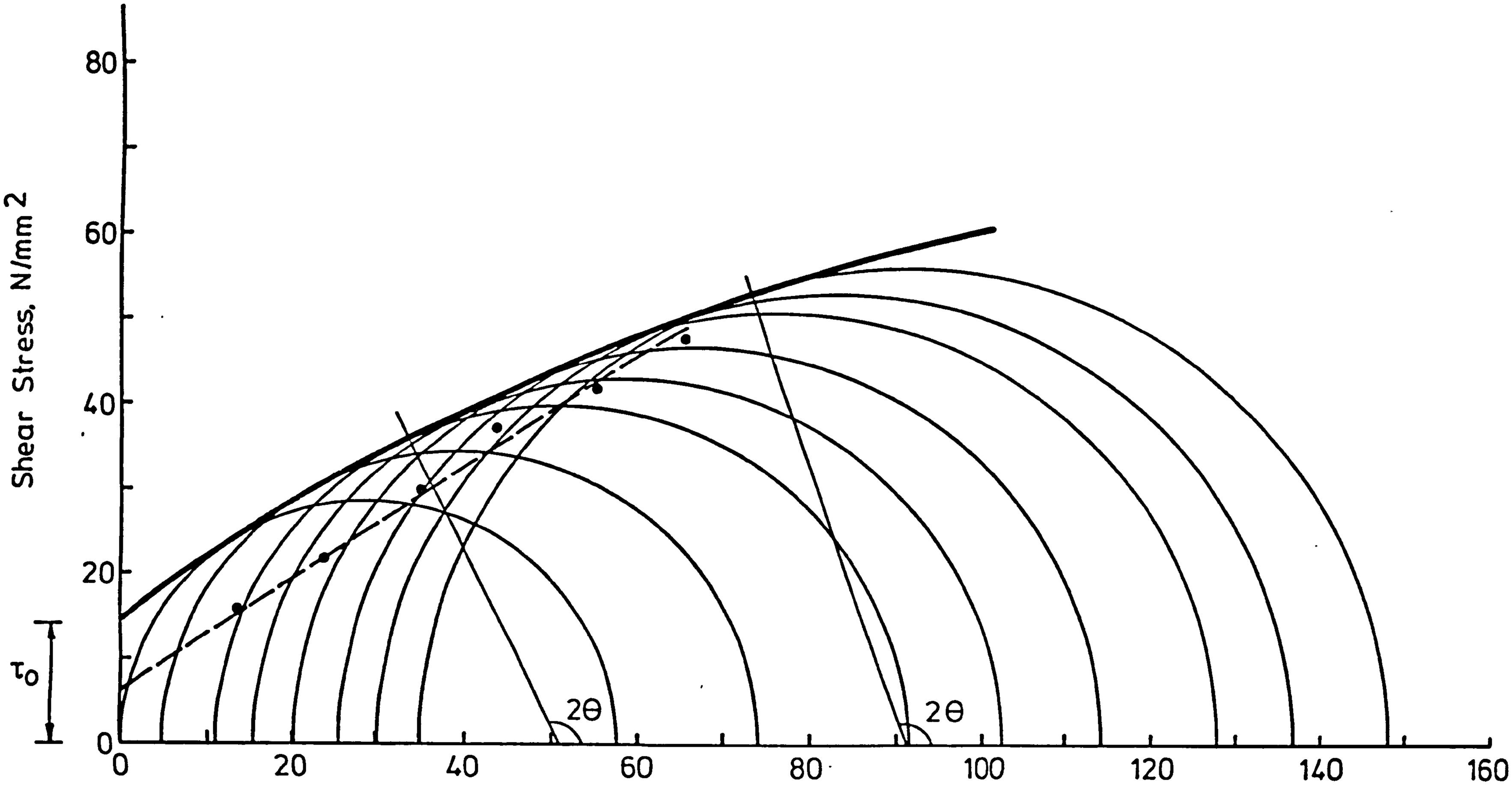

FIG. 6-14 MOHR'S ENVELOPE FOR GYPSUM

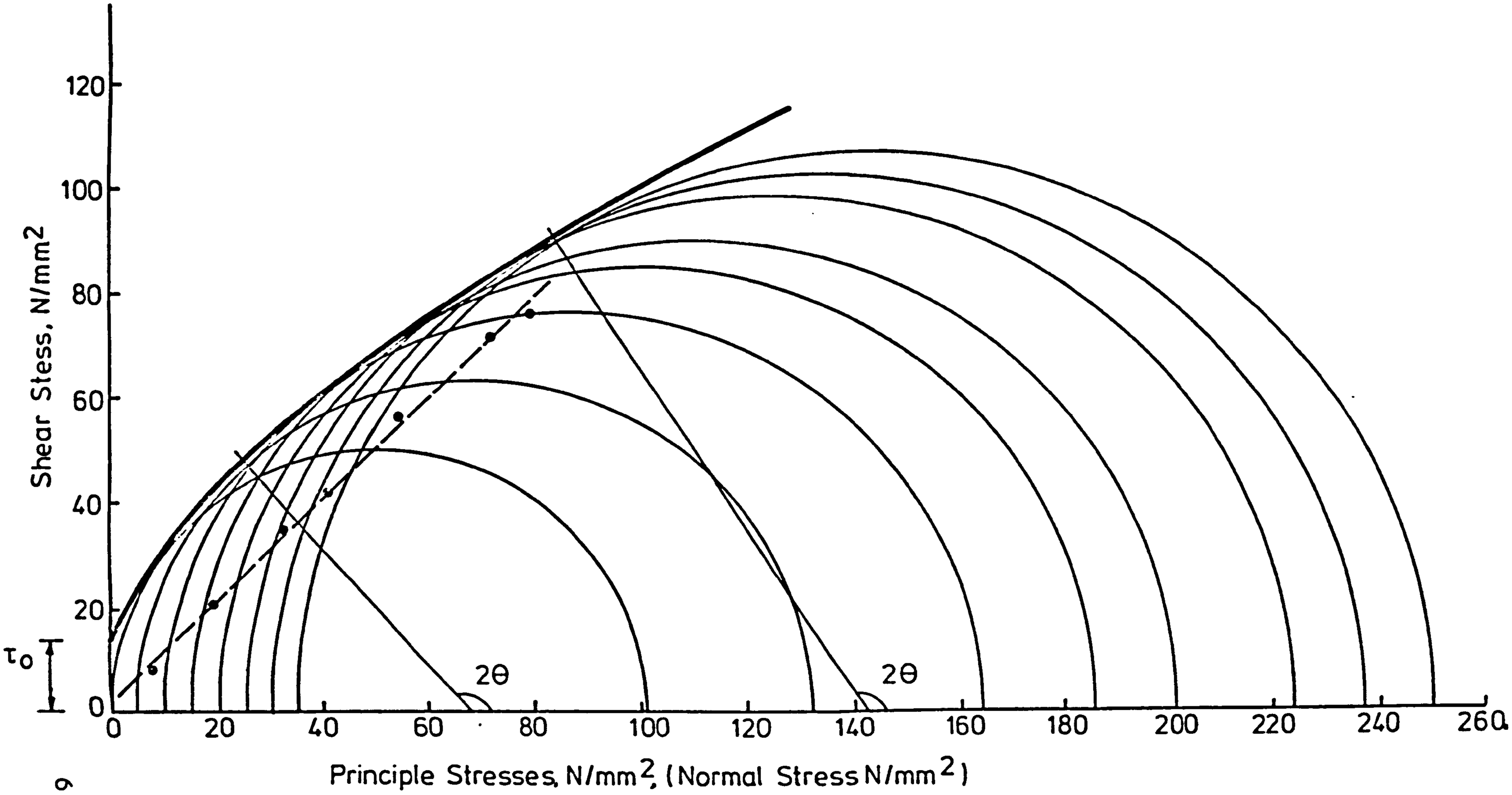

FIG. 6-15 MOHR'S ENVELOPE FOR ANHYDRITE

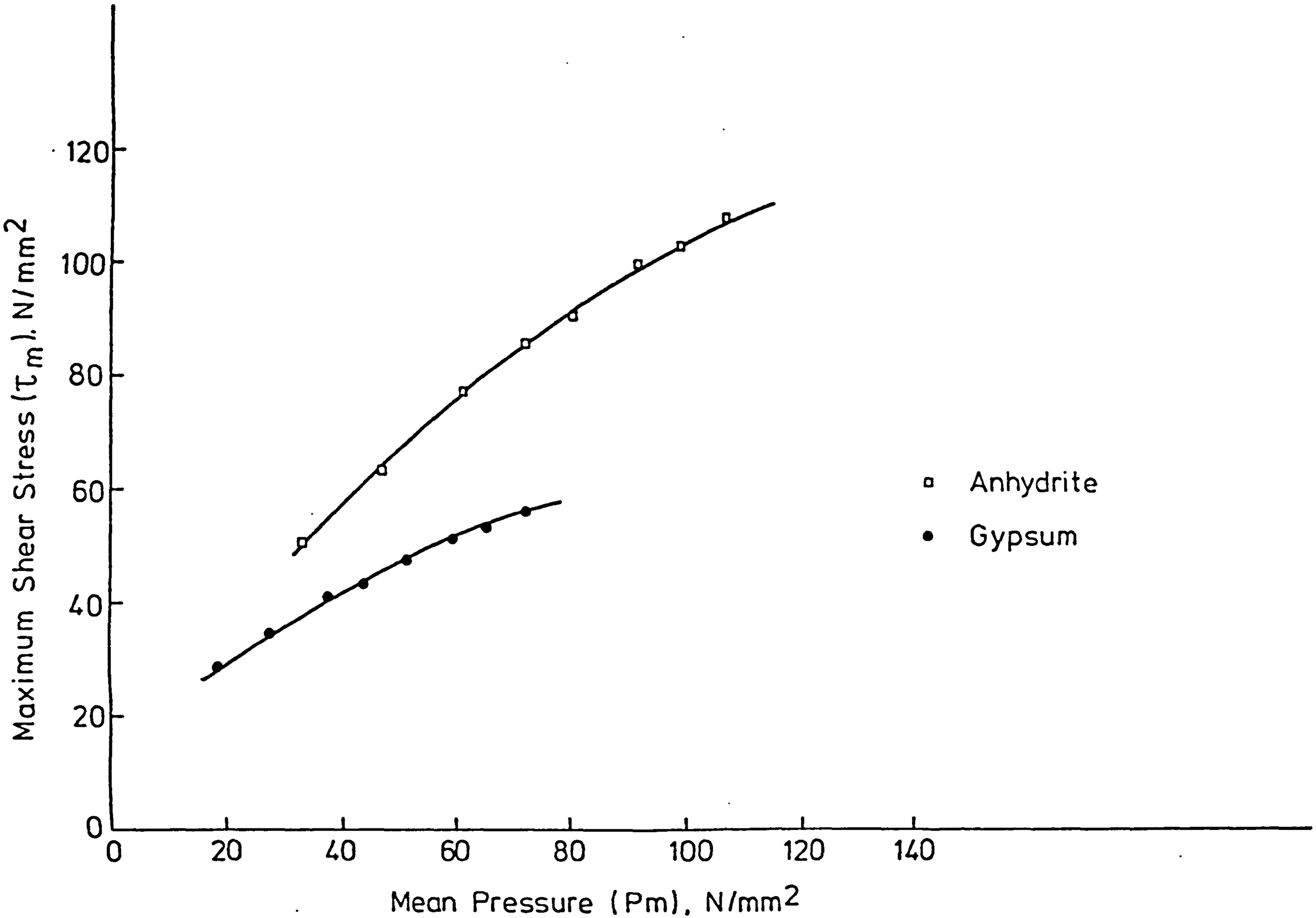

FIG. 6-16 STRENGTH PRESSURE CURVES

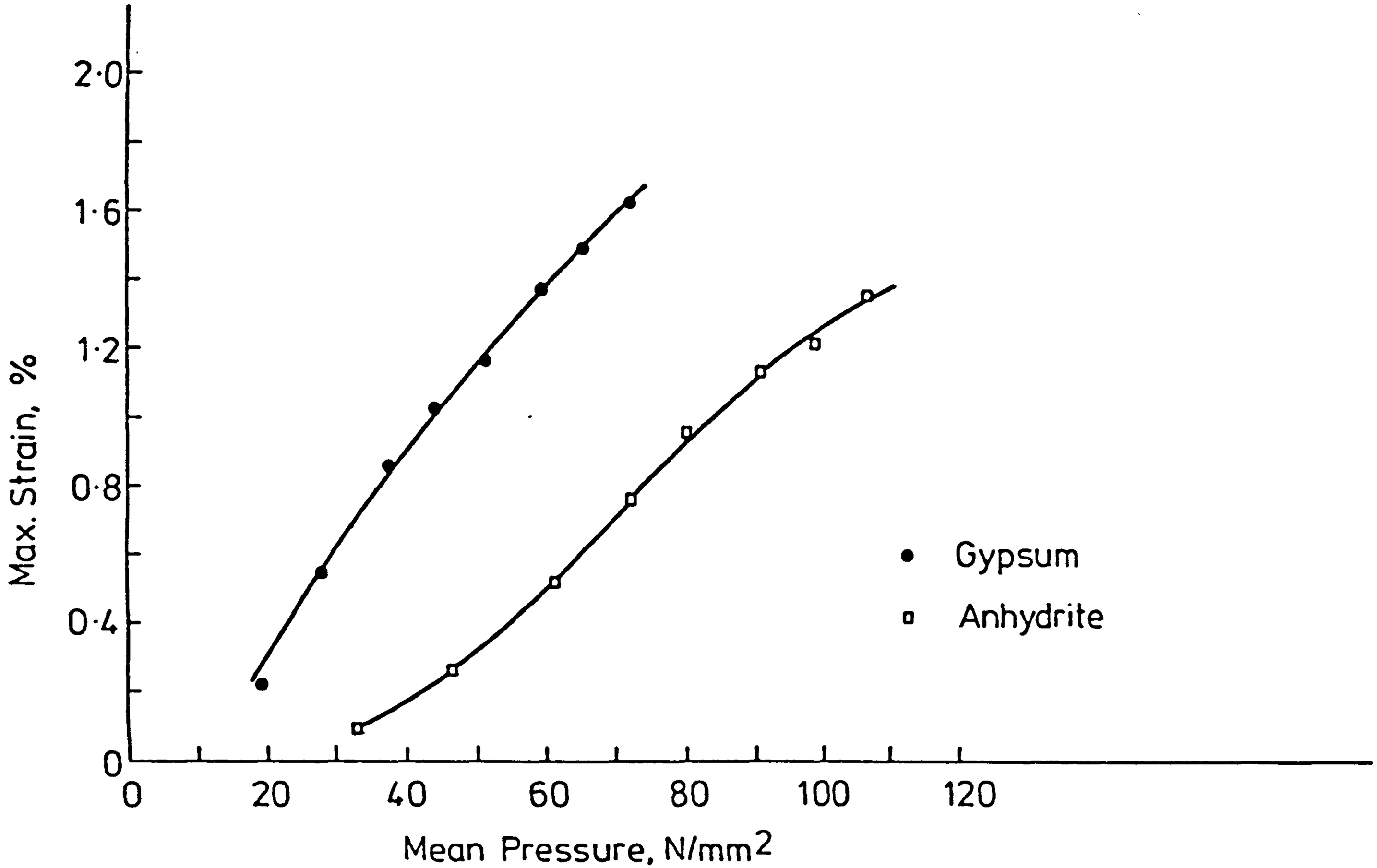

FIG. 6·17 MAX. STRAIN VERSUS MEAN PRESSURE OF GYPSUM AND ANHYDRITE

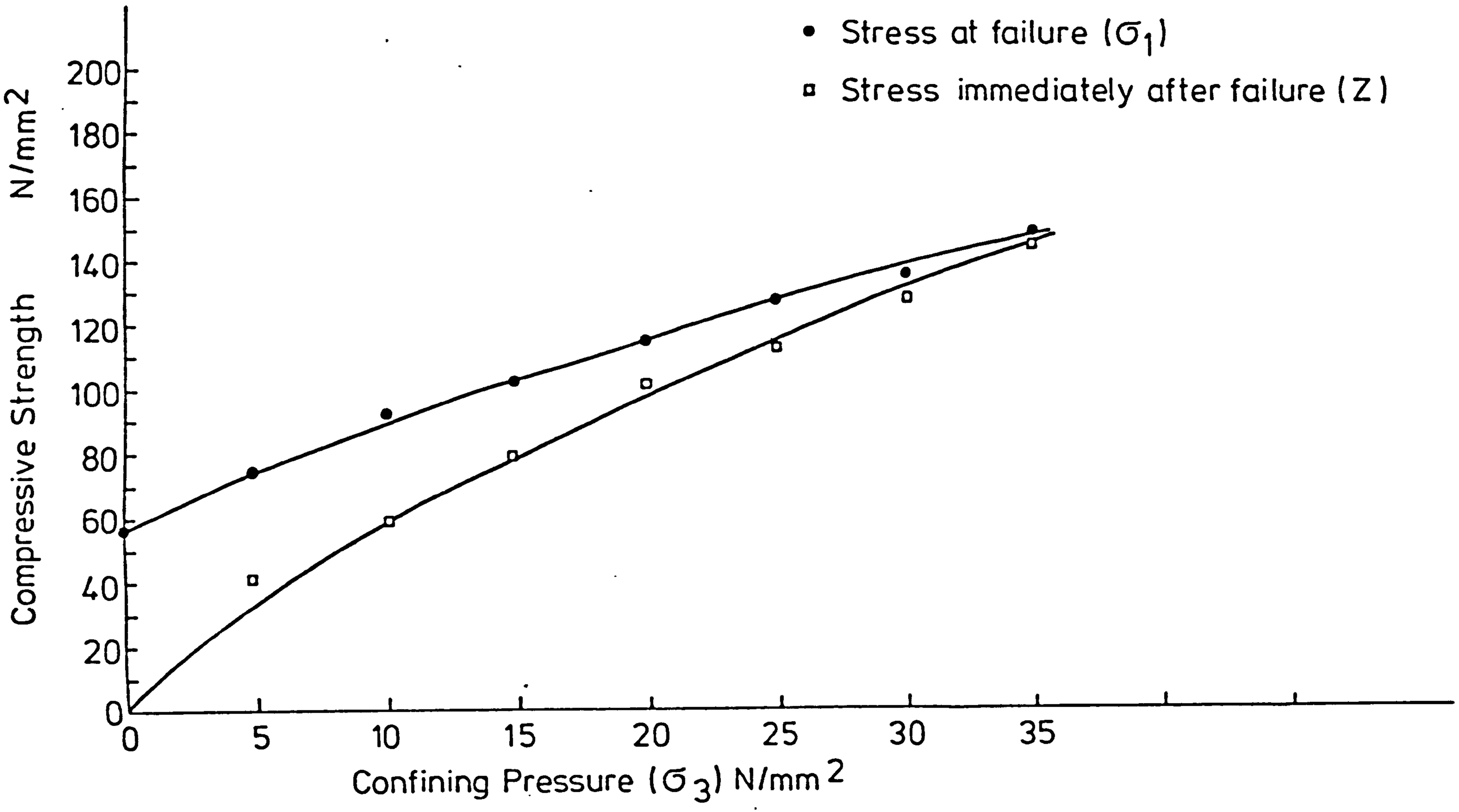

FIG. 6-18 COMRESSIVE STRENGTH OF GYPSUM AT VARIOUS CONFINING PRESSURES

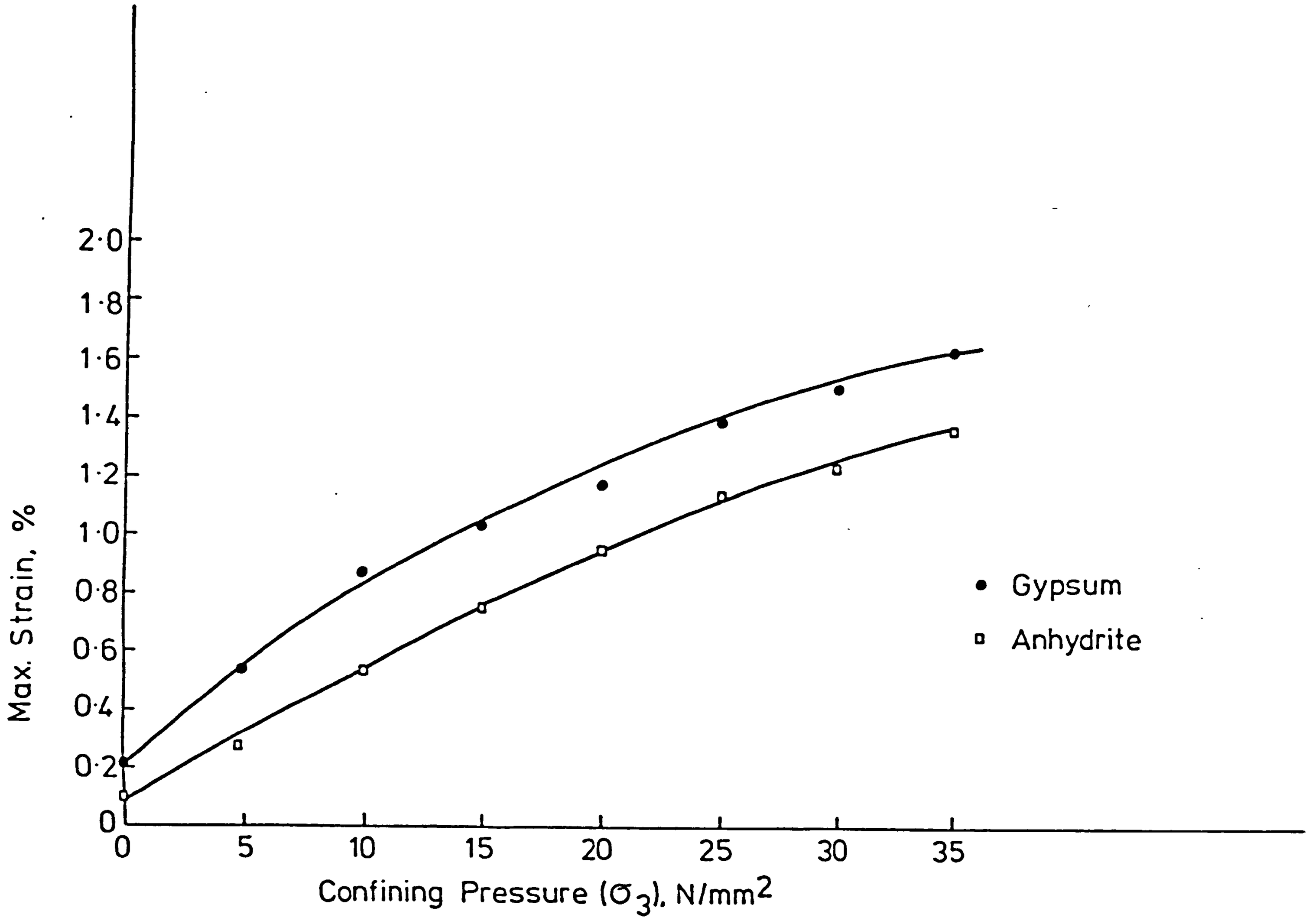

FIG. 6-20 STRAIN OF GYPSUM AND ANHYDRITE AT VARIOUS CONFINING PRESSURES

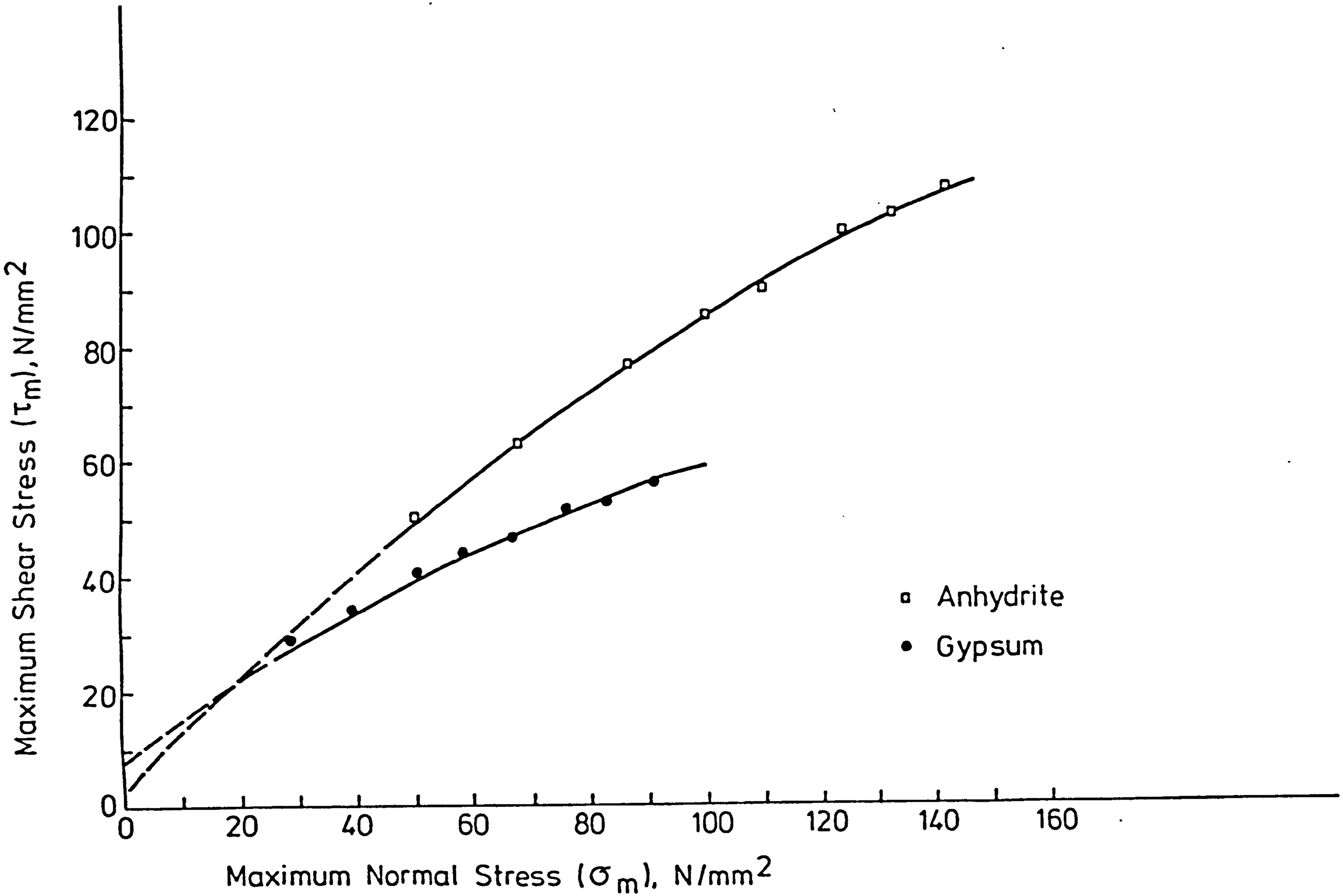

FIG.6·21 MAX. NORMAL STRESS VERSUS MAX. SHEAR STRESS IN TRIAXIAL TESTS

Chapter 7

CREEP UNDER UNIAXIAL AND BENDING SYSTEMS OF LOADING

Chapter 7

CREEP UNDER UNIAXIAL AND BENDING SYSTEMS OF LOADING

In the design of any machine for creep tests, several points must be considered, the most important of which are:

(a) The known applied stress to the specimen must be kept constant over the whole period of the test.

(b) The deformation measuring devices must be stable and unaffected by the surrounding environment changes of humidity and temperature.

In the research work described here, the first point was achieved by using dead-weight loading system in both uniaxial and bending creep machines. The second point was achieved by using suitable methods of compensation and measuring devices of proven stability which will be described later.

7-1 Uniaxial Compression Test

7-1.1 Compression Apparatus

The machine used was similar to the one used by Misra[49] in (1962). It consists, figures (7-1) and (7-2) of:

(a) Dead Weight and Lever Unit:

This unit consists of two levers, lever No.1 (h) fulcrums at the knife edge K_3 and lever No. 2, (b) fulcrums at the knife edge K_5. The knife edges K_2 on lever No.1 and K_4 on lever No.2 are connected together by means of two tie rods and a turn buckle (d). By means of the turn buckle the distance between the two knife edges K_2 and K_4 can be adjusted according to the load required. The lever system by reversing direction twice enjoys the advantage of obtaining a large ratio (mechanical advantage $\approx$ 1:120) in relatively small space. Using knife edges

minimises friction losses at all places where force direction is changed, also gives free movement of the machine elements at all necessary joints. Lever No.1 carried weight pan (ℓ) at the knife edge K_1. By loading the weight pan by means of dead weights a tensile pull is created at the vertical axis of knife edge K_6. This tensile pull is converted into compressive load by means of a load reversing jig (e) attached to the knife edge K_6. The bottom end of the reversing jig is connected to a spring (i) underneath the platform of the angle-iron framework (n). Fig.(7-3) shows the reverse jig with a specimen in position. A tensile pull applied at the ends of the jig is converted into a compression load at the axis of the rock specimen. The purpose of the spring and the hydraulic jack (j) assembly incorporated beneath the framework platform is to take up the elastic stretch of the framework and other tension members and also to initially apply the load smoothly and gradually at any required rate to the test specimen. Sponge seatings underneath the entire framework absorb any shocks in the floor due to external mechanical disturbances. A thrust ball bearing and clamping nut is provided on the connecting rod of hydraulic jack underneath the platform as means of taking up the distortion of framework. A spirit level (g) on lever No.1 indicates, when the bubble at the centre, that the applied load and the weight on the pan are balanced. A dead weight (a) at the end of lever No.2 and projected arm of lever No.1 act as balancing weights. The loading platens in the reversing jig were designed to carry a spherical seating for maintaining an uniaxial load on the specimen during the period of the test.

(b) Strain Measuring Devices:

Misra used Marten's Optical Extensometer and Linear Variable Differential Transformers in measuring the deformation in rock specimen. He actually measured the shortening in distance between the two platens above and below the specimen, assuming that no creep in the platens themselves, they were made of Jessop's H.16, creep resistant alloy steel. In this research the author used three axial electrical resistance foil strain gauges (Tinsley Telcon Ltd.-London) bonded in the central zone of the specimen spaced $\approx 120^{o}$ apart, Hawkes and Mellor[32]. Each gauge is 13 mm long, 120 ohm $\pm$ 0.1 resistance and a gauge factor of 2.15. Dummy strain gauges of the same type bonded on a similar piece of rock of the specimen were used with the active gauges to give temperature compensation. A Peekel strain gauge indicator type T-200 (Automation - Peekel N.V., Rotterdam, Holland) was used to measure the variations in strain for the whole period of the creep test. This indicator has excellent long term stability which satisfies the second point of requirements mentioned at the beginning of this chapter. Fig. (7-4) shows the method of connecting the strain gauges between themselves and to the Peekel strain indicator.

7-1.2 Specimen Size and Preparation:

Specimens were prepared as described in section (6-2.2). The middle third of the specimen was manually ground by rubbing it with fine emery cloth, the actual dimensions then measured by micrometer. Then the central zone was cleaned by acetone to make sure that this zone is free from any grease. Three axial electrical resistance strain gauges were bonded on this area spaced $\approx 120^{o}$ apart by using (P_2) adhesive following the

manufacturer's instructions in this step. Finally, leads were soldered to the gauges and connected to the strain gauges bridge for strain measuring during the test.

7-1.3 Test Procedure:

7-1.3.1 Calibration of Compression Machine:

The lever system machine described before gives a theoretical mechanical advantage of 1:120 i.e. one kilogram on the weight pan should give 120 kg on specimen. But because of friction losses in the knife edge joints where direction is changed, therefore, it was necessary to calibrate the machine to find the actual ratio between the weights on the pan and the load applied on the specimen. A 75 mm high by 25 mm diameter duralumin specimen with strain gauges attached to it was first tested in a Clockhouse compression machine and a curve was plotted of load applied to specimen v/s its deformation (strain), Fig. (7-5a). Afterwards the duralumin specimen was placed in the creep machine and another curve was plated of load on the weight-pan v/s specimen strains Fig. (7-5b). These two curves give separate linear relationships on the graph. As in the two graphs the deformation of the specimen is common, this forms a basis for comparison of the load on the pan (kg) v/s compressive load applied to the specimen (KN). A third curve was plotted to show this linear relationship, Fig. (7-5c), which is the machine calibration curve. It was found from the calibration curve that 1 kilogram on the weigh-pan gives 1.135 KN on specimen i.e. the mechanical advantage of the lever system is equal to 115.73 times approximately.

7-1.3.2 Short Term Test:

The short term uniaxial test of gypsum and anhydrite to find their instantaneous strengths was mentioned in section (6-2).

7-1.3.3 Creep Test:

To give a required stress to a specimen, a corresponding weight on the pan of the creep machine is calculated from the calibration curve and placed on the pan. Then the specimen is placed in its exact central position between the platens of the machine. With a zero load on the specimen a reading from the T-200 indicator is recorded. Then the load is carefully applied to the specimen by operating the hydraulic jack until full load is carried by bringing lever No.1 to the horizontal position, this is observed by the spirit level on the lever. Then the clamping nut provided underneath the platform is turned until it becomes firmly seated against the framework platform. At this moment another reading of the T-200 indicator is recorded. The difference between the two readings gives the "instantaneous" strain in the specimen. After that, many readings were recorded at known intervals of time which reveal the creep phenomenon of the rock specimen under uniaxial compression. All the T-200 indicator readings were adjusted according to the number of strain gauges used and to the gauge factor of the gauges following the T-200 indicator manufacturer's instructions.

7-2 Bending Creep Test:

7-2.1 Apparatus

To achieve pure bending moments in the specimens tested, the four-point loading apparatus described in section (6-1.2) was used. In order to make sure that constant stress can be maintained during the whole period of the creep test dead weight loading was used.

7-2.1.1 Loading Devices

When the corresponding load to give a certain stress

is only a few kilograms, the weight was placed directly on the platform (a) as shown in Fig. (7-6). In cases when heavy weights were needed to give the required stress, a lever system was designed to give a mechanical advantage of 1:10, i.e. one kilogram on the weight pan gives 10 kilograms on the specimen, Figs. (7-7) and (7-8). Using the lever system of loading has three main advantages; it reduces the total required weights on pan by 10 times, enables the load to be applied without shocks, and reduces the loading time. At the end of the lever (b) remote from the pan (a) a weight (e) was used to balance the weight of the lever itself, the weight of the adjustable vertical bar (c) and the weight of the pan. The friction effect of the hinge of the lever was measured and was found to be too small to consider.

7-2.1.2 Strain Measurements

Two methods were used in measuring the strain at the lower outer surface of the specimen beams.

First, a 0.002 mm dial gauge was clamped to the lower steel bar of the apparatus to measure the deflection at the centre of the specimen beam, from which the strain can be calculated by making certain assumptions.

Second, by using electrical resistance strain gauges. Two gauges are attached to the centre of the lower surface of the beam and connected with two dummy gauges of the same type mounted on an unloaded piece of similar rock to form a full bridge as illustrated in Fig. (7-4a). A Peekel strain gauge indicator type T-200 was used to measure the strain for the whole period of the test.

7-2.2 Size and Preparation of Specimens:

The beams were cut, ground and dried as described in section (6-1.3). The centre zone of the lower surface of the beam then manually ground by rubbing it with fine emery cloth, the actual dimensions then measured by micrometer to the nearest 0.01 mm. The central zone was cleaned by acetone to make sure that it is free of any grease. Two electrical resistance, foil type, strain gauges were bonded to this zone 20 mm apart by using (P2) adhesive. Finally, leads were soldered to active and dummy gauges and connected to the strain gauge indicator as described in section (7-1.1.6) to measure the strains.

7-2.3 Test Procedure:

7-2.3.1 Short Term Test:

The instantaneous strengths of gypsum and anhydrite in bending were found as described before in chapter (6).

7-2.3.2 Creep Test:

The beam was placed on the two supports K_3 and K_4, the leads of the strain gauges connected with the dummy gauges leads to the strain gauge indicator. The initial dial gauge and strain gauge readings were recorded. Then the upper steel bar and the platform (in case of low loading) were placed on the beam. Weights were placed on the platform or on the weight pan until the desired load was reached. A stop watch was then started, and the dial gauge and strain gauge readings were recorded. The difference between the initial and the loaded readings was considered as "instantaneous" strain. The subsequent strains produced were recorded at necessary intervals of time during the whole period of test.

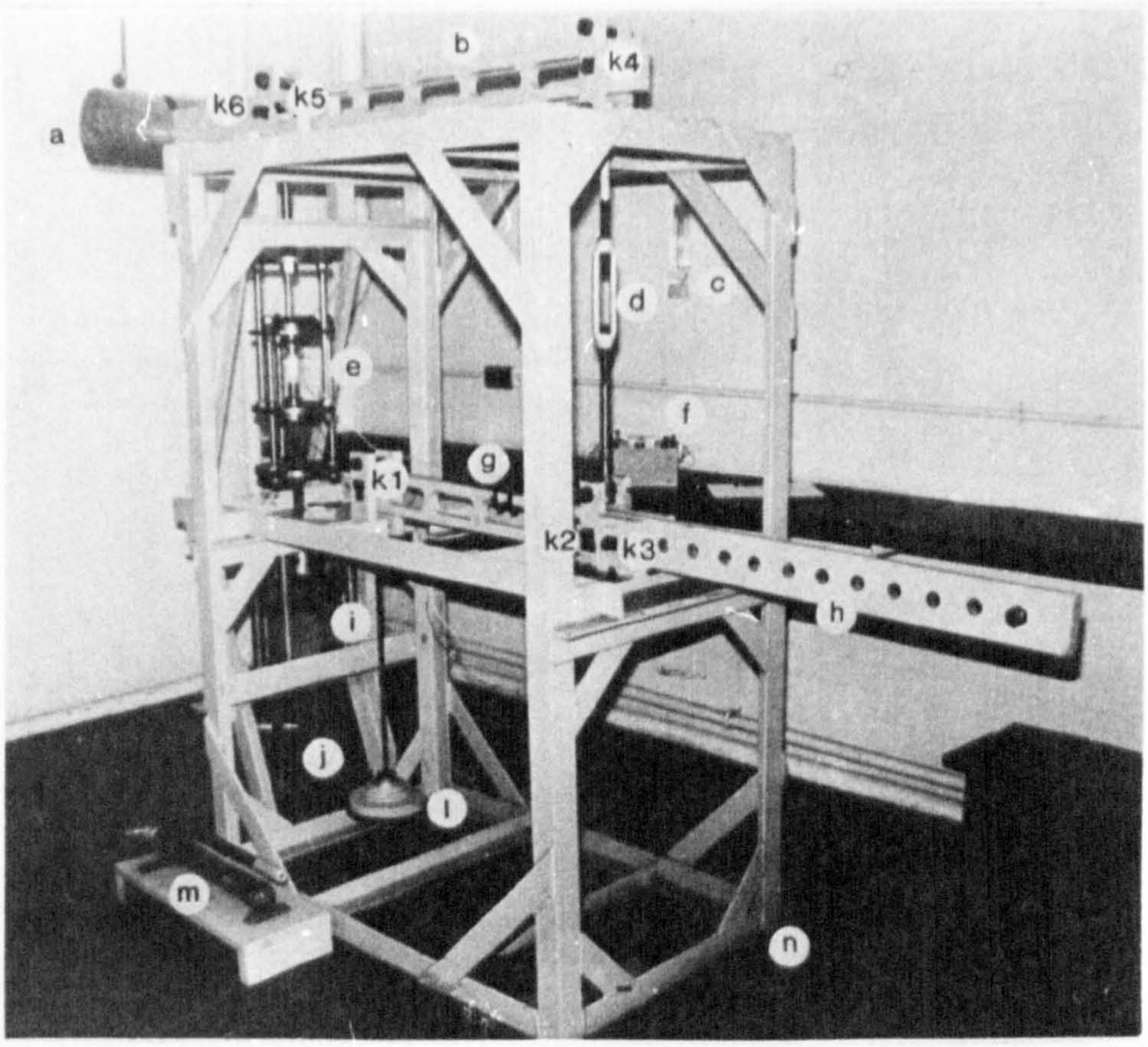

FIG. 7-1 UNIAXIAL CREEP TEST IN PROGRESS

a) Balance Weight
b) Lever No. 2
c) Thermometer
d) Turn Buckle
e) Load Reversal Jig and Specimen
f) Peekel Strain Gauges Indicator
g) Spirit Level
h) Lever No. 1
i) Spring
j) Hydraulic Jack
k_1), k_2), k_3), k_4), k_5), k_6) Knife Edges
l) Weight Pan and Weights
m) Pump
n) Angle Iron Frame and Sponge Seatings

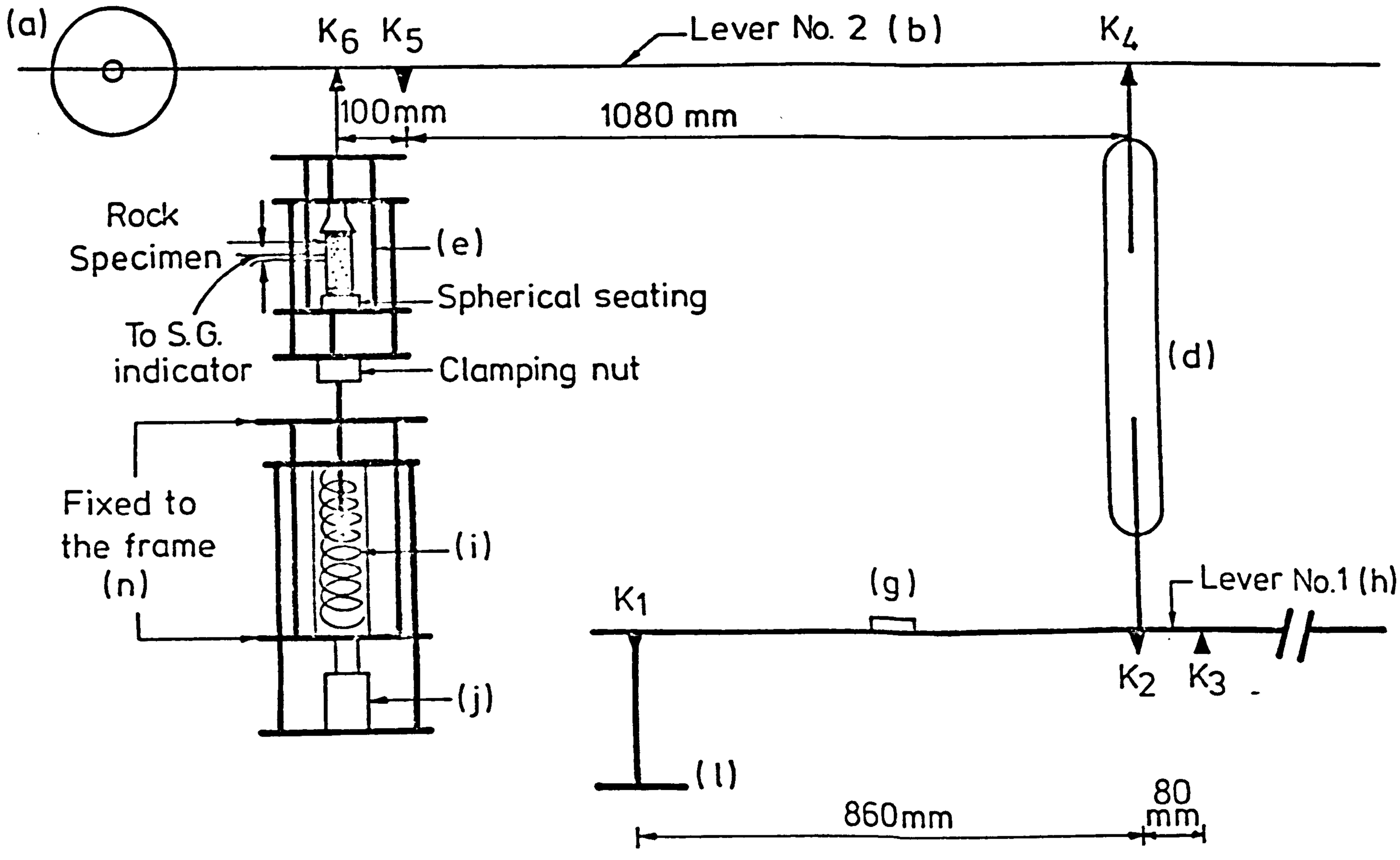

FIG.7·2 SCHEMATIC DIAGRAM OF COMPRESSION CREEP MACHINE
(FOR SYMBOLS SEE FIG.7·1)

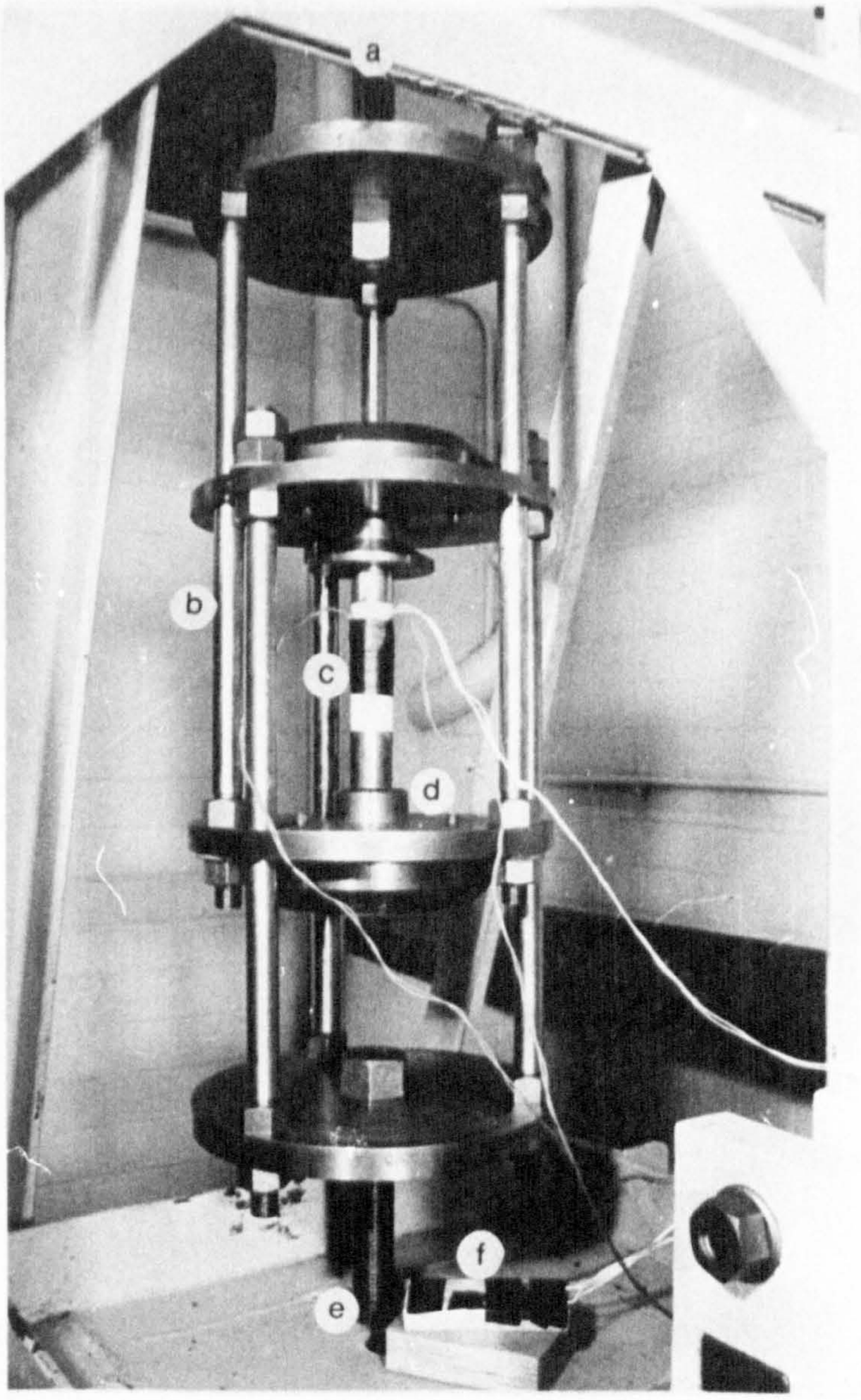

FIG. 7-3 LOAD REVERSAL JIG WITH GYPSUM SPECIMEN IN POSITION

a) Steel Rod to Knife Edge No. 6
b) Load Reversal Jig
c) Gypsum Specimen with Strain Gauges
d) Spherical Seat
e) Steel Rod to the Spring and Hydraulic Jack
f) Dummy Strain Gauges on a Piece of Gypsum

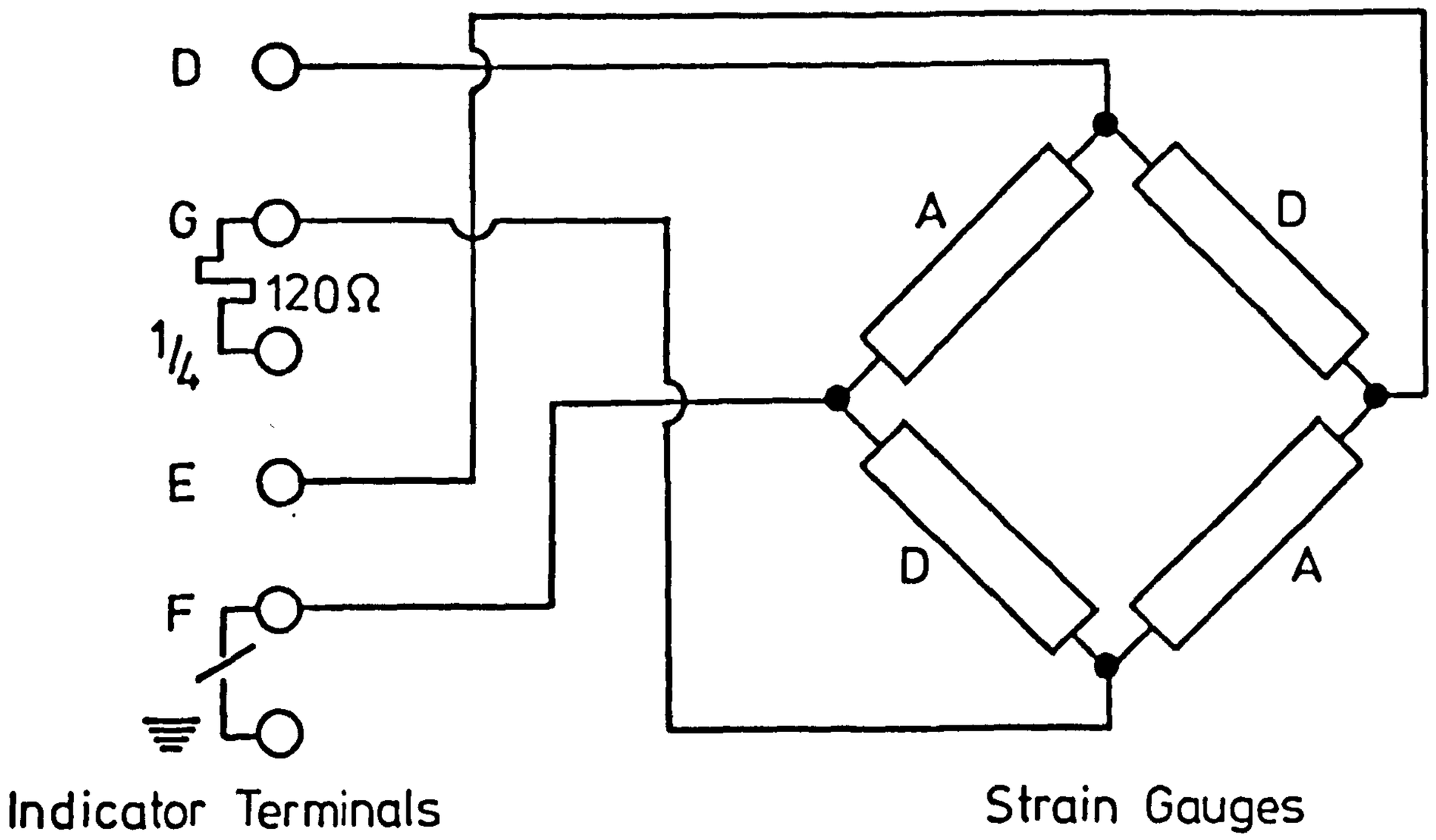

(a) Full Bridge Circuit

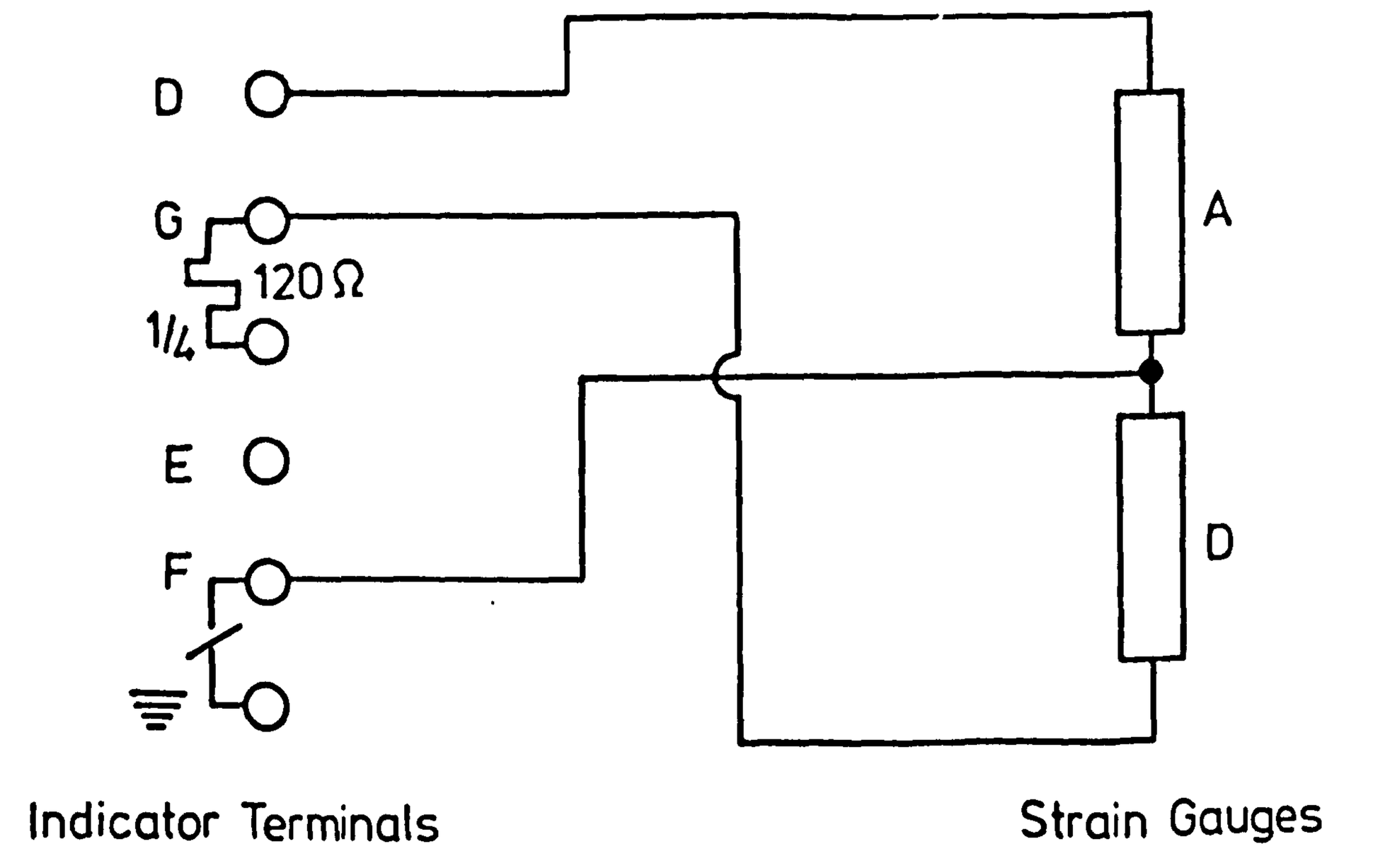

(b) Half Bridge Circuit

FIG. 7·4 CONNECTION OF STRAIN GAUGES

A. ACTIVE GAUGE
D. DUMMY GAUGE

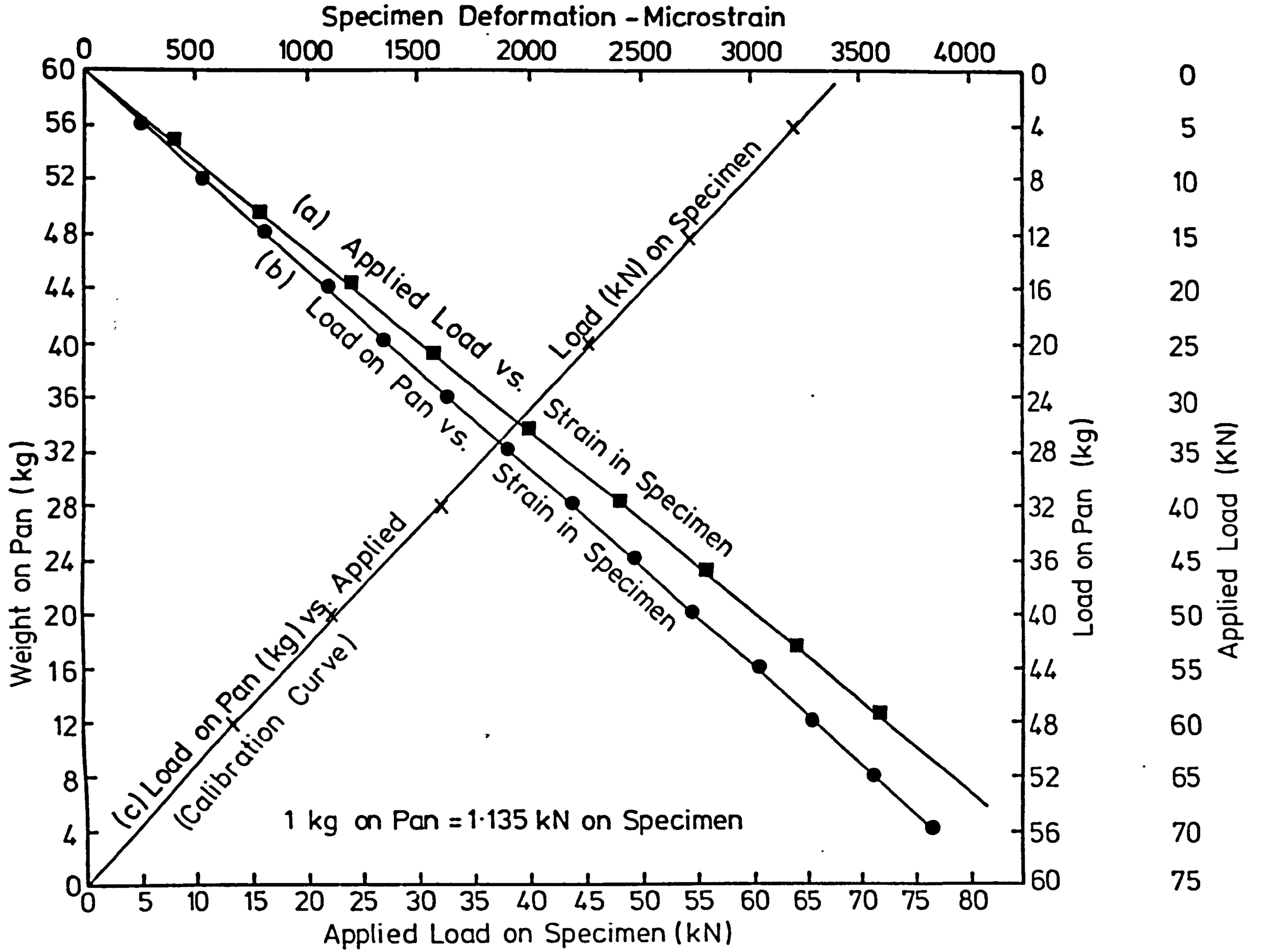

FIG. 7-5 CALIBRATION CURVE OF COMP. CREEP MACHINE

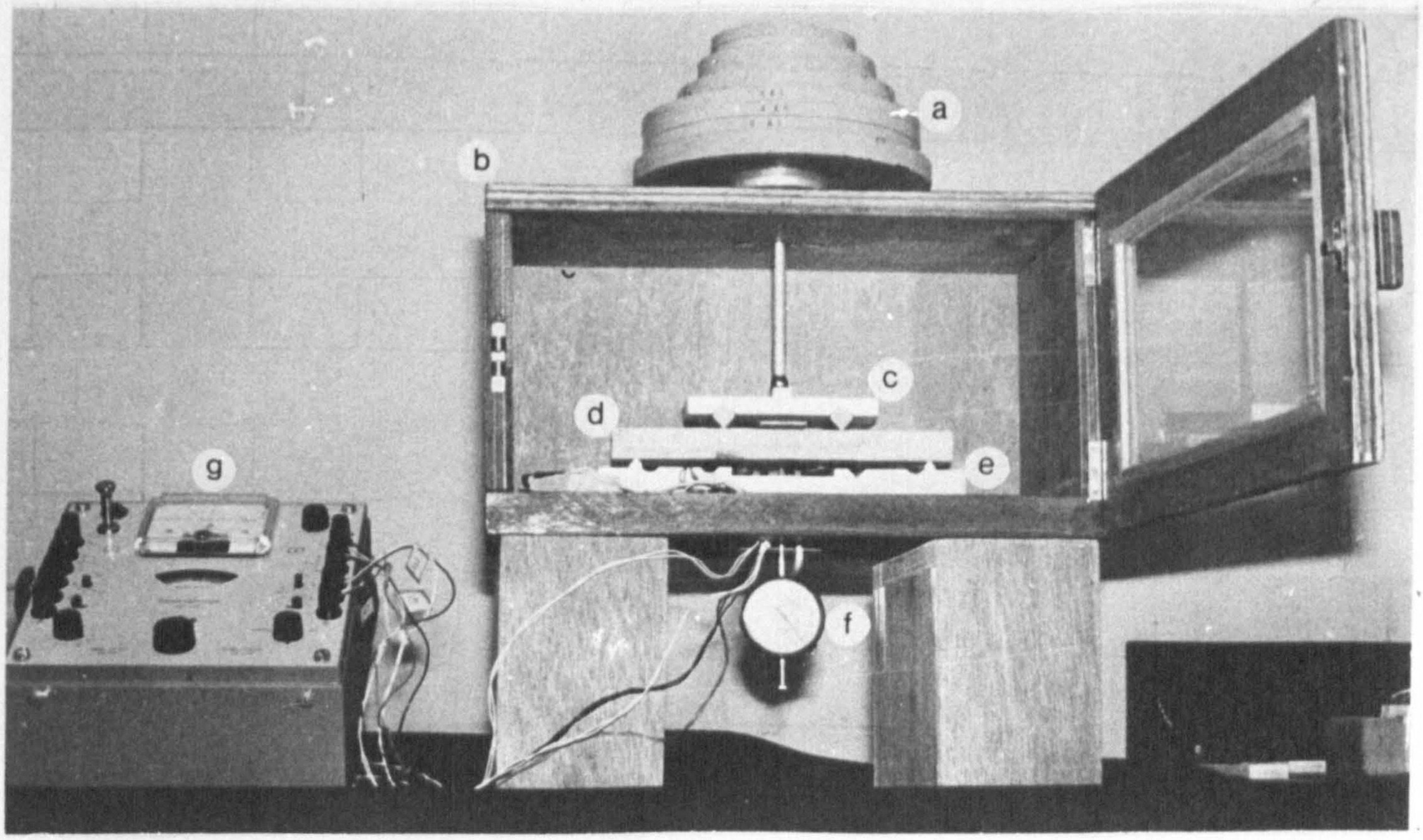

FIG. 7-6 BENDING CREEP APPARATUS WITHOUT LEVER

a) Weights and Platform
b) Wooden Box
c) Upper Steel Bar with Spherical Seat
d) Rock Specimen
e) Lower Steel Bar
f) 0·002 mm Dial Gauge
g) Peekel Strain Gauges Indicator

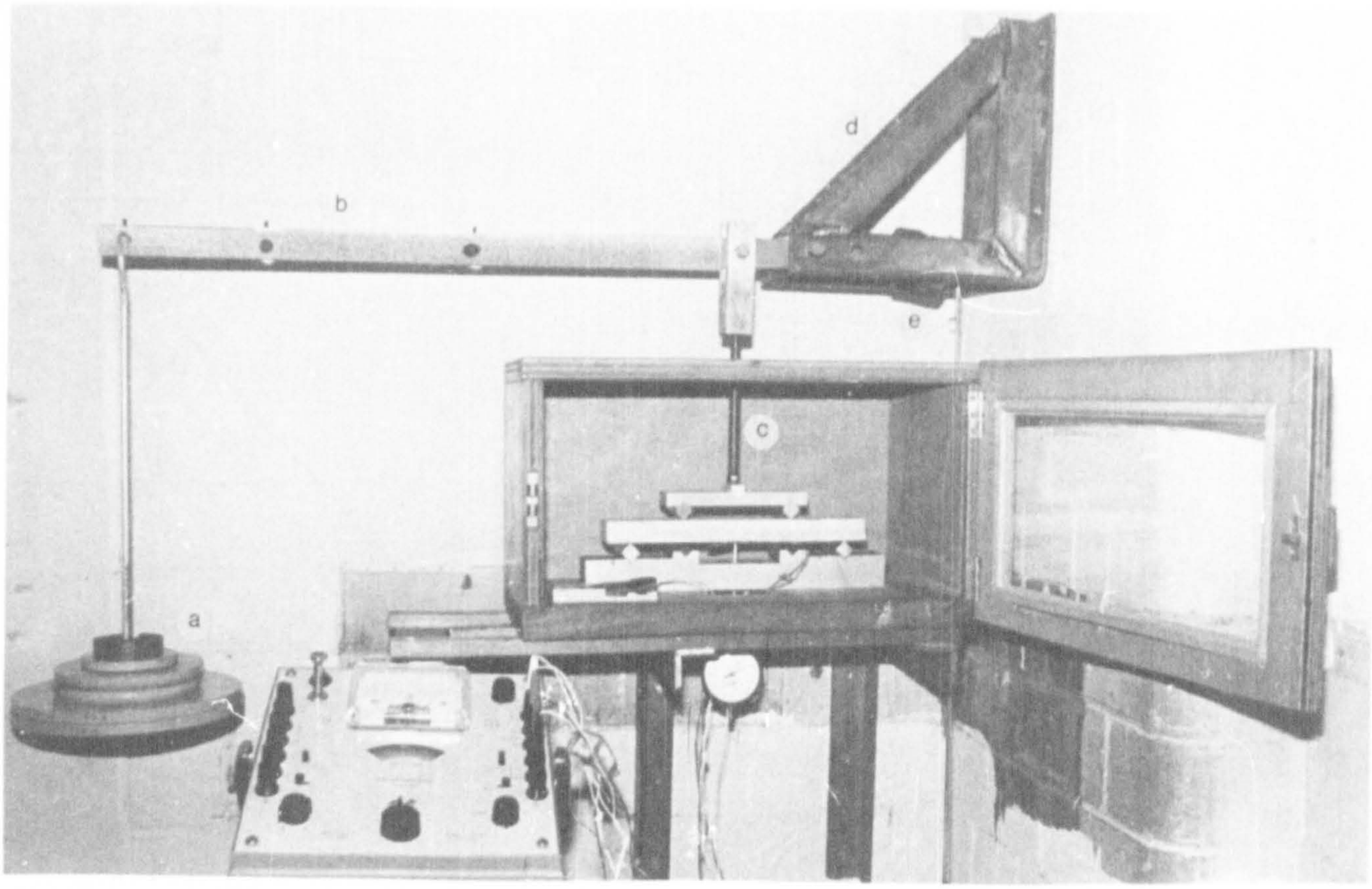

FIG.7-7 BENDING CREEP TEST IN PROGRESS WITH LEVER SYSTEM OF LOADING

a) Weights and Weight Pan
b) Lever
c) Adjustable Rod
d) Steel Frame Fixed to the Wall
e) Balance Weights

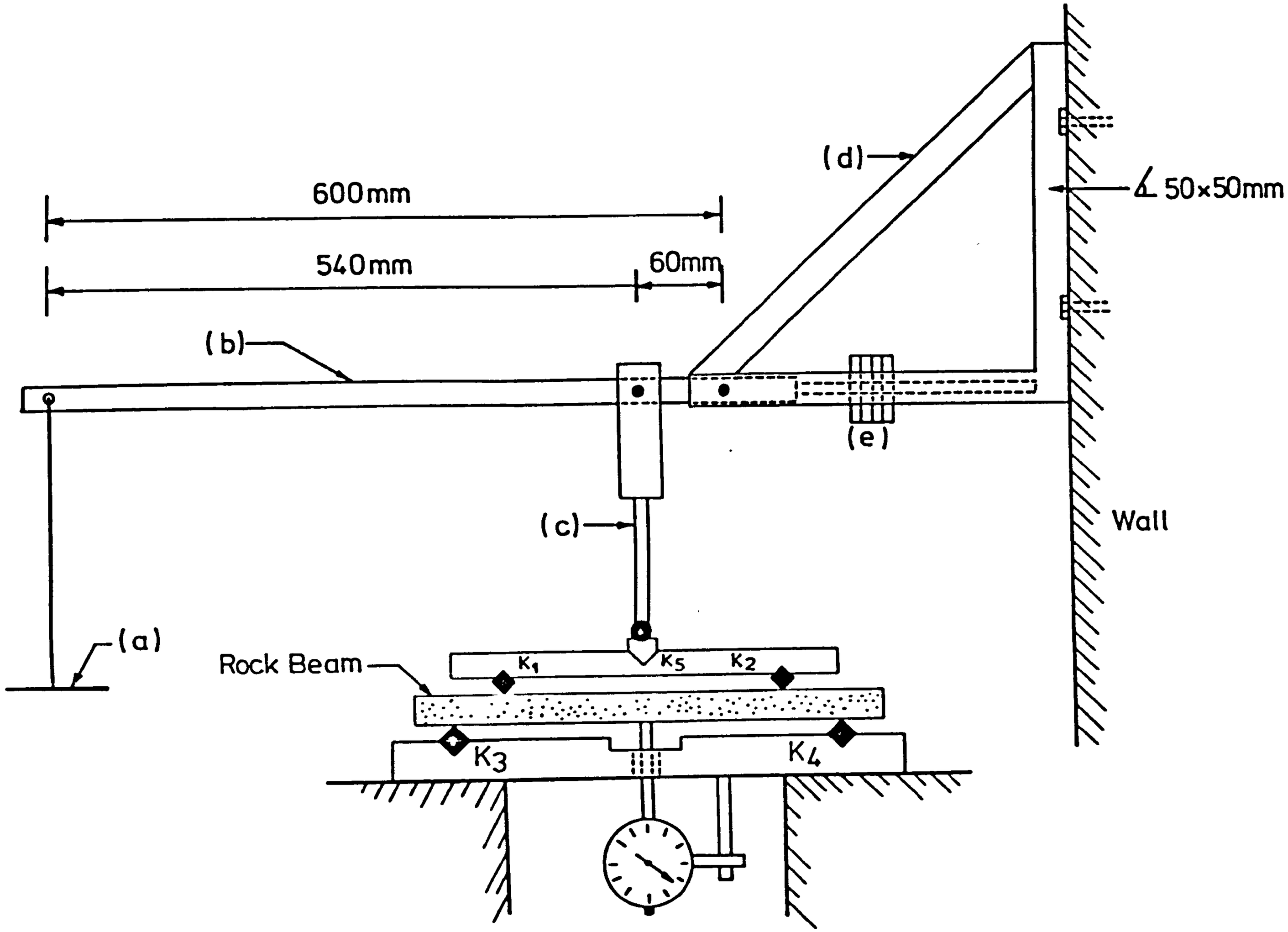

FIG 7-8 ELEVATION OF BENDING APPARATUS WITH LEVER SYSTEM OF LOADING
(For Symbols See Fig. 7-7)

Chapter 8

A NEW APPARATUS FOR EXPERIMENTAL STUDY OF CREEP IN ROCKS SUBJECTED TO TRIAXIAL STRESSES

Chapter 8

A NEW APPARATUS FOR EXPERIMENTAL STUDY OF CREEP IN ROCKS SUBJECTED TO TRIAXIAL STRESSES

8-1 Introduction:

8-1.1 General:

Much rock testing work has been carried out on a short term basis such as uniaxial, triaxial, bending, etc., whereas long term tests investigating time dependent or "creep" behaviour in rocks has been limited to simple stress systems, e.g. bending and uniaxial compression. The reason for that, maybe, the difficulties and problems associated with any long term test, and the un-availability of a suitable apparatus for carrying out the required long term combined stresses tests. One of the aims of this research was to build a new apparatus for the study of the creep properties in the more readily deformed rocks under triaxial loading. Most investigators of triaxial properties have measured the axial deformation of rock specimens by measuring externally the movement of the platens above and below the specimen, whereas in the new apparatus the axial strain of the specimen was measured within the pressure cell itself. The general layout of the apparatus is shown in the photograph, Fig. (8-1) and in the schematic diagram, Fig. (8-2).

8-1.2 Design Requirements:

Because of the nature of time dependent tests,several factors must be considered in the design of any creep apparatus. The following are the most important to be considered:

(1) Stability: The deformation measuring devices should have a high degree of stability and the applied stresses should have a negligible fluctuation, i.e. the stresses must be maintained

constant over the whole period of the test.

(2) Sensitivity: The measuring devices, within the apparatus, should be able to record any small deformation in the specimen and must also have the necessary freedom from zero drift.

(3) Independence: The apparatus must be free from difficulties due to switching off in electrical systems, power cuts, any mechanical maintenance effects, etc. It is also necessary that the apparatus would mostly operate without any attention, possibly for periods of days over weekends, holidays, etc. when safety requirements dictate that electrical motors and similar mechanical equipment cannot be left running.

The above three factors have been considered in the design of the apparatus and will be discussed later.

8-1.3 Some of The Previous Published Work Concerning Triaxial Test Methods:

Adams and Nicholson[1] in (1901) were the first who carried out triaxial tests on rocks. They found that rocks change their properties when a confining pressure is applied, so that they are no longer brittle, but behave plastically. The confining pressure was applied by placing the rock specimens in a tightly fitting steel jacket. Fig.(8-3) shows a schematic diagram of Adam's triaxial cell. The defects of using a solid confining medium, as used above, were summarized by Griggs[26] which are: (a) It is nearly impossible to measure exactly the confining pressure; (b) The confining pressure is not constant, depending on the deformation of the specimen, i.e. as the deformation increases the confining pressure increases as well; (c) The specimen is not free to fracture by shear, since a fracture would have to tear through the walls of the steel jacket. To overcome the above defects fluid was used to transmit the confining pressure to the specimen. Considere[12] in (1903) and (1906)

carried out triaxial tests on cement mortar specimen cylinders 790 mm long by 295 mm in diameter. The confining pressures on the mortar specimens were applied by water. Von Karman[83] in (1911) was the first who used fluid (glycerine) to transmit lateral pressure to rock specimens in triaxial compression tests. He used a red sandstone and Carrara marble cylindrical specimens of 40 mm diameter by 100-110 mm length within 0.1 mm thick brass jackets to prevent direct contact between confining fluid and the specimens. The axial deformation of the rock specimen was determined by measuring the displacement of the ram into the pressure cell using a dial gauge. It was Ros and Eichinger[73] in (1928) who suggested the use of rubber instead of metal jackets for the rock specimens. They used a Von Karman apparatus in carrying out triaxial tests on Carrara marble. Griggs[26] in (1936) built a triaxial apparatus, see Fig.(8-4), similar to Von Karman's but operating at confining pressures up to 13000 atmospheres. The confining pressure was measured by the change in resistance of coil of manganin wire in a special gauge within the cell. This technique was suggested by Bridgman[9]. Griggs studied the deformation properties of marble and solenhofen limestone under high confining pressures at room temperature. The deformation of the specimen was determined by measuring the movement of the upper piston in the cell by a micrometer dial gauge. He used unjacketed specimens for all tests except for two experiments where he used a drawn copper tube of 0.01 inch in wall thickness as a specimen jacket. Serdengecti and Boozer[78] in (1961) described an apparatus in which the axial load and the axial deformation were measured inside the pressure

cell and pore pressure could be applied. Heating devices were developed with the apparatus up to 300° C. They also developed a method of deforming the specimen at various strain rates in the range 10^{-3} to 10^{2} percent per second. This was done by applying the axial load hydraulically with a large hydraulic accumulator to keep the ram moving steadily forward and releasing an equalising pressure by means of a calibrated needle valve. Murrell[50] in (1962) developed a triaxial apparatus to carry out experiments on rocks. Confined compression, tension and extension tests have been carried out by him on siliceous sandstone. Both the longitudinal and the diametral strains were measured inside the pressure chamber by means of extensometers. The cell was designed to sustain a confining pressure up to 400 N/mm^2. This apparatus was used in the present research in carrying out short term triaxial tests on gypsum and anhydrite as described in Chapter (6). In 1965, Comte[11] used a triaxial apparatus similar to the one used by Griggs with the addition of heating devices. He studied the effects of temperature to 300° C, confining pressures to 1000 bars, differential stresses up to 138 bars and the effect of grain size on the creep behaviour of artificial rock-salt specimens. Hoek and Franklin[35] in (1968) developed a triaxial cell for rock testing which is capable of confining pressures up to 70 N/mm^2. The cell can be used for short term and creep triaxial tests. The axial and the diametral strains can be measured by strain gauges mounted on the specimen. Figures (8-5) and (8-6) show different parts of the cell. Full details of the design and description of the performance of the cell are given by Hoek and Franklin[35]. In this research Hoek's cell has been used in carrying out some of the

triaxial creep tests on gypsum and anhydrite. The cell was placed in the load reverser jig of the lever operated uniaxial creep machine, see Fig. (8-7). The axial load was applied in similar method to that described in section (7-1.3.3) for the uniaxial creep tests. The confining pressure was applied and controlled by a similar method to that used in the new apparatus which will be described later in this chapter. Boy[8], in (1972) developed a triaxial cell to study the strength and behaviour of concrete under triaxial stresses. The cell can accommodate a concrete specimen of 375 mm long by 150 mm diameter. He measured the longitudinal and lateral strain by LVDTs inside the pressure cell. The cell was used up to 84 N/mm^2 confining pressure.

Many other investigators have used different triaxial cells for short and long term tests all of which have used methods of operation which were common in principle to those described above.

8-1.4 General Specification:

The apparatus was designed and constructed to fulfil the following requirements:-

(1) To accommodate rock specimens 75 mm long and 25 mm diameter, nominal size.

(2) To accommodate confining pressures up to 50 N/mm^2.

(3) To provide axial stresses in the rock specimens up to 135 N/mm^2 which can be increased to 400 N/mm^2 by adding an extra axial intensifier.

(4) To maintain constant loads with the minimum of manual adjustment for the whole duration of the test.

(5) To measure the axial strain over the middle third of the specimen inside the pressure chamber.

(6) To measure the axial stress of the specimen by using a load cell inside the pressure chamber in addition to an external pressure gauge.

(7) To be able to change the axial and confining stresses separately, quickly and easily if it is required according to the nature of the test.

(8) To be as compact as possible and can be easily and safely operated by one person.

8-2 Triaxial cell:

As previously mentioned in section (8-1.4), it was decided to design a cell to accommodate rock specimens of 75 mm long by 25 mm diameter and to sustain maximum confining pressure up to 50 N/mm^2. The triaxial cell which is shown in Figures (8-1), (8-8), (8-9) and (8-10) has overall dimensions of 341 mm height by 100 mm diameter and is made from rust resisting steel No.EN.57 (British standard 970:1955). Details of the composition and mechanical properties of this steel are given in table (8-1). The cell mainly consists of:

8-2.1 Cell Body:

Figures (8-8), (8-9), (8-10c) and (8-11h) give full details of the cell body which is a hollow steel cylinder of internal diameter 64 mm to give enough clearance for the strain measurement instrumentation clamped on a 25 mm diameter rock specimen. The length of the cylinder is 228 mm to accommodate the 75 mm high rock specimen, specimen seat (load cell) and the spherical seating. The thickness of the walls was calculated according to Love[47] analysis of the stress in a hollow cylinder subjected

Table (8-1)

Details of the steel EN.57 used in the construction of the creep triaxial cell (see British Standard 970:1955)

(a) Chemical composition, The steel shall contain:

Element	Per cent	
	min	max.
Carbon	-	0.25
Silicon	0.10	1.00
Manganese	-	1.00
Nickel	1.00	3.00
Chromium	15.50	20.00
Sulphur	-	0.045
Phosphorus	-	0.045

(b) Mechanical properties:

Limiting ruling section, in.	6	2.50
Tensile strength tons/sq.in.,min.	55	55
Yield stress tons/sq.in.,min.	44	44
Elongation, percent, min.	15	15
Izod impact value ft.lb.,min.	15	25
Brinell hardness number,min.	248	248

to internal or external pressure. There is a factor of 3 between the yield stress of the steel and the design working stress. This factor is adequate and safe particularly as the apparatus will be used at maximum confining pressure for only few of the tests. An oil inlet which is shown in Fig.(8-11g) was fitted near the bottom of the cylinder. At the top and bottom ends

o-rings were fitted as oil seals in special turned grooves. The cylinder was internally ground and lapped to give a good finish.

8-2.2 Cell Head:

As shown in Figures (8-8), (8-9) and (8-10b) the head consists of a piston of 63.4 mm in diameter and an anvil of 31.7 mm in diameter which give a ratio of area of 4 to 1 so that the stress applied at the end of the anvil near the specimen is 4 times the oil pressure applied to the piston, i.e. the head itself acts as an axial intensifier. In each of the two pistons a set of two o-rings was used as an oil seal. In order to prevent any extrusion of the o-ring between the piston and its cylinder due to oil pressure a nylon backing ring was placed behind each o-ring. Similar arrangements were used in all intensifiers.

8-2.3 Cell Base:

The base as shown in Figures (8-8), (8-9), (8-10d), (8-11b) and (8-12a) is also made from rust resisting steel No. EN.57. It is fitted with twenty three insulated sockets and leads which are carried through the base via an epoxy resin sealed hole enabling external connections to be made to the strain gauges mounted on the load cell and the LVDTs around the specimen inside the pressure cell. The number of sockets fitted to the base is more than were required for the purpose of this work, so more parameters may be measured in the future tests, e.g. the lateral strain in the specimen.

8-2.4 Specimen Seat (load cell):

The specimen seat which is shown in figures (8-8), (8-9), (8-11c) and (8-12b) is made from tempered creep resisting steel No. EN 26 (British Standard 970:1955). Details of the composition and mechanical properties of this material are given in table (8-2).

The seat is of top-hat shape upon which the rock specimen stands. It was designed to be used as an axial stress measuring device. Although the load on the specimen is readily obtained from the measured gas pressure (as will be discussed later) and the known magnifying ratio through the axial intensifiers some frictional losses are expected in both the operation of the intensifier

Table (8-2)

Details of the steel EN.26 used in the construction of the specimen seat (load cell) of the creep apparatus.(see British Standard 970:1955).

(a) Chemical composition, the steel shall contain:

Element	Per cent	
	min	max.
Carbon	0.36	0.44
Silicon	0.10	0.35
Manganese	0.50	0.70
Nickel	2.30	2.80
Chromium	0.50	0.80
Molybdenum	0.40	0.70
Sulphur	-	0.050
Phosphorus	-	0.050

(b) Mechanical properties:

Limiting ruling sec.,in	4
Tensile strength, tons per sq.in.,min.	80
Yield stress, tons/sq.in., min.	68
Elongation, per cent, min.	14
Izod impact value, ft.lb., min.	25
Brinell hardness number	415

pistons and at the oil seal at the point of entry of the loading ram into the pressure cell. These losses can be readily measured by a suitable calibration method, (will be described later) but it was felt that over long periods under pressure, changes in such effects due to "welding" of the oil seals to the steel surfaces or possible an improved lubrication due to oil penetration were possible. This uncertainty is overcome by designing the specimen seat to be used as an internal load cell. The measuring zone of the seat being tubular, is fitted with 8 foil strain gauges, see Fig.(8-12b), four of which are vertical and four horizontal. They are connected in series pairs to form a full bridge circuit giving temperature compensation. The load cell was calibrated before use, and loaded over long time periods to check for any drift. The method and the curves of calibration will be given later in this chapter.

8-3 Pressure Control System, Fig.(8-13):

8-3.1 Pressure Source and Gas Lines:

Commercially available cylinders of compressed nitrogen were used as a suitable power source, the cylinders being connected to the gas pipes via a high pressure hose, Fig.(8-13a). High pressure 0.5 inch outside diameter steel pipes were used in the system, all the joints and connections were of the nut and olive fittings types.

The nominal pressure of the nitrogen in a full bottle is 2000 psi, the existing pressure can be checked at any time by the pressure gauge (c). Several shut-off and blow-off valves (b) are provided for the relief of excess pressure when required.

The compressed nitrogen passes through a filter (d) (I.V. Pressure Controllers, Ltd., Feltham, Middlesex) of maximum capacity 40 N/mm^2 (6000 psi) to ensure that scale and other foreign

matter does not affect the operation of the system.

8-3.2 Pressure Control and Relief Valves:

The filtered nitrogen then passes through one of two automatic control valves (I.V. Pressure Controllers, Ltd.), valve (f) for the axial pressure and (e) for the confining pressure. Each valve is an automatic device which maintains gas pressure constant on the output side provided that the input pressure is in excess of the required output. The valves are spring loaded devices the output pressure being controlled by screwing or unscrewing the end dome. Any excess pressure can be relieved via one of the blow-off valves (b). In the confining pressure subsystem it was found necessary to add an automatic blow-off valve, (relief valve), (g) which is a variable pressure setting device (I.V. Pressure Controller Ltd.) adjusted to operate at a pressure slightly above the required gas pressure. This becomes necessary when possible rapid deformation of the rock specimen, under high axial stress, results in the steel axial ram entering the pressure cell so displacing the confining pressure oil and generating pressures in excess of that required in the control system. The range of this valve is 2 to 7 N/mm^2.

8-3.3 Pressure Gauges:

Several pressure gauges (Budenberg Gauge Co.Ltd., Broadheath, Manchester) were used in the system where necessary:

1. Nitrogen bottle gauge, Fig.(8-13c).
2. Axial gas pressure gauge (h) which can be used to determine the axial stress on the rock specimen by considering the known dimensions of the axial intensifiers and some frictional losses in the oil seals.
3. Confining gas pressure gauge (i) which is used in

a similar way to gauge (h) on the confining pressure sub-system side.

4. Confining oil pressure gauge, Fig. (8-1j), which gives directly the confining pressure in the pressure cell and can be used as a check on the behaviour of the confining pressure intensifier, Fig.(8-1k).

8-4 Measuring Systems:

8-4.1 Stresses:

As it mentioned previously, in any creep test all the stresses must be kept constant in magnitude and direction during the whole period of the test. In this research two stresses were dealt with, the axial stress and the lateral (confining) stress.

8-4.1.1 Axial stress:

The maximum pressure which can be used from the nitrogen bottle is about 10 N/mm^2, and in order to produce higher pressures, intensifiers have to be used. These simply consist of a pair of high pressure cylinders with a double-ended piston, by means of which a low pressure is multiplied by the ratio of the piston areas. Two intensifiers were used, the first, figures (8-1m), (8-2m), (8-8) and (8-10a) gives a magnification ratio of 2.25 to 1, while the second which is within the cell head, see section (8-2.2), gives a ratio 4 to 1, so the two intensifiers give a 9:1 pressure increase from gas pressure to the end of the steel anvil near the specimen in the pressure cell. Due to the difference in areas between the steel anvil (31 mm diam.) and the rock specimen (25 mm diam.) the stress in the specimen was increased by about 1.5 times. The accurate total magnification factor was found by calibration the apparatus which will be described later in this chapter.

8-4.1.2 Lateral Stresses:

The two minor principal stresses (σ_2 and σ_3) in all the experiments were equal to the confining pressure, this being measured directly by means of the pressure gauge (j) in figures (8-1) and (8-2).

In order to obtain the required confining pressure, (up to 30 N/mm^2) in the pressure cell from the maximum available pressure in the nitrogen bottle another intensifier was used, see figures (8-1k), (8-2k) and (8-8) which gives an increase of 4.7:1 in the pressure from the gas side to the oil in the pressure cell. Another pressure gauge (i), Fig. (8-13), was used on the gas side of the confining pressure sub-system as a check gauge on the behaviour of this intensifier (k). The confining pressure was kept constant by means of the automatic control valve (e) and the automatic relief valve (g), Fig.(8-13), as already described in section (8-3.2).

8-4.2 Longitudinal Strain:

In order that the effects of frictional contact between the steel platens and the rock specimen are eliminated from the strain results, it is necessary to confine measurement to portions of specimen remote from the sample ends. In this research measurement was restricted to the middle third of the specimen. For this reason the axial strain measuring devices were installed on the sample inside the pressure cell. Three Linear Variable Differential Transformers (LVDT's) manufactured by Sangamo Weston Control Ltd. of North Bersted, Sussex, U.K. mounted on the specimen were used to measure the longitudinal strain.

The transducers employed were of the type classed as linear variable differential transformers. Each consists of two parts,

a cylindrical tube containing two sets of windings, a primary and a secondary and a core which is in the form of a thin brass tube containing a short length of sintered dust-iron core at one end, this being inserted into the windings section. The secondary winding is split into two halves one each side of the primary and these are differentially wound. When the core is centrally situated in the windings and the primary is fed with alternating current (5 KHz) from an oscillator the secondary produces no signal. Movement of the core changes the electromagnetic interaction between the primary and each half of the secondary in such a manner that a secondary output is produced which is linearly related to the core displacement. Essentially, therefore, the LVDT is a displacement transducer which is suitable as a strain measuring device when installed over a known gauge length.

The technique of using these transducers satisfies the following conditions:

1. The ability to measure very small deformation down to 2 microstrain, which is necessary in creep tests.
2. Stability over long periods of time which is necessary in creep tests as was mentioned previously in the design requirements, sect. (8-1.2).
3. Insensitivity to environmental changes of temperature and confining pressure.
4. Easy mounting of the transducer on the specimen due to its separate armature assembly.
5. Small overall size, especially important in triaxial cells.

The three LVDT's were spaced at 120^{o} intervals around an annular steel ring, Fig.(8-14c), which is clamped by three steel

pointed grub screws to the specimen, figures (8-15) and (8-16). The LVDT cores are attached to spherical mountings on a similar steel ring, figures (8-14b) and (8-16), similarly clamped to the specimen at a gauge length of (25) mm, figures (8-15) and (8-16).

A special set of jigs was designed and constructed, Fig. (8-14a) in order to initially mount the transducers correctly on the specimen, figures (8-15) and (8-16). The LVDT's were connected together via a balancing circuit, Fig.(8-15b) mounted within the pressure cell. Fig. (8-17) shows the connection circuit of the transducers between themselves and to the transducer multimeter (C52/5). Table (8-3) gives information about all resistances connected to each transducer (TDR). The combined output of the transducers being obtained by leads, Fig.(8-15g), to the sockets in the cell base. The displacement readings are then obtained by the use of a Sangamo Weston C52/5 transducer multimeter which is a combined 5 KHz oscillator and output meter containing further balancing, amplification and attenuation circuits, Fig. (8-1r).

Table (8-3).

Resistances connected to transducers.

Transducer Serial No.	R_2 0.1%	R_3 2%	R_4 2%	R_5 2%
TDR 1	5.0 kΩ +1.0 kΩ	68 kΩ	120 kΩ	330 kΩ
TDR 2	5.0 kΩ	27 kΩ	47 kΩ	560 kΩ
TDR 3	5.0 kΩ	33 kΩ	330 kΩ	-

In the case of a few experiments when high axial stress was applied and failure was expected at any time, a pen recorder manufactured by Record Electrical Co.Ltd., of Altringham, Cheshire, U.K. was connected to the transducer multimeter, Fig. (8-1s) to record the time and the displacement on a special graphic chart. Calibration of the transducers was performed as described in Sect. (8-5.3), before any test was carried out.

8-5. Calibration of the Apparatus:

Before any creep experiments were carried out the load cell and the transducers were calibrated and the friction forces between the moving parts at the oil seals were determined.

8-5.1 Calibration of the Load Cell:

The load cell (specimen seat) was loaded by the Avery Testing machine up to 100 KN. by increments of 10 KN., the output of the strain gauge bridge was read on a strain gauge indicator. The cell was further tested under confining pressures to check the effect of the confinement on the strain gauges. Fig.(8-18) shows the calibration of the load cell. Loads were also applied to the cell for periods up to two weeks to check drift in the gauge outputs and/or creep in the cell material. The results obtained indicated that the behaviour of the cell was extremely stable.

8-5.2 Calibration of Intensifiers for Friction Effects:

The two axial intensifiers give a theoretical increase in pressure of 9:1 between the end of the anvil near the specimen and the gas pressure. Because of friction losses in the oil seals of the intensifiers and the anvil entering the pressure chamber, and the difference between the ram and the rock specimen cross-sectional areas, it was necessary to calibrate the apparatus

to find the actual ratio between the axial load gauge gas pressure reading (bar) and the applied load on the specimen (KN). A 75 mm high by 25 mm diameter duralumin specimen was placed on the load cell (specimen seat) of the creep apparatus and tested in an Avery Testing Machine, a curve was plotted of load applied to the specimen versus the output of the strain gauges set on the load cell as shown in Fig. (8-19a), this curve is similar to the curve of Fig.(8-18). Afterwards the duralumin and the load cell were placed in the creep apparatus and another curve was plotted of the axial gas pressure gauge (Fig.8-1h) versus the output of the strain gauges on the load cell, Fig. (8-19b). These two curves give separate linear relationships on the graph. As in the two graphs the output of the strain gauges set of the load cell is common, this forms a basis of comparison between the axial load applied to the specimen in KN's and the axial gas pressure gauge reading in bars. A third line, Fig. (8-19c), was plotted to show this linear relationship which is the apparatus calibration curve. It was found from this that to apply one KN on the specimen the reading on the axial pressure gauge should be 1.448 bar. A relationship between the required axial stress in the rock specimen, the confining pressure and the upper (axial) gas pressure gauge reading was found as follows:

Let:

A_s : Specimen cross-sectional area, mm^2

σ : Required axial stress in the specimen N/mm^2

P : Confining oil pressure, N/mm^2

R : Axial gas pressure gauge reading, bar (gauge (h) in Fig. (8-1)).

A_r : Ram cross-sectional area, mm^2 (which enters the pressure cell).

1. The load on specimen = $(A_s)(\sigma)$, N.

2. Upward force due to the effect of confining pressure on the difference between the ram and specimen areas will equal to $(A_r - A_s)(P)$, N.

3. Total applied load must be = $A_s . \sigma + (A_r - A_s).P$.

4. From the calibration curve

$$R = (1.448)(\text{Applied load in KN})$$

$$\therefore R = (1.448)\{ A_s . \sigma + (A_r - A_s) . P\} \times 10^{-3}$$

$$R = (A_s . \sigma + A_r . P - A_s P)(1.448)(10)^{-3}$$

$$R = \{ A_s(\sigma - P) + A_r . P\} (1.448)(10)^{-3} \qquad (8\text{-}1)$$

As the diameter of the ram equals 31.7 mm therefore, A_r = 789.24 mm^2. Substituting this value of A_r in equation (8-1) and simplifying the new equation we get

$$R = [1.448\ A_s.(\sigma - P) + 1142.82\ P] \times 10^{-3} \qquad (8\text{-}2)$$

In applying any required axial stress to a rock specimen under confining pressure either of the two methods described in sections (8-5.1) and (8-5.2) can be used. In the first method, the axial pressure control valve is operated to apply the load to the specimen until the corresponding strain gauge output of the load cell, which is pre-determined from the curves of Fig. (8-18), to the required axial stress is read on the external strain gauge indicator, Fig.(8-1q). In the second method, the equation (8-2) is used to determine the pressure reading (R) which gives the required axial stress (σ) under the confining pressure (P). The axial control valve is then adjusted until the required axial gas pressure gauge reading (R) is reached. In practice the second method was used to give the first

adjustment and the load cell was used to provide the final check. During the progress of a test both the axial gauge and the load cell output were monitored to ensure correct functioning of the apparatus.

8-5.3 Calibration of the Strain Measurement Transducers:

On receipt, each transducer had been inspected and calibrated by the manufacturer (Sangamo Weston Controls Ltd.). Table (8-4) gives the inspection certificate and the calibration details provided. After the three transducers were connected via balancing circuit as mentioned previously in section (8-4.2), it was found necessary to calibrate the new combination.

The three transducers and their corresponding cores were assembled on the annular rings at a gauge length of 1 inch. The assembly was placed between the Clock house machine platens with a 0.001 inch dial gauge fixed between them to measure the displacement. The balancing circuit of the transducers was connected to the (C52) transducer multimeter and a graph was plotted of the reading of the (C52) multimeter versus the movement of the platens recorded by the dial gauge. The total movement was (0.1) inch which gave full scale on the multimeter scale. Fig. (8-20) shows the linear relationship between the displacement of the annular rings and the output of the transducer multimeter.

8-6 Preparation of Rock Specimens:

The rock specimens were prepared in a similar manner to that described in section (6-2.2). The specimens were jacketed in a P.V.C. tube, the ende of which extended over two steel platens where o-rings are used, see figures (8-12) and (8-15d), to prevent the access of the hydraulic oil to the specimen. Since the screws of the two annular rings are required to penetrate the

Table (8-4)

Inspection certificates of the transducers.

Transducer type: A1/0.1" MOD

Calibrated range ± 0.100"

Excitation : 5 volts. AC @ 5 KHz

Calibration load: As supplied, ohms

Sensitivity: 1.6 mv/v/0.001"

Calibration details

Transducer No.	Armature in (from zero)		Armature out (from zero)	
	Displacement in	Output	Displacement in	Output
TDR1	0.100	9990	0.100	10000
	0.075	7501	0.075	7511
	0.050	5000	0.050	5003
	0.025	2496	0.025	2496
TDR2	0.100	10020	0.100	9990
	0.075	7515	0.075	7505
	0.050	5005	0.050	5000
	0.025	2500	0.025	2500
TDR3	0.100	10015	0.100	10005
	0.075	7515	0.075	7515
	0.050	5008	0.050	5005
	0.025	2504	0.025	2500

PVC jacket on the rock specimen, oil may possibly penetrate at these points. This difficutly has been overcome by sliding 0.05 mm thick feeler strip between the jacket and the specimen. The feeler strip is strong enough and ductile that the screws do not penetrate it, and at the same time the PVC jacket makes a good seal against the polished strip. Finally, the strain measurement assembly was clamped to the specimen, as described previously in section (8-4.2), before insertion into the cell.

8-7 Test Procedure:

8-7.1 Short Term Test:

Triaxial compression short term tests were carried out on gypsum and anhydrite specimens to find their instantaneous triaxial compressive strengths. These were described in Chapter 6. Different percentages of these strengths were then used in several series of triaxial compression creep tests.

8-7.2 Creep Test:

Following the preparation of rock specimen, section (8-6), the leads from the transducers are plugged into the base sockets and the sample is located on its seat (load cell). The apparatus is then filled with hydraulic oil, suitable bleed plugs, figures (8-8) and (8-9), being provided to ensure no air locks exist in the pressure cell. The transducer meter is then switched on to be warmed for ten minutes in order to ensure stable operation. The multimeter is connected to the pen recorder when necessary.

To apply the desired load to the specimen under a given confining pressure, the reading on the axial pressure gauge corresponding to the load required was calculated by equation (8-2). Also the corresponding output of the strain gauges on

the load cell was found from the calibration curve, Fig.(8-18).

Initial (zero) readings are taken from the instruments indicating load and displacement and by operation of the gas pressure control valves, the confining pressure and the axial load are in turn increased to the required values. A check is made of reasonable correspondence between the axial load calculated from the gas pressure and the load indicated by the internal load cell and between the gas pressure and direct oil pressure in the confining pressure sub-system. The amount of deformation recorded during the time of loading gives the instantaneous deformation (strain). Further strain readings are then obtained according to a pre-arranged timetable to obtain time dependent or "creep" behaviour of the rock specimen. Checks are made from time to time on the behaviour of the confining pressure and axial load systems. Apart from some small initial fluctuations probably due to temperature changes resulting from sudden large gas pressure changes, the pressure control systems were found to be reliable in maintaining loading conditions.

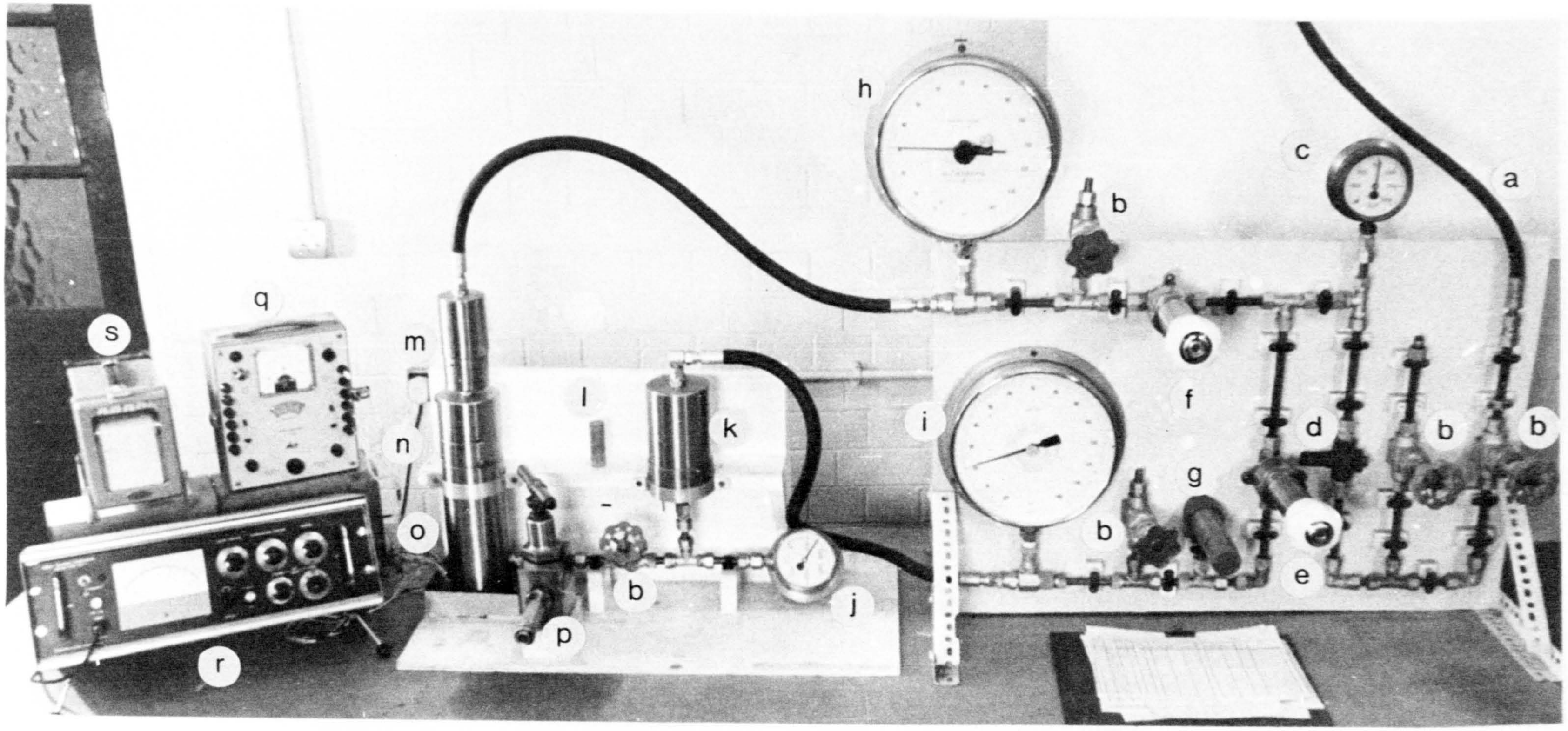

FIG. 8-1 TRIAXIAL CREEP APPARATUS

a. To nitrogen bottle
b. Shut off valve
c. Nitrogen bottle pressure gauge
d. Filter
e. Confining pressure control valve
f. Axial pressure control valve
g. Automatic relief valve
h. Axial pressure gauge (N_2)
i. Confining pressure gauge (N_2)
j. Confining pressure gauge (oil)
k. Confining pressure intensifier
l. Rock specimen
m. Axial load intensifier
n. Pressure cell head
o. The cell
p. Oil inlet valve
q. Strain gauge indicator
r. Transducer multimeter
s. Graphic recorder

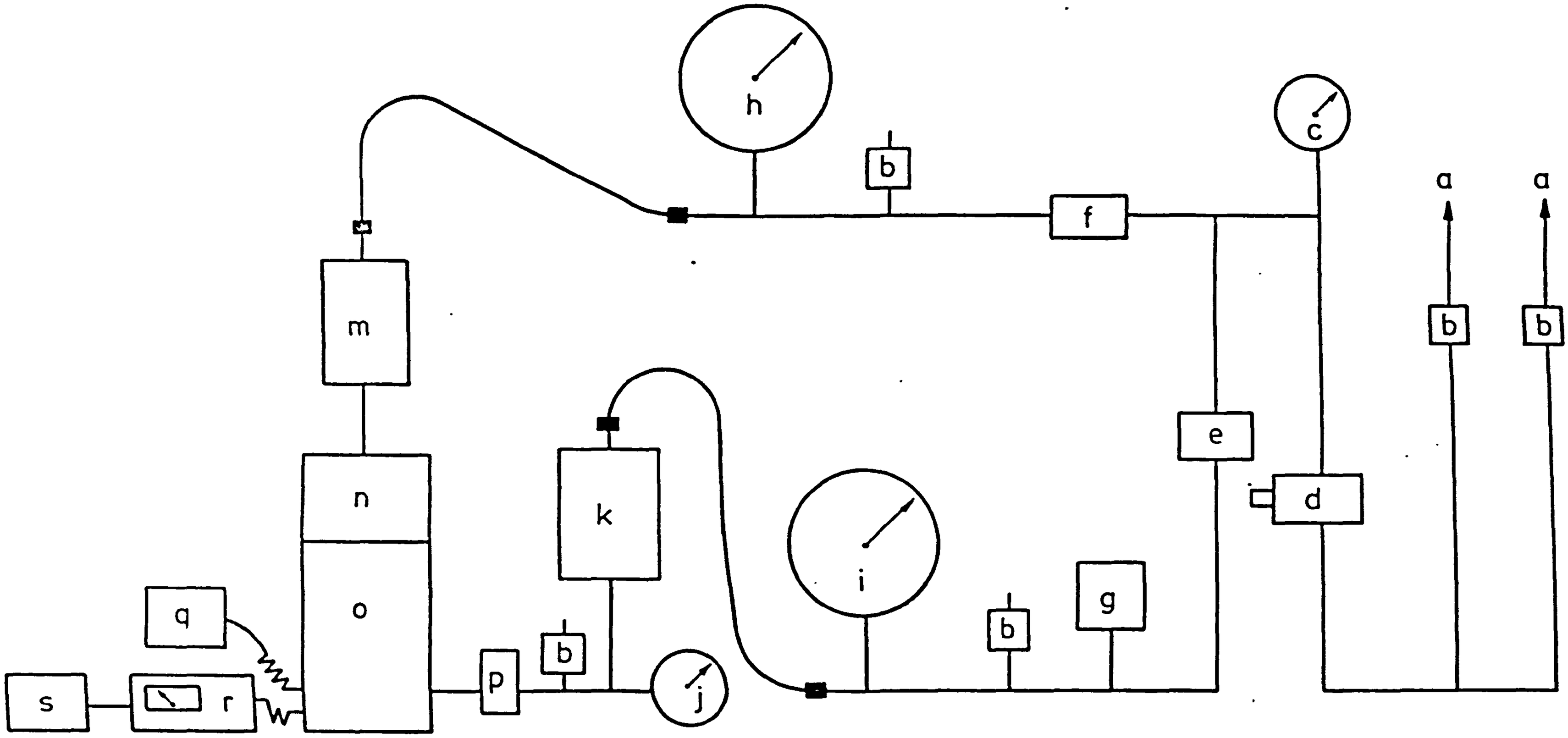

FIG 8-2 SCHEMATIC DIAGRAM OF CREEP APPARATUS

(For Symbols see Fig 8-1)

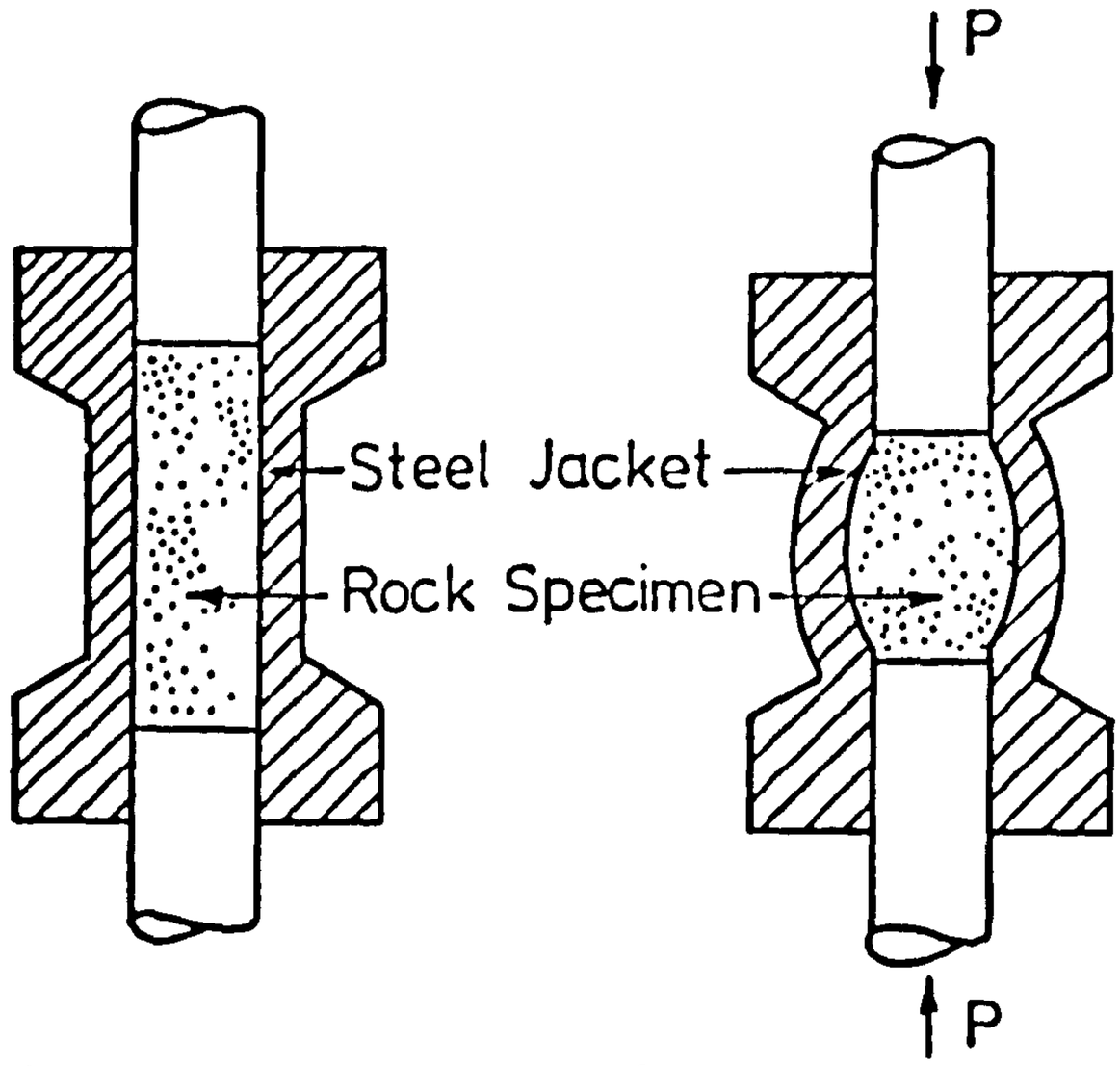

FIG. 8-3 SCHEMATIC DIAGRAM OF ADAM'S TRIAXIAL CELL

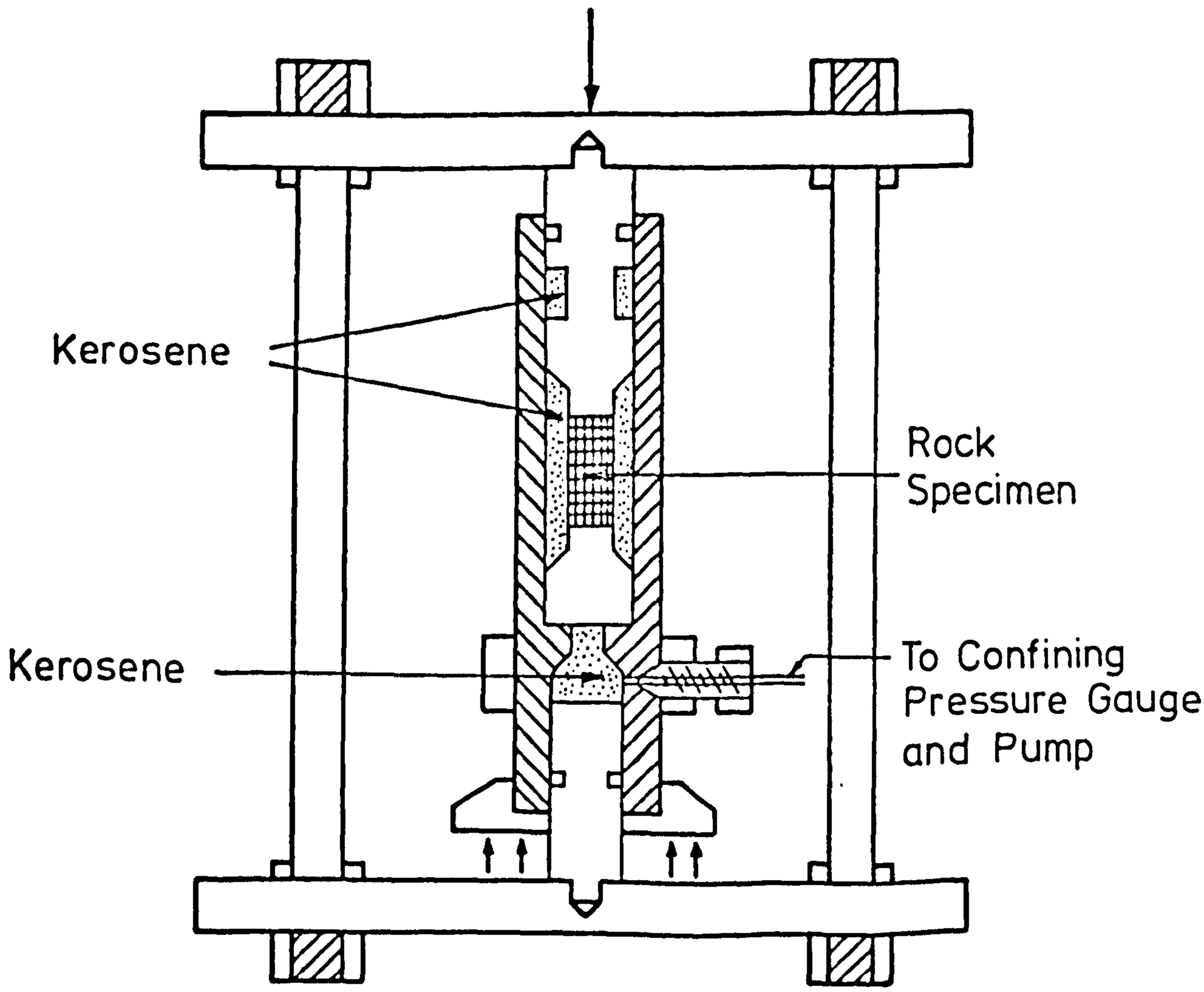

FIG. 8-4 SCHEMATIC DIAGRAM OF GRIGGS TRIAXIAL APPARATUS

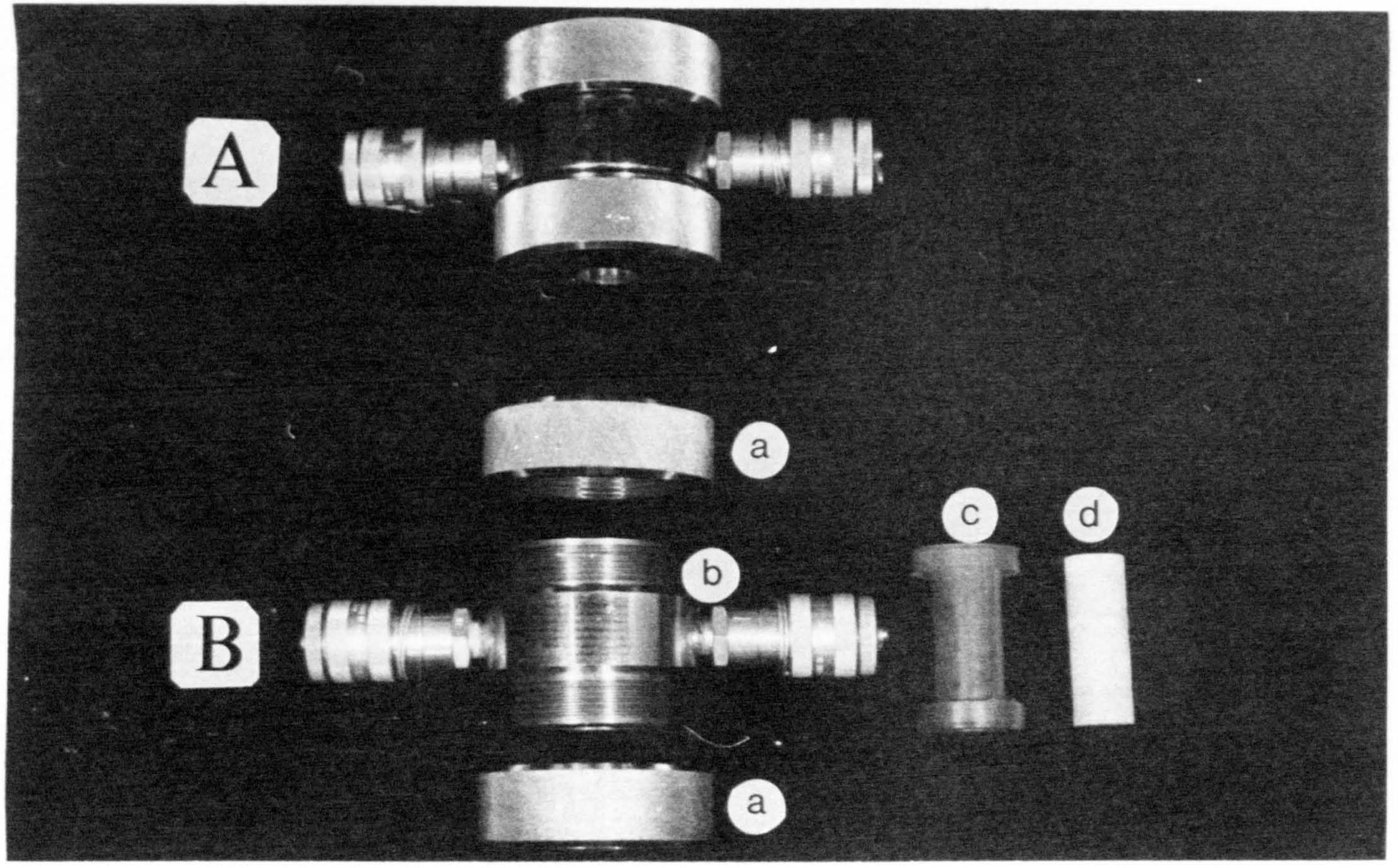

FIG. 8-5 HOEK AND FRANKLIN TRIAXIAL CELL

A: Assembled

B: Exploded

a) End Cap
b) Cell Body
c) Rubber Sealing Sleeve
d) Rock Specimen

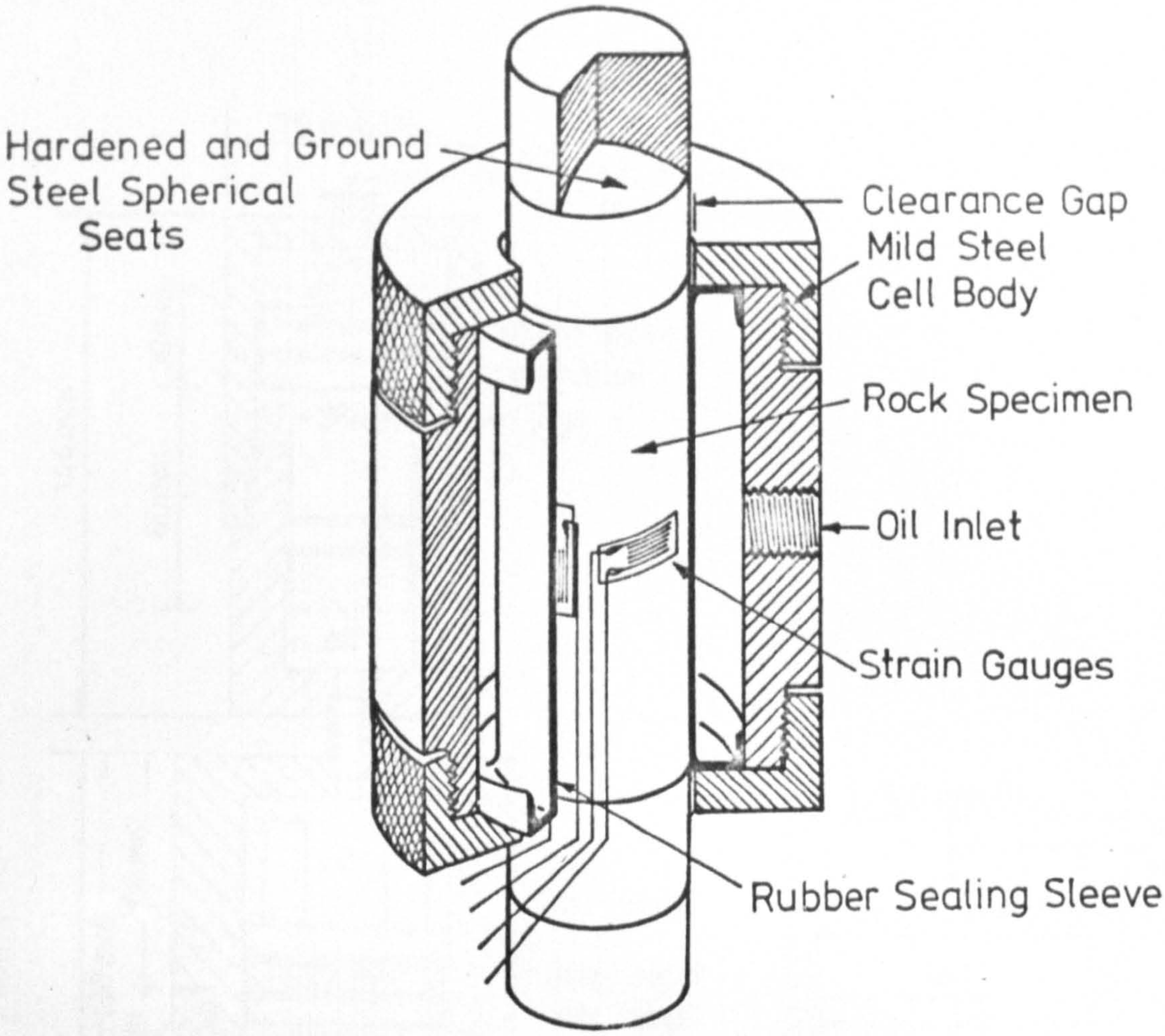

FIG. 8-6 CUTAWAY VIEW OF HOEK'S TRIAXIAL CELL

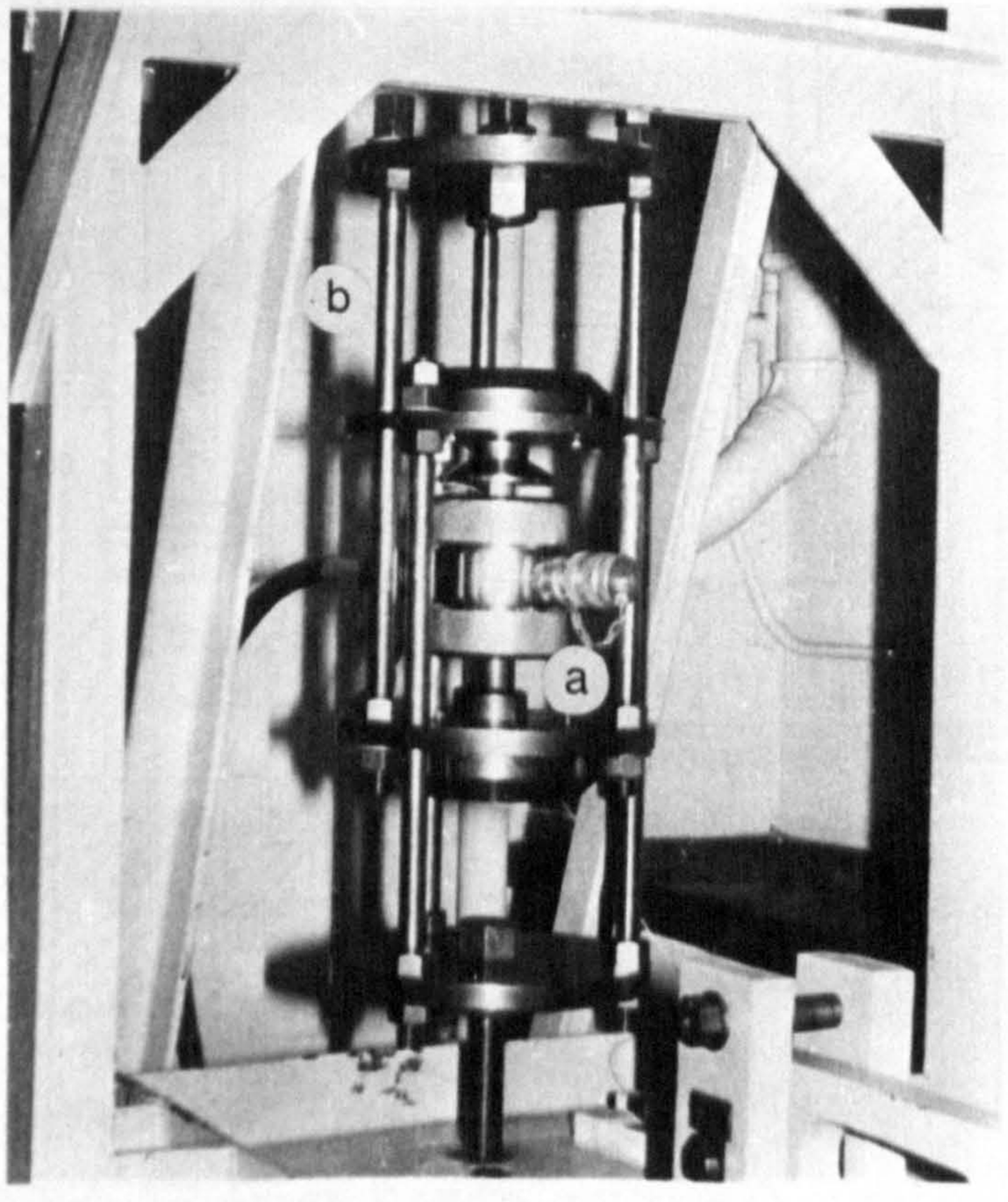

FIG. 8-7 HOEK'S CELL IN THE CREEP MACHINE

a) The Cell
b) Load Reverser of the Creep Machine

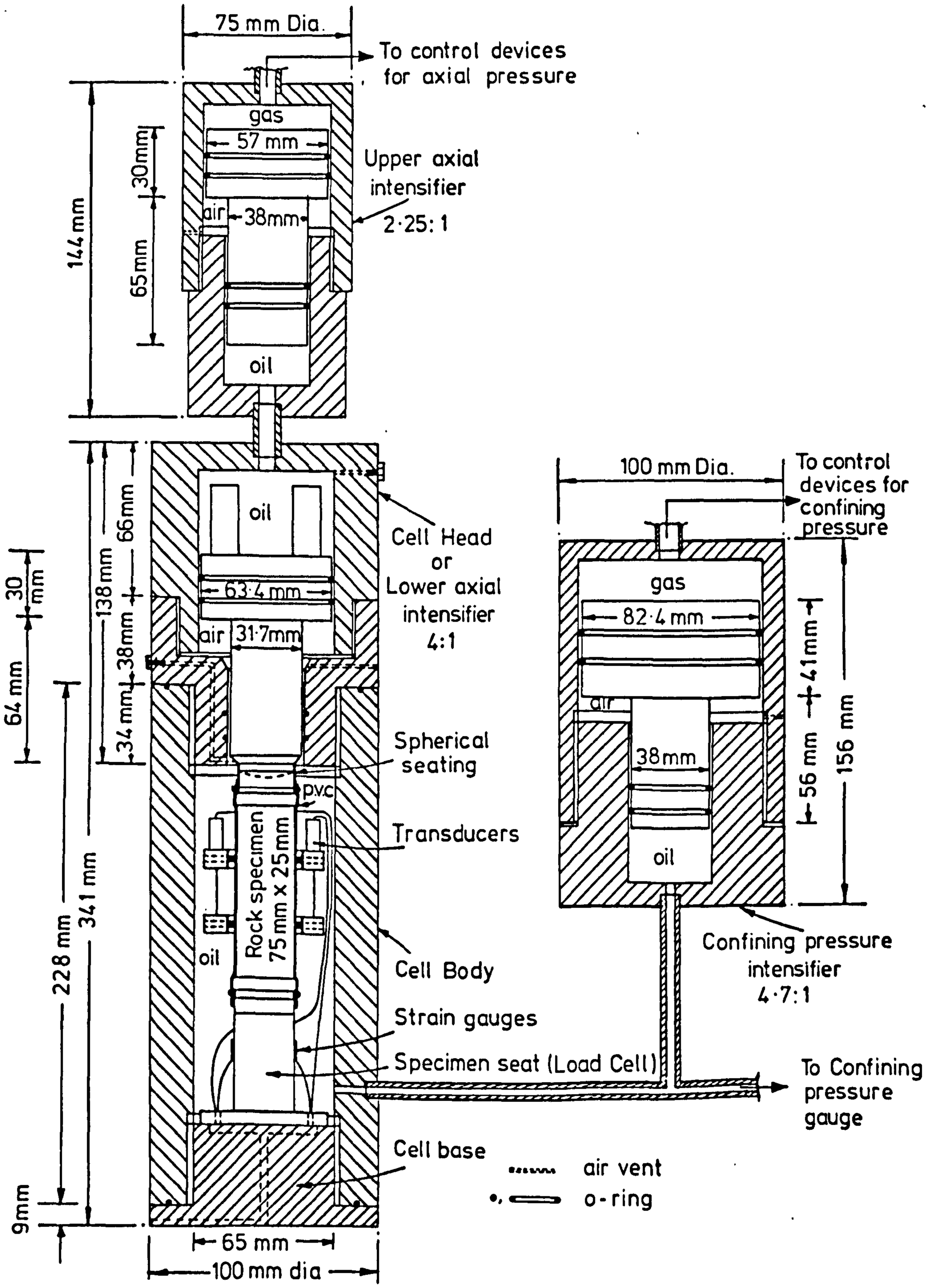

FIG. 8-8 TRIAXIAL CREEP CELL AND INTENSIFIERS

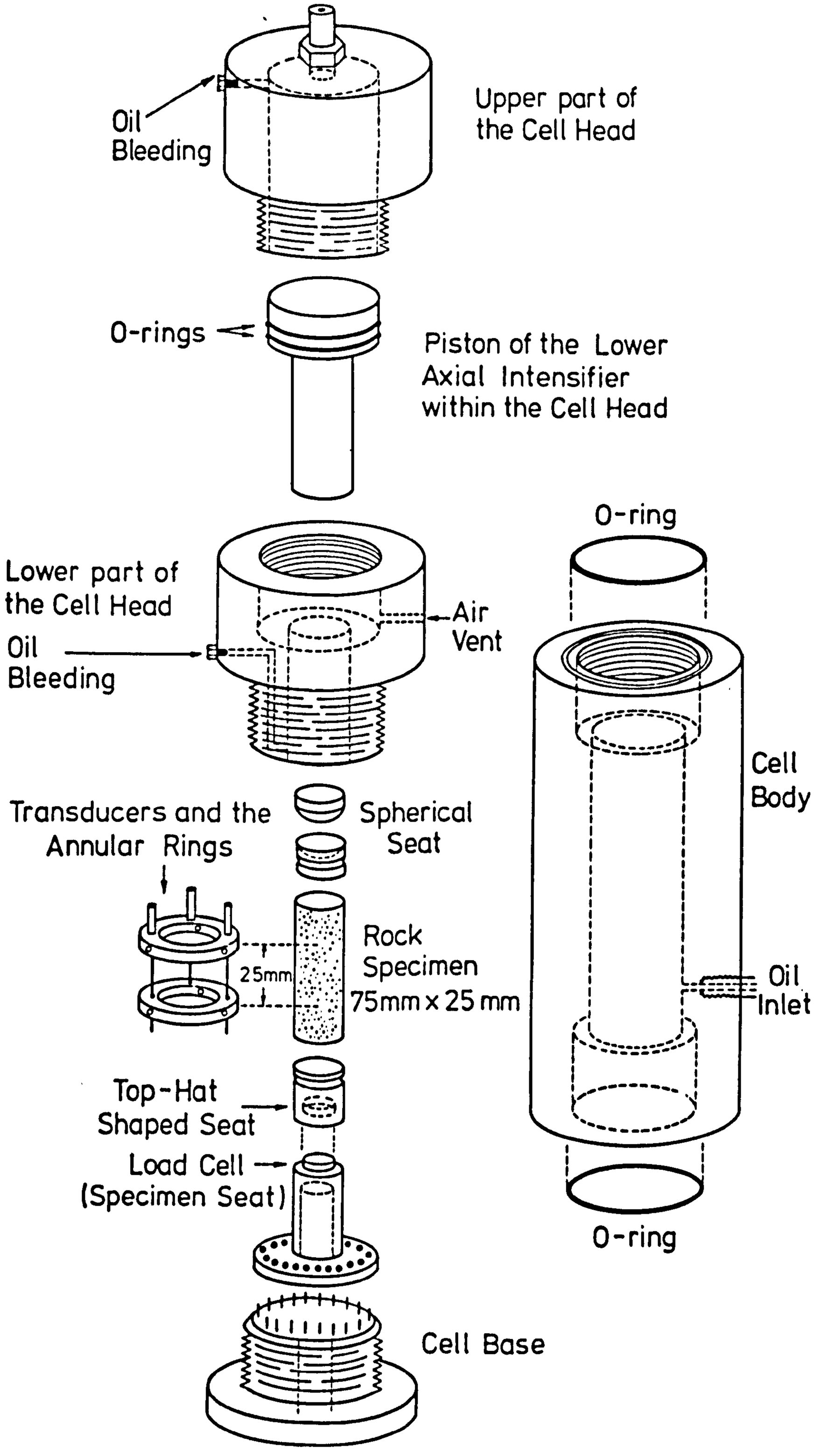

FIG. 8-9 EXPLODED VIEW OF TRIAXIAL CELL

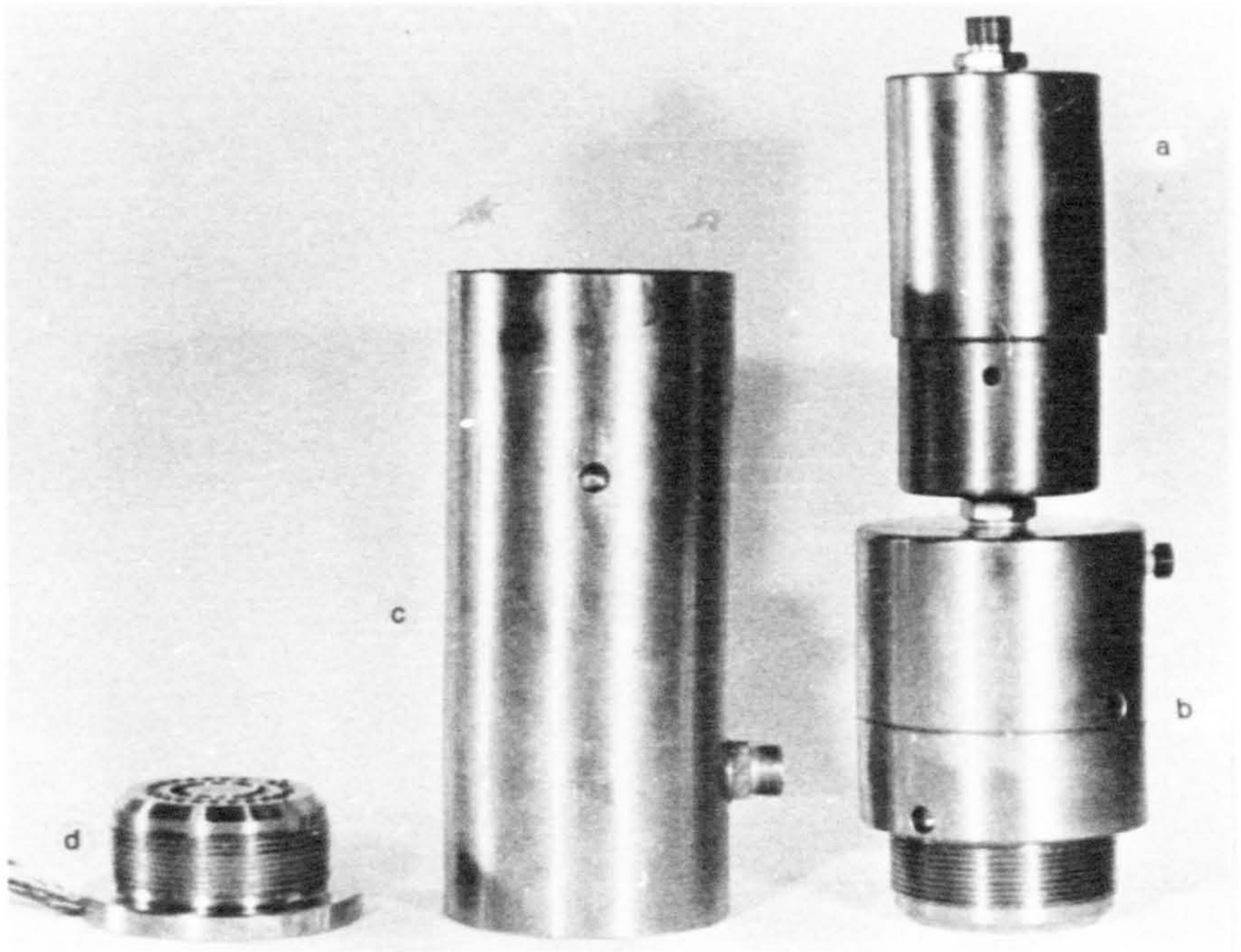

FIG. 8-10 TRIAXIAL CELL DISMANTLED

a) Upper Axial Intensifier
b) Cell head (Lower Axial Intensifier)
c) Cell Body
d) Cell Base

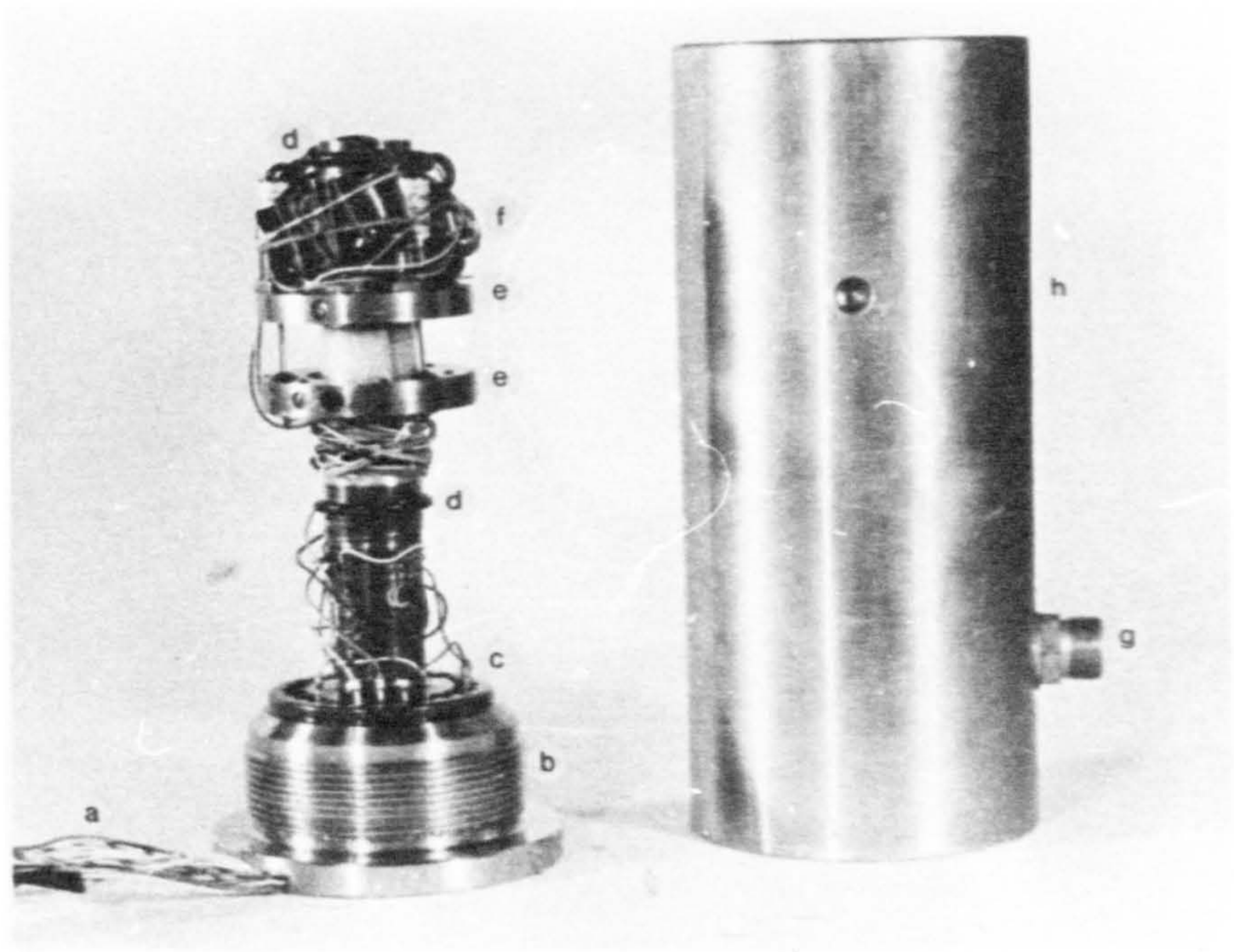

FIG. 8-11 ASSEMBLED TRANSDUCERS, LOAD CELL, CELL BASE AND BODY

a) External leads
b) Cell Base
c) Load Cell (Specimen Seat)
d) Oil Seals
e) Annular Transducer Rings
f) Transducers and Balancing Circuit
g) Oil Inlet
h) Cell Body

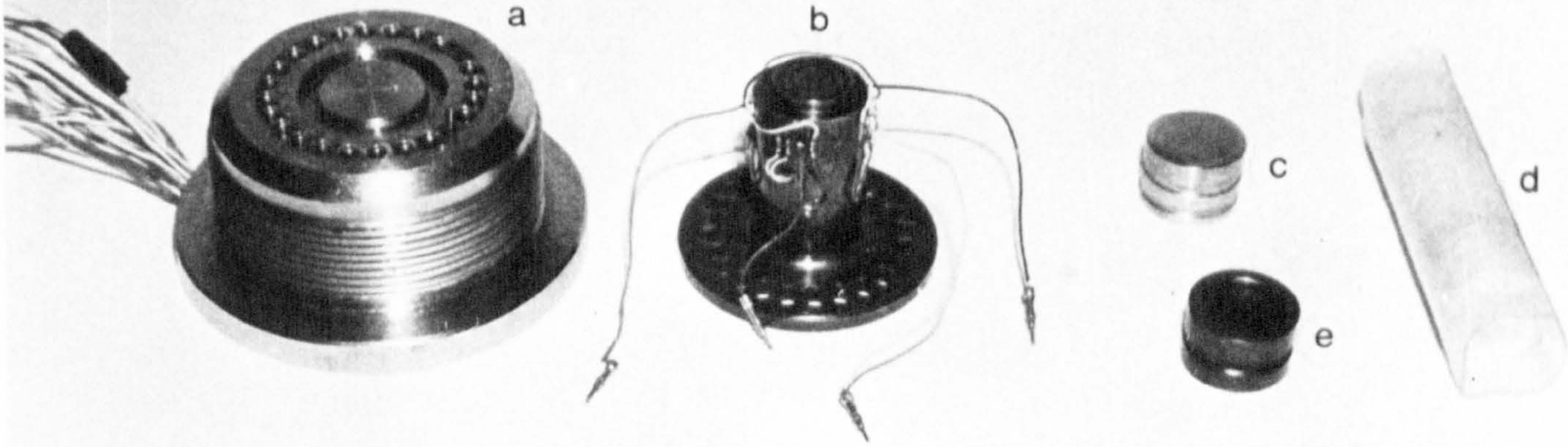

FIG. 8-12 CELL BASE, LOAD CELL, AND JACKETED ROCK SPECIMEN

a) Cell Base with Electrical Sockets
b) Load Cell (Specimen Seat) with Strain Gauges
c) Spherical Seating
d) Jacketed Rock Specimen
e) Hat-Shape Top Steel Platen

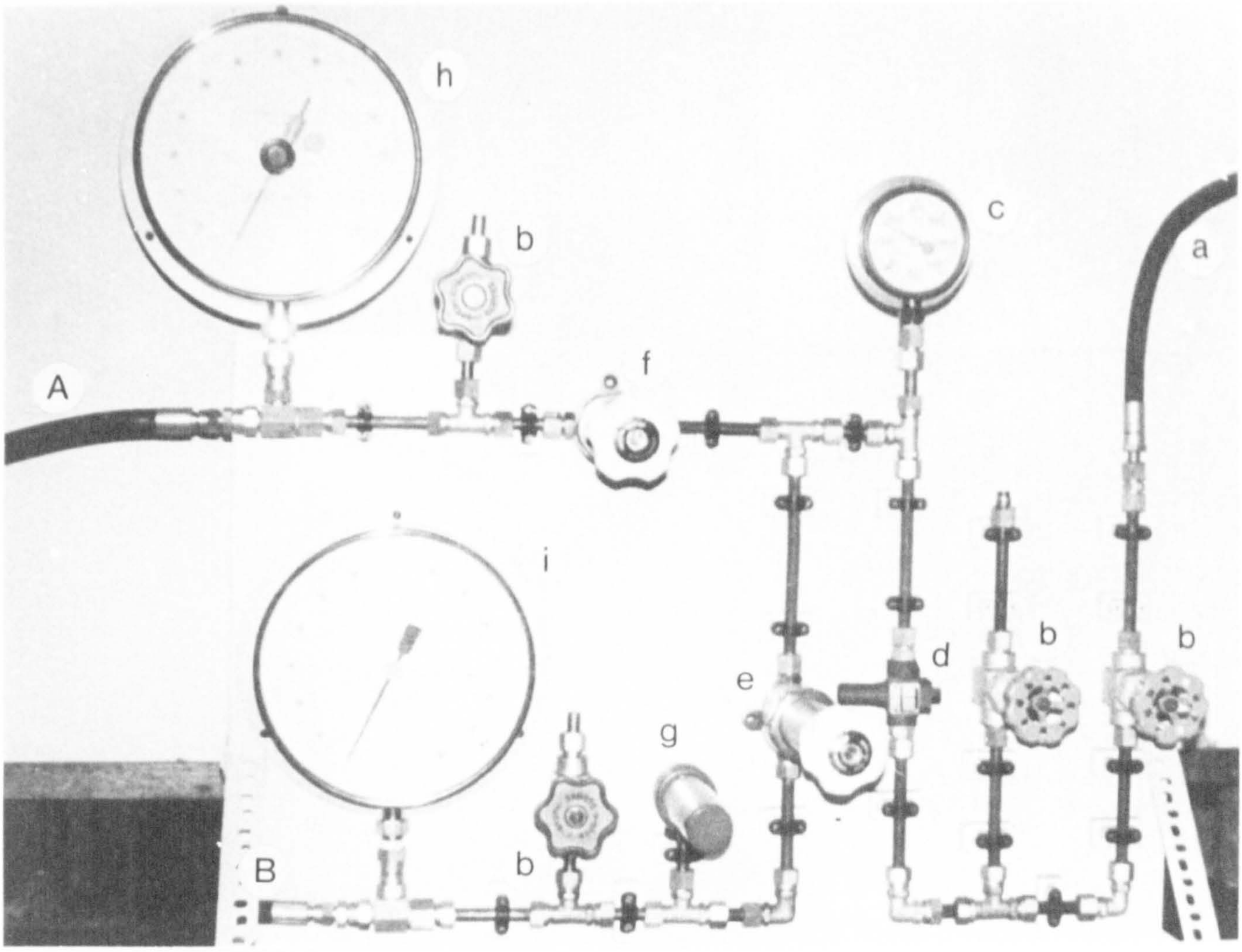

FIG. 8-13 PRESSURE CONTROL SYSTEM

a) To Nitrogen Bottle
b) Shut-Off Valve
c) Nitrogen Bottle Pressure Gauge
d) Filter
e) Confining Pressure Control Valve
f) Axial Pressure Control Valve
g) Automatic Relief Valve
h) Axial Pressure Gauge (N_2)
i) Confining Pressure Guage (N_2)
A) To the Axial Pressure Intensifiers
B) To the Confining Pressure Intensifier

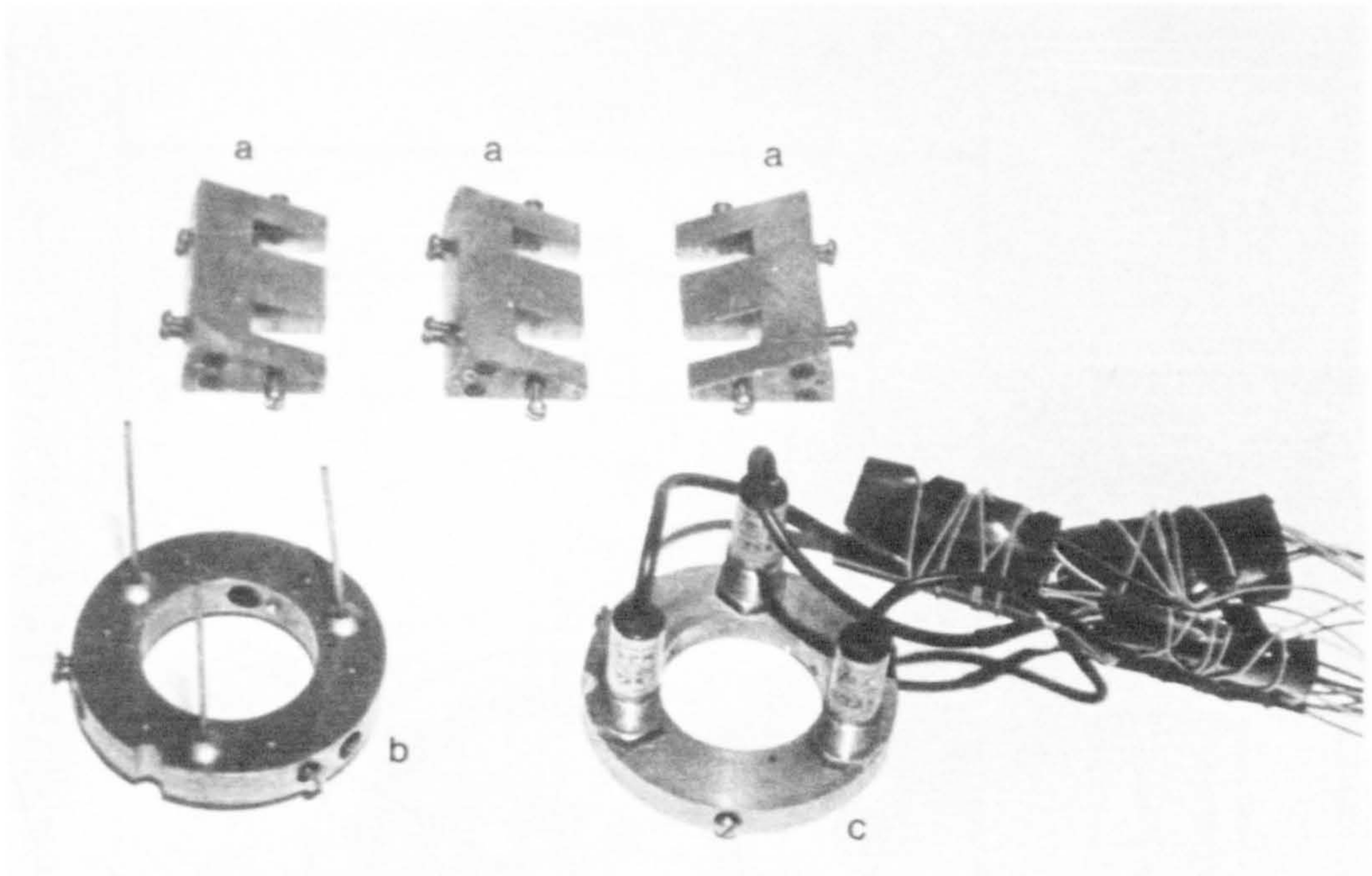

FIG. 8-14 TRANSDUCERS, ANNULAR RINGS AND JIGS

a) Transducers Jig
b) Lower Annular Ring
c) 3 Transducers Mounted on the Upper Annular Ring and Balancing Circuit

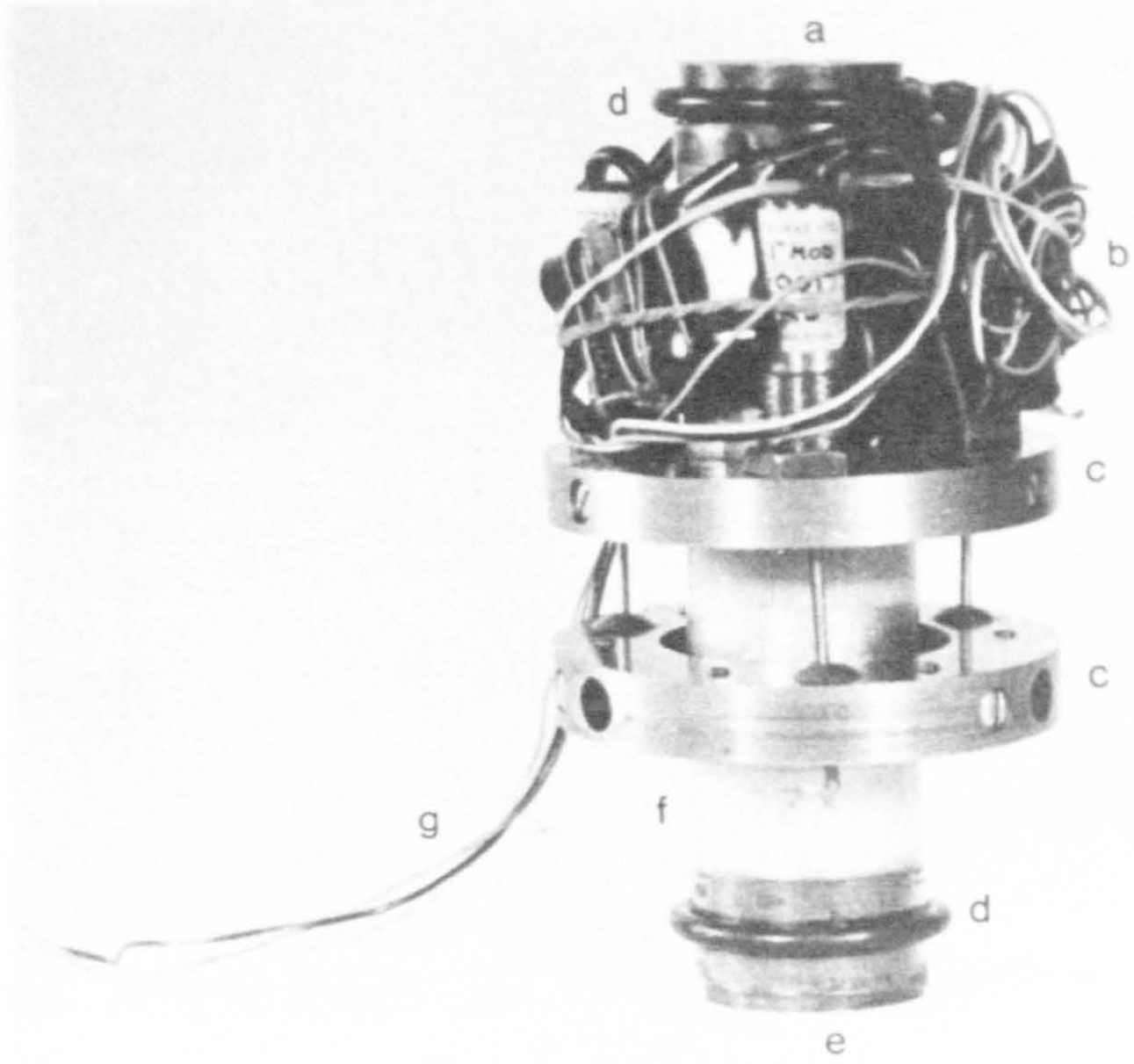

FIG. 8-15 TRANSDUCERS MOUNTED ON THE ROCK SPECIMEN

a) Spherical Seat
b) Transducers and Balancing Circuit
c) Annular Rings
d) O-Ring (Oil Seal)
e) Hat-Shaped Top Platen
f) Jacketed Rock Specimen
g) Electrical Leads to the Cell Base

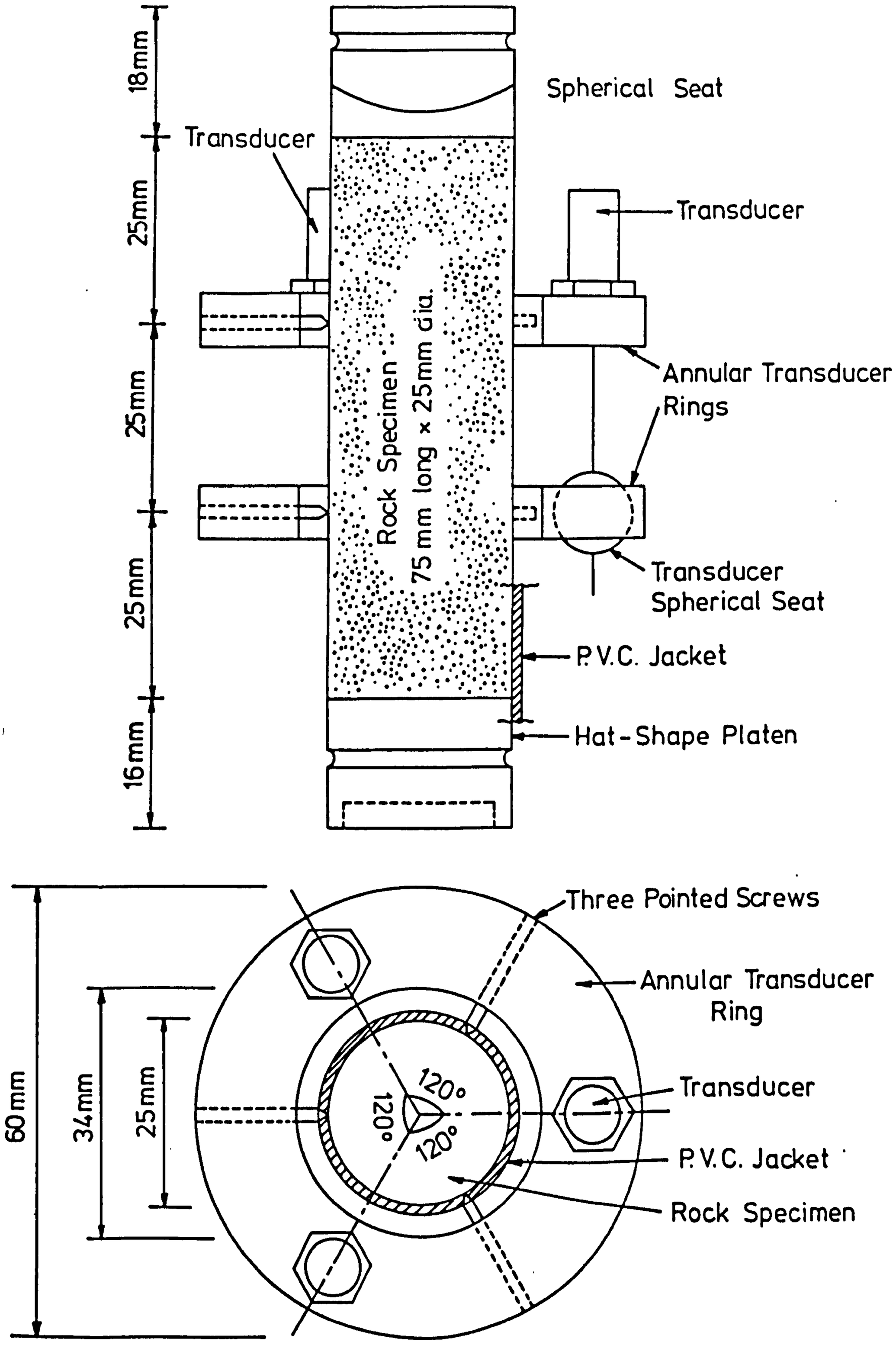

FIG. 8-16 METHOD OF ATTACHING TRANSDUCERS TO THE SPECIMEN

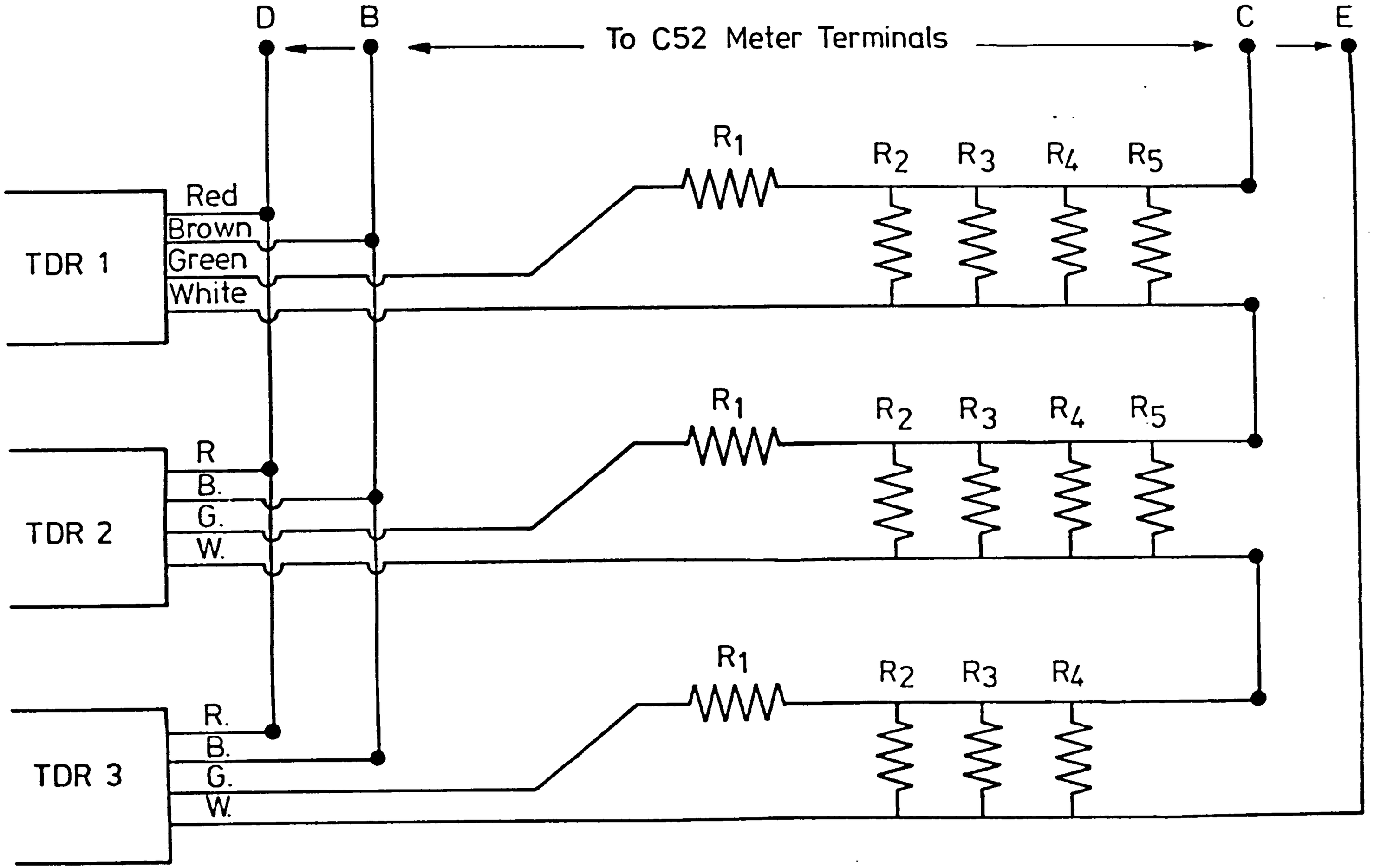

FIG. 8-17 BALANCING CIRCUIT OF THE THREE TRANSDUCERS

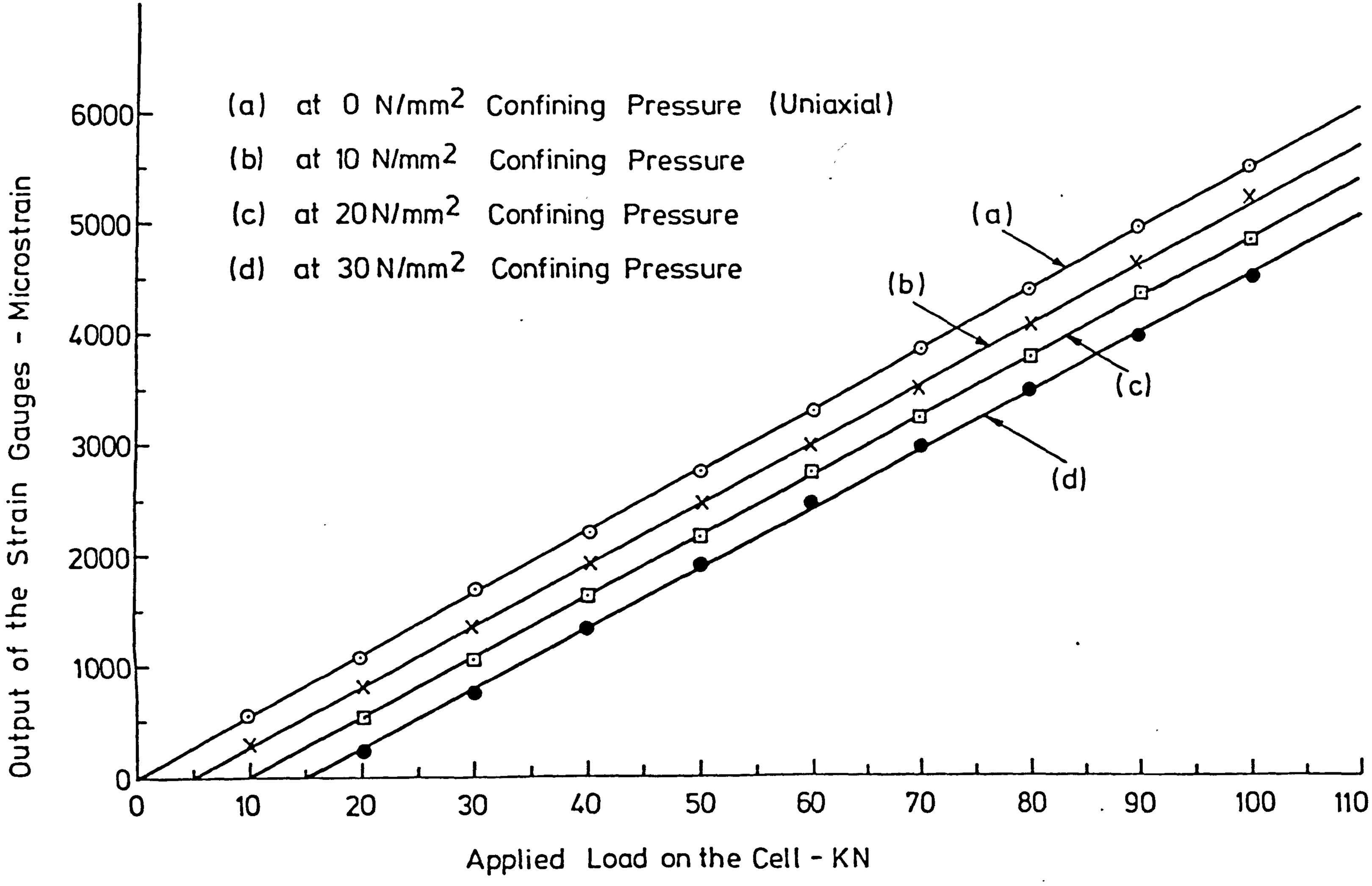

FIG. 8-18 CALIBRATION CURVE OF THE LOAD CELL (Specimen Seat)

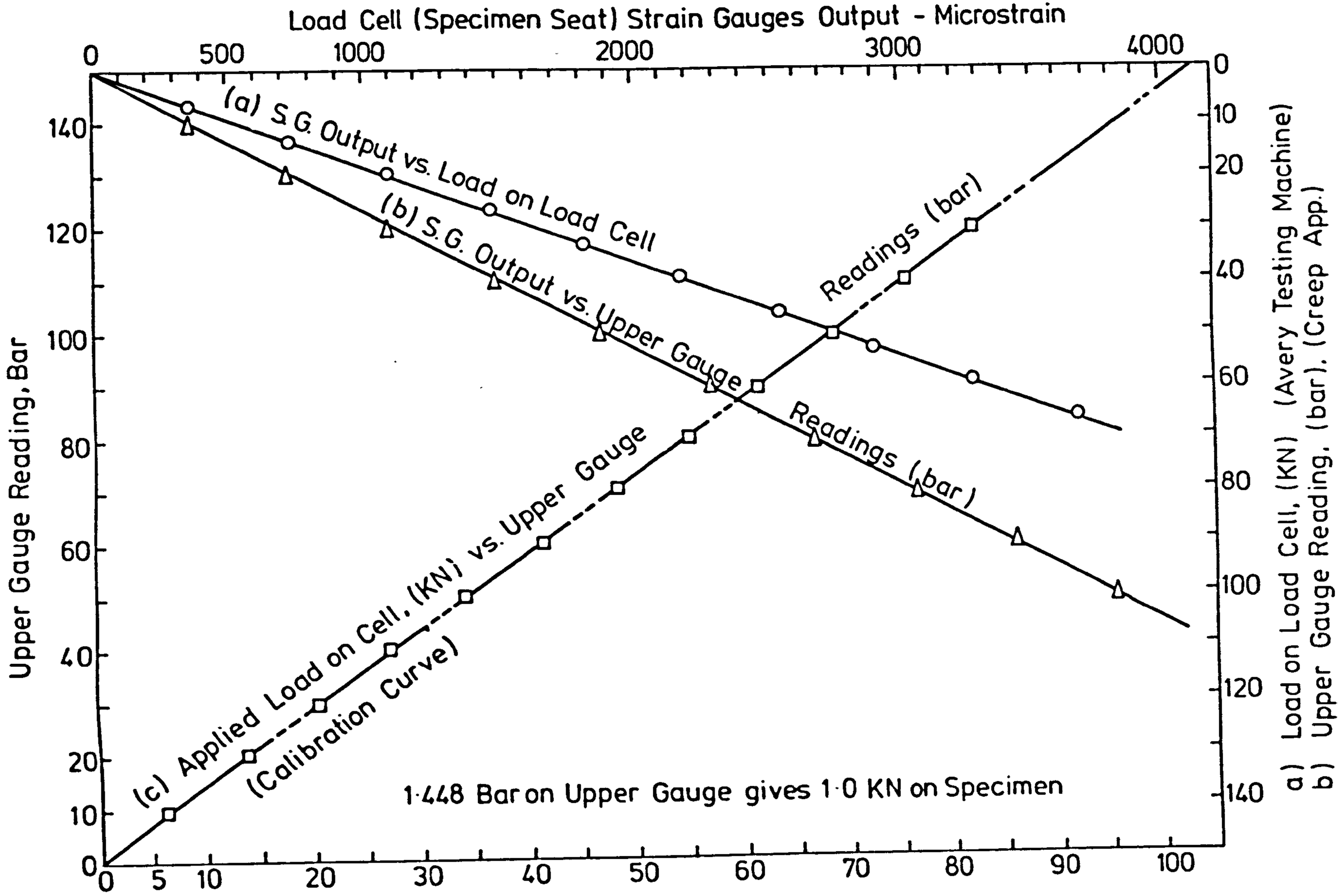

FIG.8-19 CALIBRATION CURVE OF THE TRIAXIAL CREEP APPARATUS

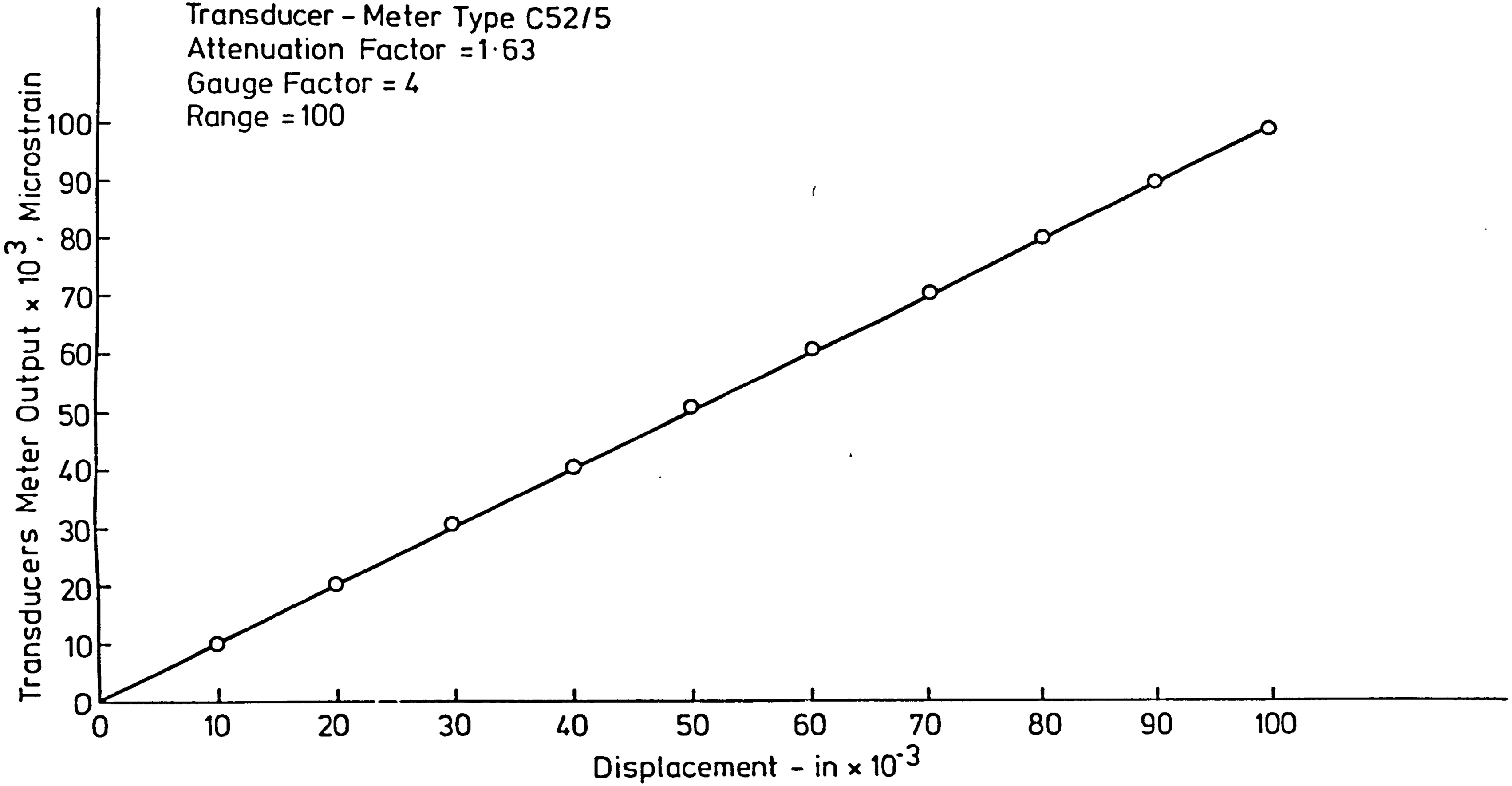

FIG. 8-20 TRANSDUCERS CALIBRATION CURVE

CHAPTER 9

RESULTS AND DISCUSSION

Chapter 9

RESULTS AND DISCUSSION

Although the aim of this work is to study the creep behaviour of the previously mentioned evaporite rocks, namely, gypsum and anhydrite, and to develop a suitable apparatus to extend this investigation into the triaxial field, in this chapter, it is useful to commence with a brief discussion of the rocks' short term test results to make clear the relation between the creep behaviour of these materials and their short term property. The short term and creep results will first be discussed and compared with other investigators' results, where necessary and possible, in both bending and comrpession tests.

9-1 Bending:

Most of the tests were carried out on air dried rock beams 240 mm long by 40 mm wide and 20 mm thick subjected to simple bending in a four-point loading apparatus for both short term and creep tests at room temperature.

9-1.1 Short Term Tests:

Several gypsum and anhydrite beams, type 1, were tested to determine their instantaneous strengths. Table (6-1) and (6-2) give full data, the mean values and the standard deviation of the strength of each rock. The tensile and compressive strains were measured at the lower and upper surfaces of each beam respectively. It was found that, at most of the stress levels employed, the compressive strain measured is greater than the tensile. Fig.(9-1) shows the stress-strain relationship in a single gypsum beam subjected to bending stress. Fig. (9-2) shows stress-strain data of five gypsum beams in bending. It can

be seen that even for the beams of the same dimensions, (20 G11, 20 G23) and (12 G1, 12 G4, 12 G23) there are noticeable differences in their stress-strain behaviours. This due, probably, to the petrological differences in these beams, i.e. size of grains, cementing material, inhomogeneity, etc. and/or due to possible humidity and temperature differences.

The position of the neutral axis or zero strain was determined for two gypsum rock beams as follows: At various stress levels both the tensile and compressive strains were measured at the bottom and top surfaces of the beam. In Fig.(9-3) the position of the neutral axis at any stress level is shown by the dotted line defined by drawing a horizontal line through the intersection point of the line joining any values of tensile and compressive strains corresponding to a certain stress level and the vertical axis of zero strain.

It was found that for both rocks the neutral axis moves up from the tension side towards the compression side as the stress increases. It was also found that in most of the beams tested the neutral axis is below the centre of the beam (plane of symmetry) even at failure stress which is in agreement with Forster's[25] results on rock salt beams, whereas Datta[15] reported that, in his work on sandstone, granite and marble beams, the neutral axis moves up and passes the centre of the beam when the stress increases to near fracture. Fig.(9-1) shows the differences in values of the compressive and tensile strains, and Fig. (9-3) shows that the neutral axis of the rock beam is not at its centre. Both figures show an agreement with the assumption made previously in section (6-1.5) which states that for most rocks the stress-strain behaviour is not the same in tension

and compression and the neutral axis of the beam thus cannot be assumed to be located at the middle of the section.

9-1.2 Creep Tests:

All bending creep tests were carried out on gypsum and anhydrite air dried specimen beams at room temperature. The stress applied was determined as a percentage of each rock instantaneous strength (σu). The percentages used were 30, 40, 60 and 80%. As it was mentioned previously the creep strain at the centre of the bottom face of each rock beam was determined by both measuring the strain using strain gauges and measuring the deflection by a dial gauge. Fig. (9-4) shows an example of the creep strain determined by the above two methods. The average strain was used in drawing most of these conclusions in this investigation.

Two or three beams were tested at each stress level, the average of the results of these beams was plotted as creep strain (in microstrain) versus time in hours. Figures (9-5) and (9-6) show the effect of stress on the bending creep of gypsum and anhydrite respectively. Tables (9-1) and (9-2) give full data of creep strains for both rocks. It can be seen from the figures and the tables that as the stress increases, both the creep strain and the instantaneous strain increase. It was found that the bending creep in gypsum follows one of the following equations according to the magnitude of the applied stress:

(1) At low stress level, 30%σu, it follows the logarithmic law, $\varepsilon = A + B \log t$, where ε is the creep strain, t is the time after loading in hours and A and B are constants depend on the tested material at the stress conditions. This behaviour indicates that the crrep diminishes asymptotically with time. The creep strain

Table (9-1)

Bending creep strain in Gypsum

Time hours	Applied stress - N/mm^2			
	30% σu 4.5	40% σu 6.0	60% σu 9.0	80% σu 12.1
	Instantaneous strain - microstrain			
	118.2	142.5	231.9	295.9
	Creep strain - microstrain			
0.1,(6 min.)	0.8	4.3	5.1	8.0
0.33,(20 min.)	2.5	4.8	8.2	11.5
0.5,(30 min.)	3.6	5.7	9.7	14.7
1	3.9	6.7	12.5	17.8
2	3.9	9.5	15.5	22.3
6	4.4	13.3	20.4	29.5
12	5.0	15.2	25.0	36.4
24	5.0	19.0	28.6	45.1
48	5.5	23.8	35.5	55.8
72	6.2	27.6	36.2	58.0
96	6.6	29.5	44.6	62.5
120	6.9	30.4	47.6	67.0
144	7.2	34.2	50.8	67.4
168	7.4	36.1	56.6	71.9
192	7.7	40.3	57.8	83.1
216	7.7	41.7	59.8	83.5
240	7.7	42.8	63.7	88.3
264	-	43.1	64.1	93.8
288	-	43.1	65.2	94.2
312	-	44.5	66.8	96.2
336	-	45.0	67.7	98.2
360	-	44.8	-	100.3
384	-	-	-	119.1 Failure

Table (9-2)

Bending creep strain in Anhydrite

Time hours	Applied stress - N/mm^2		
	40% σu =7.1	60% σu =10.6	80% σu =14.2
	Instantaneous strain - microstrain		
	99.8	153.7	184.2
	Creep strain - microstrain		
0.1,(6 min.)	2.0	5.8	6.6
0.33,(20 min.)	3.2	8.0	10.7
0.5,(30 min.)	2.9	10.0	11.4
1	4.5	10.5	13.3
2	4.0	12.1	15.3
3	4.2	12.4	16.0
4	4.5	13.0	17.5
5	4.4	14.3	19.2
6	4.5	14.8	18.5
12	5.5	17.8	21.5
24	6.3	19.7	23.3
48	6.6	20.6	26.4
72	6.7	21.0	28.9
96	7.4	20.8	29.5
120	6.6	21.1	30.8
144	7.3	22.0	31.0
168	-	22.2	30.4
192	-	-	30.5
216	-	-	31.5
240	-	-	31.5
			-

was plotted versus the time on a semi-log paper, a straight line was obtained, Fig. (9-7d). The constant A in the above relationship is the creep strain at t = 1 hour, whereas B is the slope of the straight line on the semi-log graph.

The following equation was found for the creep of gypsum in bending under stress of 30% σu (4.5 N/mm^2):

$$\varepsilon = 3.53 + 1.45 \log t \qquad (9\text{-}1)$$

(2) At medium stress levels, namely 40% and 60% of the ultimate instantaneous stress it was found that the creep curve followed a power relationship throughout the tests of the form $\varepsilon = Ct^n$. When the results were plotted on log-log paper, Fig. (9-8), straight lines were obtained where C is the creep strain at t = 1 hour and n is the slope of the straight line. It was also found that $n \simeq 1/3$.

The following equations were obtained

(a) At σ = 40% σu = 6.0 N/mm^2

$$\varepsilon = 7.22\ t^{0.31} \qquad (9\text{-}2)$$

(b) At σ = 60% σu = 9.0 N/mm^2

$$\varepsilon = 11.83\ t^{0.30} \qquad (9\text{-}3)$$

(3) At the higher stress level, σ = 80% σu, it was found that the creep strain followed the power law, mentioned previously, at the beginning of the test, see Fig. 9-8a, followed by a steady state creep of the form $\varepsilon = Dt$ which led finally to fracture.

The following equations were obtained:

$$\varepsilon = 16.70\ t^{0.32}, \quad 0 < t < 288 \text{ hr} \qquad (9\text{-}4)$$

$$\varepsilon = 94.2 + 0.09\ t, \quad 288 < t < 360 \text{ hr} \qquad (9\text{-}5)$$

$$\varepsilon = f(t), \quad 360 < t \qquad (9\text{-}6)$$

The constant 94.2 in equation (9-5) represents the creep

strain at the beginning of the steady-state creep stage at t = 288 hrs.

For anhydrite the creep behaviour followed the logarithmic relationship for all the stress levels, Fig.(9-9). The following equations were obtained:

(a) At σ = 40% σu = 7.1 N/mm^2

$$\varepsilon = 3.83 + 1.55 \log t \quad (9\text{-}7)$$

(b) At σ = 60% σu = 10.6 N/mm^2

$$\varepsilon = 11.19 + 5.20 \log t \quad (9\text{-}8)$$

(c) At σ = 80% σu = 14.2 N/mm^2

$$\varepsilon = 13.31 + 7.55 \log t \quad (9\text{-}9)$$

Tables (9-3) and (9-4) give summary of the constants C and n for gypsum and A and B for anhydrite, respectively.

Table (9-3)

Constants of the power equation of the bending creep in gypsum.

$$\varepsilon = Ct^n$$

$\frac{\sigma}{\sigma u}$ x 100 percent.	Equation No.	C	n
40	9-2	7.22	0.31
60	9-3	11.83	0.30
80	9-4	16.70	0.32

Table (9-4)

Constants of the logarithmic equation of the bending creep in anhydrite

$$\varepsilon = A + B \log t$$

$\frac{\sigma}{\sigma u}$ x 100 percent.	Equation No.	A	B
40	9-7	3.83	1.55
60	9-8	11.19	5.20
80	9-9	13.31	7.55

From the data of table (9-3) for gypsum and the corresponding equations it can be seen that as the stress increases the constant C increases whereas n remains nearly constant. Misra[49] reported that both constants, C and n, increase as the stress increases for the rocks.

On the other hand, the constants A and B, given in table (9-4) for anhydrite, increase as the stress increases. Misra[49], Griggs[28] and others observed the same behaviour in other different rocks.

In a bending creep test on a gypsum beam the stress was increased by steps at various periods of time. Fig. (9-10) shows the total strain versus time, i.e. the instantaneous strains are also shown on the graph. It can be seen that at any time the load was increased there was an instantaneous strain followed by a creep strain. This means that further elastic strain was produced by stress increase even after high creep strain had occurred in the beam.

Fig. (9-11) shows the instantaneous strains of gypsum and anhydrite versus the applied stress as a percentage of σu.

From these curves the modulus of elasticity was calculated for each rock as follows:

(a) For gypsum:

$$E_g = \frac{100}{100} \times \frac{15.07}{381.4} \times 10^6 = 3.95 \times 10^4 \text{ N/mm}^2$$

(b) For anhydrite:

$$E_a = \frac{100}{100} \times \frac{17.73}{245.8} \times 10^6 = 7.21 \times 10^4 \text{ N/mm}^2$$

The above tensile Young's moduli will be compared with the compressive Young's moduli for each rock when the compression tests results will be discussed later in section (9-2.1).

9-2 Compression:

All the tests were carried out on air dried type 1 rock specimens, (The axial load was applied perpendicular to rock bedding) 75 mm long by 25 mm diameter (nominal size) at room temperature.

9-2.1 Short Term Tests:

Uniaxial and triaxial compression tests were carried out on gypsum and anhydrite specimens.

Uniaxial tests were performed on eight specimens of each rock whereas triaxial tests were performed on varying numbers of specimens of each rock at every chosen pressure level.

The confining pressure levels were 5, 10, 15, 20, 25, 30 and 35 N/mm^2.

The determined strengths of gypsum and anhydrite at various confining pressures are given in tables (6-3) and (6-4) and shown in figures (6-18) and (6-19). The curves show a non-linear increase in rock strength as the confining pressure increases.

Mohr's circles for gypsum and anhydrite are shown in

figures (6-14) and (6-15) respectively and an envelope was fitted to the stress circles for each rock. It can be observed that some of the stress circles do not touch the envelope, indicating lower strength values than those predicted from the Mohr envelope drawn. These small differences can be attributed to possible errors arising from random variations in the initial condition of the rock specimens and/or to the anisotropy of the material tested. Mohr envelopes for both gypsum and anhydrite are approximately parabolic in shape and similar to the shape of the envelopes of rocks obtained by previous investigators; Murrell[50], Franklin[23], Handin and Hager[30] and others.

The values of the axial stress immediately after fracture (z) at various confining pressures are given in table (6-3) and (6-4). From these values and the measured angles of fracture, the values of the normal stress σn and shear stress τ_s have been calculated using equations (6-5) and (6-6). These values are given in tables (6-3) and (6-4) and are plotted in figures (6-14) and (6-15), where they are shown by dotted straight lines for gypsum and anhydrite, respectively. The slope of the mentioned line gives the coefficient of friction within the fractured specimen of the rock. It is clear then that if the above straight line meets the Mohr envelope, there will be stresses at which no reduction of load will occur after fracture since the applied shear stress on the fracture surface does not exceed the frictional force on the surface.

It can be seen from tables (6-3) and (6-4) that there is a marked difference between the measured angles of fracture (θ) and those calculated from Griffith's, (θ_G), equation (6-7). This can be attributed to the fact that the Griffith theory predicts only

the orientation of the dangerous crack which propagates and initiates fracture, Murrell[50]. There is also the possibility that the Griffith crack under shear may not propagate in the direction of its major axis and that the observed fracture surface develops by the linking up of a number of propagating cracks.

On the other hand, the measured fracture angles (θ) agree reasonably well with those predicted from Mohr envelopes (θ_M). The small differences between them are possibly due to anisotropy or incipient fracture planes in the rock. In anisotropic material, fracture will not necessarily take place along the maximum shear stress plane, since the material may be stronger in this direction than in another along which the shear stress is lower but sufficient to cause fracture.

The stress-strain curves of gypsum and anhydrite at various confining pressures are shown in Figs. (9-12) and (9-13) respectively. Each curve represents the average values obtained from several specimens tested at the mentioned confining pressure. In order to get an idea of the reliability of the results, two sets of stress-strain curves for gypsum specimens, tested at uniaxial and 30 N/mm^2 confining pressure, are given in Figs.(9-14) and (9-15), respectively. The average curve of each set is also shown as a dotted line. It can be seen that there is a clear scatter in the results of different specimens deformed under similar conditions. Among the possible causes of these differences are (a) effect of anisotropy, (b) slight variations of temperature from test to test, (c) small differences in mechanical properties of specimens, etc.

The load/displacement of gypsum at various confining pressures

is shown in Fig. (9-16).

It can be noticed from the stress-strain curves and the load-displacement of gypsum mentioned previously that there is a linear section in each curve during the early stages of the deformation. This section of the curve is frequently assumed to be the elastic zone. It can be also seen that at a constant axial stress, see Figs. (9-12) and (9-13), as the confining pressure increases the strain, deformation, decreases. At high both confining and axial stress, Fig.(9-12), the stress-strain curve tends to become parallel to the strain-axis, indicating plastic behaviour of rock materials under high confining pressure. It can be noticed that the slope of each stress-strain curve increases with confining pressure.

The total strain before fracture (maximum strain) versus both the mean pressure Pm, that is, one-third of the sum of the three principal stresses (σ_1, σ_2 and σ_3) and the confining pressure is plotted in Figs. (6-17) and (6-20), respectively for both gypsum and anhydrite. These curves are sometimes known as ductility curves. It can be seen that at any mean pressure or confining pressure the maximum strain (ductility) of gypsum is higher than that of the anhydrite indicating that, under triaxial loading, the gypsum starts to deform plastically at a lower stress than the anhydrite. The relationship between the mean pressure, P_m, and the maximum shear stress, τ_m, is shown in Fig. (6-16) for both gypsum and anhydrite. This curve is sometimes called the strength pressure curve, (Handin and Hager[30].) The curves for both rocks are slightly concave downward but nearly linear. The slope of each curve decreases with increasing the mean pressure. It is clear that this slope can never exceed

1.5 which is the slope of the curve at uniaxial compression. Handin and Hager[30] reported that the strength curves they obtained for anhydrite and dolomite are nearly straight lines. Their anhydrite curve was constructed depending on results from one specimen only. It can be seen from Fig.(6-16) that the anhydrite curve lies above that of gypsum and its slope at any value of mean pressure is more than that of the gypsum which is to be expected because the anhydrite is stronger than the gypsum.

The relationship between the maximum shear stress, $\tau_m = \frac{\sigma_1 - \sigma_3}{2}$, and the maximum normal stress, $\sigma_m = \frac{\sigma_1 + \sigma_3}{2}$, is shown in Fig.(6-21) for both tested rocks. The gradient of both curves decreases with increasing the normal stress. It is expected that these curves tend to merge into straight lines parallel to σ_m-axis as would be expected in a material deforming plastically.

The modulus of elasticity of each rock at various confining pressures was determined by making use of the instantaneous strains and their corresponding stresses applied during the creep tests. The instantaneous strain versus the axial stress (as a percentage of the ultimate strength) at various confining pressures are plotted in Figs (9-17) and (9-18) for gypsum and anhydrite respectively. From these curves the moduli of elasticity of each rock were determined at every confining pressure employed. They are given in table (9-5) together with the moduli of elasticity from bending creep tests, see section (9-1.2).

Table (9-5)

Moduli of Elasticity of Gypsum and Anhydrite at Various modes of loading, N/mm^2.

Mode of stress	Gypsum	Anhydrite
Bending (Tension)	$3.95x10^4$	$7.21x10^4$
Uniaxial (Comp.)	$3.17x10^4$	$7.05x10^4$
Triaxial (Comp.)		
Confining pressure N/mm^2	Gypsum	Anhydrite
10	$3.19x10^4$	$8.27x10^4$
20	$3.26x10^4$	-
30	$3.32x10^4$	-

The moduli of elasticity in compression tests are plotted versus the confining pressure as shown in Fig.(9-19). It can be seen that the modulus of elasticity of each rock increases linearly with confining pressure. Murrell[50] reported the same behaviour for Darley Dale sandstone under triaxial compression. From table (9-5) it is clear that the modulus of elasticity in uniaxial compression of each rock is less than the corresponding modulus of elasticity in tension from bending tests. This confirms the behaviour of the rock in bending tests where the stress-strain curve in compression lies below the curve in tension, see Fig.(9-1), and the neutral axis being nearer the tension face of the beam than the compression.

9-2.2 Creep Tests:

One aim of this research was to develop an apparatus for triaxial creep experiments, and to study the triaxial creep behaviour of some evaporite rocks, using the above mentioned

apparatus. Gypsum and anhydrite were chosen initially to be tested. A full description and details concerning the development of the apparatus have been given in Chapter 8 of this thesis. A brief description of the tested rocks mineralogical and chemical composition is given in Chapter 4. All the tests were carried out on air dried 75 mm long by 25 mm rock core samples (the exact dimensions of each specimen were measured individually) at room temperature, (the temperature was $68^{o}F \pm 2$ and the humidity was $51\% \pm 1.5$).

From the results published by previous investigators in the field of creep in rocks and confirmed in this work it is established that the applied stress has a great effect on the creep behaviour of any rock. The value of the applied stress necessary to cause an appreciable amount of creep to occur in a reasonable time from an experimental viewpoint, apart from other factors, depends on the ultimate strength of the tested rock under the loading conditions of the experiment. It was therefore decided to apply different axial stresses as a percentage of the ultimate strength, at every confining pressure, namely 30%, 50%, 65% and 80% of the ultimate strength σu. Various confining pressure levels were chosen for this study. They are: 0 (uniaxial), 10, 20 and 30 N/mm^2.

The results of the creep tests are, in the form of tables and figures, given in tables from (9-6) to (9-11) and figures from Fig. (9-20) to (9-34). In each table the axial stress is given as a percentage of the ultimate strength of the rock (σu) at the given confining pressure and in N/mm^2. The instantaneous strain in each case is also given. The data given for each stress level and the corresponding graph is the average value

obtained from two or three rock specimens tested at similar applied stresses, axial and confining , and at similar environmental conditions. In order to give an idea of the reliability of the results, one set of creep results of three gypsum specimens tested under 68.2 N/mm^2 (=50%σu) axial stress at 30 N/mm^2 confining pressure is given in table (9-12)and plotted in Fig. (9-35). The average is also shown in both the table and the figure. It can be seen from the above example that there are clear differences in the results of different specimens deformed under similar stress conditions. These differences were, possibly, the result of the effect of anisotropy in the specimens, small differences in the chemical composition between the specimens, slight variations of temperature and humidity from test to test, small differences in mechanical properties of specimens etc.

Table (9-6)

Uniaxial creep strain in Anhydrite

Time hours	Axial stress - % σu, N/mm²			
	30% σu 30.4	40% σu 40.5	60% σu 60.8	80% σu 81.0
	Instantaneous strain - microstrain			
	430.6	655.8	918.6	997.5
	Creep strain - microstrain			
0.1,(6 min.)	3.2	6.0	4.2	8.8
0.33,(20 min.)	4.1	9.7	13.3	16.6
0.5,(30 min.)	5.5	11.6	16.1	18.5
1	7.4	14.4	21.5	26.4
2	10.2	18.5	27.0	33.3
3	-	24.0	-	37.9
4	12.5	25.5	33.9	40.7
5	13.9	27.8	34.7	44.4
6	14.8	29.6	39.3	47.2
12	17.1	31.0	44.0	56.0
24	18.5	35.7	46.8	61.1
48	24.1	41.7	54.8	68.0
72	24.1	46.3	56.1	75.9
96	26.2	48.9	60.0	80.5
120	27.1	48.2	61.8	81.5
144	26.4	48.2	63.2	82.5
168	30.5	49.1	64.5	84.6
192	30.5	53.3	68.5	85.9
216	30.8	53.8	69.0	86.3
240	30.4	54.6	68.2	88.9
264	31.3	53.6	70.1	88.9
288	-	54.8	71.8	91.0
312	-	55.9	70.8	90.2
336	-	56.4	70.3	89.9
360	-	-	72.1	92.3
			-	-

Table (9-7)

Triaxial creep strain in Anhydrite at 10 N/mm^2 confining pressure

Time hours	Axial stress - % σu, N/mm^2		
	40% σu =65.8	60% σu =98.8	80% σu =131.7
	Instantaneous strain - microstrain		
	756.1	1236.2	1601.8
	Creep strain - microstrain		
0.1,(6 min.)	4.6	2.8	8.3
0.33,(20min.)	8.3	11.5	14.1
0.5,(30 min.)	11.6	15.6	16.2
1	13.9	22.3	23.0
2	20.8	27.8	28.4
3	22.2	32.0	34.1
6	27.9	39.5	44.2
12	32.4	42.4	47.0
24	35.4	48.1	56.2
48	39.8	58.7	62.9
72	44.5	62.5	72.5
96	45.7	63.8	79.3
120	47.0	65.7	87.8
144	46.1	65.9	90.8
168	48.5	67.0	91.3
192	52.0	67.7	93.2
216	51.6	68.3	99.0
240	52.5	71.3	104.6
264	52.3	-	105.3
288	52.2	72.8	106.4
312	-	-	107.7
336	54.8	73.0	110.3
360	54.3	74.5	114.1
384	-	-	-
408	-	74.6	118.0
432	-	75.7	-
456	-	75.4	119.1
480	-	75.4	119.0

Table (9-7)

contd.

Triaxial creep strain in Anhydrite at 10 N/mm^2 confining pressure

Time hours	Axial stress - % σu, N/mm^2		
	40% σu =65.8	60% σu =98.8	80% σu =131.7
	Instantaneous strain - microstrain		
	756.1	1236.2	1601.8
	Creep strain - microstrain		
504	-	-	-
528	-	-	120.5
552	-	-	-
576	-	-	121.3
600	-	-	123.6
624	-	-	123.8
648	-	-	123.8
672	-	-	124.0
692	-	-	124.4
720	-	-	124.2

Table (9-8)

Uniaxial creep strain in Gypsum

Time hours	Axial stress - % σu, N/mm^2				
	30% σu =17.2	40% σu =23.0	50% σu =28.7	65% σu =37.3	80% σu =46.0
	Instantaneous strain - microstrain				
	520.3	648.7	937.4	1207.0	1411.5
	Creep strain - microstrain				
0.1,(6 min.)	12.2	14.3	30.5	33.9	51.7
0.33,(20 min.)	18.3	24.3	-	45.7	74.6
0.5,(30 min.)	23.1	27.4	47.3	55.3	78.5
1	27.0	43.1	53.5	60.5	95.5
2	33.7	50.0	61.0	71.4	118.4
3	44.2	60.3	68.1	78.0	135.1
4	48.6	64.9	70.3	82.5	150.3
6	50.1	70.2	74.9	95.3	161.7
12	53.2	77.6	86.1	115.6	191.0
24	64.3	94.6	110.4	139.7	225.2
48	72.5	-	128.4	167.7	269.2
72	82.5	103.1	131.7	184.8	309.3
96	88.6	115.0	140.5	195.1	331.5
120	95.3	117.5	145.0	203.9	340.4
144	99.7	118.3	150.5	209.4	359.1
168	102.9	117.8	158.8	220.5	376.9
192	106.1	120.2	168.4	224.7	389.8
216	107.0	124.9	173.2	229.1	410.7
240	110.4	125.7	181.3	235.3	425.0
264	110.4	127.3	184.7	241.0	432.1
288	110.5	127.7	186.8	252.0	441.8
312	-	128.3	189.3	255.3	450.3
336	-	129.4	-	270.1	459.4
360	-	130.3	-	266.8	465.2
384	-	-	-	362.6	474.5
408	-	-	-	368.5	483.3
432	-	-	-	-	494.0
456	-	-	-	-	494.3
480	-	-	-	-	495.8
					-

Table (9-9)

Triaxial creep strain in Gypsum at 10 N/mm^2 confining pressure

Time hours	Axial stress - % σu, N/mm^2				
	30% σu =27.6	40% σu =36.8	50% σu =46.0	65% σu =59.8	80% σu =73.7
	Instantaneous strain - microstrain				
	726.9	1109.3	1470.5	2002.3	2220.1
	Creep strain - microstrain				
0.1,(6 min.)	21.3	35.1	42.5	55.9	69.5
0.33,(20min.)	28.1	47.2	56.3	79.1	100.7
0.5,(30 min.)	32.5	51.9	62.4	90.3	115.3
1	38.9	62.0	75.1	106.7	140.3
2	46.2	71.8	89.2	130.2	175.5
3	50.3	78.3	98.3	145.4	196.2
4	54.4	85.5	105.0	160.7	215.1
5	56.2	90.0	113.7	171.8	230.7
6	58.6	94.3	120.0	181.3	241.9
12	64.8	111.5	142.5	215.0	301.3
18	70.1	125.0	157.8	235.2	338.1
24	78.3	131.3	173.1	265.4	371.1
48	90.1	155.0	200.3	320.1	462.2
72	101.9	171.3	226.4	359.4	512.4
96	105.7	185.3	245.2	391.3	560.4
120	111.8	197.4	256.4	410.7	601.7
144	117.5	205.1	271.1	438.1	639.1
168	120.1	208.7	281.7	460.5	668.7
192	122.4	212.5	289.8	475.0	688.8
216	124.8	218.6	300.1	490.3	715.0
240	126.3	222.6	310.1	505.3	750.1
264	-	228.1	316.3	516.1	770.3
288	-	233.4	322.8	528.2	789.2
312	-	238.2	328.1	540.4	805.0
336	-	241.9	334.3	551.5	821.1
360	-	245.1	341.8	559.1	836.6
384	-	-	347.1	570.2	854.5
408	-	-	351.2	579.3	874.4

Table (9-9)

contd.

Triaxial creep strain in Gypsum at 10 N/mm^2 confining pressure

Time hours	Axial stress - % σu, N/mm^2				
	30% σu =27.6	40% σu =36.8	50% σu =46.0	65% σu =59.8	80% σu =73.7
	Instantaneous strain - microstrain				
	726.9	1109.3	1470.5	2002.3	2220.1
	Creep strain - microstrain				
432	-	-	355.7	588.4	892.1
456	-	-	360.2	600.7	903.3
480	-	-	365.7	610.0	913.2
504	-	-	-	619.7	924.8
528	-	-	-	628.1	937.7
552	-	-	-	638.8	948.3
576	-	-	-	644.7	962.1
600	-	-	-	650.1	971.3
624	-	-	-	-	982.7
648	-	-	-	-	990.3
					-

Table (9-10)

Triaxial creep strain in Gypsum at 20 N/mm^2 confining pressure

Time hours	Axial stress %σu, N/mm^2			
	30% σu =34.4	50% σu =57.3	65% σu =74.5	80% σu =91.7
	Instantaneous strain - microstrain			
	1069.3	1710.3	2284.1	2815.7
	Creep strain - microstrain			
0.1,(6 min.)	39.0	45.2	59.7	71.4
0.33,(20 min.)	50.1	62.5	70.1	107.0
0.5,(30 min.)	55.7	70.8	98.3	122.1
1	61.3	82.1	119.0	145.2
2	71.1	98.3	140.3	182.7
3	76.5	112.5	165.0	215.2
4	82.1	120.5	180.1	235.3
5	86.4	129.5	191.4	256.1
6	89.3	140.1	200.7	263.3
12	102.6	165.3	235.7	330.3
18	107.1	180.5	269.1	379.7
24	116.9	191.7	290.8	411.7
48	130.3	240.1	370.2	540.1
72	144.8	261.3	419.3	619.8
96	155.1	280.8	440.1	665.4
120	161.7	300.2	469.7	710.4
144	165.2	312.1	501.8	761.5
168	171.3	322.5	520.9	798.8
192	175.1	341.7	550.1	830.1
216	177.3	350.3	570.8	861.7
240	178.4	360.4	591.3	888.1
264	179.1	371.3	608.5	911.8
288	-	379.1	630.1	950.3
312	-	380.5	640.3	980.5
336	-	386.3	648.1	991.4
360	-	390.1	665.3	1019.7

Table (9-10)

contd.

Triaxial creep strain in Gypsum at 20 N/mm^2 confining pressure

Time hours	Axial stress $\%_\sigma$ u, N/mm^2			
	30% σ u =34.4	50% σ u =57.3	65% σ u =74.5	80% σ u =91.7
	Instantaneous strain - microstrain			
	1069.3	1710.3	2284.1	2815.7
	Creep strain - microstrain			
384	-	-	690.1	1048.8
408	-	-	695.7	1073.1
432	-	-	704.1	1100.7
456	-	-	710.3	1120.8
480	-	-	712.1	1137.2
504	-	-	715.3	1149.2
528	-	-	718.1	1161.1
552	-	-	-	1172.3
576	-	-	-	1179.1
600	-	-	-	1192.4
624	-	-	-	1199.5
648	-	-	-	1202.7
672	-	-	-	1207.2
696	-	-	-	1208.1
720	-	-	-	1210.9
				-

Table (9-11)

Triaxial creep strain in Gypsum at 30 N/mm^2 confining pressure

Time hours	Axial stress %σu, N/mm^2			
	30% σu =40.9	50% σu =68.2	65% σu =88.7	80% σu =109.2
	Instantaneous strain - microstrain			
	1249.7	1828.7	2788.9	3355.0
	Creep strain - microstrain			
0.1,(6 min.)	44.5	49.3	58.1	83.4
0.33,(20 min.)	56.3	71.5	81.5	110.3
0.5,(30 min.)	60.1	79.7	104.0	127.7
1	71.3	94.1	140.1	162.0
2	79.2	118.8	164.7	231.8
3	90.3	132.1	187.0	245.5
4	93.7	136.8	195.7	261.1
5	96.8	145.1	210.3	288.7
6	102.1	166.2	215.1	307.8
12	115.5	201.5	275.2	380.4
18	131.5	212.0	322.3	439.0
24	140.7	235.5	340.7	481.2
48	153.0	270.5	421.1	635.1
72	172.7	312.1	483.1	735.3
96	185.3	360.9	585.2	790.7
120	191.8	380.2	585.9	855.5
144	195.4	369.1	602.1	936.6
168	205.3	370.7	635.7	970.1
192	209.5	405.6	671.8	1015.3
216	208.5	419.1	635.0	1095.2
240	215.6	420.1	740.4	1150.5
264	-	448.8	737.1	1147.7
288	-	460.2	760.1	1180.8
312	-	463.7	779.8	1217.1
336	-	487.1	800.5	1241.0
360	-	483.3	823.4	1261.2
384	-	487.7	838.2	1285.3
408	-	489.1	850.4	1315.1

Table (9-11)

contd.

Triaxial creep strain in Gypsum at 30 N/mm^2 confining pressure

Time hours	Axial stress %σu, N/mm^2			
	30% σu =40.9	50% σu =68.2	65% σu =88.7	80% σu =109.2
	Instantaneous strain - microstrain			
	1249.7	1828.7	2788.9	3355.0
	Creep strain - microstrain			
432	-	-	862.1	1342.5
456	-	-	873.3	1361.2
480	-	-	881.0	1390.7
504	-	-	888.3	1412.8
528	-	-	890.7	1441.3
552	-	-	897.2	1473.4
576	-	-	901.1	1493.2
600	-	-	907.3	1508.1
624	-	-	-	1527.0
648	-	-	-	1539.2
672	-	-	-	1550.8
696	-	-	-	1561.1
720	-	-	-	1571.7
				-

Table (9-12)

Creep strain in three Gypsum specimens deformed under 68.2 N/mm^2 (50% σu), axial stress at 30 N/mm^2 confining pressure - microstrain

Time hr.	Specimen No.93 G	Specimen No.94 G	Specimen No.97 G	Average
0,(Inst.)	1890.3	1877.1	1718.6	1828.7
0.1,(6 min.)	51.2	55.1	41.5	49.3
0.33,(20 min.)	74.5	72.7	67.2	71.5
0.5,(30min)	79.3	76.4	83.3	79.7
1	88.3	102.7	91.2	94.1
2	110.2	126.1	120.0	118.8
3	120.3	139.2	136.8	132.1
4	127.1	145.9	137.4	136.8
5	138.3	153.7	143.2	145.1
6	170.3	178.1	150.3	166.2
12	217.5	211.7	175.2	201.5
18	235.1	-	188.9	212.0
24	270.1	225.3	211.2	235.5
48	304.9	260.5	246.2	270.5
72	325.4	335.2	275.8	312.1
96	351.7	405.8	325.2	360.9
120	355.3	455.1	330.3	380.2
144	360.8	394.8	351.7	369.1
168	363.5	408.3	340.2	370.7
192	400.4	430.7	385.8	405.6
216	405.8	430.7	420.7	419.1
240	410.5	429.3	420.6	420.1
264	425.5	475.8	445.2	448.8
288	430.4	471.8	478.4	460.2
312	438.4	470.2	482.4	463.7
336	462.0	484.1	515.3	487.1
360	453.5	478.2	518.1	483.3
384	467.8	468.8	526.5	487.7
408	471.3	470.3	525.8	489.1

The creep curves obtained for the two chosen rocks under different axial and confining stresses obey reasonably well the following laws:

Logarithmic law, $\varepsilon = A + B \log t$ (9-10)

or/and Power law, $\varepsilon = Ct^n$ (9-11)

where, ε is the creep strain at any time in microstrain, t is the time after loading in hours and A, B, C and n are constants which depend on the material and the test conditions. For anhydrite and gypsum creep behaviour, under uniaxial and triaxial compression, the following equations were found:

(a) For Anhydrite:

Uniaxial compression and triaxial compression at 10 N/mm^2 confining pressure creep tests were carried out on anhydrite specimens at room temperature. The triaxial creep tests were confined to 10 N/mm^2 due to limitations of available time.

In all cases, except that at high stress of the triaxial tests, the creep curves followed the logarithmic law, Eq.(9-10), indicating that the creep diminishes asymptotically with time.

1). For uniaxial compression the following relationships were obtained, see table (9-6) and Figs. (9-20) and (9-21):

at σ_1 = 30% σu = 30.4 N/mm^2:

$$\varepsilon = 8.62 + 8.29 \log t \quad (9\text{-}13)$$

at σ_1 = 40% σu = 40.5 N/mm^2:

$$\varepsilon = 17.11 + 15.15 \log t \quad (9\text{-}14)$$

at σ_1 = 60% σu = 60.7 N/mm^2:

$$\varepsilon = 22.42 + 18.70 \log t \quad (9\text{-}15)$$

at σ_1 = 80% σu = 81.0 N/mm^2:

$$\varepsilon = 26.81 + 26.10 \log t \quad (9\text{-}16)$$

The values of the creep strain given in table (9-6) were

plotted versus time on semi-log graph as shown in Fig.(9-21). The relationships so obtained were straight lines, indicating that the logarithmic law well fits the given data. In the equations (9-13) to (9-16) the first term, A in equation (9-10), represents the amount of creep strain after one hour and the number proceeding log t, B in equation (9-10), represents the slope of the straight line drawn of the creep strain versus time on semi-log graph, see Fig.(9-21), which can be calculated by $B = \frac{\varepsilon_2 - \varepsilon_1}{\log t_2 - \log t_1}$. Another method in calculating A and B were used which is called the least square method which will be described when the gypsum results are discussed later in this chapter.

2). For triaxial compression at 10 N/mm^2 confining pressure the following relationships were obtained, see table (9-7) and Figs. (9-22), (9-23) and (9-24):

at σ_1 = 40% σu = 65.8 N/mm^2:

$$\varepsilon = 16.31 + 14.38 \log t \qquad (9\text{-}17)$$

at σ_1 = 60% σu = 98.8 N/mm^2=

$$\varepsilon = 21.50 + 20.16 \log t \qquad (9\text{-}18)$$

at σ_1 = 80% σu = 131.7 N/mm^2:

$$\varepsilon = 28.21 + 15.05 \log t \qquad (9\text{-}19)$$

for $0 < t < 2$ hrs.

and $\varepsilon = 25.54 t^{0.245}$ (9-20)

for $t > 2$ hrs.

It can be seen from the above equations that the creep in anhydrite at 10 N/mm^2 confining pressure followed the logarithmic law, Eq. (9-10), for the whole periods of all the tests except under high axial stress, 80% σu, where a departure from the logarithmic relationship was obtained after 2 hours loading.

In the initial stage, $0 < t < 2$ hrs, the creep curve followed the logarithmic law, Eq. (9-10), which later on changed into the power law, Eq.(9-11), ($\varepsilon = Ct^n$). The value of the exponent "n" being only fractionally greater than zero. Fig.(9-24) shows the creep strain plotted versus time on a log-log graph which gives a straight line curve after t = 2 hrs. indicating that the power law, Eq.(9-11), well fits the creep behaviour of anhydrite at 10 N/mm^2 confining pressure under high axial stress, 80%σu. The value of "n" is the slope of the straight line on the log-log graph, calculated by $n = \frac{\log\varepsilon_2 - \log\varepsilon_1}{\log t_2 - \log t_1}$. The value of "C" is the creep strain at t = 1 hour. Equation (9-11) can be rewritten in the form:

$$\log\varepsilon = \log C + n \log t \qquad (9\text{-}21)$$

which is an equation of a straight line of a slope equal to "n" and an intercept on the $\log\varepsilon$ axis equal to $\log C$. Therefore, the least square method mentioned previously can be used in calculating "n" and "C". An example of using this method will be given later in this chapter.

(b) For Gypsum:

Uniaxial compression and triaxial compression at 10, 20, 30 N/mm^2 confining pressure creep tests were carried out on air dried gypsum specimens at room temperature. It was found that the creep behaviour of gypsum followed the logarithmic law, Eq. (9-10), and/or the power law, Eq.(9-11), according to the magnitude of the applied axial stress and the confining pressure. From the creep results obtained the following relationships were found:

1). For uniaxial compression, see table (9-8) and Figs. (9-25), (9-26) and (9-27), the creep behaviour followed either

the logarithmic law, Eq. (9-10), or the power law, Eq. (9-11), according to the applied stress as given below:

at σ_1 = 30% σu = 17.3 N/mm^2:

$$\varepsilon = 32.51 + 26.92 \log t \qquad (9\text{-}22)$$

at σ_1 = 40% σu = 23.0 N/mm^2:

$$\varepsilon = 45.19 + 31.60 \log t \qquad (9\text{-}23)$$

at σ_1 = 50% σu = 28.7 N/mm^2:

$$\varepsilon = 53.49\ t^{0.215} \qquad (9\text{-}24)$$

at σ_1 = 65% σu = 37.6 N/mm^2:

$$\varepsilon = 62.10\ t^{0.245} \qquad (9\text{-}25)$$

at σ_1 = 80% σu = 46.0 N/mm^2:

$$\varepsilon = 90.21\ t^{0.284} \qquad (9\text{-}26)$$

It is clear from the above equations that at low axial stress, namely 30% σu and 40% σu, the creep of gypsum followed the logarithmic law, Eqs.(9-22) and (9-23). Whereas under medium and high axial stress (50% σu, 65% σu and 80% σu) the creep-time relationship followed the power law: Eqs.(9-24), (9-25) and (9-26).

The uniaxial creep data were plotted on semi-log graph, Fig.(9-26), and on log-log graph, Fig.(9-27). It can be seen from the above two figures that the creep of gypsum under 30% σu and 40% σu give straight line relationship between the creep strain and the time on the semi-log graph (lines d and e in Fig. (9-26)), indicating that the logarithmic law ($\varepsilon = A + B \log t$) well fits the results obtained. The constants "A" and "B" were calculated in similar method described in the previous section of anhydrite. On the other hand, when the stress was increased to 50% σu, 65% σu and 80% σu the creep data gave a straight line relationship of creep strain versus time on log-log graph; lines

a, b and c in Fig.(9-27), indicating that the power law ($\varepsilon = Ct^n$) well fits the creep results under the above mentioned stress levels. The constants "C" and "n" were calculated by the least square method, mentioned previously, and equation (9-21).

2). For triaxial compression at various confining pressures the following relationships were obtained:

a - At 10 N/mm^2 confining pressure, table (9-9) and Figs. (9-28), (9-29) and (9-30). The creep behaviour of gypsum at this level of confining pressure followed the power law, Eq. (9-11), for all axial stress levels except under low axial stress, 30% σu where it followed the logarithmic relationship, Eq. (9-10), at the beginning of the test then a departure from this law to the power law was obtained. The relationships obtained were:

at σ_1 = 30% σu = 27.6 N/mm^2:

$$\varepsilon = 38.22 + 22.70 \log t \qquad (9\text{-}27)$$

for $0 < t \leq 24$ hours

and $\varepsilon = 43.91\ t^{0.189}$ (9-28)

for $t > 24$ hours

at σ_1 = 40% σu = 36.8 N/mm^2:

$$\varepsilon = 60.95\ t^{0.238} \qquad (9\text{-}29)$$

at σ_1 = 50% σu = 46.0 N/mm^2:

$$\varepsilon = 74.21\ t^{0.250} \qquad (9\text{-}30)$$

at σ_1 = 65% σu = 59.8 N/mm^2:

$$\varepsilon = 107.24\ t^{0.285} \qquad (9\text{-}31)$$

at σ_1 = 80% σu = 73.7 N/mm^2:

$$\varepsilon = 140.10\ t^{0.307} \qquad (9\text{-}32)$$

b - At 20 N/mm^2 confining pressure, table (9-10) and Figs. (9-31) and (9-32). The creep curves of gypsum under all axial

stress levels followed the power law, Eq. (9-11), throughout the tests. The following relationship were obtained:

at σ_1 = 30% σu = 34.4 N/mm^2:

$$\varepsilon = 62.11\ t^{0.199} \tag{9-33}$$

at σ_1 = 50% σu = 57.3 N/mm^2:

$$\varepsilon = 83.30\ t^{0.267} \tag{9-34}$$

at σ_1 = 65% σu = 74.5 N/mm^2

$$\varepsilon = 118.44\ t^{0.288} \tag{9-35}$$

at σ_1 = 80% σu = 91.7 N/mm^2:

$$\varepsilon = 148.28\ t^{0.313} \tag{9-36}$$

c- At 30 N/mm^2 confining pressure, table (9-11) and Figs. (9-33) and (9-34). The creep curves at this level of confining pressure and under all the applied axial stresses followed the power equation, Eq. (9-11), from the beginning of each test. The creep equations were as follows:

at σ_1 = 30% σu = 40.9 N/mm^2:

$$\varepsilon = 69.38\ t^{0.214} \tag{9-37}$$

at σ_1 = 50% σu = 68.2 N/mm^2:

$$\varepsilon = 97.74\ t^{0.271} \tag{9-38}$$

at σ_1 = 65% σu = 88.7 N/mm^2:

$$\varepsilon = 131.74\ t^{0.307} \tag{9-39}$$

at σ_1 = 80% σu = 109.2 N/mm^2:

$$\varepsilon = 164.18\ t^{0.344} \tag{9-40}$$

In the previous equations from (9-22) to (9-40) all the constants were found by using the least square method and checked with the values obtained from the semi-log and log-log graphs. All the results were in agreement. An example is given in Appendix B to illustrate the use of the least square method.

The degree of correctness is also shown in the same example by calculating the correlation coefficient (R). Analysis of the creep results and their discussions is made under the following major headings:

1). Effect of axial stress.

2). Effect of confining pressure.

9-2.2.1 Effect of Varying Axial Stress

Effect of varying axial stress on creep was studied under uniaxial and triaxial compression on gypsum and anhydrite. It can be seen from tables (9-6) to (9-11) that creep strain occurred at every axial stress. It is also clear from the above mentioned tables that the instantaneous strain increased with the applied axial stress. These deformations are not completely elastic in nature but consist of reversible and some irreversible deformations, specially at high axial stress. These irreversibly deformations, compared to the elastic deformations, are very small. The instantaneous deformations (strains) versus the corresponding axial stresses are plotted in Figs. (9-17) and (9-18) for gypsum and anhydrite respectively. The moduli of elasticity were also found by making use of these instantaneous strain-stress graphs, see section (9-2.1).

For anhydrite at uniaxial compression and triaxial at 10 N/mm^2 it was found that the creep curves followed the logarithmic relationships, see equations (9-13) to (9-19) except at triaxial compression under 80% σu, see equation (9-20). Misra[49] reported the same behaviour of most of the rocks tested under uniaxial compression. Griggs[28] indicated that creep in Solenhofen limestone, halite single crystals, shale and other rocks followed the logarithmic law under uniaxial compression. Phillips[62]

found the same behaviour in different metal wires subjected to uniaxial tension, see Eq. (5-1). The constants A and B of the logarithmic equation for anhydrite creep in both uniaxial and triaxial compression are given in table (9-13). It can be seen from this table that as the axial stress increases the values of both constants increase. In other words, the effect of increase the axial stress is to increase the creep rate, as well as the instantaneous strain.

Table (9-13)

The constants A and B of the logarithmic equation ($\varepsilon = A + B \log t$) for anhydrite.

Confining pressure	Axial stress % σu	Equation No.	A	B
Uniaxial	30%	9-13	8.62	8.29
	40%	9-14	17.11	15.15
	60%	9-15	22.42	18.70
	80%	9-16	26.81	26.10
10 N/mm^2	40%	9-17	16.31	14.38
	60%	9-18	21.50	20.16
	80%*	9-19	28.21	15.05

* The creep curve changed to the power law ($\varepsilon = Ct^n$) after 2 hours of creep.

For gypsum at uniaxial compression; Figs. (9-25),(9-26) and (9-27); the creep curves followed the logarithmic law, Eqs. (9-22) and (9-23), under low axial stress, namely 30% σu and 40% σu. Whereas under medium and high stress; 50% σu, 65% σu and 80% σu; they followed the power law; see Eqs. (9-24), (9-25) and (9-26). It can be seen from equations (9-22) and (9-23) that

the constants A and B of the logarithmic law increase with the stress. This behaviour was reported by many other investigators, Misra[49], Griggs[28] and others. Comparing the anhydrite uniaxial creep equations with those of the gypsum it can be seen that the creep curves of gypsum changed from logarithmic law to power equation at lower stress level (given as % σu), than that of the anhydrite. It seems likely that the weaker the rock the lower the stress level at which the creep law changes to a power law. Hedley[34] and Comte[11] in their uniaxial creep tests on rock salt reported that the creep curves followed the power law from the very beginning of the test. Their work conforms the above conclusion because, generally, rock salt is weaker than gypsum. The power equations (9-24), (9-25) and (9-26) and their constants C and n will be discussed later with triaxial creep results. For triaxial compression at 10, 20 and 30 N/mm^2 confining pressure the creep curves followed the power law, equation (9-11), for all the cases, see equations (9-28) to (9-40), except for the first 24 hours of the creep test at 10 N/mm^2 confining pressure under 30% σu axial stress where it followed the logarithmic law, equation (9-27). This behaviour of gypsum is in agreement with many investigators work on various rocks. Kendall[43] on rock salt and Solenhofen limestone, Comte[11] on artificial rock salt, Hedley[34] on potash, and others reported that the creep of rocks tested under triaxial compression followed the power law, Eq. (9-11). The power "n" was found to be $0 < n < 1$. Table (9-14) gives the creep equations, the constants C and n of the power equation ($\varepsilon = Ct^n$) and the creep rate at various times after loading for gypsum deformed under uniaxial and triaxial compression.

Table (9-14)

C and n of the power law and the creep rate of gypsum at uniaxial and triaxial compression creep tests.

σ_3 N/mm^2	$\frac{\sigma_1}{\sigma_u} \times 100$ / σ_1 N/mm^2	Creep Equation	Equation constants C	n	Creep rate, microstrain, at t = 1 hr.	12 hr.	24 hr.	48 hr.	96 hr.	120 hr.	192 hr.	240 hr.	360 hr.	480 hr.	600 hr.	720 hr.
0 Uni-axial	30% 17.2	$\varepsilon=32.5 + 26.9 \log t$	-	-	26.90	2.24	1.12	0.56	0.28	0.22	0.14	0.11	0.07	0.06	0.04	0.04
	40% 23.0	$\varepsilon=45.2 + 31.6 \log t$	-	-	31.60	2.63	1.32	0.66	0.33	0.26	0.16	0.13	0.08	0.07	0.05	0.04
	50% 28.7	$\varepsilon=53.5t^{0.215}$	53.5	.215	11.50	1.64	0.95	0.55	0.32	0.27	0.19	0.16	0.11	0.09	0.08	0.07
	65% 37.3	$\varepsilon=62.1t^{0.245}$	62.1	.245	15.21	2.33	1.38	0.82	0.48	0.41	0.29	0.24	0.18	0.14	0.12	0.11
	80% 46.0	$\varepsilon=90.2t^{0.284}$	90.2	.284	25.62	4.32	2.63	1.60	0.98	0.82	0.59	0.49	0.37	0.30	0.26	0.23
10	30% 27.6	$t \leq 24$ hr $\varepsilon=38.2 + 22.7 \log t$	-	-	22.70	1.89	0.84	-	-	-	-	-	-	-	-	-
		$t > 24$ hr $\varepsilon=43.9t^{0.189}$	43.9	.189	-	-	-	0.36	0.20	0.17	0.12	0.10	0.07	0.05	0.05	0.04
	50% 46.0	$\varepsilon=74.2t^{0.250}$	74.2	.250	18.55	2.87	1.71	1.02	0.60	0.51	0.36	0.30	0.22	0.18	0.15	0.13
	65% 59.8	$\varepsilon=107.2t^{0.285}$	107.2	.285	30.55	5.16	3.15	1.92	1.17	1.00	0.71	0.61	0.55	0.37	0.32	0.28
	80% 73.7	$\varepsilon=140.1t^{0.307}$	140.1	.307	43.01	7.68	4.75	2.94	1.81	1.56	1.12	0.97	0.73	0.60	0.51	0.45

Table (9-14) contd.

C and of the power law and the creep rate of gypsum at uniaxial and triaxial compression creep tests

σ_3 N/mm^2	$\frac{\sigma_1}{\sigma_u} \times 100$ / σ_1 N/mm^2	Creep Equation	Equation constants		Creep rate, microstrain, at t =											
			C	n	1 hr.	12 hr.	24 hr.	48 hr.	96 hr.	120 hr.	192 hr.	240 hr.	360 hr.	480 hr.	600 hr.	720 hr.
20	30% 34.4	$\varepsilon=62.1t^{0.199}$	62.1	.199	12.36	1.69	0.97	0.56	0.32	0.27	0.18	0.15	0.11	0.09	0.08	0.06
	50% 57.3	$\varepsilon=83.3t^{0.267}$	83.3	.267	22.24	3.60	2.16	1.30	0.78	0.67	0.47	0.40	0.30	0.24	0.21	0.18
	65% 74.5	$\varepsilon=118.4t^{0.288}$	118.4	.288	34.10	5.81	3.54	2.17	1.32	1.13	0.81	0.69	0.52	0.42	0.36	0.32
	80% 91.7	$\varepsilon=148.3t^{0.313}$	148.3	.313	46.42	8.41	5.23	3.25	2.02	1.73	1.25	1.08	0.82	0.67	0.57	0.51
30	30% 40.9	$\varepsilon=69.4t^{0.214}$	69.4	.214	14.85	2.15	1.22	0.71	0.41	0.34	0.24	0.20	0.15	0.12	0.10	0.08
	50% 68.2	$\varepsilon=97.7t^{0.271}$	97.7	.271	26.48	4.31	2.61	1.58	0.95	0.81	0.57	0.49	0.37	0.30	0.25	0.22
	73.3	$\varepsilon=106.2t^{0.280}$	106.2	.280	29.74	4.97	3.02	1.83	1.11	0.95	0.68	0.57	0.43	0.35	0.30	0.26
	65% 88.7	$\varepsilon=131.7t^{0.307}$	131.7	.307	40.43	8.25	4.47	2.76	1.71	1.46	1.06	0.91	0.68	0.56	0.48	0.42
	80% 109.2	$\varepsilon=164.2t^{0.334}$	164.2	.344	56.48	11.07	7.02	4.46	2.83	2.44	1.79	1.55	1.19	0.98	0.85	0.75

Table (9-14) contd.

C and of the power law and the creep rate of gypsum at uniaxial and triaxial compression creep tests

σ_3 N/mm^2	$\frac{\sigma_1}{\sigma_u}$x100 / σ_1 N/mm^2	Creep Equation	Equation constants		Creep rate, microstrain, at t =											
			C	n	1 hr.	12 hr.	24 hr.	48 hr.	96 hr.	120 hr.	192 hr.	240 hr.	360 hr.	480 hr.	600 hr.	720 hr.
20	30% 34.4	$\varepsilon=62.1t^{0.199}$	62.1	.199	12.36	1.69	0.97	0.56	0.32	0.27	0.18	0.15	0.11	0.09	0.08	0.06
	50% 57.3	$\varepsilon=83.3t^{0.267}$	83.3	.267	22.24	3.60	2.16	1.30	0.78	0.67	0.47	0.40	0.30	0.24	0.21	0.18
	65% 74.5	$\varepsilon=118.4t^{0.288}$	118.4	.288	34.10	5.81	3.54	2.17	1.32	1.13	0.81	0.69	0.52	0.42	0.36	0.32
	80% 91.7	$\varepsilon=148.3t^{0.313}$	148.3	.313	46.42	8.41	5.23	3.25	2.02	1.73	1.25	1.08	0.82	0.67	0.57	0.51
30	30% 40.9	$\varepsilon=69.4t^{0.214}$	69.4	.214	14.85	2.15	1.22	0.71	0.41	0.34	0.24	0.20	0.15	0.12	0.10	0.08
	50% 68.2	$\varepsilon=97.7t^{0.271}$	97.7	.271	26.48	4.31	2.61	1.58	0.95	0.81	0.57	0.49	0.37	0.30	0.25	0.22
	73.3	$\varepsilon=106.2t^{0.280}$	106.2	.280	29.74	4.97	3.02	1.83	1.11	0.95	0.68	0.57	0.43	0.35	0.30	0.26
	65% 88.7	$\varepsilon=131.7t^{0.307}$	131.7	.307	40.43	8.25	4.47	2.76	1.71	1.46	1.06	0.91	0.68	0.56	0.48	0.42
	80% 109.2	$\varepsilon=164.2t^{0.334}$	164.2	.344	56.48	11.07	7.02	4.46	2.83	2.44	1.79	1.55	1.19	0.98	0.85	0.75

From table (9-14) and the corresponding equations it is clear that the constants "C" and "n" increase with the axial stress at any particular confining pressure. The values of C and n are plotted against the axial stress in Figs. (9-36) and (9-37) respectively. Hedley[34] reported similar behaviour in rock salt and potash. The creep rate increases with the axial stress as shown in table (9-14) and Figs. (9-38) and (9-39) and therefore shorten the time to fracture. The values of creep rate given in table (9-14) were plotted against the axial stress on log-log graph. Straight lines were obtained indicating that the relationship between the creep rate "ε'" and the axial stress σ_1 follows a power equation of the form $\varepsilon' = k\sigma_1^{g}$, see equation (9-11), where k is a constant equal to the creep rate ε' at $\sigma_1 = 1\ N/mm^2$ and g is another constant equal to the slope of the straight line of ε' versus σ_1 on a log-log graph. Fig.(9-40) gives two sets of straight lines for creep rate versus σ_1 on log-log graph at 20 and 30 N/mm^2 confining pressure at various values of t. It can be seen from Fig. (9-40) that at each level of σ_3 the set of relationships consists of several straight lines parallel or nearly parallel to each other, in other words, they have one slope. The equations for these sets of straight lines are:

at $\sigma_3 = 20\ N/mm^2$

$$\varepsilon' = k\ \sigma_1^{1.857} \qquad (9\text{-}41)$$

at $\sigma_3 = 30\ N/mm^2$

$$\varepsilon' = k\ \sigma_1^{1.801} \qquad (9\text{-}42)$$

Misra[49] and Hedley[34] reported the same relationships between the creep rate and the stress in their uniaxial creep tests on different rocks.

The safe axial creep stress applied to a gypsum specimen for an assumed service life can be determined from the creep data available as follows:

Experimental data of creep in gypsum under triaxial compression at 10 N/mm^2 confining pressure have been chosen to be used in determining the working stress (σ_w) under the given conditions.

$$\sigma_w = \frac{\sigma_c}{f} \tag{9-43}$$

where σ_w is the working stress, σ_c is the stress that would just cause failure by excessive creep in the given expected life and f is a safety factor that suitably covers uncertainties of material variability and operating conditions. At room temperature and at the given confining pressure the creep strength σ_c is determined from the series of the creep strain-time curves of Fig. (9-28) as follows:

Assume that the expected life is 1,000,000 hours and the critical strain is 3000 microstrain, for the determination of the critical strain see Potts[66] and Hedley[34]. The creep curves of Fig.(9-28) are plotted on log-log graph and the critical strain is drawn as shown in Fig. (9-41). The creep relationships, straight lines, are extrapolated to intersect the horizontal line of the critical strain. The time at each point of intersection represents the time required for that specimen to reach the critical strain at the given stresses. In Fig. (9-42) the time to reach the critical creep strain, determined from Fig.(9-41), is plotted against the axial stress on a log-log graph. A straight line is obtained from which the creep stress which causes the critical creep strain for the assumed expected life can be determined by means of the projection on the stress axis from the

point of intersection of the straight line and t = 1,000,000 hours.

Using a similar procedure any creep strength and any assumed life can be accommodated. Knowing the creep strength σ_c and factor of safety f, the safe working stress σ_w for the service life can be calculated by Eq. (9-43). From Fig. (9-42) it is clear that the service life of the specimen increases as the creep strength decreases for a certain critical strain. The above mentioned method can be used for any engineering rock structure providing creep data of the rock concerned is available, and it is clear that triaxial results greatly increase the field of application of the procedure in rock engineering problems.

At constant differential stress $(\sigma_1-\sigma_3)$ it was found that the creep rate increases with the axial stress. Fig. (9-43) shows the relationship between the creep rate and σ_1 at constant $(\sigma_1-\sigma_3)$ at various times. It can be observed that all the relationships are straight lines emanating from one point on σ_1-axis (negative value). Therefore, for any constant differential stress there will be a set of ε' vs σ_1 straight lines emanate from one point on the σ_1-axis so that a general equation can be written for this relationship in the form:

$$\varepsilon' = (K + \sigma_1)R \qquad (9-44)$$

where ε' is the creep rate, K is the absolute value of σ_1 at $\varepsilon' = 0$ and R is the slope of the straight line. From Fig. (9-43) the following general equation was found:

$$\varepsilon' = (7.5 + \sigma_1) \times R \qquad (9-45)$$

For different values of t, the values of R are given in table (9-15).

Table (9-15)

Values of R for various values of t

at $(\sigma_1-\sigma_3)$ = 40 N/mm^2

Time hours	R x 10^{-3}
24	35.5
120	11.1
240	6.7
600	3.3

9-2.2.2 Effect of Confining Pressure

At a constant axial stress a rapid decrease in the creep rate was observed as the confining pressure increased. Fig. (9-44) shows the relationship between the creep rate of gypsum and the confining pressure at constant axial stress (σ_1=73.3 N/mm^2). The figure shows a set of curves at various times. The curves are concave upward and nearly parallel to each other. An explanation for this behaviour is that the confining pressure may decrease the size, number and propagation of fractures during creep. Comte[11], Hedley[34], Robertson[72] and others reported the same behaviour in different rocks subjected to triaxial creep. At a constant axial stress it can be also seen from table (9-14) that both constants C and n of the power equation, Eq.(9-11), decrease as the confining pressure increases, Fig. (9-45). Both curves are not linear and concave upwards.

From table (9-14) at an axial stress corresponding to a constant percentage of the short term strength (%σu) such as 50% σu or 65% σu, it can be seen that the creep rate at any time, C and n increase as the confining pressure increases. Creep of anhydrite in uniaxial compression followed the logarithmic law, Eq.(9-10),

for all axial stress levels, whereas at 10 N/mm^2 confining pressure the creep curves changed to the power law, Eq.(9-11), at 80% σu. The same behaviour can be observed in gypsum subject to creep under uniaxial and triaxial compression. Therefore, it can be stated that varying the confining pressure affects the creep behaviour of these rocks by controlling the form of the creep strain versus time law at a certain percentage of their short term strengths.

Increasing the confining pressure on any rock changes some of its mechanical properties; it makes that rock more ductile than its nature at atmospheric pressure; it makes the rock deform under suitable axial load, plastically rather than in a brittle manner, Murrell[50]. The creep property is one of the rock's mechanical characteristics that is also affected by the change of the confining pressure even under constant differential stress. Patchet[59] reported that the creep rate of a specimen is dependent on the differential stress applied and is independent of the magnitude of either the axial or lateral stresses. In this research it was found that varying the confining pressure has an effect on the creep behaviour of gypsum at constant differential stress. Williams and Elizzi[92] confirmed the effect of varying the confining pressure on the creep phenomenon at constant differential stress. Figs. (9-46) and (9-47) show that at constant differential stress as the confining pressure increases the creep strain and the creep rate increase slightly. The constants "C" and "n" of the creep power equation, Eq.(9-11), were also affected by varying the confining pressure at constant differential stress. Fig. (9-48) shows that both "C" and "n" increase with confining pressure. It was also found that at a constant differential

stress up to $\sigma_1 - \sigma_3$ = 42.5 N/mm^2, the creep rate increases linearly with confining pressure whereas above $\sigma_1 - \sigma_3$ = 42.5 N/mm^2 the curve starts to take a parabolic shape concave upwards as shown in Fig. (9-49). At any differential stress below the limit (42.5 N/mm^2) there is a set of straight lines of creep rate versus confining pressure at different times. These straight lines emanate from one point on the σ_3-axis as shown in Fig. (9-50). This behaviour is similar to that given in Fig. (9-43).

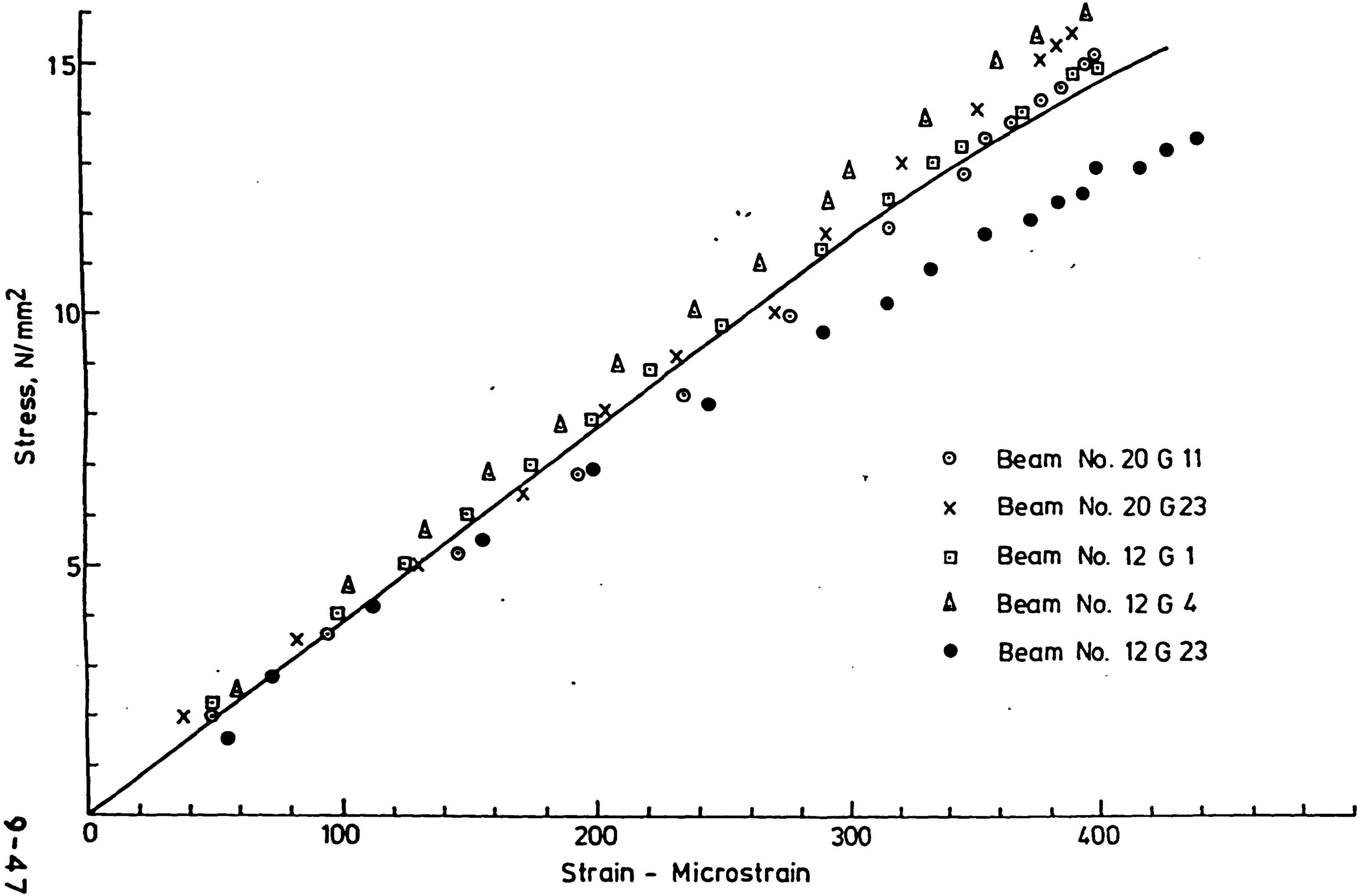

FIG. 9-2 STRESS - STRAIN RELATION OF GYPSUM IN TENSION FROM BENDING TESTS

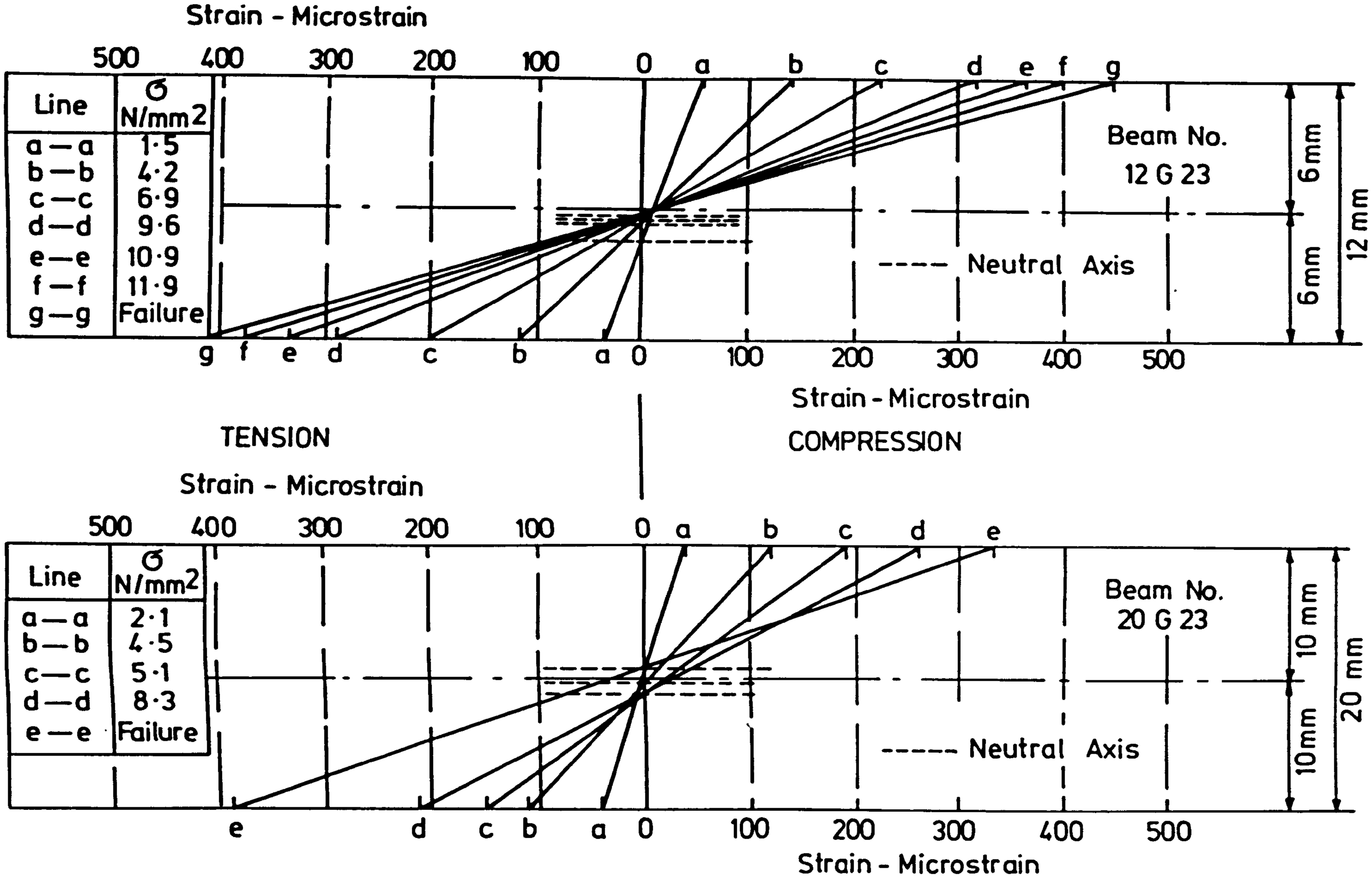

FIG. 9-3 DISTRIBUTION OF STRAIN OF GYPSUM AT VARIOUS STRESSES

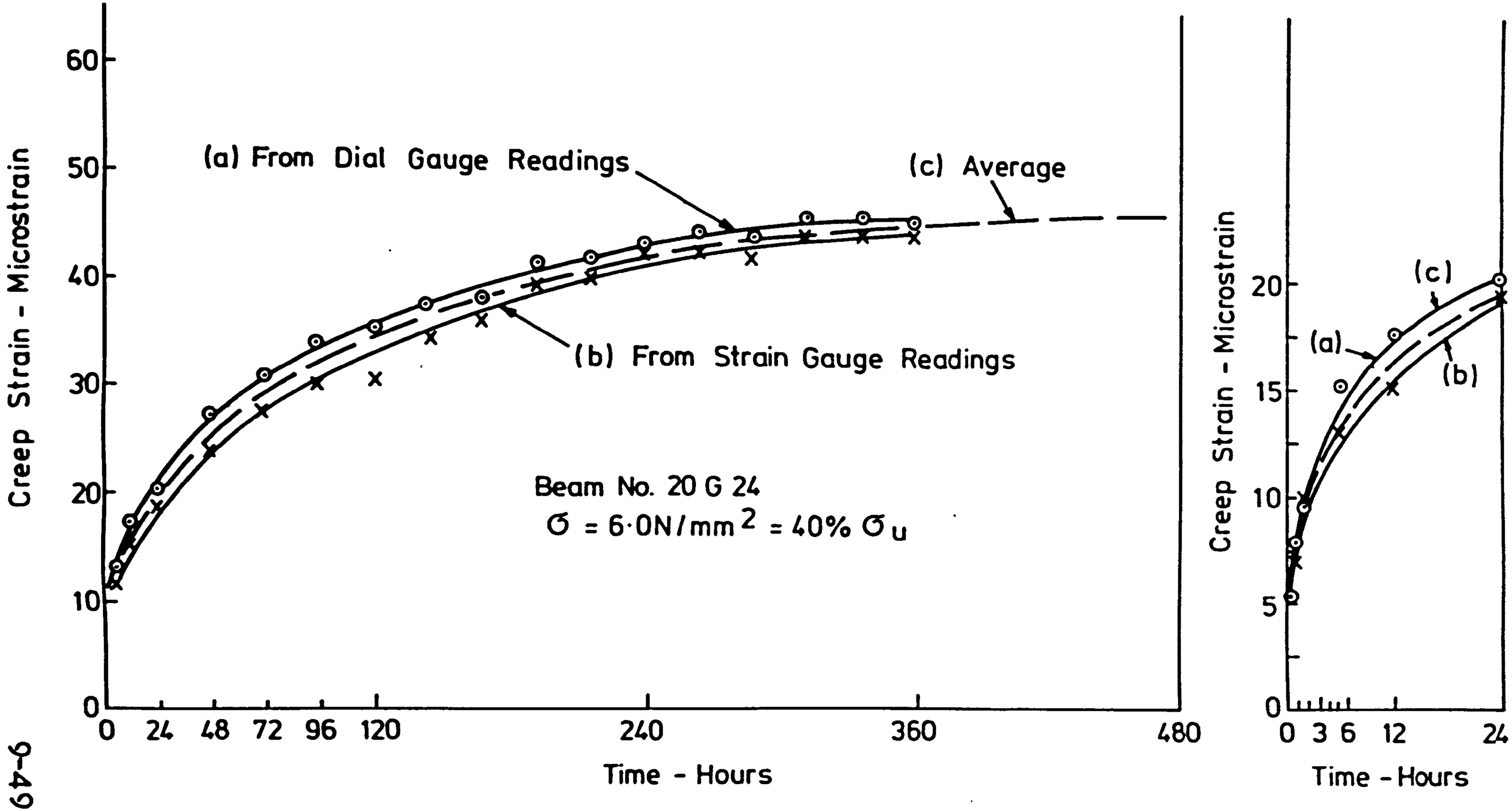

FIG. 9-4 CREEP OF GYPSUM IN BENDING (Average)

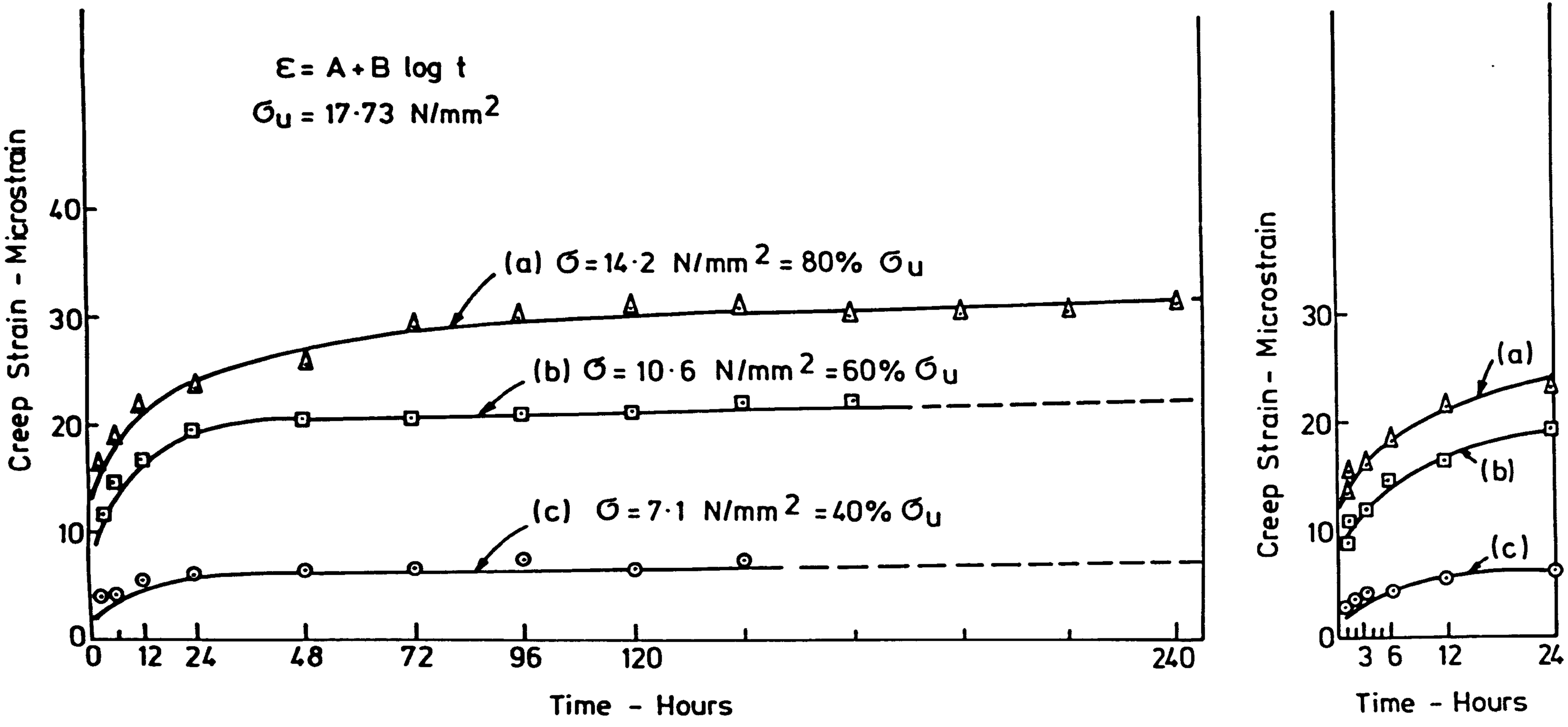

FIG. 9-6 CREEP OF ANHYDRITE IN BENDING AT VARIOUS STRESSES

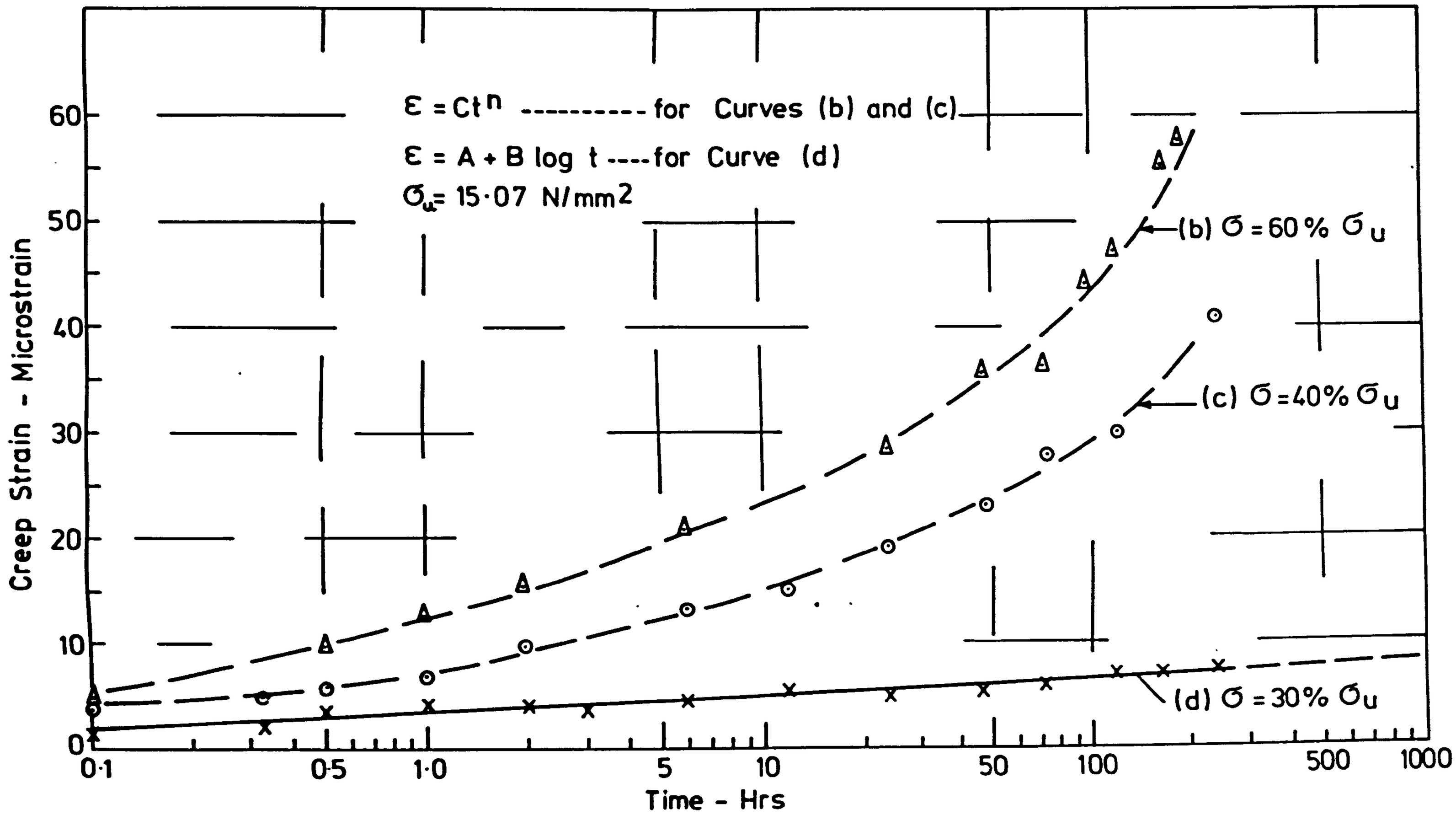

FIG. 9-7 CREEP OF GYPSUM IN BENDING
(Semi - Log Graph)

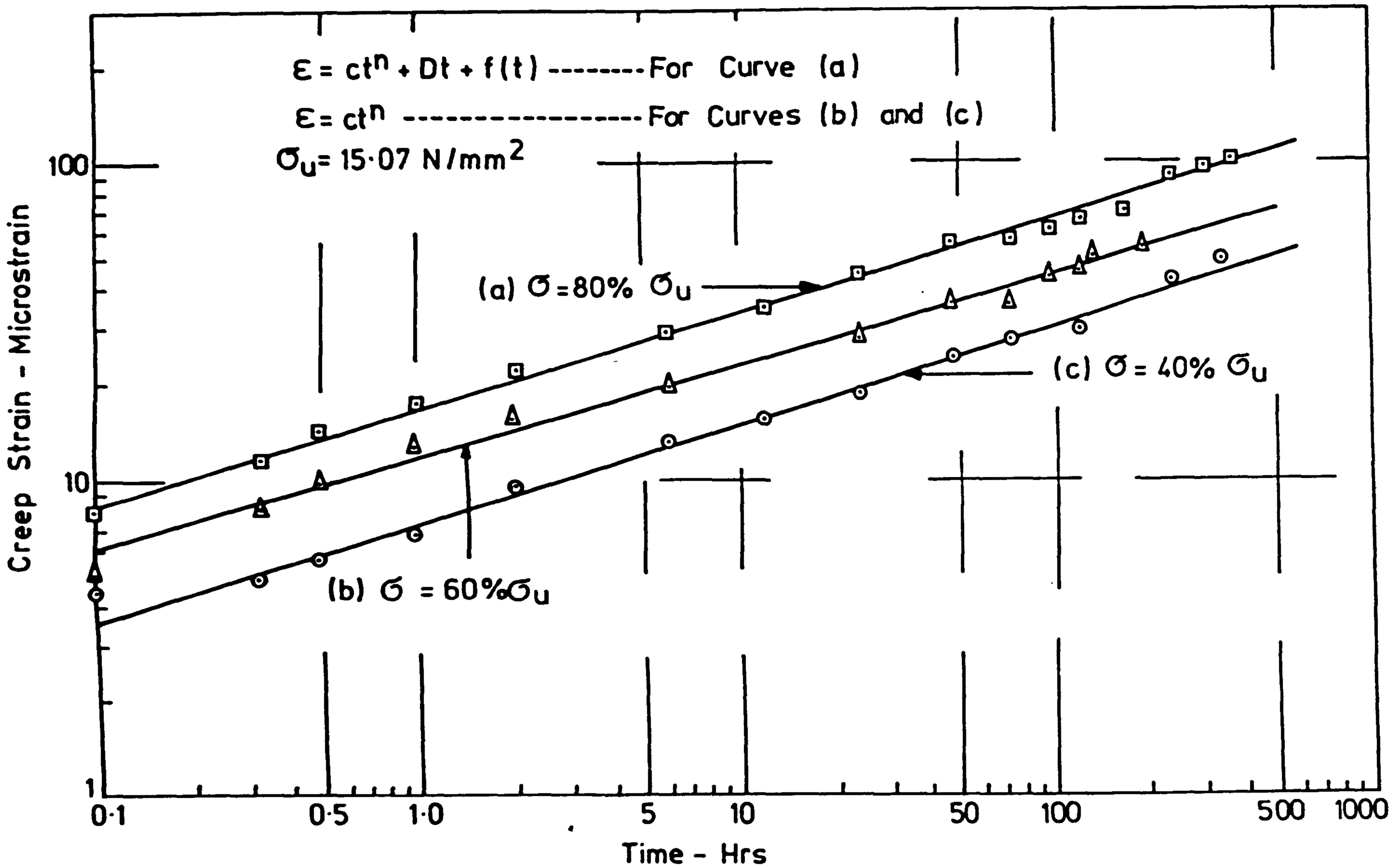

FIG. 9-8 CREEP OF GYPSUM IN BENDING
(Log-Log Graph)

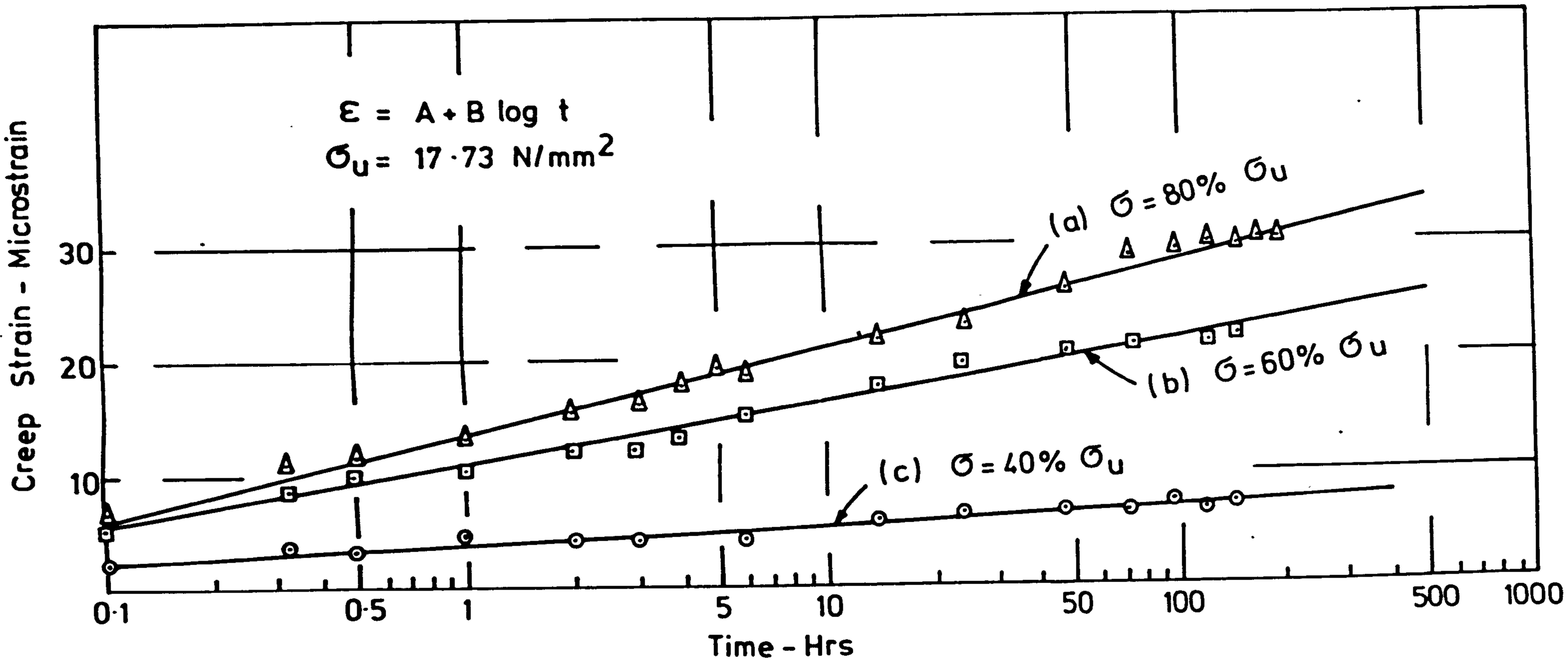

FIG. 9-9 CREEP OF ANHYDRITE IN BENDING
(Semi-Log Graph)

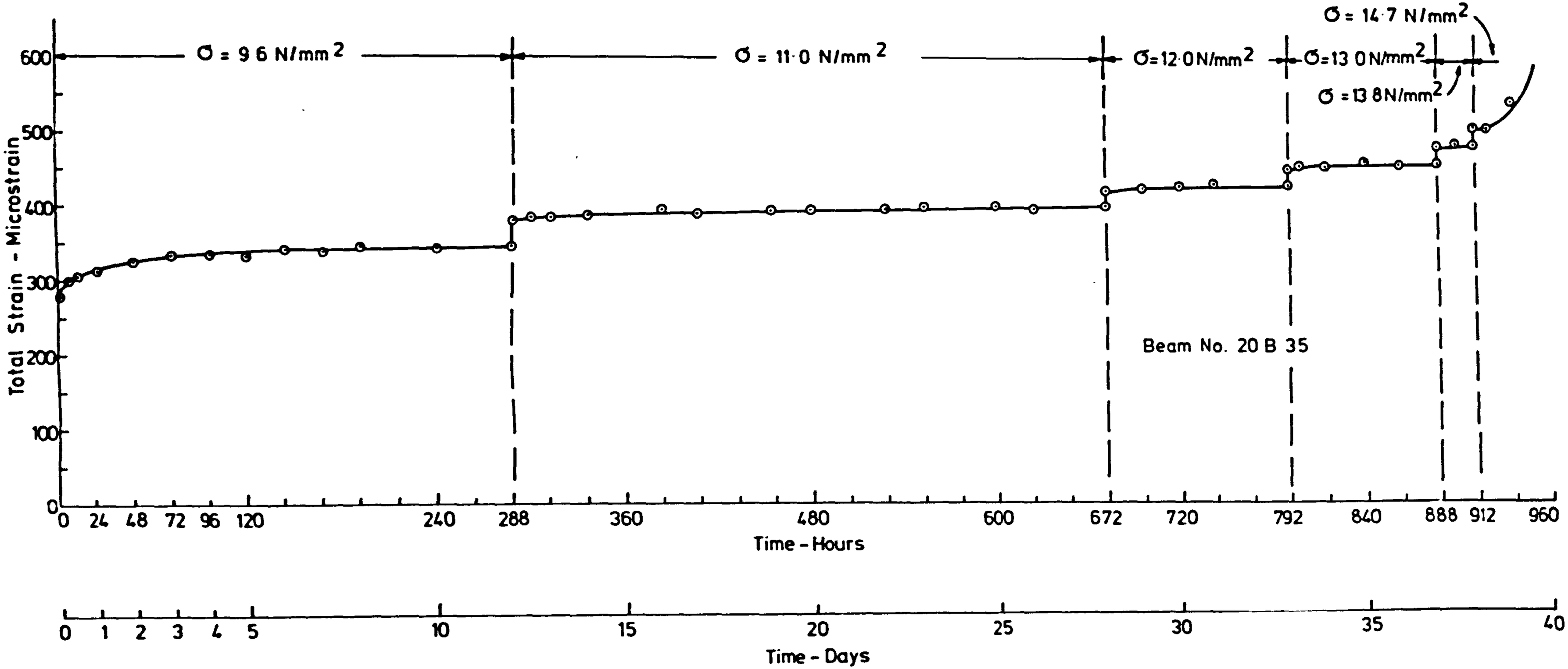

FIG. 9-10 CREEP OF GYPSUM SPECIMEN IN BENDING AT VARIOUS STRESSES

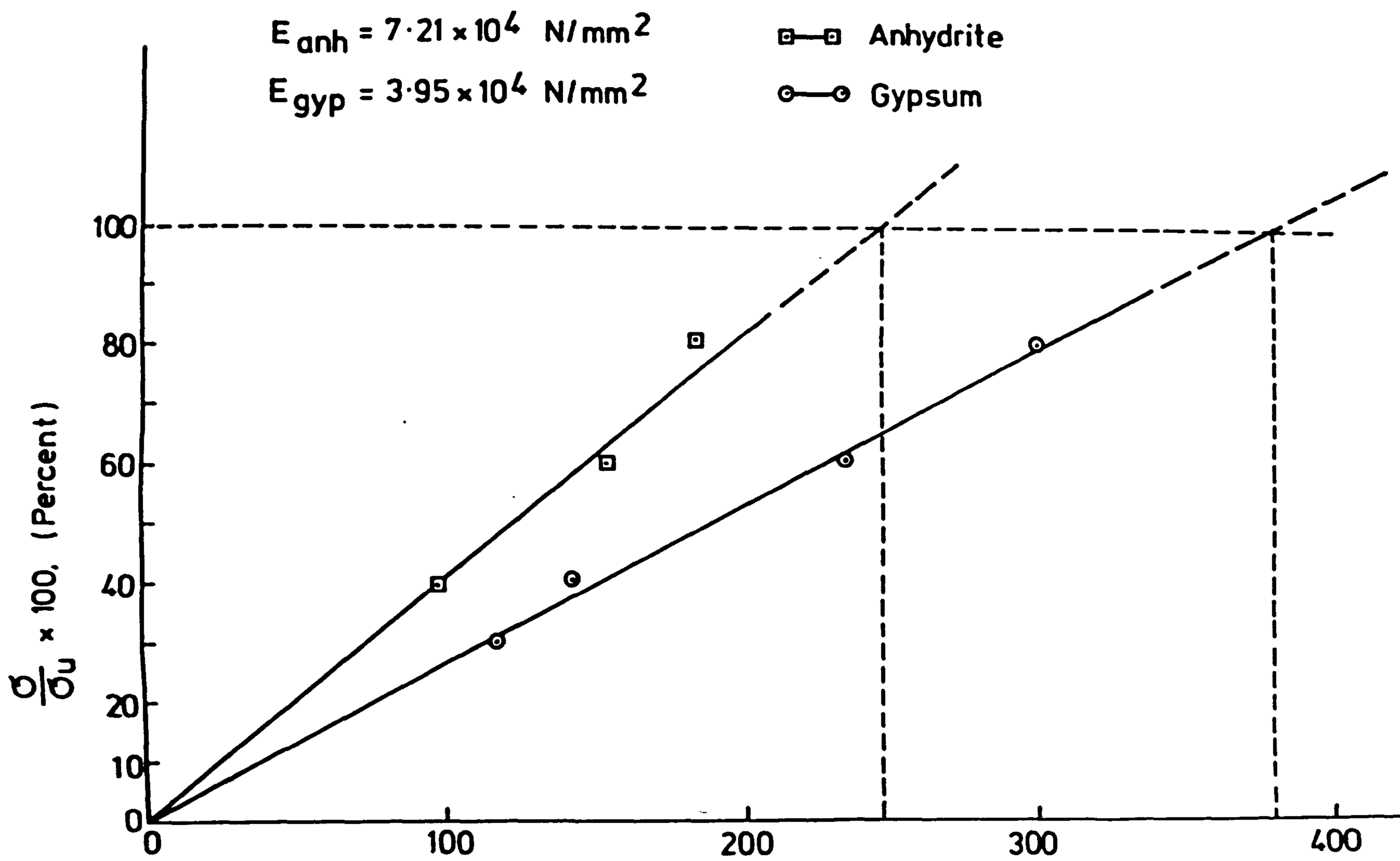

FIG. 9-11 DETERMINATION OF MODULUS OF ELASTICITY OF GYPSUM AND ANHYDRITE FROM BENDING CREEP TESTS

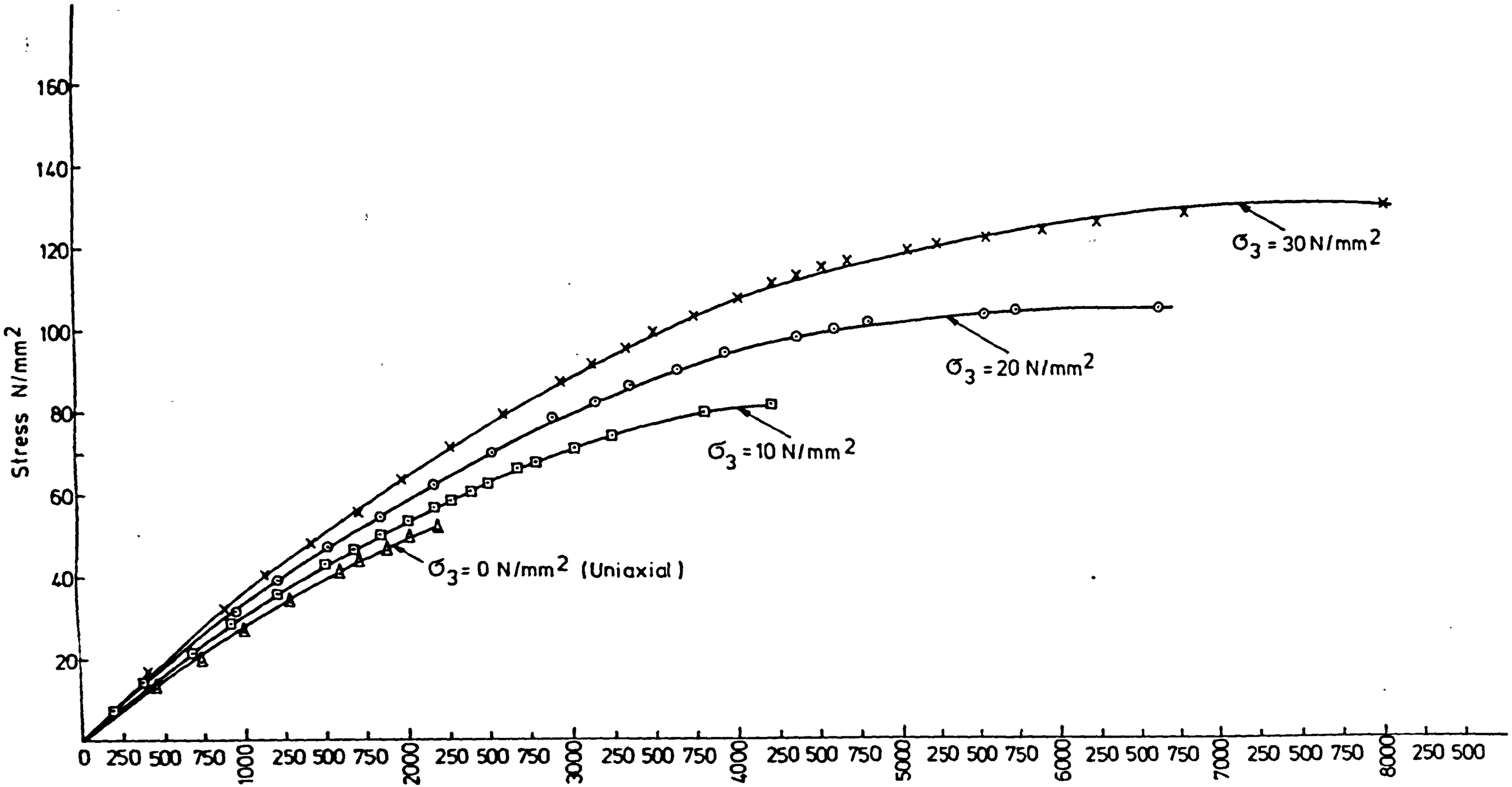

FIG. 9-12 STRESS-STRAIN CURVES OF GYPSUM AT VARIOUS CONFINING PRESSURES

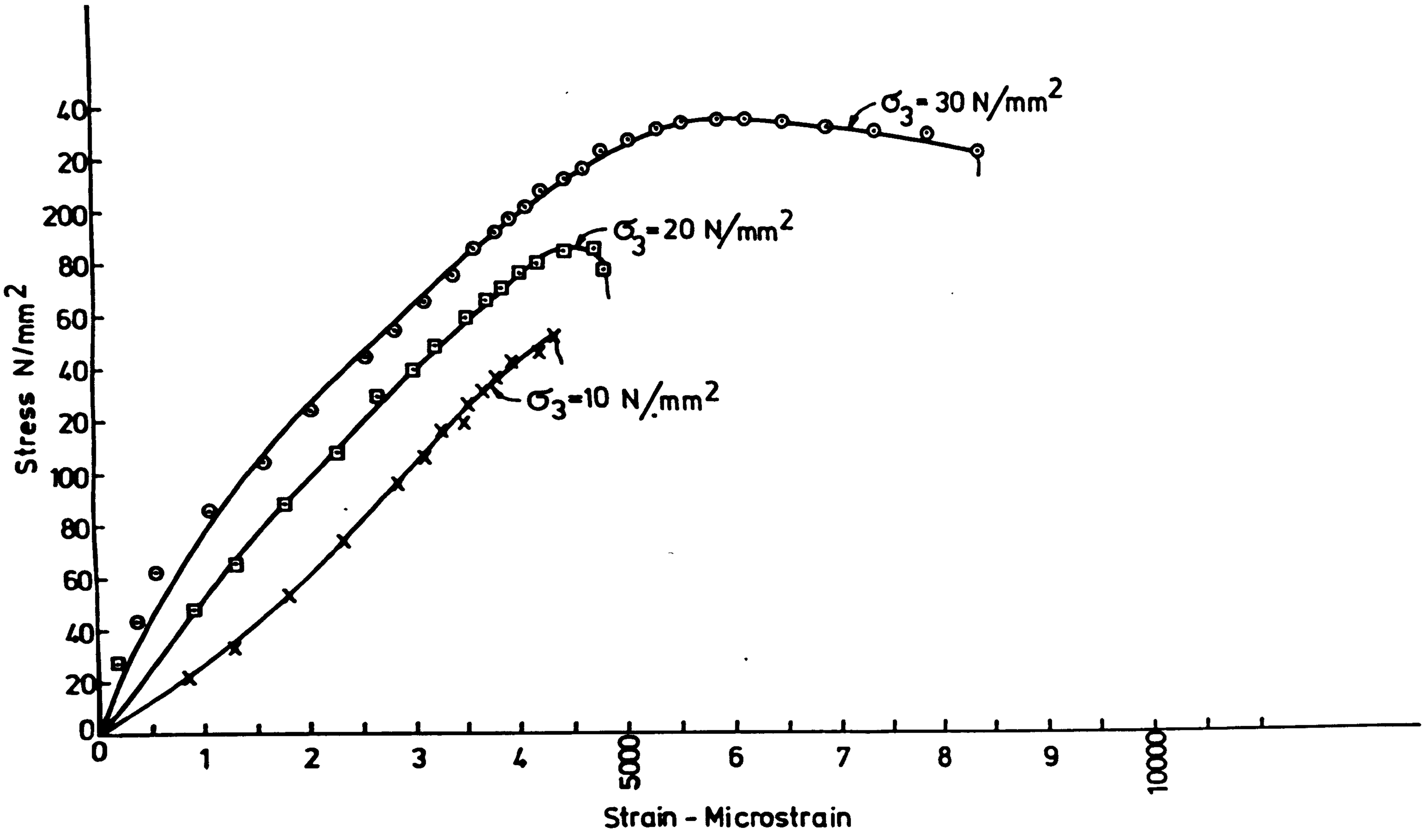

FIG. 9-13 STRESS-STRAIN CURVES OF ANHYDRITE AT VARIOUS CONFINING PRESSURES

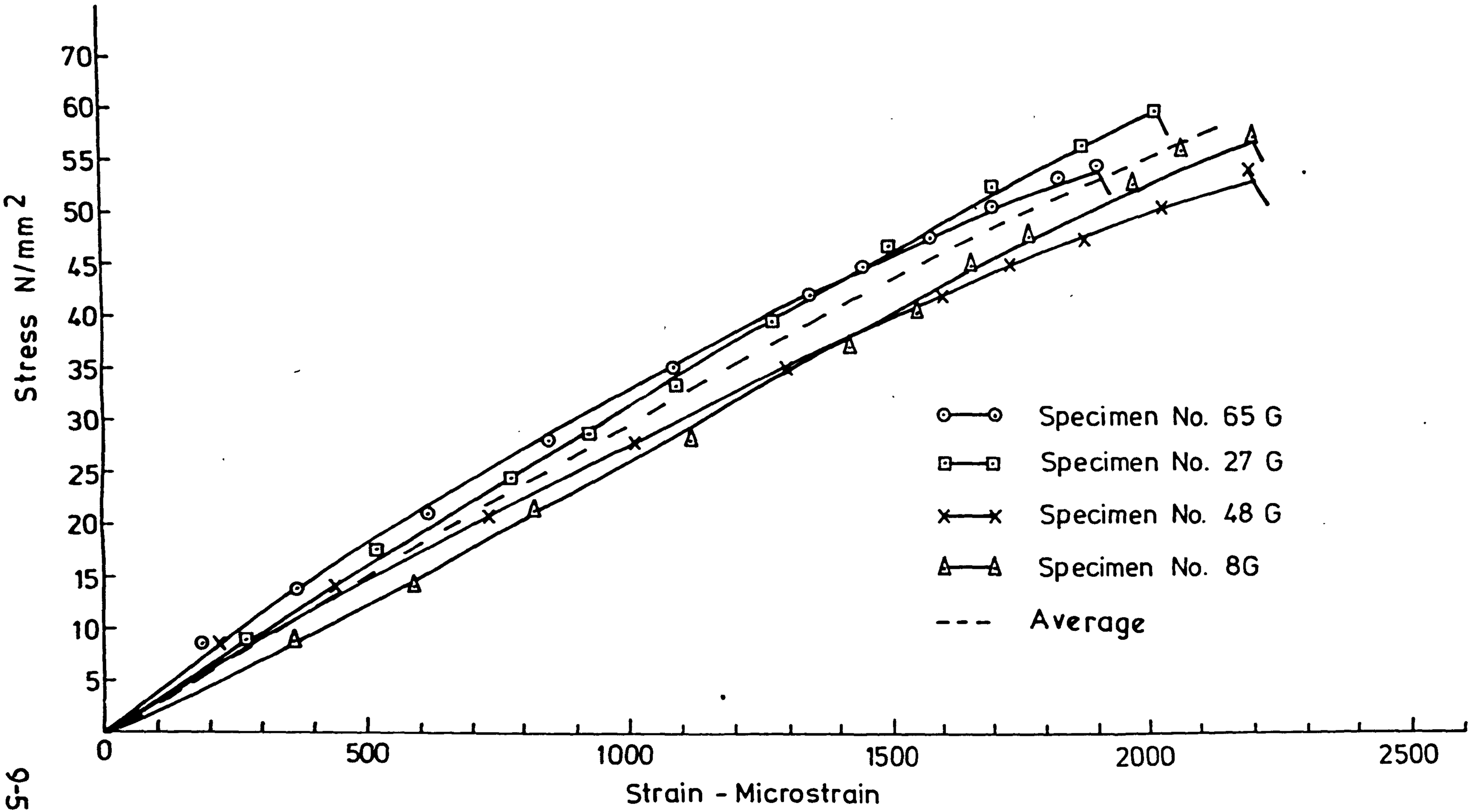

FIG. 9-14 STRESS-STRAIN CURVES OF GYPSUM IN UNIAXIAL COMPRESSION

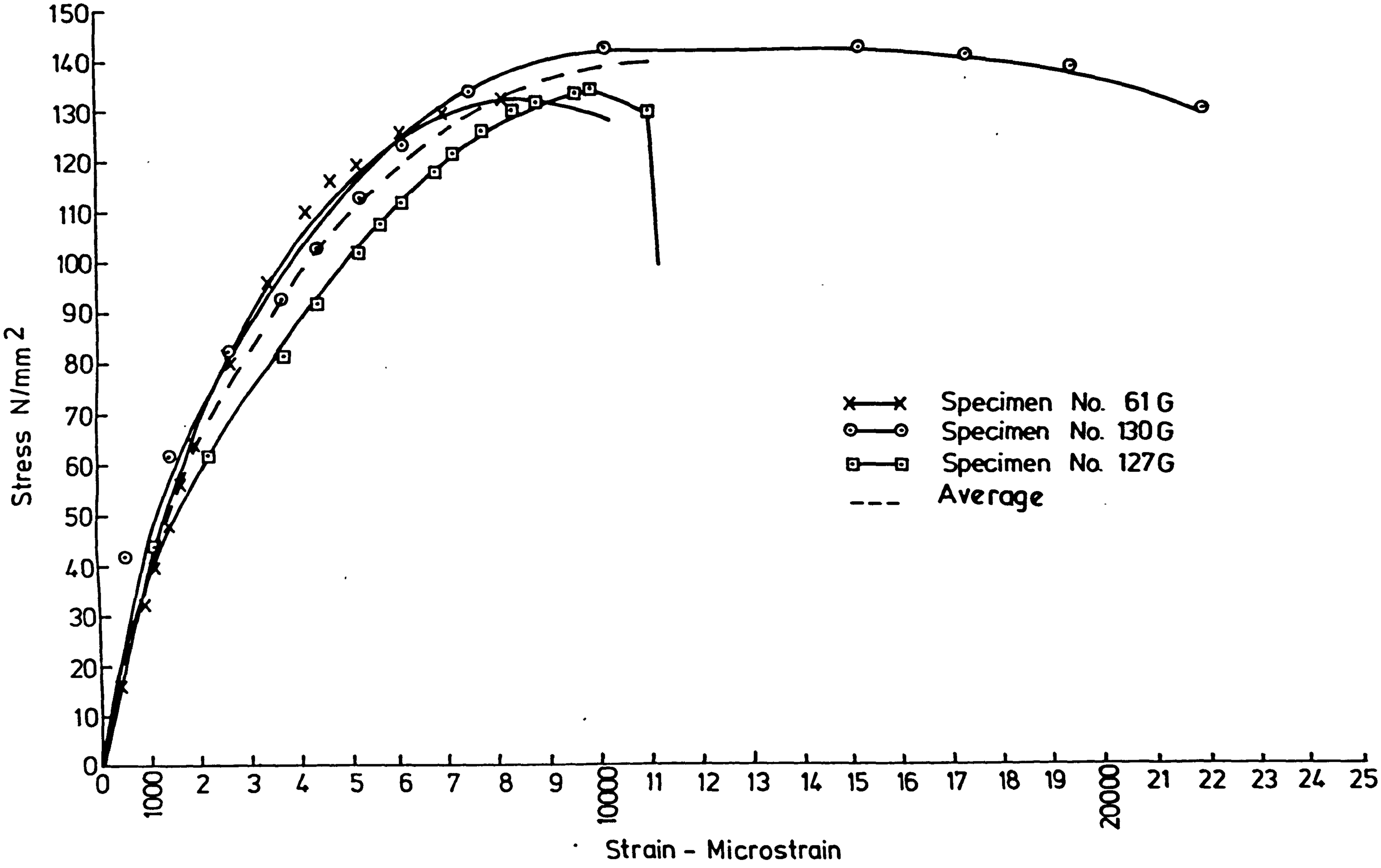

FIG. 9-15 STRESS-STRAIN CURVES OF GYPSUM AT 30 N/mm^2 CONFINING PRESSURE

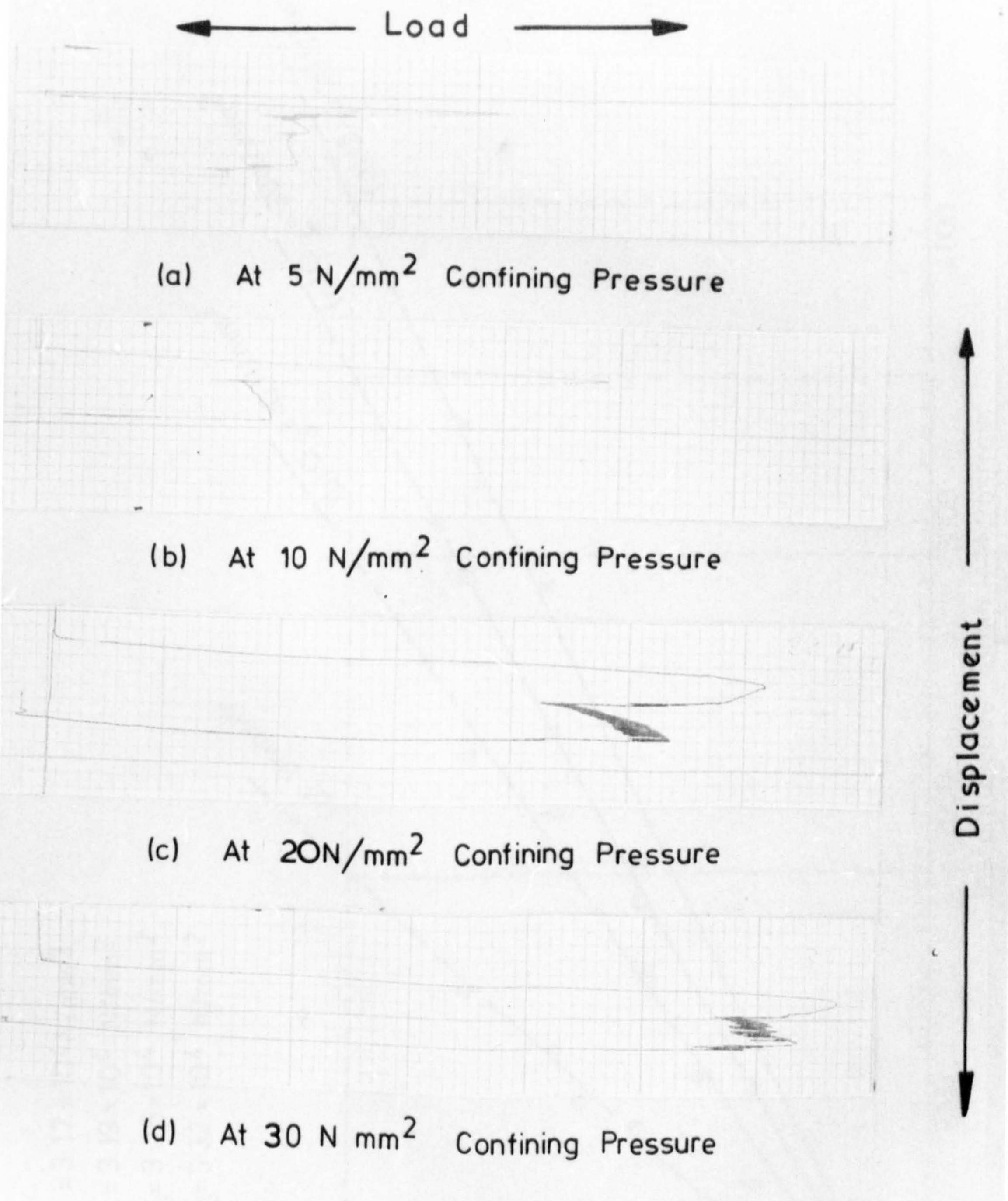

FIG 9–16 LOAD – DISPLACEMENT CURVES OF GYPSUM AT VARIOUS CONFINING PRESSURES

(a) $E_0 = 3{\cdot}17 \times 10^4 N/mm^2$

(b) $E_{10} = 3{\cdot}19 \times 10^4 \ N/mm^2$

(c) $E_{20} = 3{\cdot}26 \times 10^4 \ N/mm^2$

(d) $E_{30} = 3{\cdot}32 \times 10^4 \ N/mm^2$

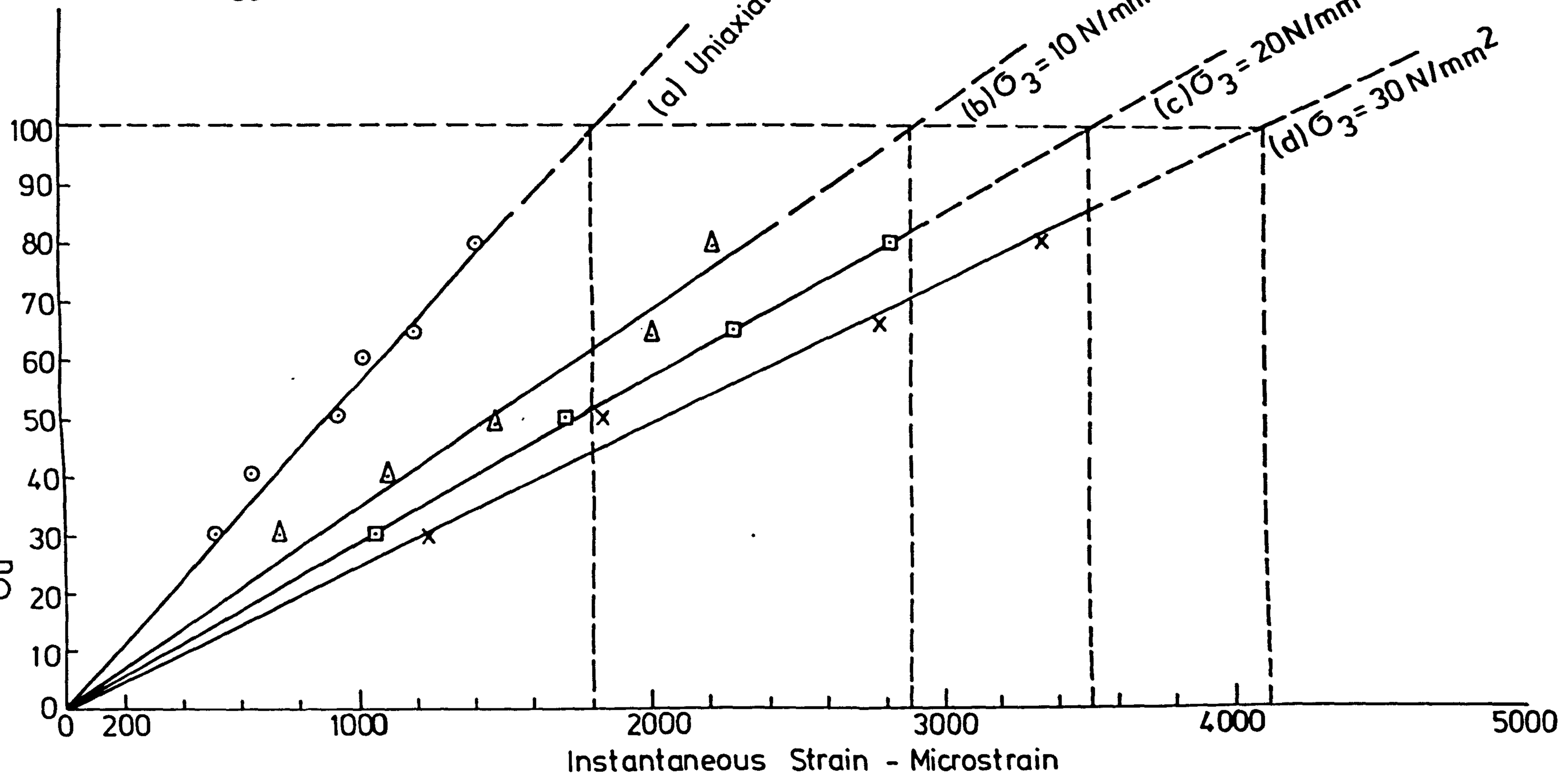

FIG. 9-17 DETERMINATION OF MODULUS OF ELASTICITY OF GYPSUM AT VARIOUS $\bar{\sigma}_3$

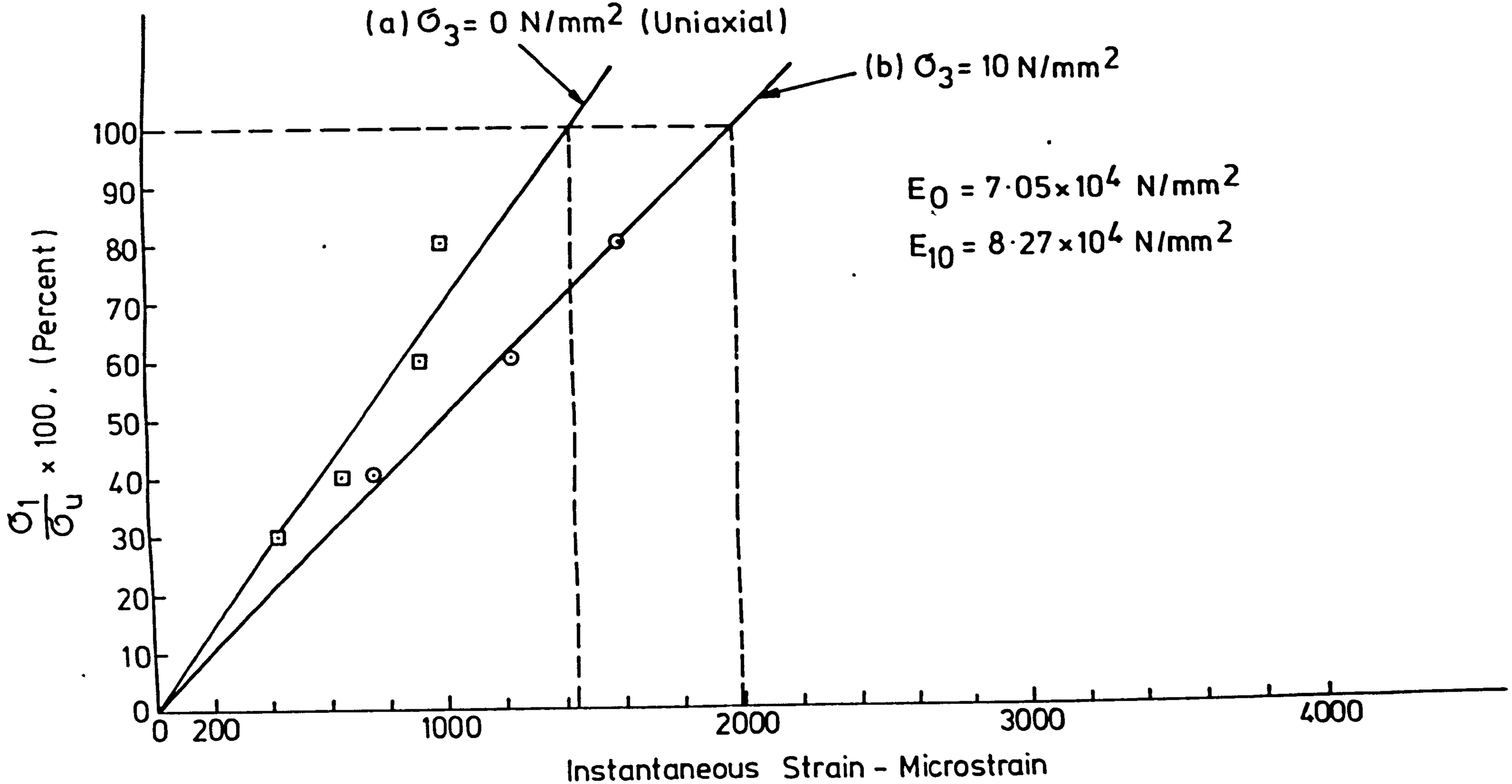

FIG. 9-18 DETERMINATION OF MODULUS OF ELASTICITY OF ANHYDRITE AT VARIOUS σ_3

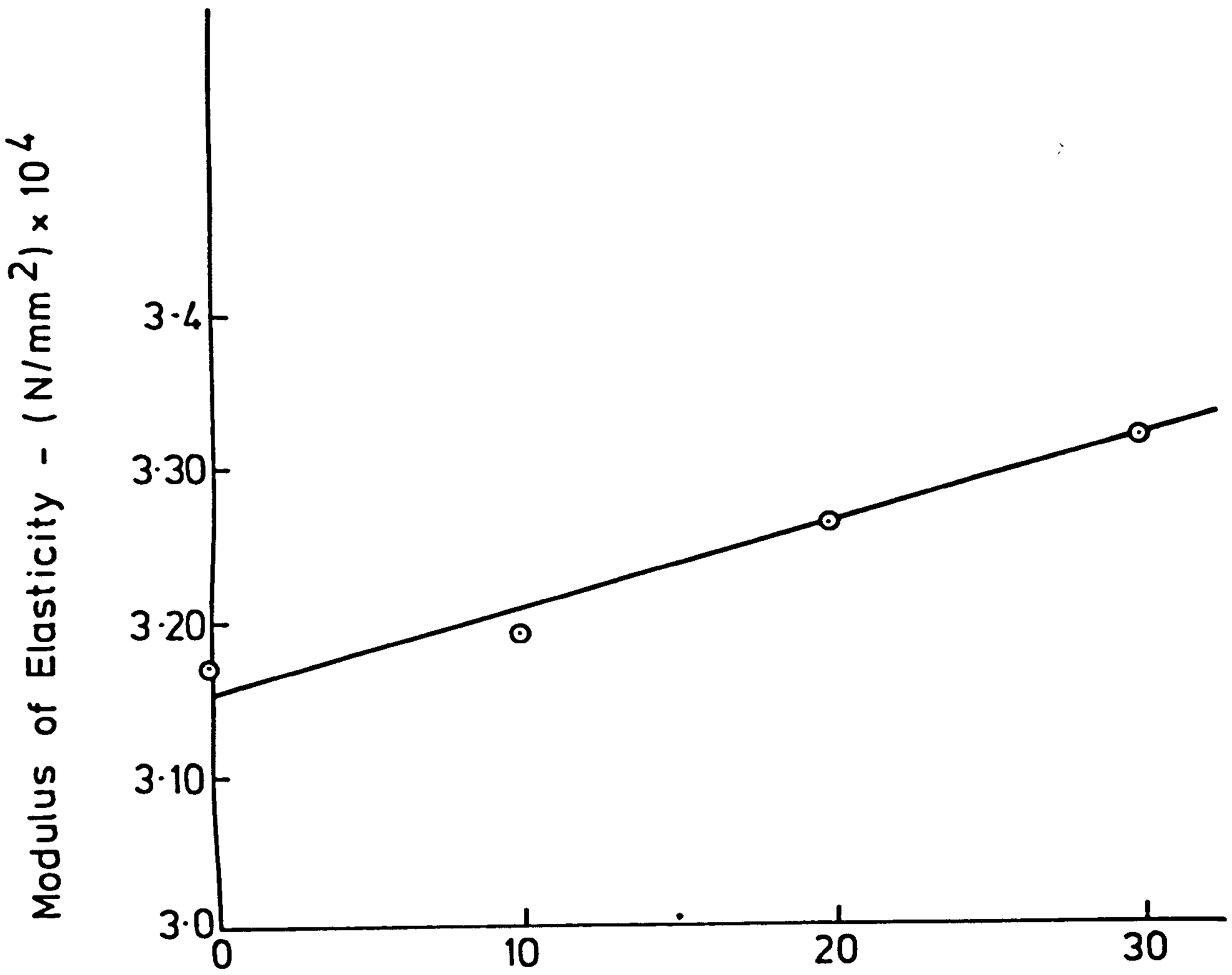

GYPSUM

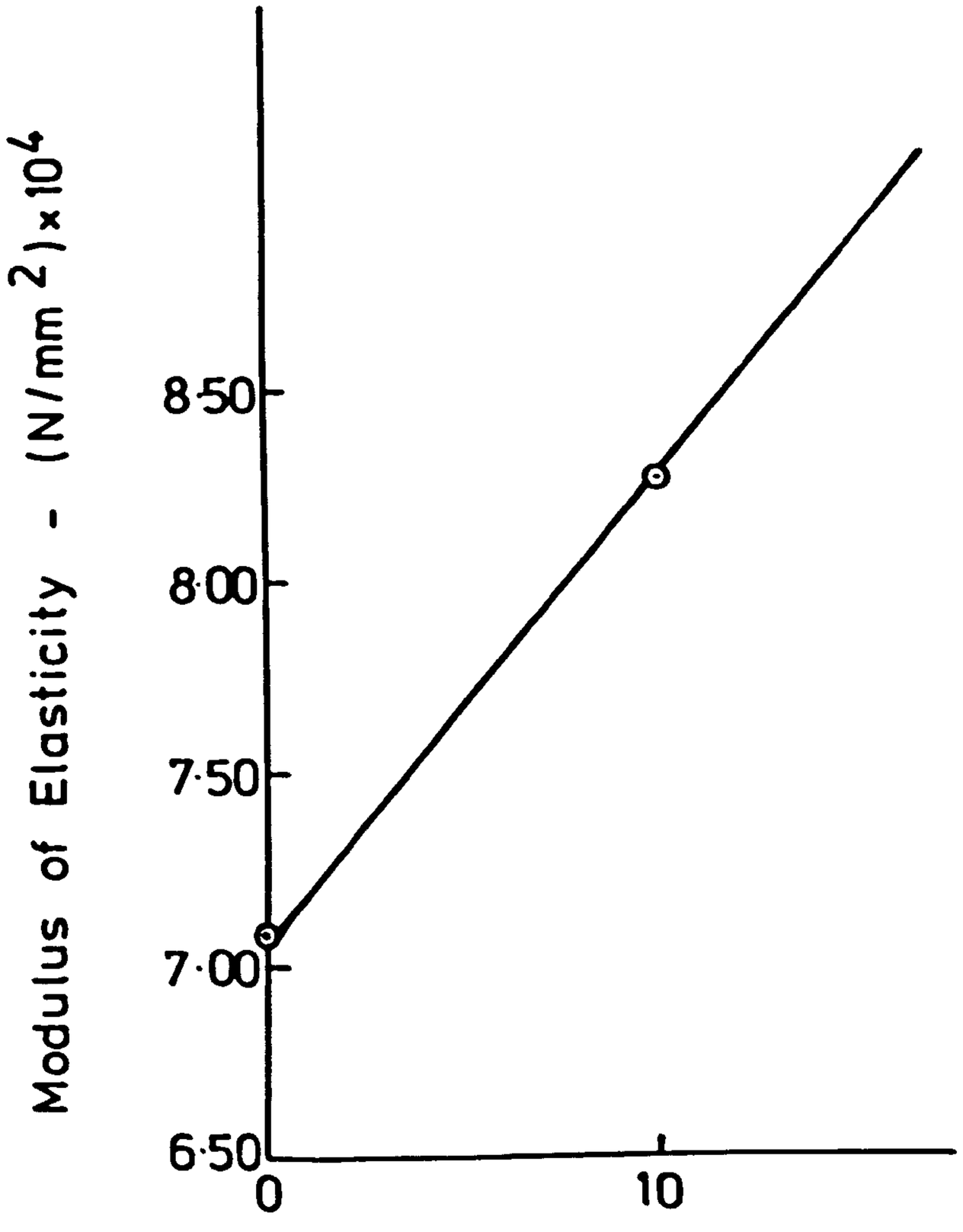

ANHYDRITE

FIG. 9-19 MODULUS OF ELASTICITY OF GYPSUM AND ANHYDRITE AT VARIOUS CONFINING PRESSURES

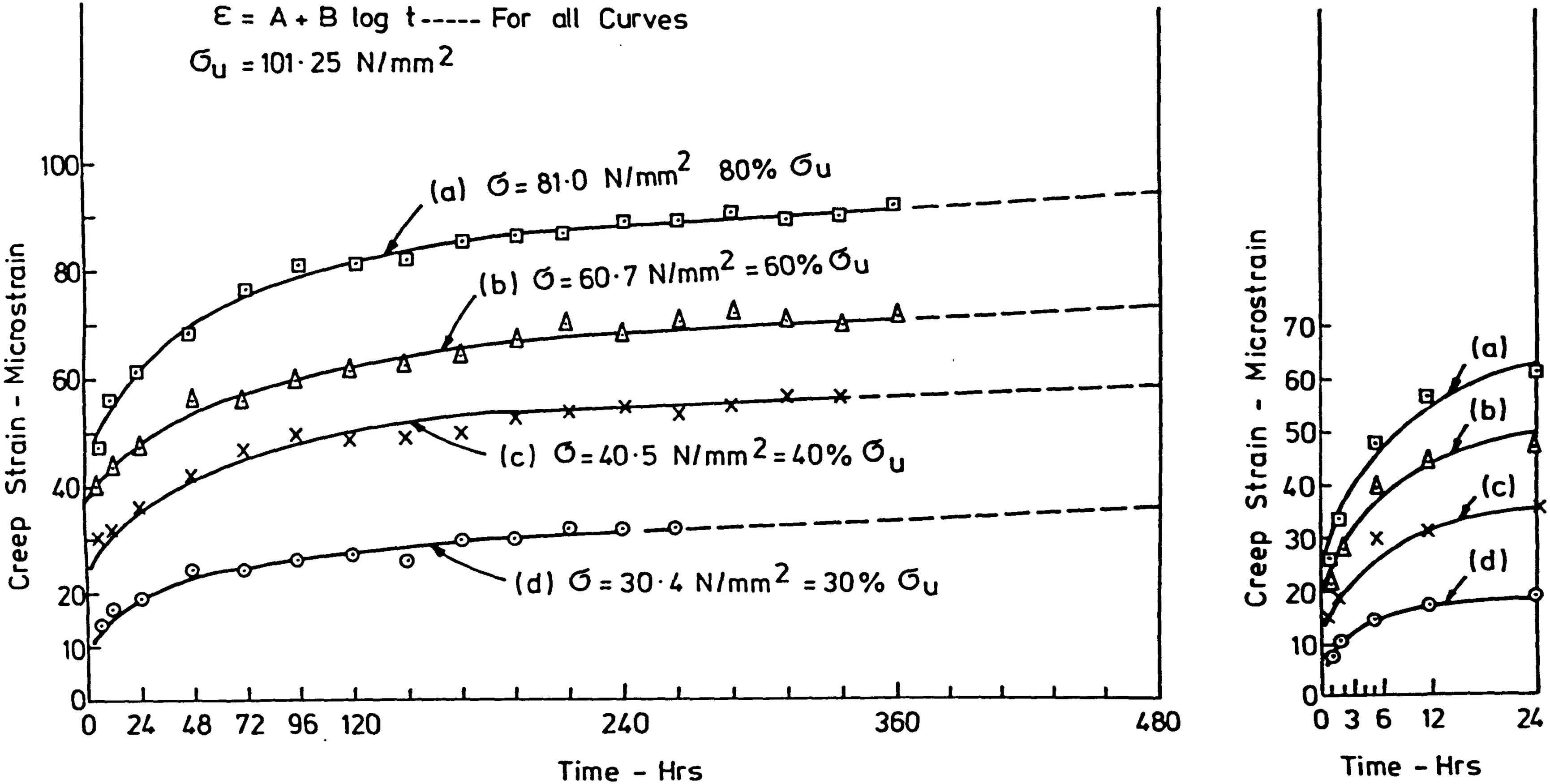

FIG. 9-20 CREEP OF ANHYDRITE IN UNIAXIAL COMPRESSION

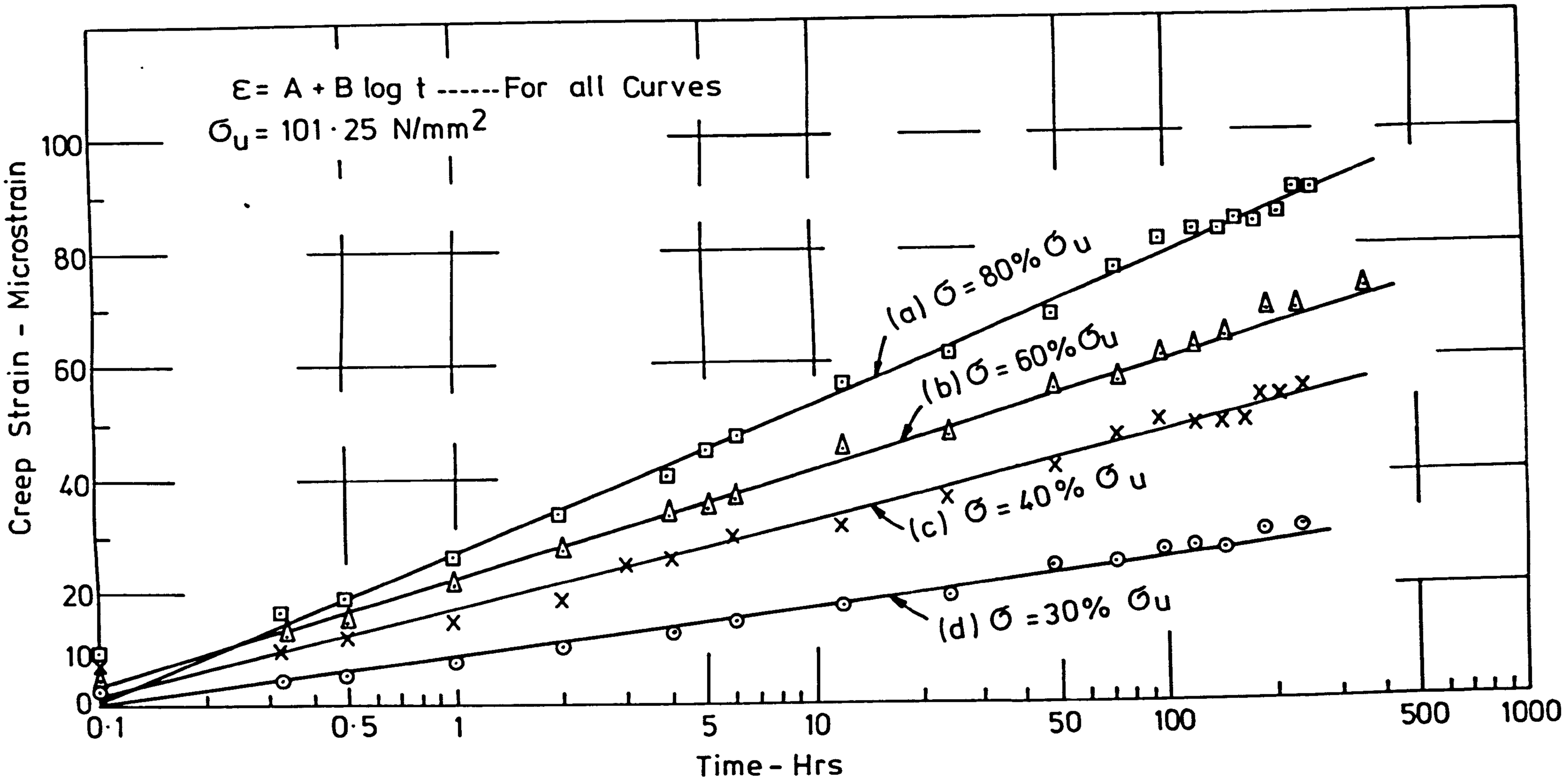

FIG.9-21 CREEP OF ANHYDRITE IN UNIAXIAL COMPRESSION
(Semi - Log Graph)

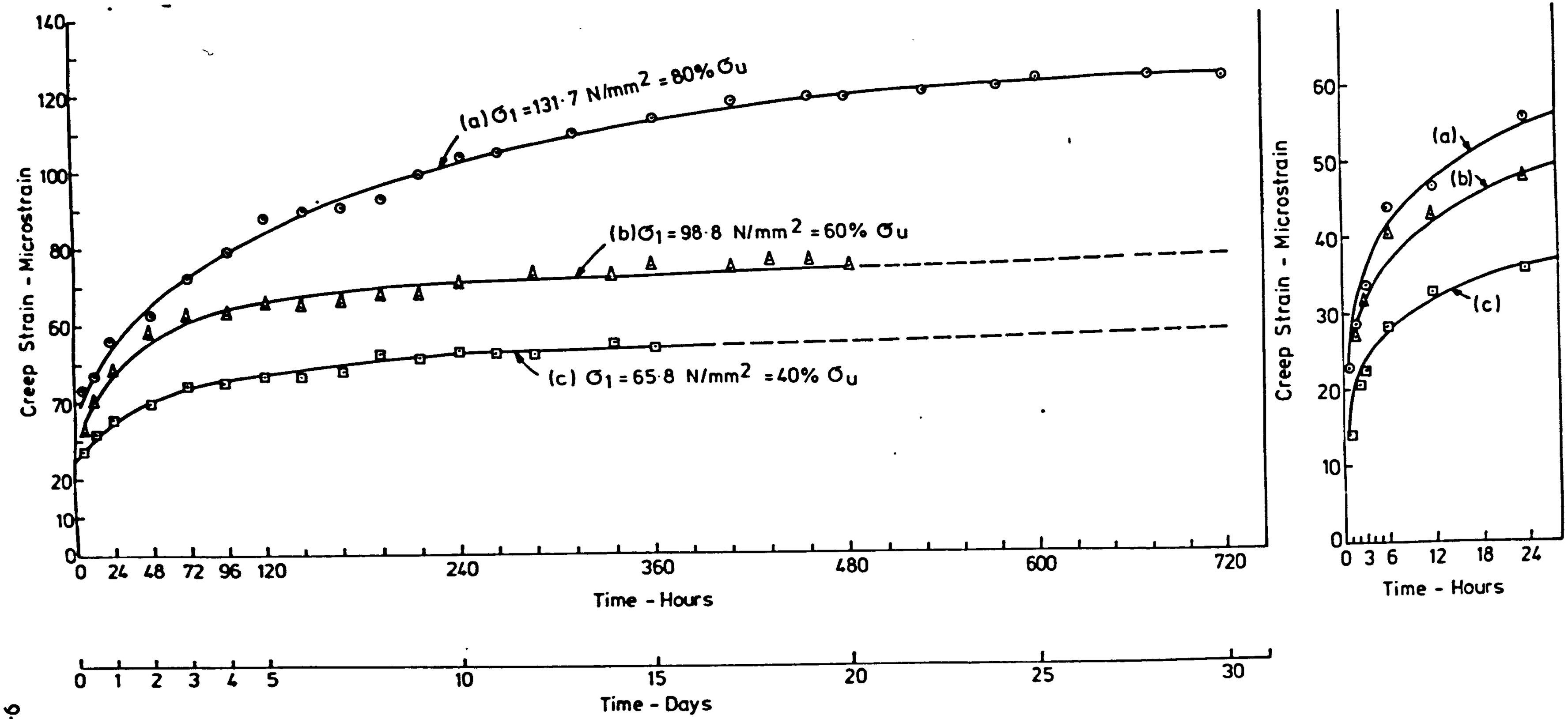

FIG. 9-22 CREEP OF ANHYDRITE IN TRIAXIAL COMPRESSION AT 10 N/mm^2 CONFINING PRESSURE

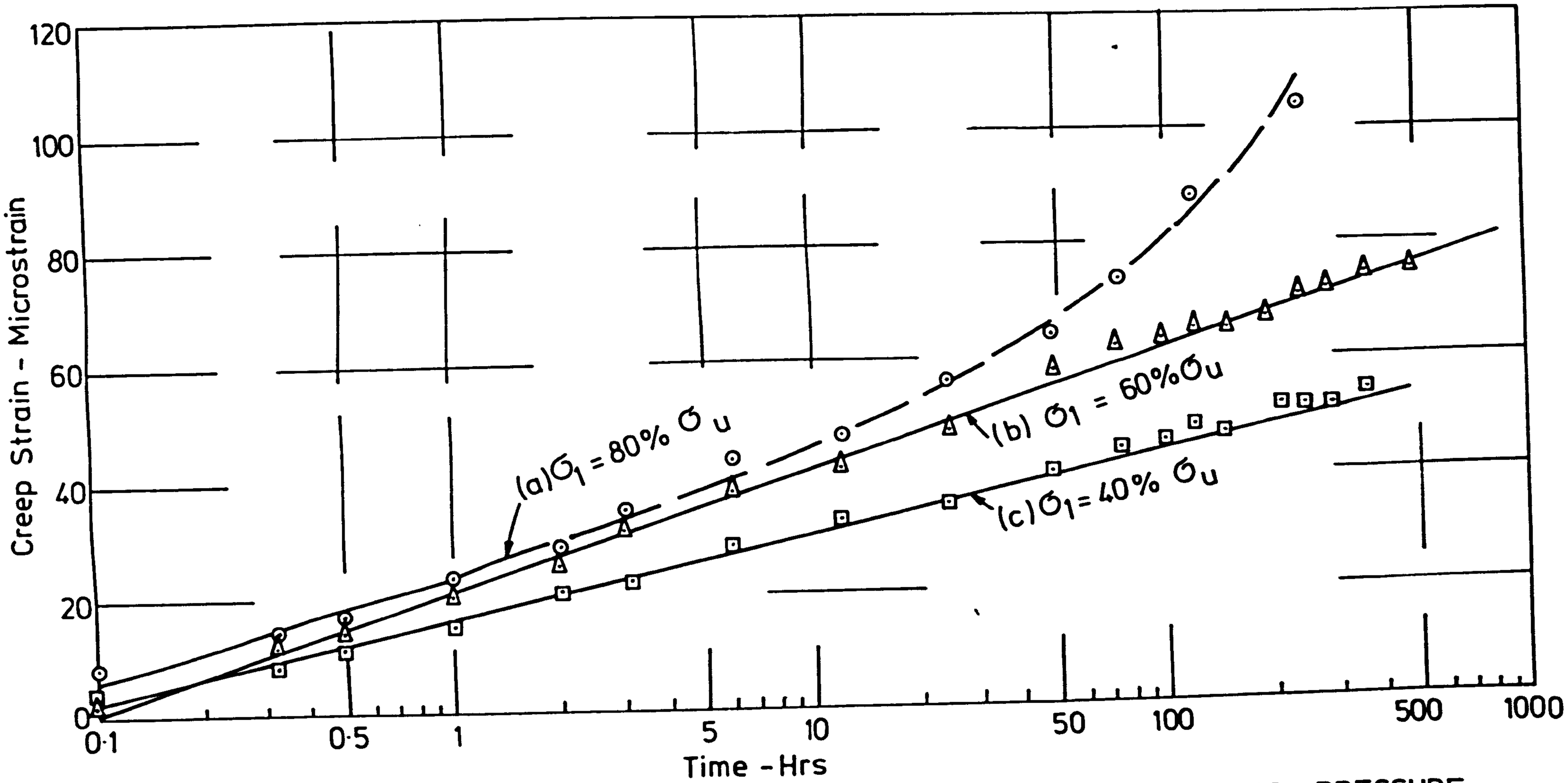

FIG. 9-23 CREEP OF ANHYDRITE IN TRIAXIAL COMPRESSION AT 10 N/mm CONFINING PRESSURE
(Semi-Log Graph)

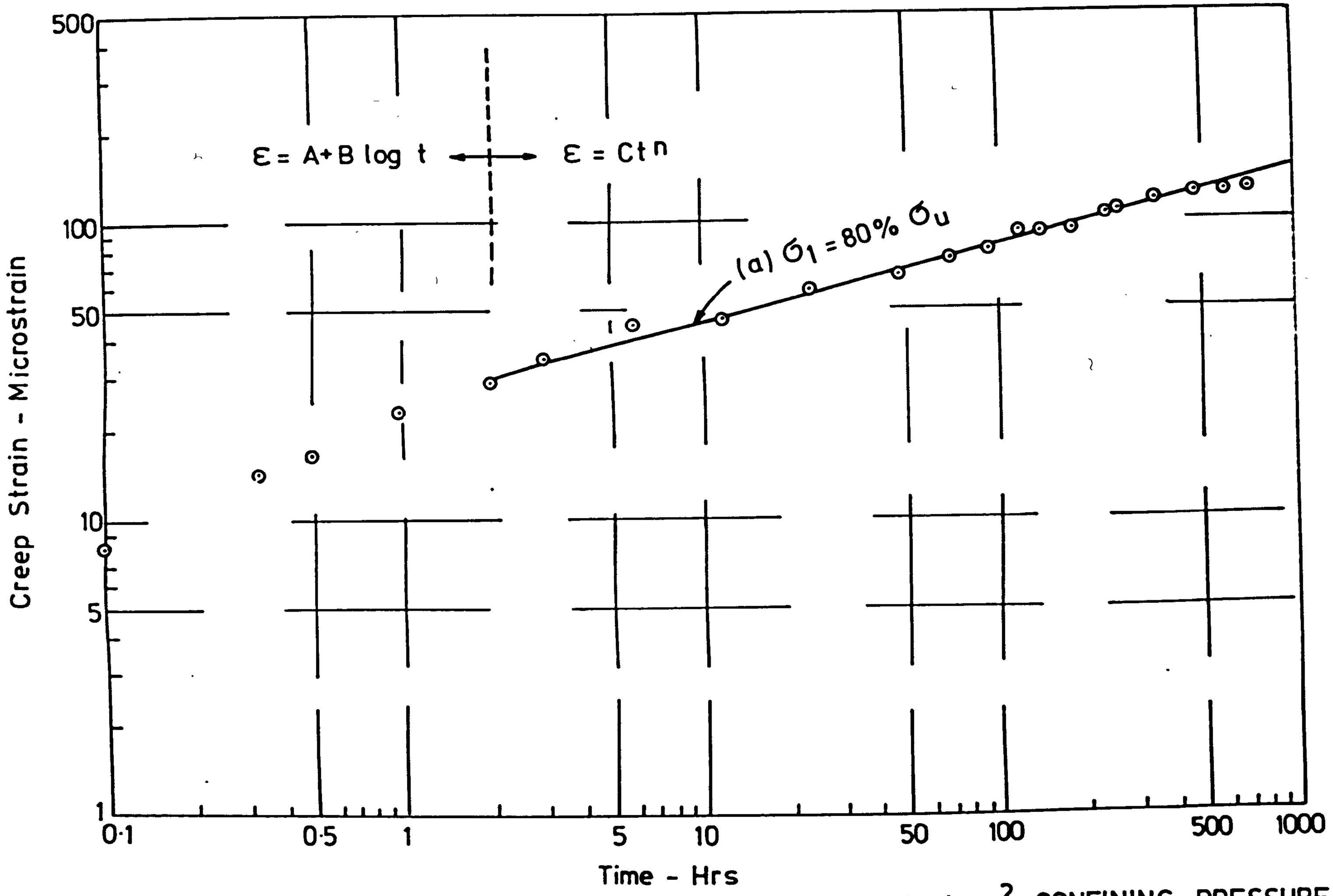

FIG. 9-24 CREEP OF ANHYDRITE IN TRIAXIAL COMPRESSION AT 10 N/mm^2 CONFINING PRESSURE
(Log-Log Graph)

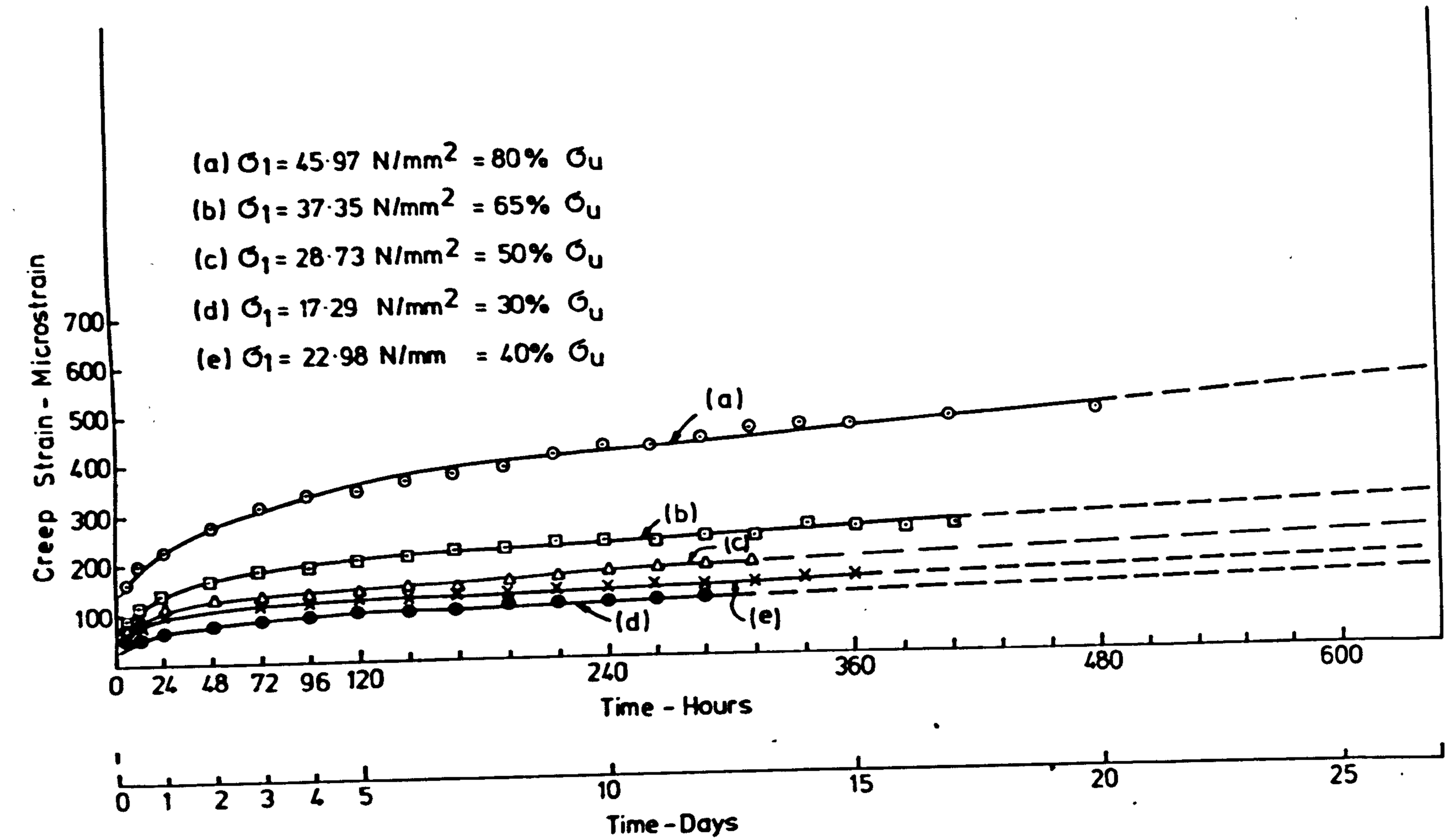

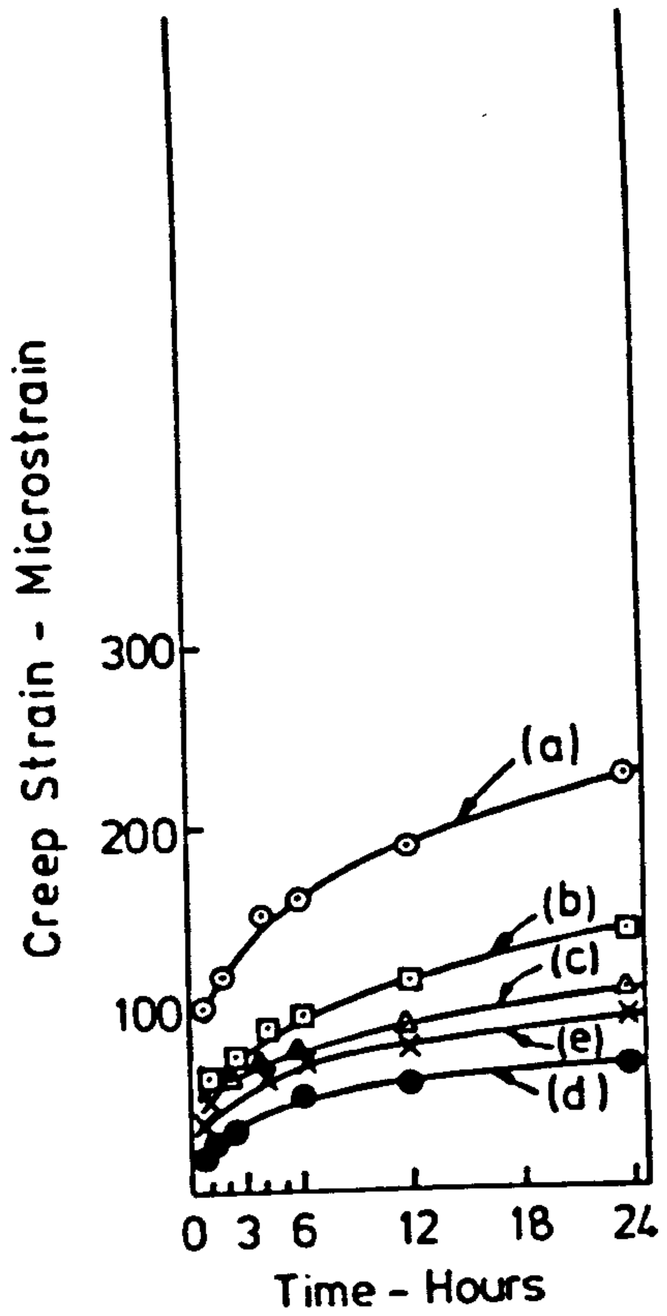

FIG. 9-25 CREEP OF GYPSUM IN UNIAXIAL COMPRESSION

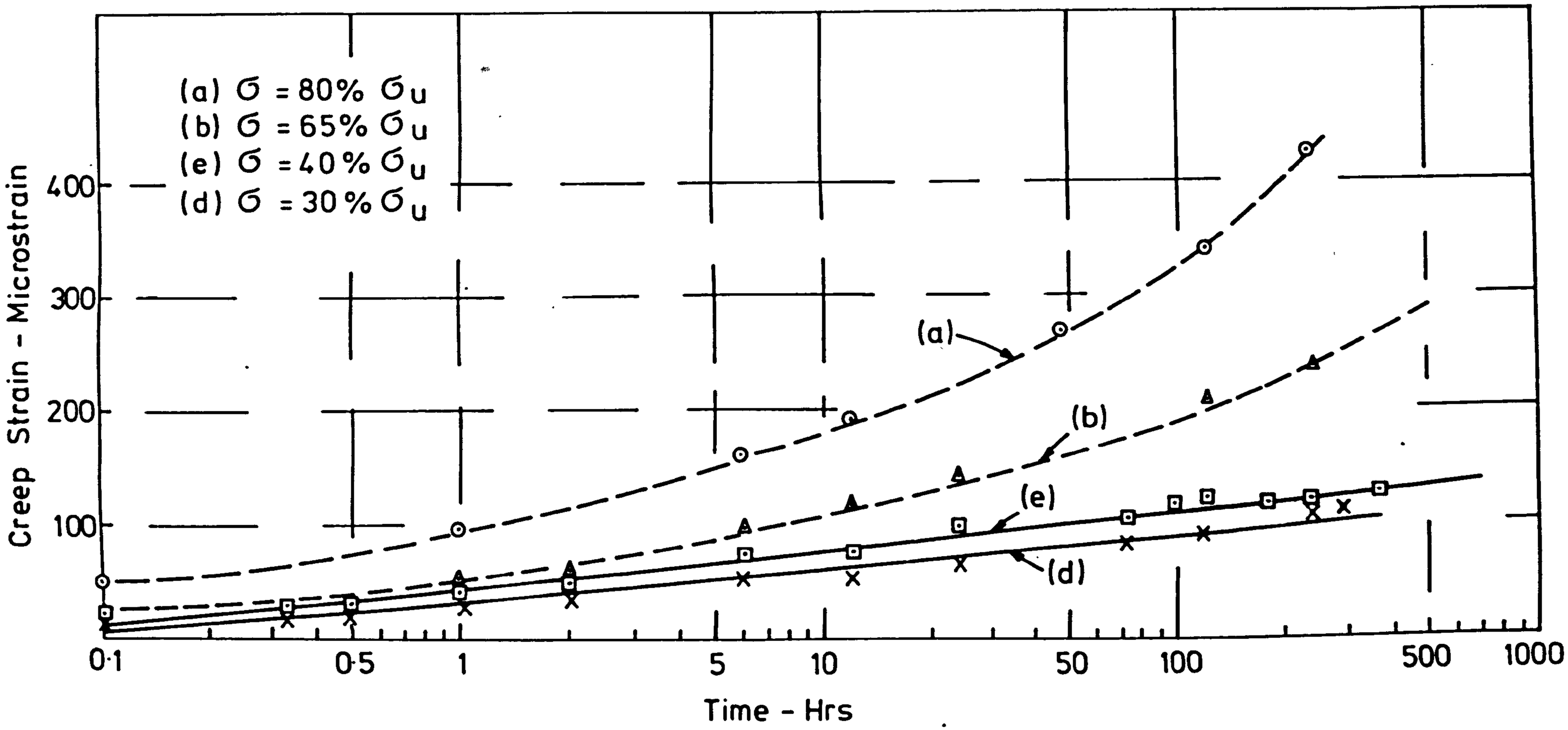

FIG. 9-26 CREEP OF GYPSUM IN UNIAXIAL COMPRESSION
(Semi - Log Graph)

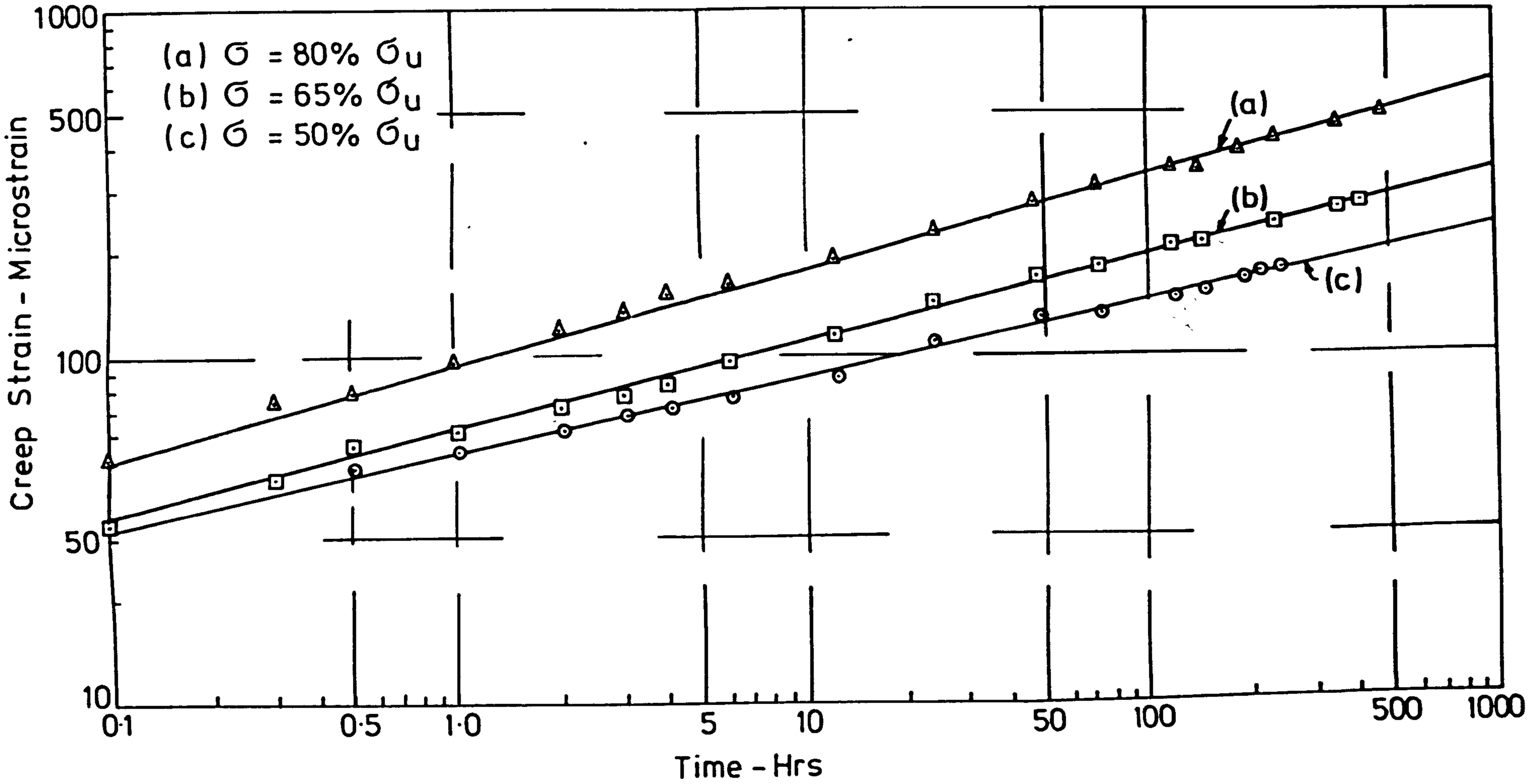

FIG. 9-27 CREEP OF GYPSUM IN UNIAXIAL COMPRESSION
(Log-Log Graph)

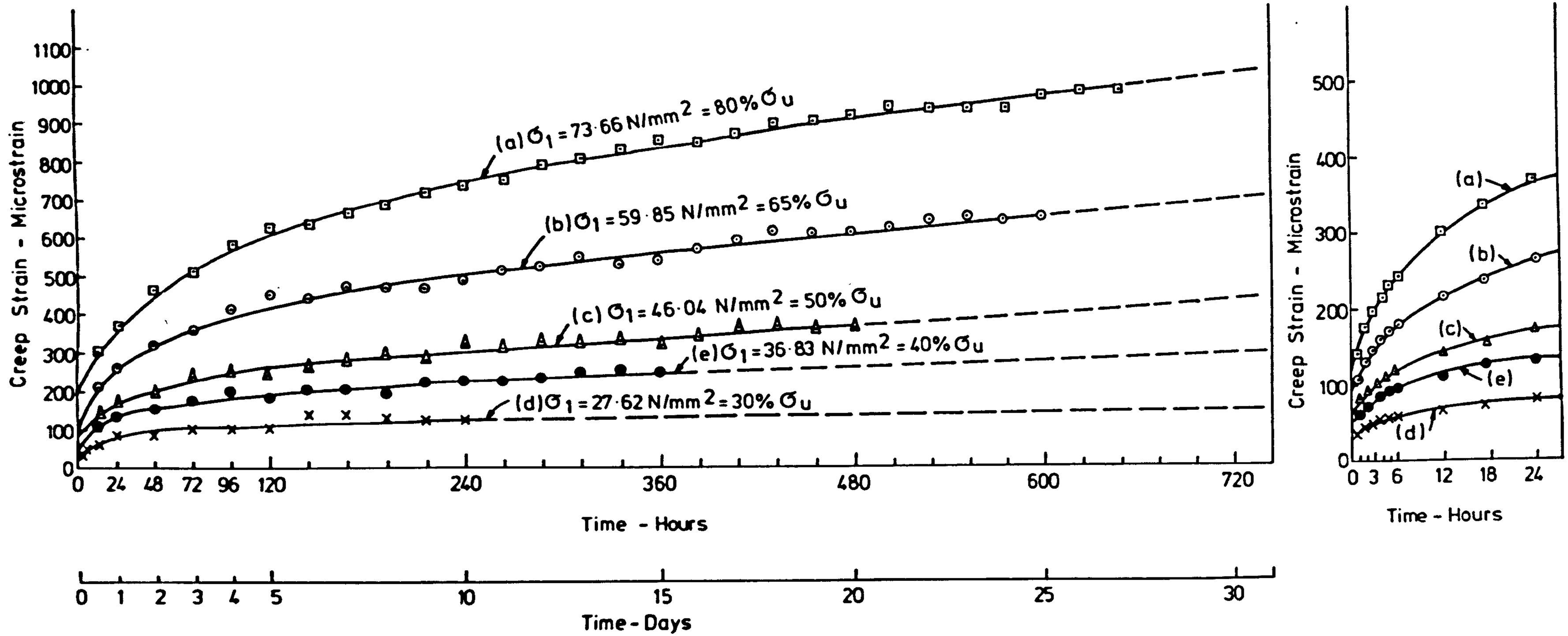

FIG. 9-28 CREEP OF GYPSUM IN TRIAXIAL COMPRESSION AT 10N/mm^2 CONFINING PRESSURE

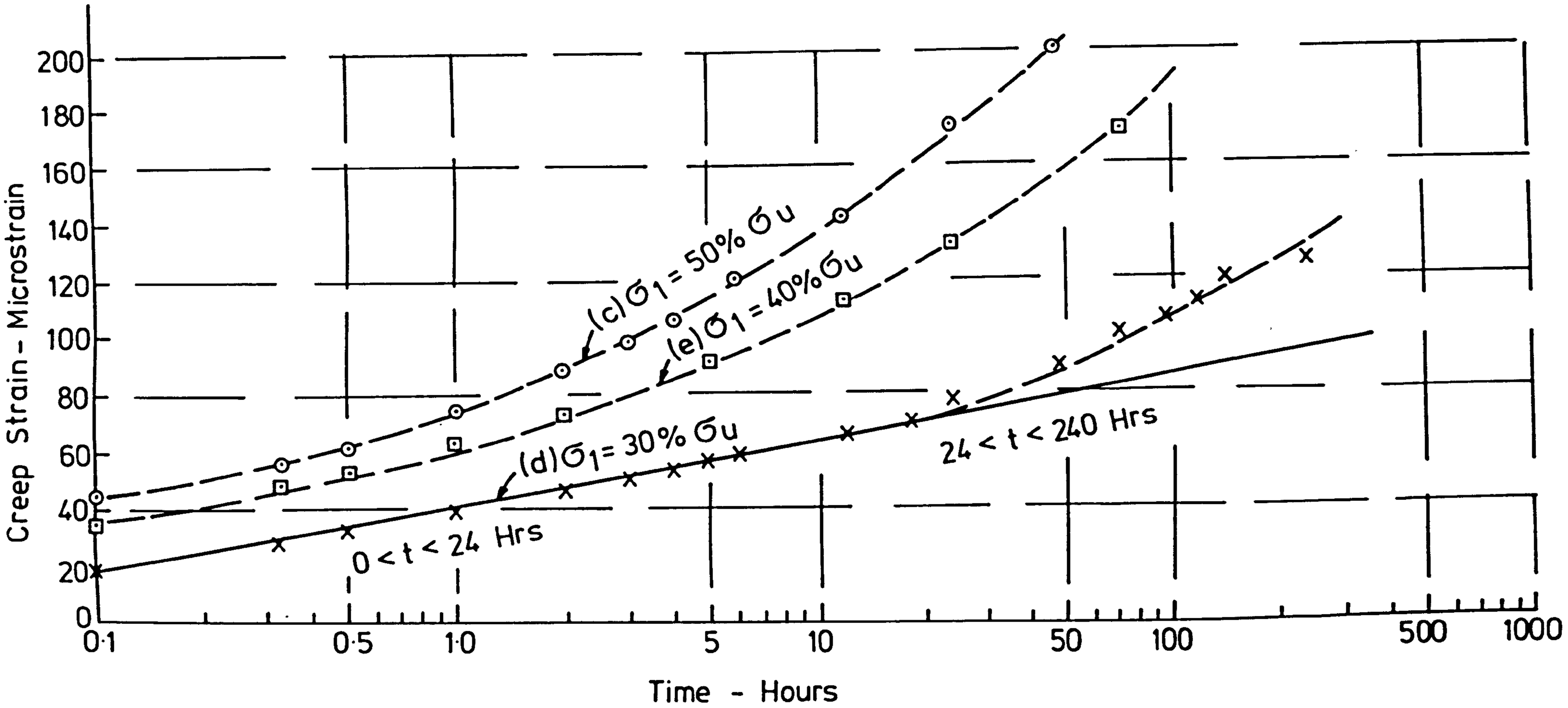

FIG. 9-29 CREEP OF GYPSUM IN TRIAXIAL COMPRESSION AT 10/Nmm^2 CONFINING PRESSURE
(Semi-Log Graph)

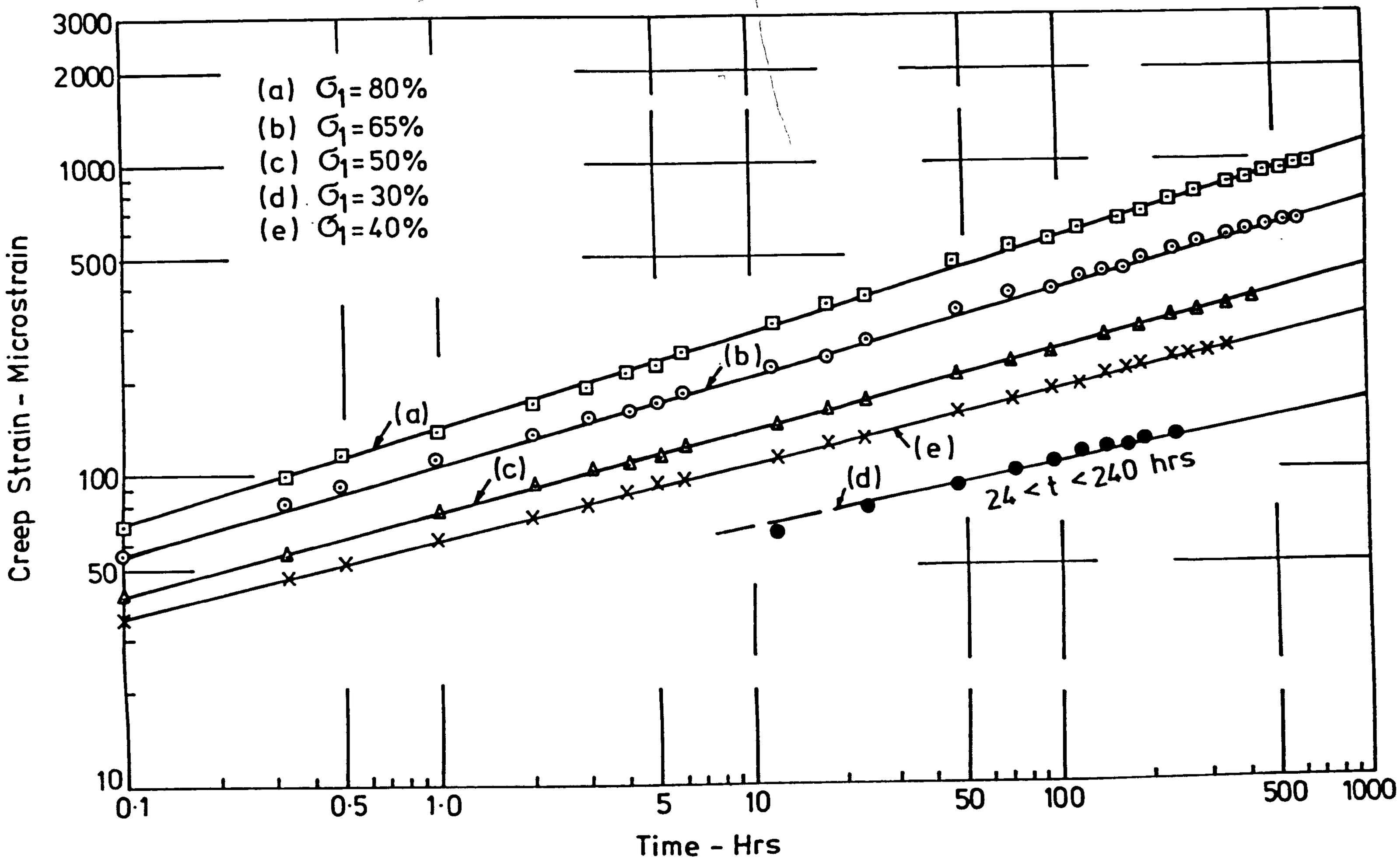

FIG. 9-30 CREEP OF GYPSUM IN TRIAXIAL COMPRESSION AT 10 N/mm^2 CONFINING PRESSURE
(Log - Log Graph)

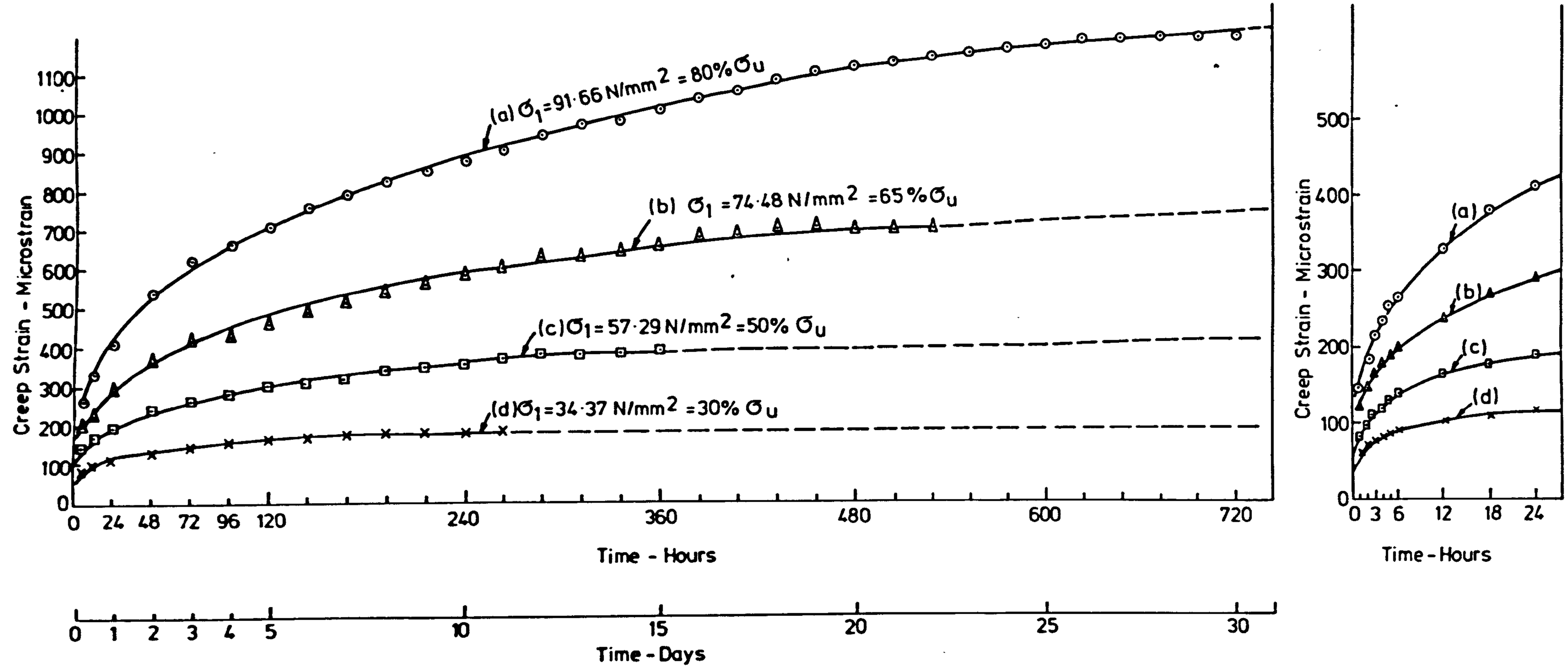

FIG.9-31 CREEP OF GYPSUM IN TRIAXIAL COMPRESSION AT 20 N/mm^2 CONFINING PRESSURE

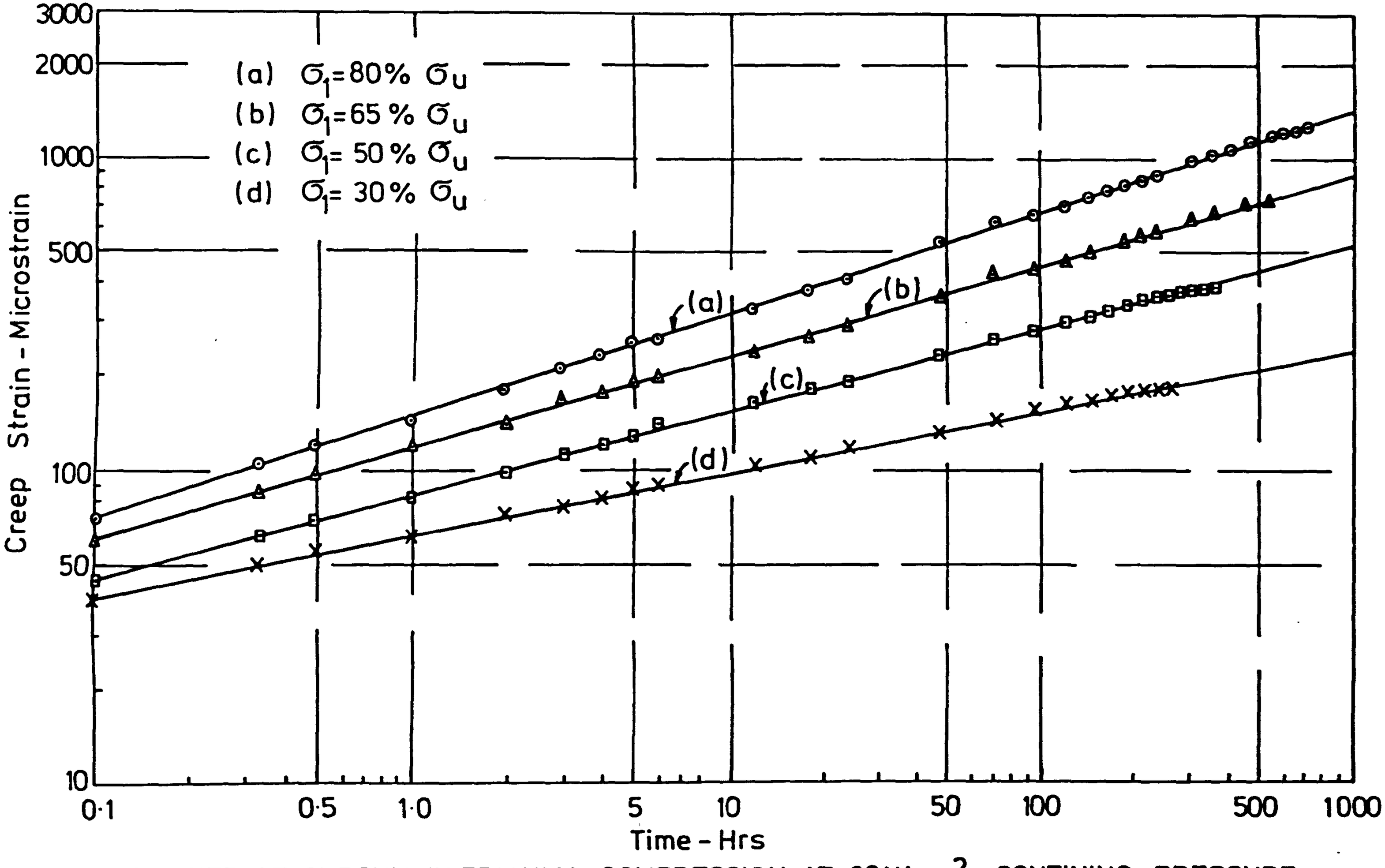

FIG.9-32 CREEP OF GYPSUM IN TRIAXIAL COMPRESSION AT 20N/mm^2 CONFINING PRESSURE
(Log-Log Graph)

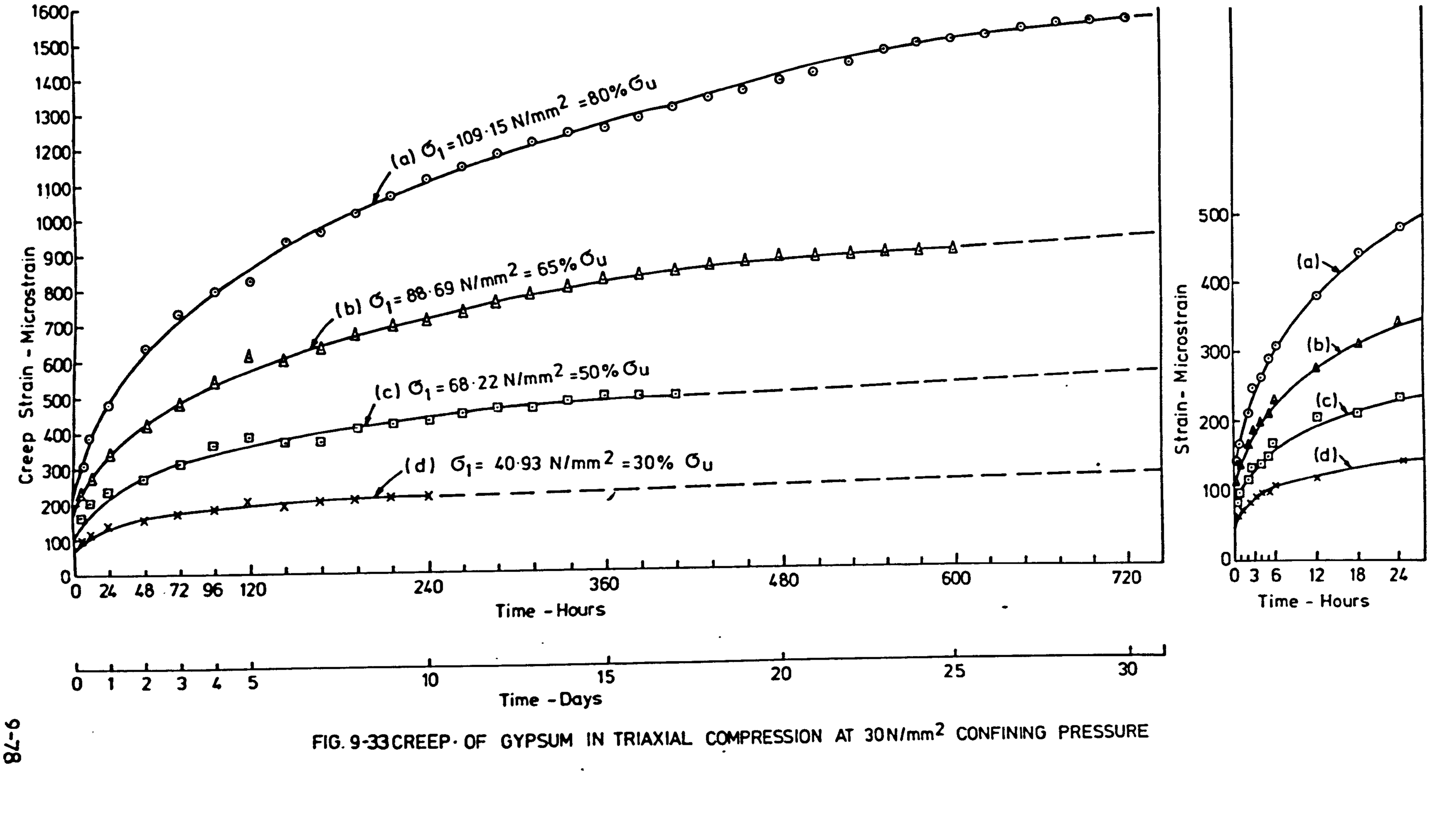

FIG. 9-33 CREEP OF GYPSUM IN TRIAXIAL COMPRESSION AT 30 N/mm² CONFINING PRESSURE

84-6

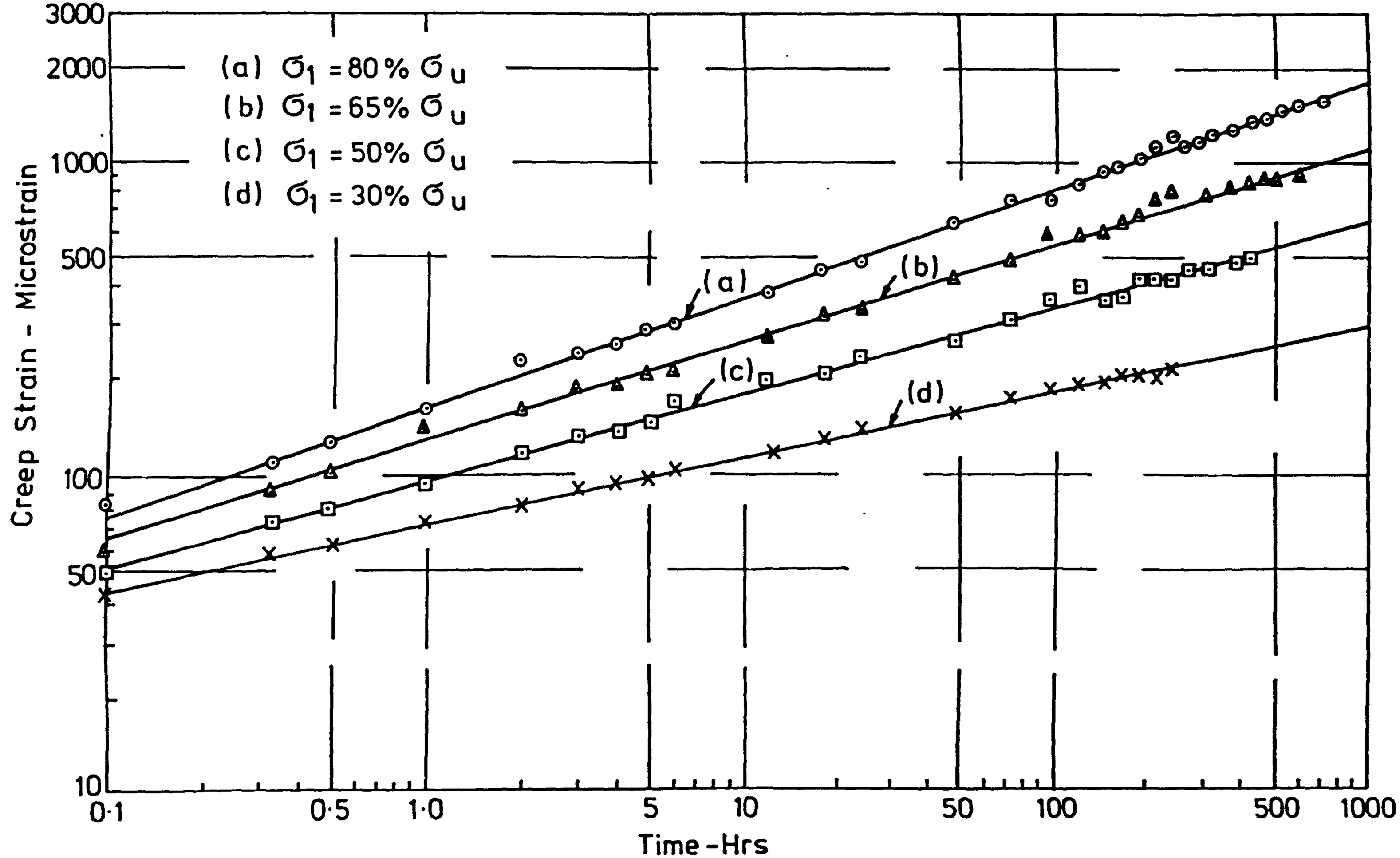

FIG. 9-34 CREEP OF GYPSUM IN TRIAXIAL COMPRESSION AT 30 N/mm^2 CONFINING PRESSURE (Log-Log Graph)

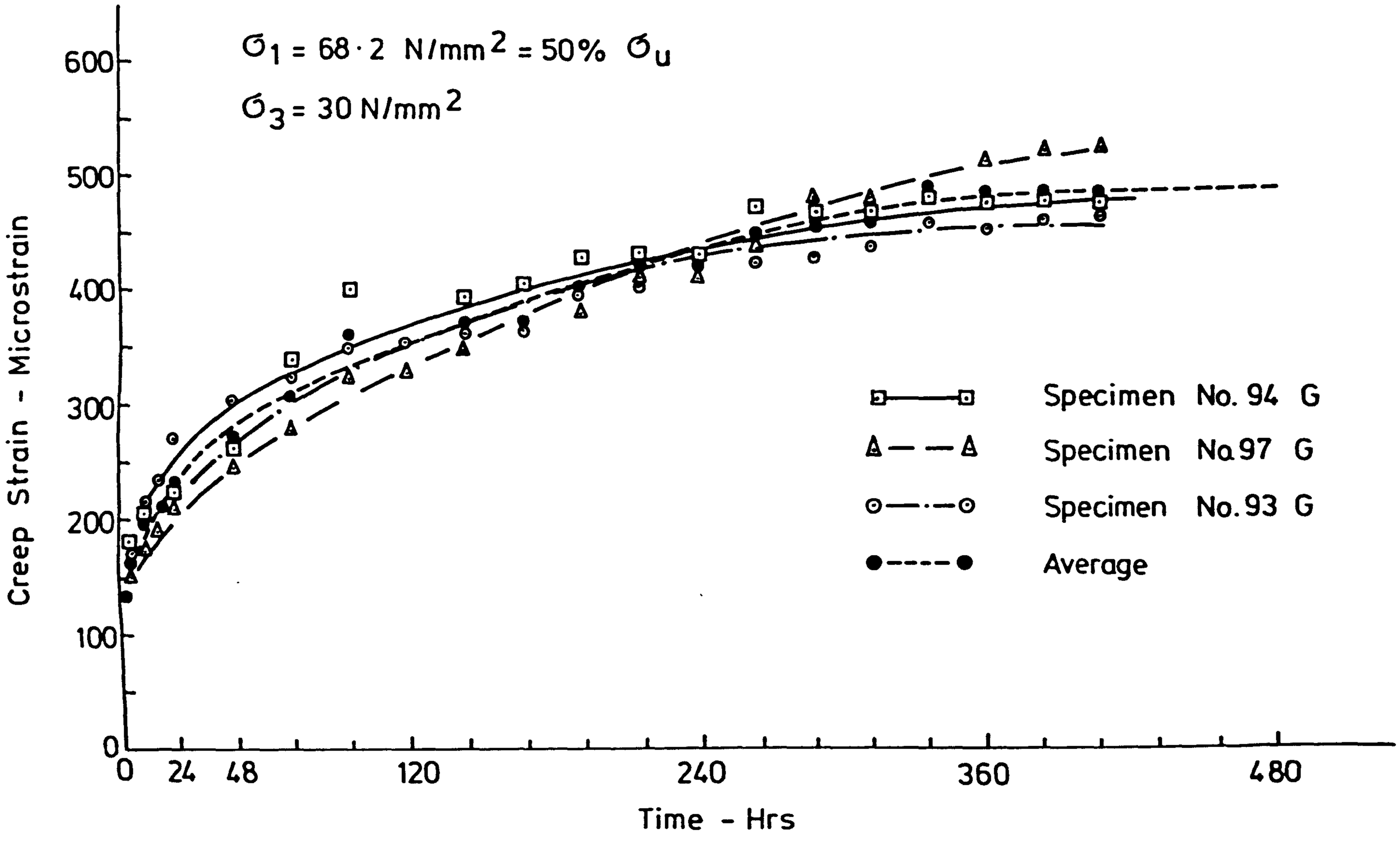

FIG. 9-35 CREEP CURVE OF GYPSUM IN TRIAXIAL COMPRESSION TAKEN AS AN AVERAGE OF THREE TESTS

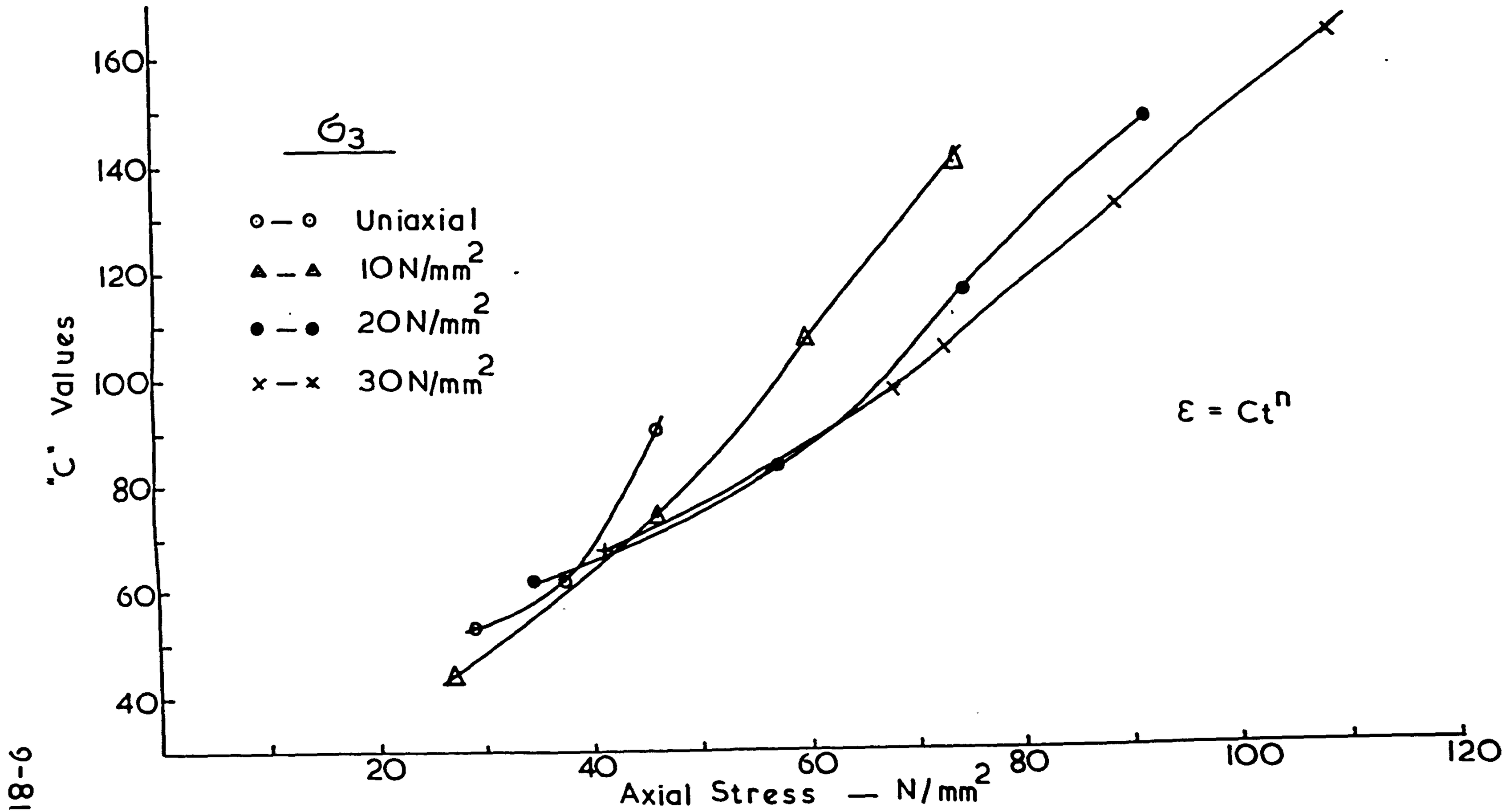

FIG 9 — 36 'C' VERSUS σ_1 AT CONSTANT σ_3

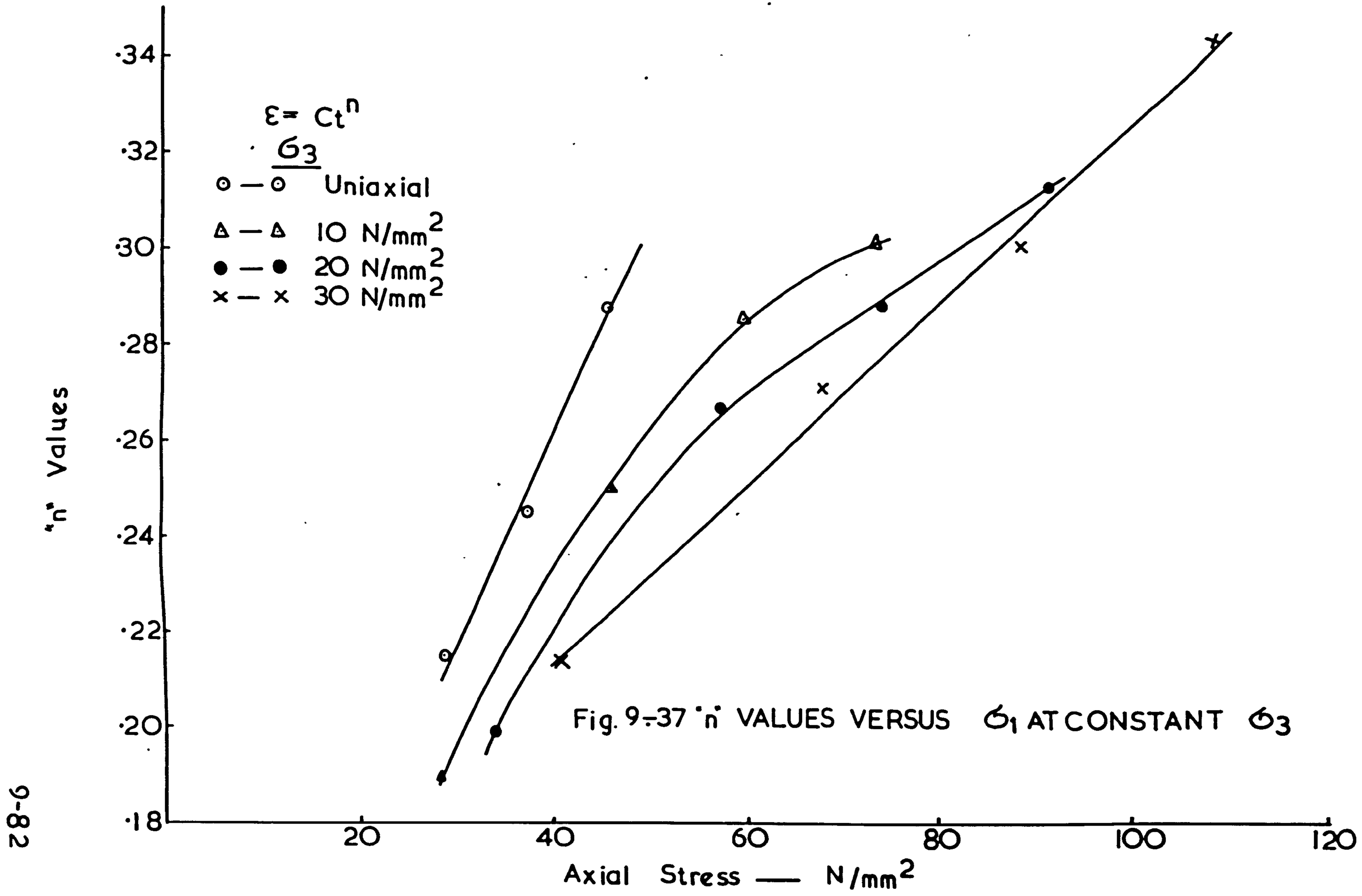

Fig. 9-37 "n" VALUES VERSUS σ_1 AT CONSTANT σ_3

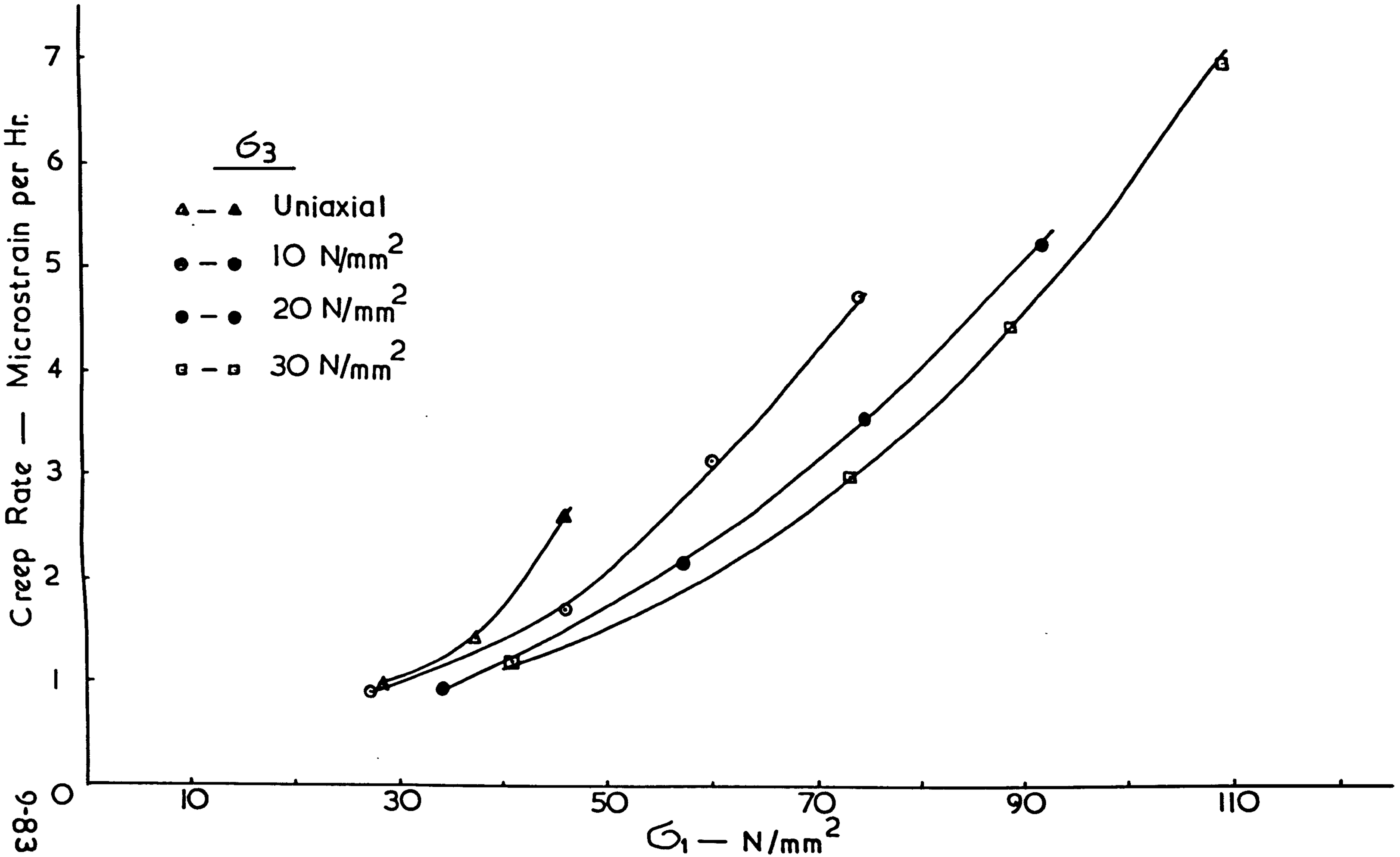

FIG. 9-38 CREEP RATE VERSUS σ_1 AT CONSTANT σ_3 (AT t = 24 hrs)

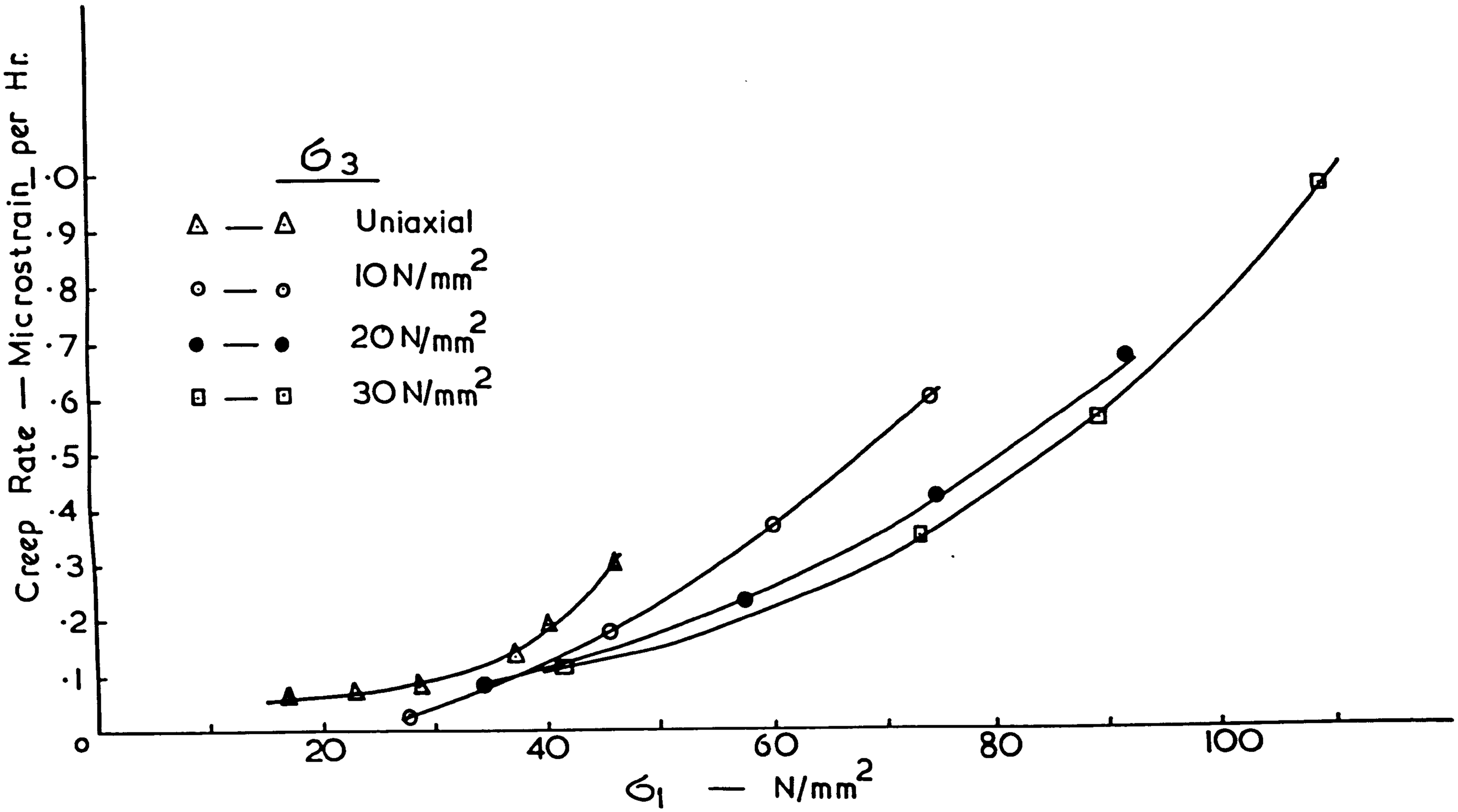

FIG 9-39 CREEP RATE VERSUS σ_1 AT CONSTANT σ_3 (at t = 480 hr)

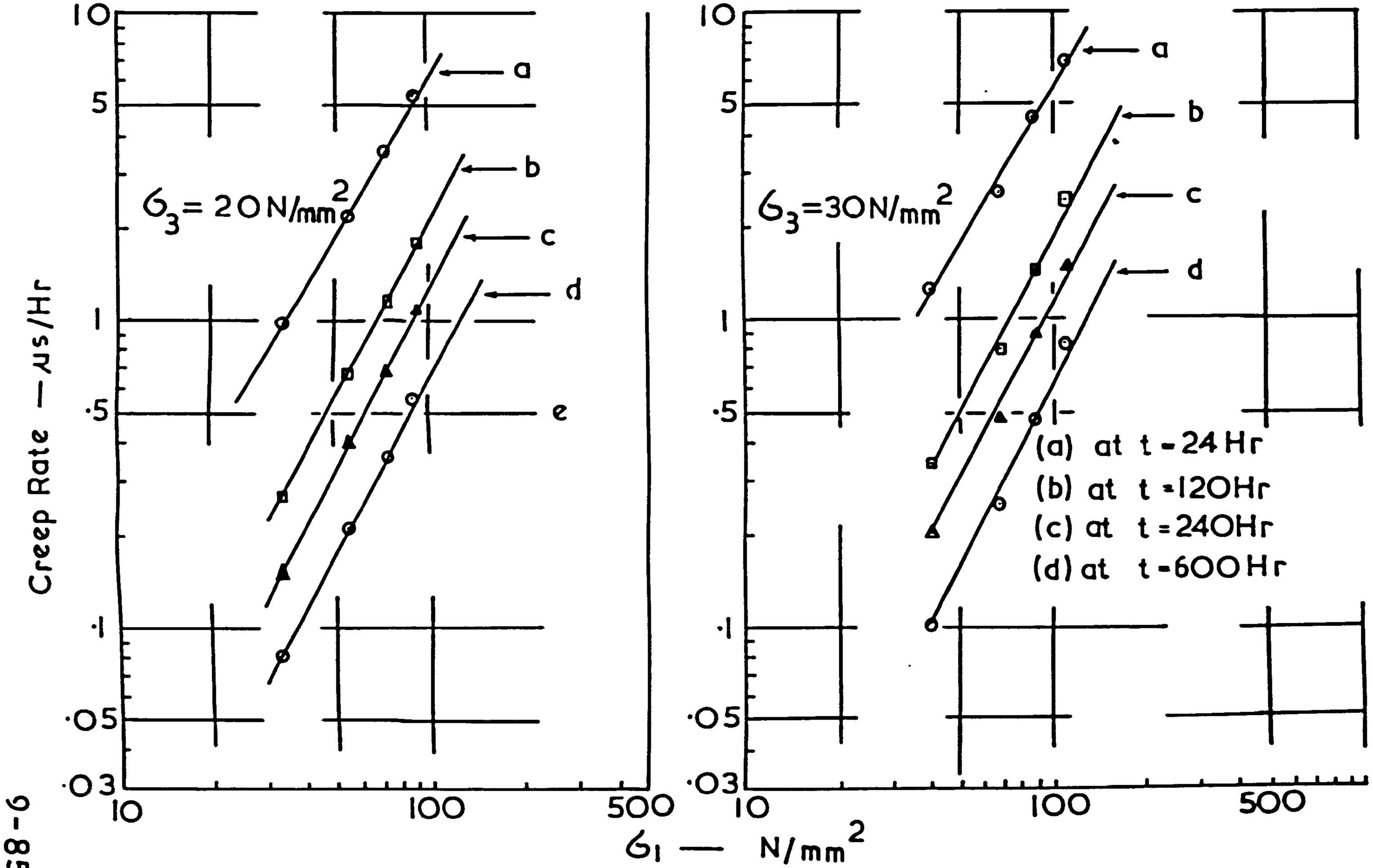

58-6

FIG.9—40 CREEP RATE VERSUS σ_1 AT VARIOUS σ_3 —(LOG—LOG GRAPH)

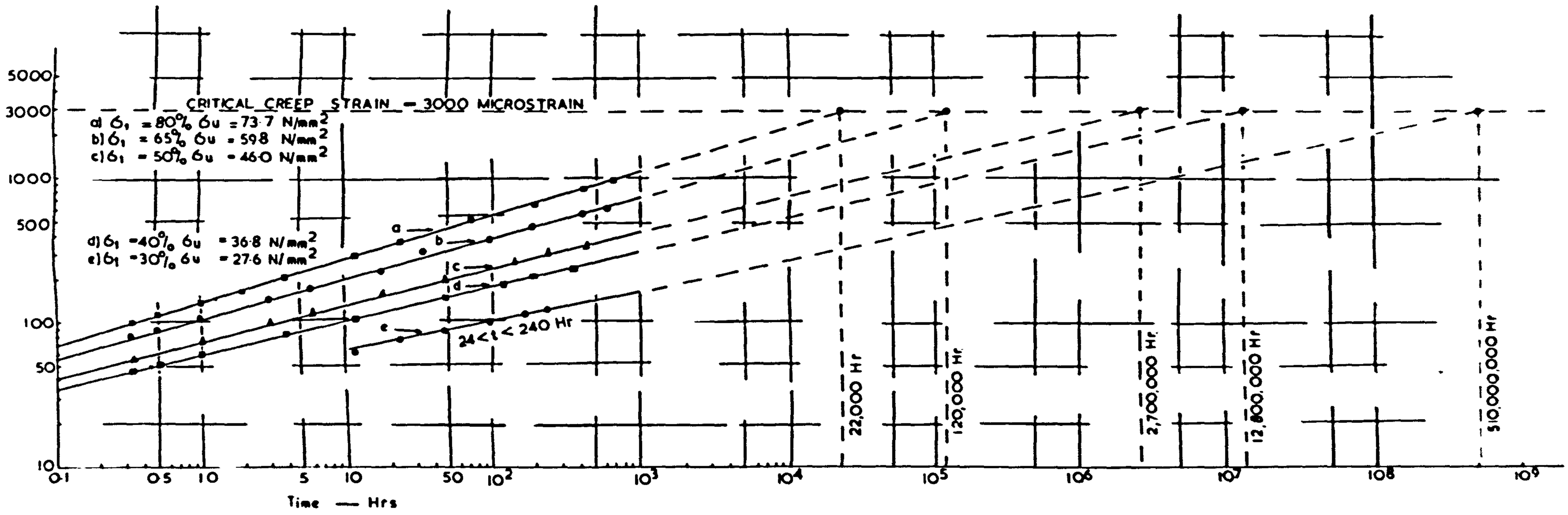

FIG 9-41 CREEP OF GYPSUM IN TRIAXIAL COMPRESSION AT 10N/mm² CONFINING PRESSURE (LOG — LOG GRAPH)

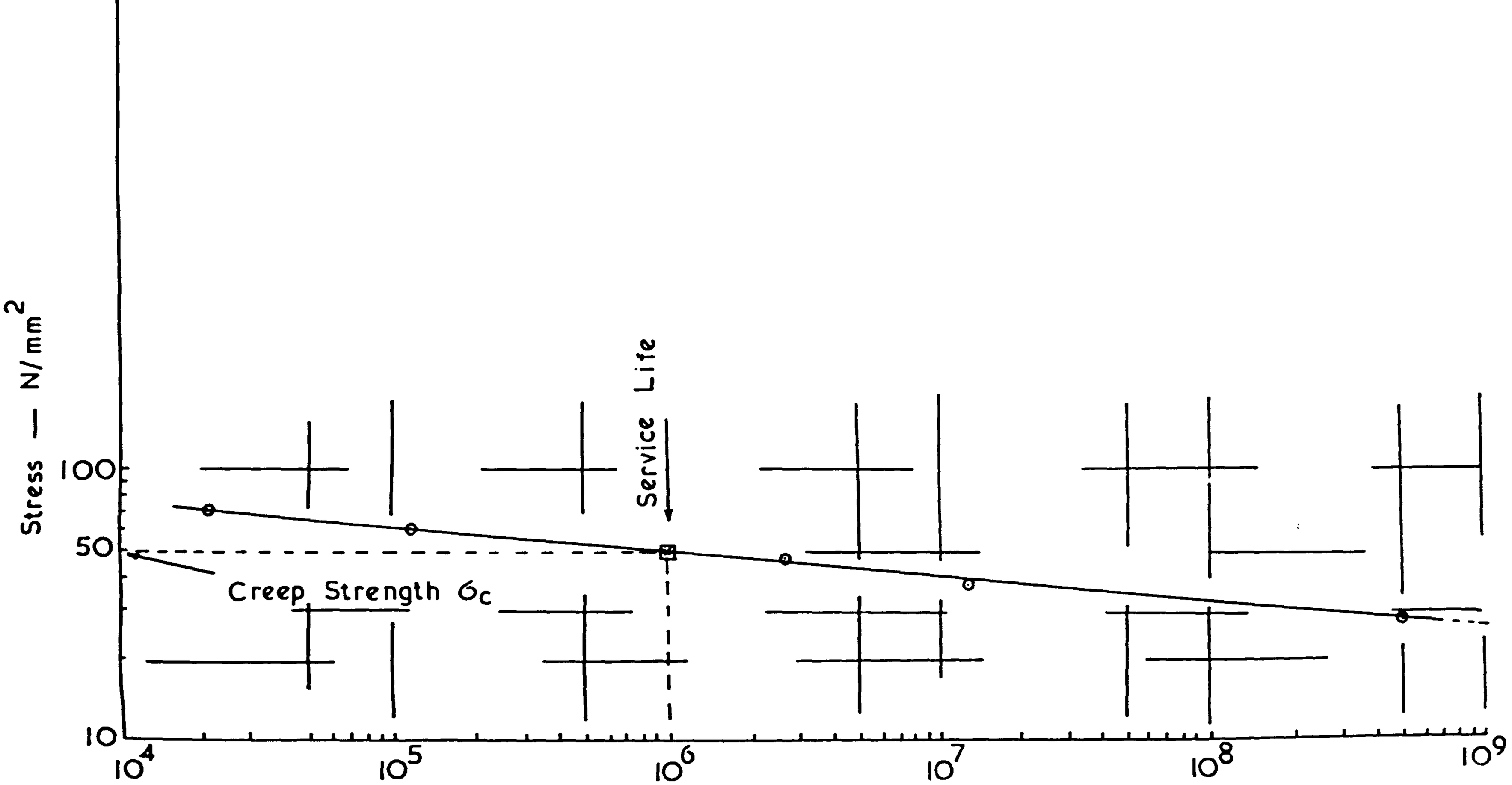

FIG 9—42 TIME VERSUS AXIAL STRESS (LOG — LOG GRAPH)

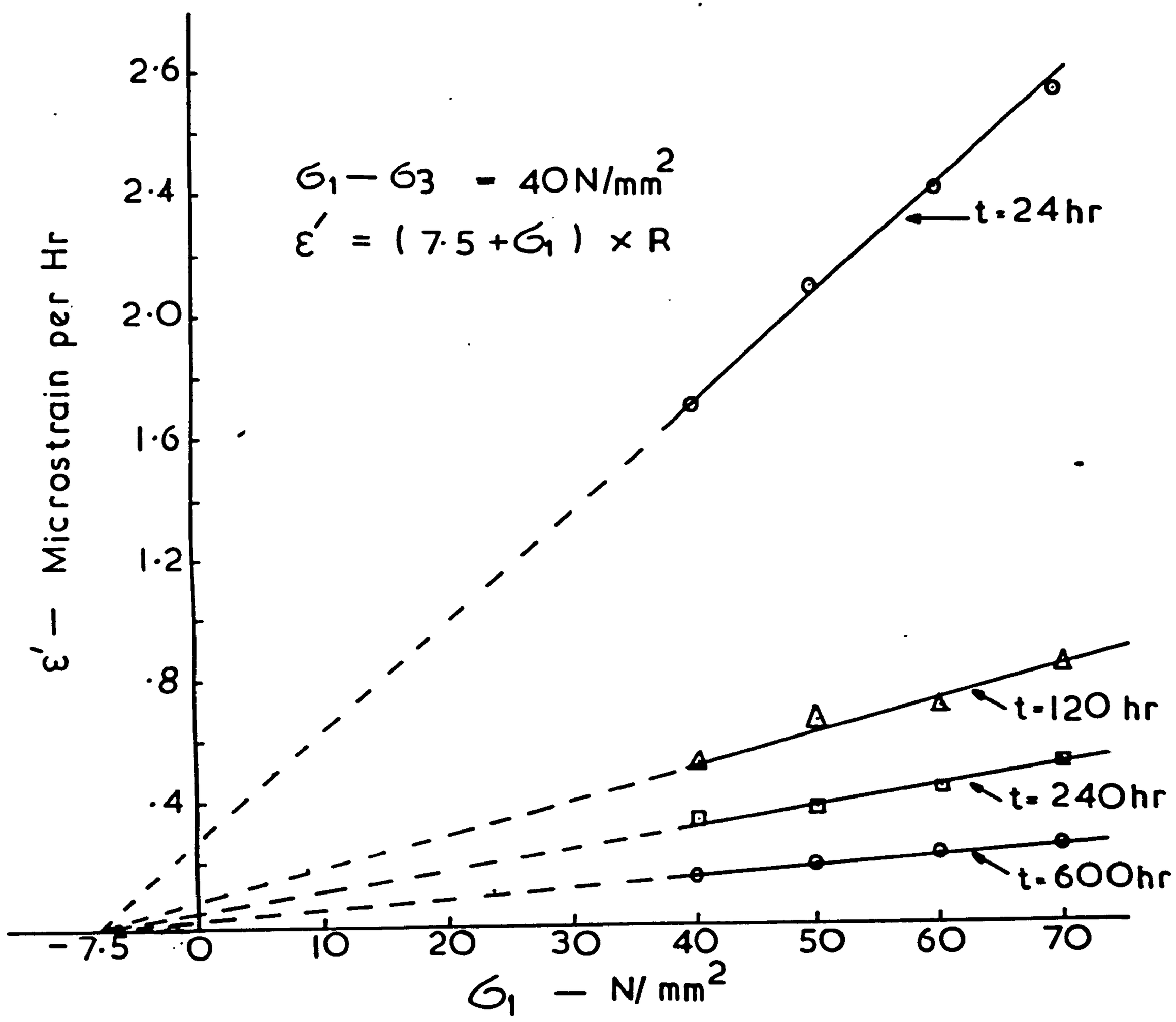

FIG 9-43 CREEP RATE VERSUS σ_1 AT CONSTANT $(\sigma_1 - \sigma_3) = 40 N/mm^2$

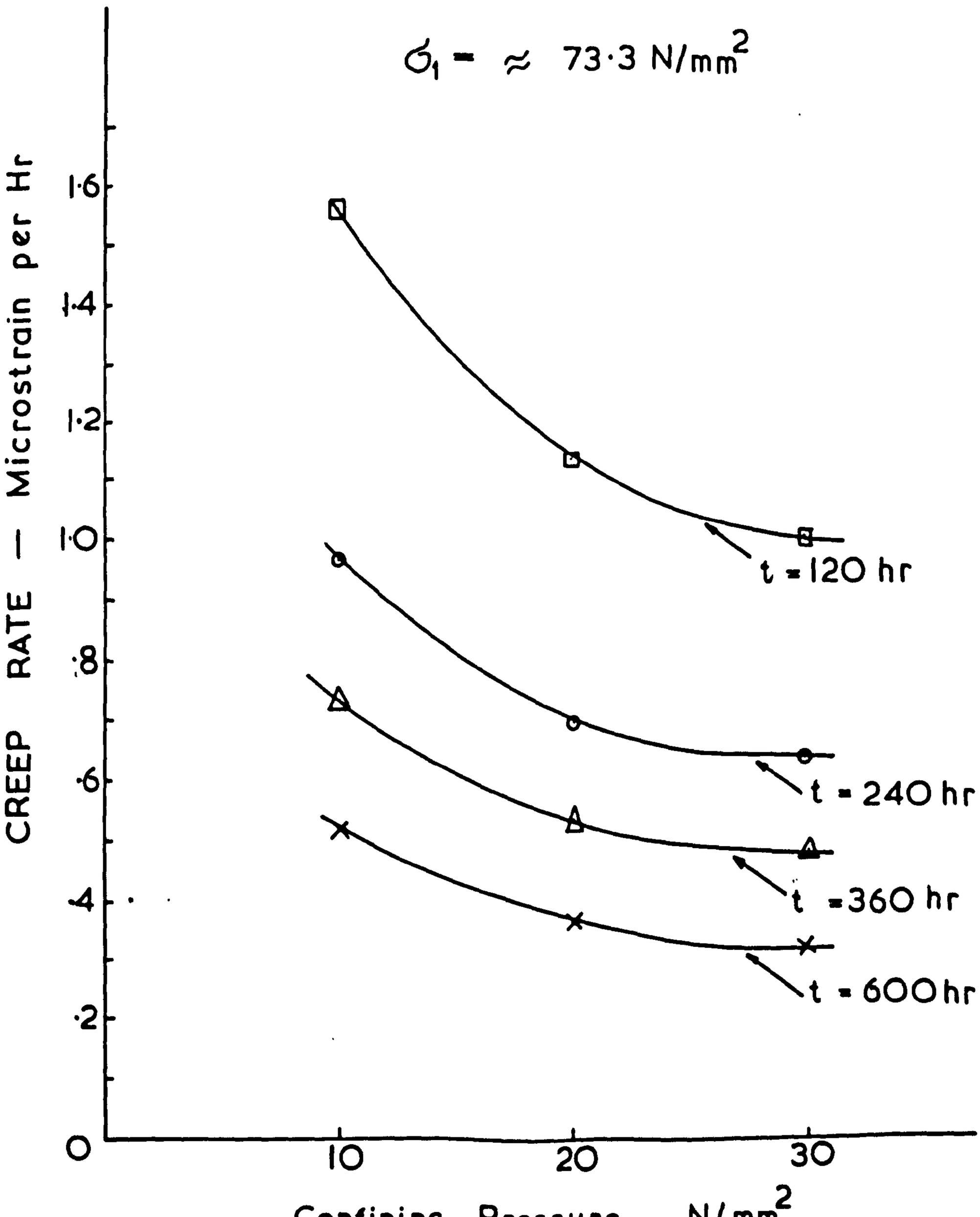

FIG 9-44 CREEP RATE VERSUS CONFINING PRESSURE AT CONSTANT σ_1

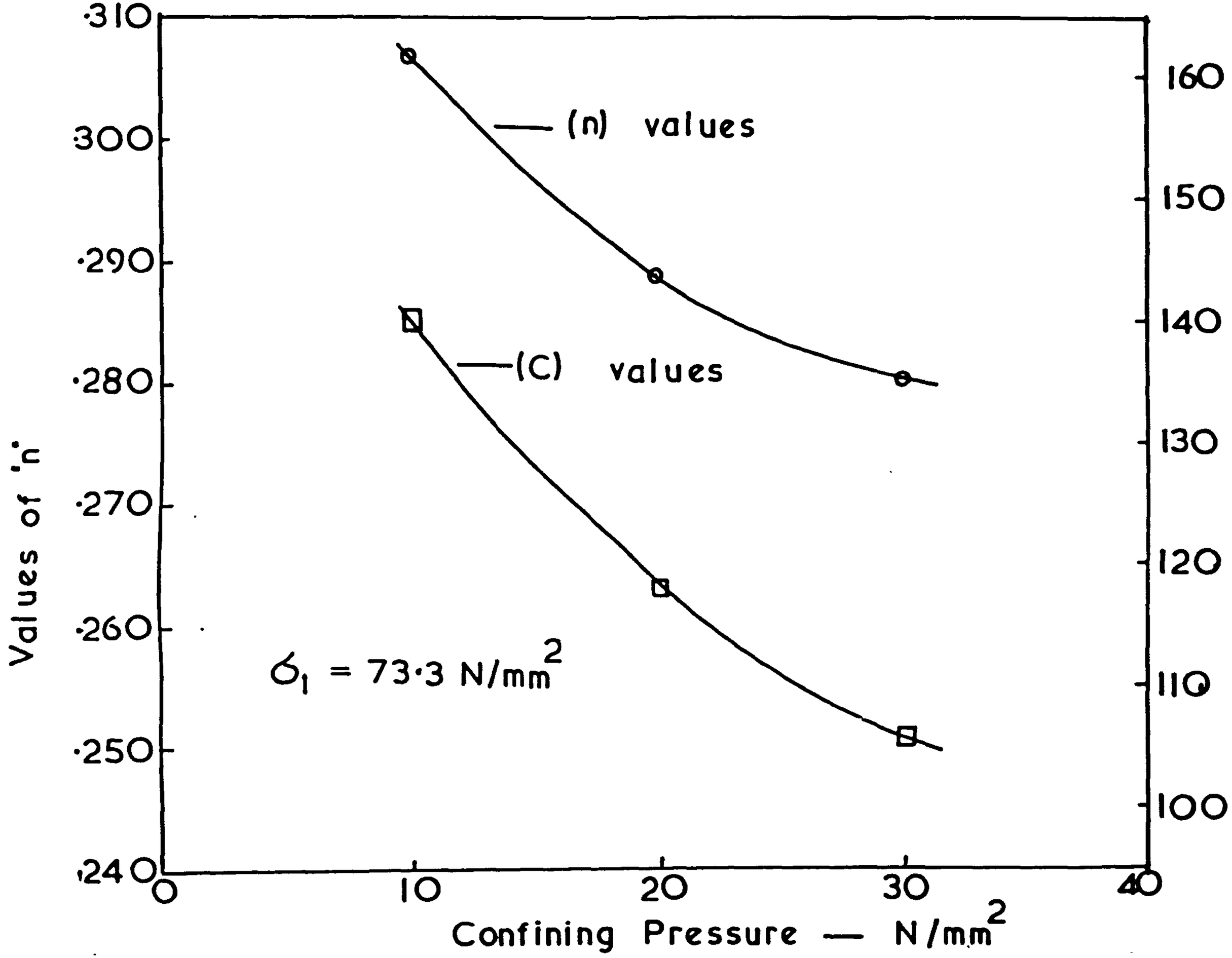

FIG 9-45 EFFECT OF CONFINING PRESSURE ON 'C' AND 'n' AT CONSTANT σ_1

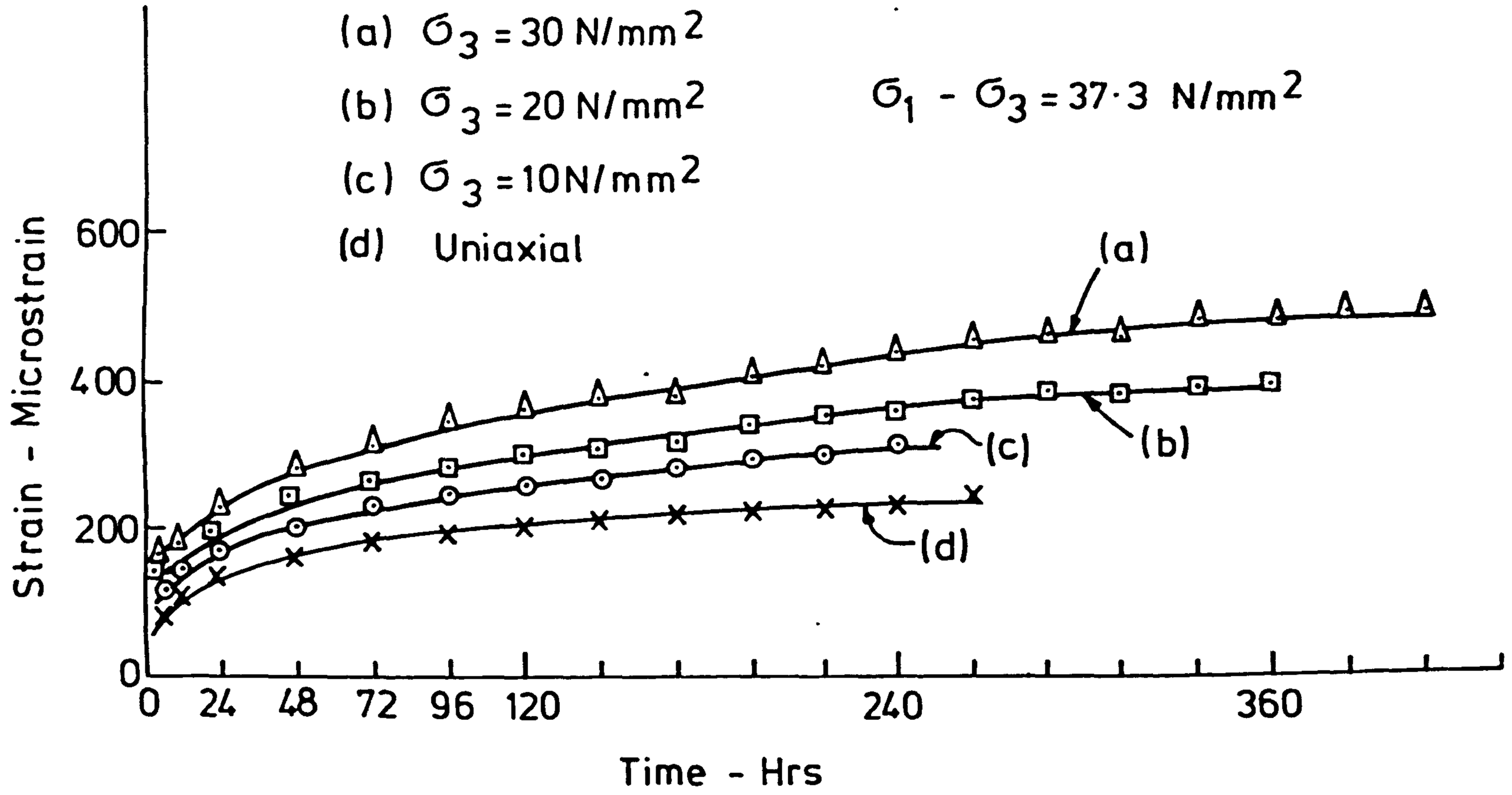

FIG.9-46 EFFECT OF CONFINING PRESSURE ON CREEP OF GYPSUM AT CONSTANT DIFFERENTIAL STRESS

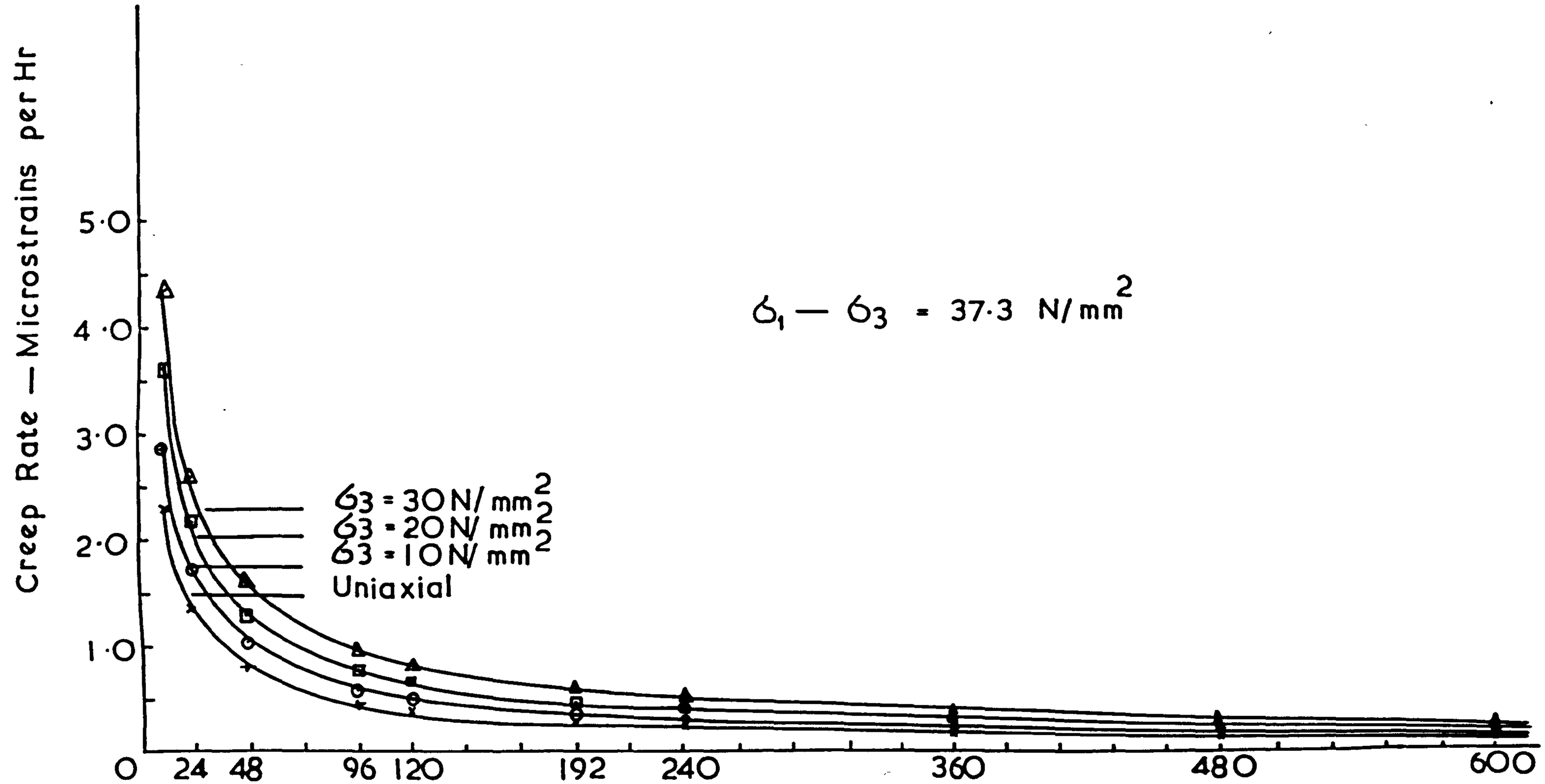

FIG 9-47 CREEP RATE OF GYPSUM VERSUS TIME AT CONSTANT DIFFERENTIAL STRESS

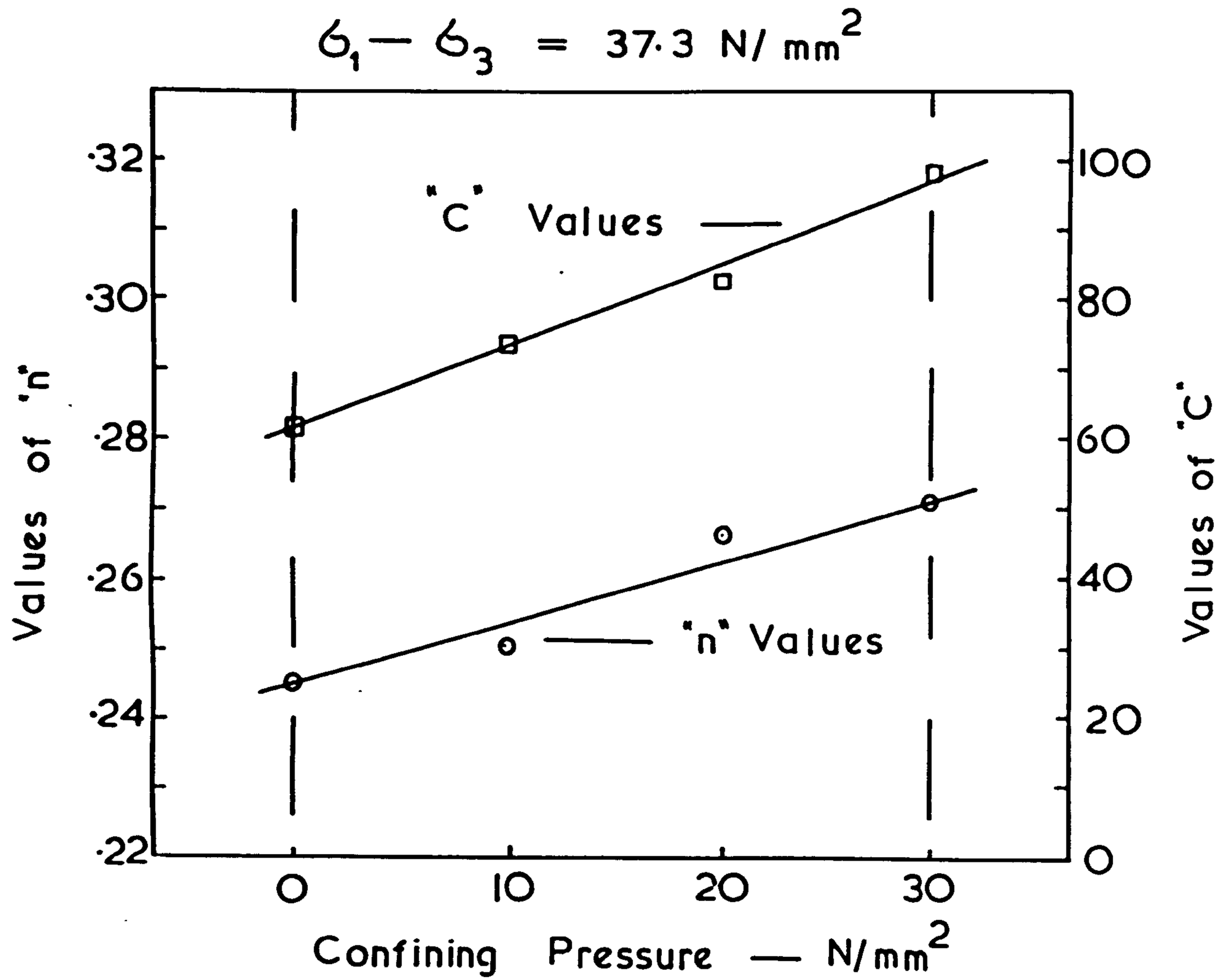

FIG 9—48 EFFECT OF CONFINING PRESSURE ON 'C' AND 'n' AT CONSTANT $\sigma_1 - \sigma_3$

t = 120 Hr

Curve No.	$\sigma_1 - \sigma_3$ N / mm^2
a	60
b	50
c	45
d	42·5
e	40
f	35
g	30
h	20

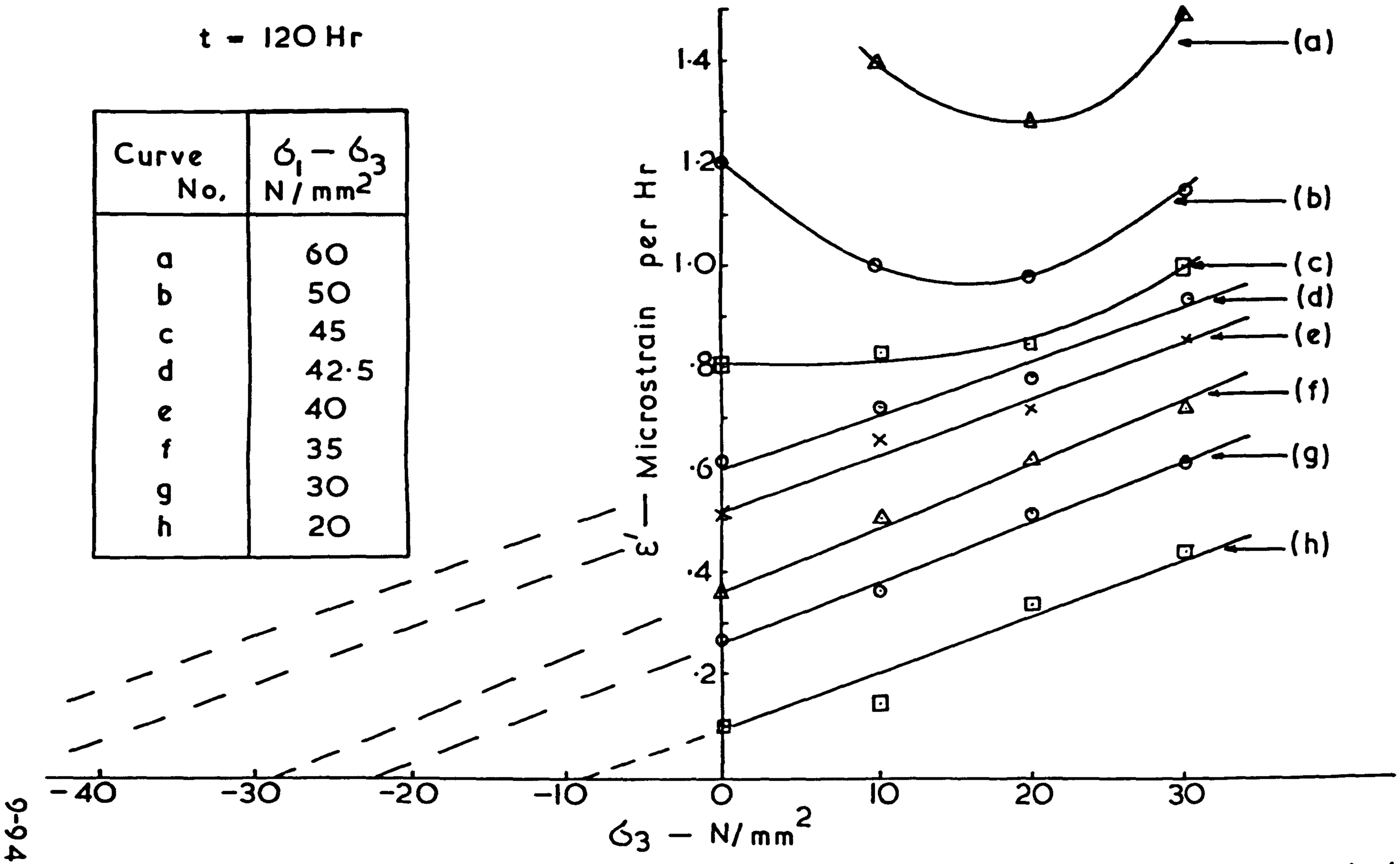

FIG 9–49 EFFECT OF CONFINING PRESSURE ON CREEP RATE AT CONSTANT (σ_1-σ_3)

$\sigma_1 - \sigma_3 = 37.3\ N/mm^2$

$\varepsilon' = (30.5 + \sigma_3) \times R$

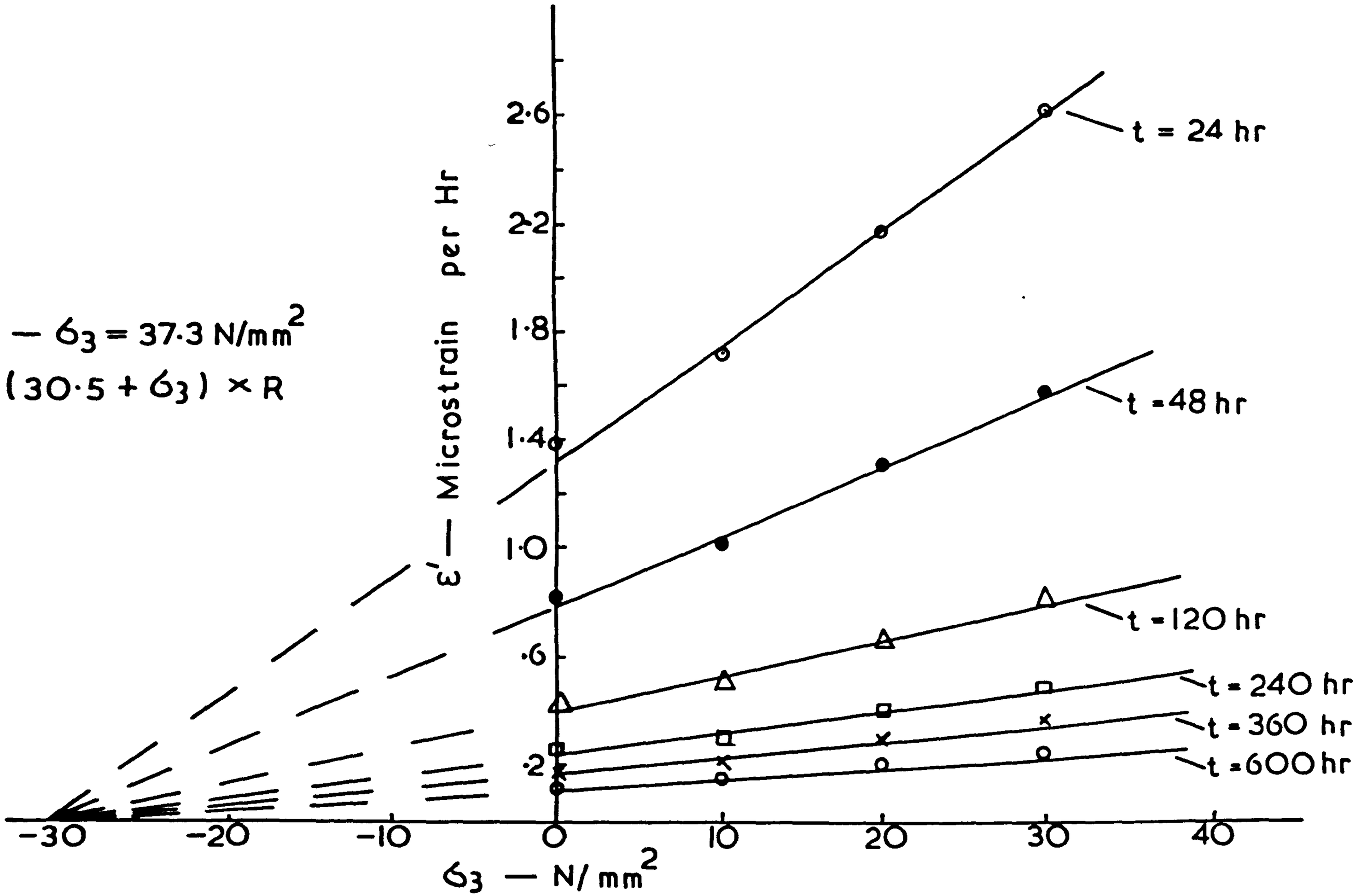

FIG 9–50 CREEP RATE VERSUS σ_3 AT CONSTANT $\sigma_1 - \sigma_3$

CHAPTER 10

CONCLUSIONS AND FUTURE DEVELOPMENTS

Chapter 10

CONCLUSIONS AND FUTURE DEVELOPMENTS

The aim of this work was in two parts:

(a) To design and build an apparatus to carry out triaxial compression creep tests on some evaporite rocks.

(b) To investigate the creep behaviour of some evaporite rocks, namely gypsum and anhydrite under triaxial and uniaxial compression and bending modes of loading.

The results of this investigation could be briefly summarised as follows:

(1) In short term tests it was found that the strength of rock increases with the confining pressure in non-linear relationship.

(2) Creep in the rocks tested takes place at all stress levels and is affected by confining pressure.

(3) At room temperature the creep of gypsum and anhydrite follows the logarithmic law ($\varepsilon = A + B \log t$) at low stresses and low confining pressure, whereas it changes to a power equation ($\varepsilon = Ct^n$) at higher stress or confining pressure, where $0 < n < 1$.

(4) The instantaneous strain increased with increasing stress. The moduli of elasticity were evaluated making use of the instantaneous strains.

(5) The constants A and B of the logarithmic equation increase with the axial stress.

(6) The constants C and n of the power equation increase with the axial stress at constant confining pressure. On the contrary they decrease as the confining pressure increases at

constant axial stress.

(7) The axial stress has a great effect on the creep rate (ε'). It was found, for both the rocks tested, that the creep rate increased with the axial stress at constant confining pressure.

(8) The increase in confining pressure reduces the creep rate at constant axial stress.

(9) At constant differential stress the creep rate increases with the axial stress and the confining pressure.

(10) Both constants C and n of the creep power law increase linearly with the confining pressure at constant differential stress.

(11) The relationship between the creep rate and the axial stress for gypsum was found to follow the power equation.

$$\varepsilon' = k\sigma_1^{\,g} \quad \text{where} \quad g > 1.$$

k and g are constants which depend on the material and the test conditions. "g" was found to be constant at any time in the creep period at a given confining pressure.

(12) A method suggested to determine the working creep stress σ_w from the creep data available at any assumed service life, becomes of wider application as a result of the more complete knowledge of creep behaviour made possible in triaxial tests.

(13) At axial stresses corresponding to constant percentages of the short term strength, the constants C and n of the creep power law and the creep rate, at any time, increase as the confining pressure increases. This explains the rapid change in the creep curve from the logarithmic law to the power equation as the confining pressure increases.

The author suggests that it would be of interest to carry on similar creep tests on other evaporite rocks such as rock salt, potash, etc., to obtain a wider knowledge of the behaviour of evaporite rocks before making any generalization. Triaxial creep tests on gypsum and anhydrite at higher confining pressure may also throw more light on their behaviour under these conditions.

With reference to the triaxial creep apparatus, the author suggests the following points for future work:

(1) The construction of more powerful apparatus both in confining and axial stress. This will enable the extension of triaxial creep study of the tested rocks at higher stresses or into harder rock materials outside the evaporite range.

(2) Design and use of a lateral strain measuring device to measure the diameteral creep strain in the pressure cell itself.

(3) Means of controlling the pore pressure in the specimen under stress and the possible use of pore fluids consisting of various solutions to study the effect of both the presence of solutions and pore pressure on the creep behaviour of different rock materials.

(4) Finally, the possibility of investigating the creep property of rock materials in triaxial compression at various temperatures.

REFERENCES

1. Adams, F.D. and Nicholson, J.D., 1901. "An experimental Investigation Into the Flow of Marble", Phill. Trans. Soc., London, A, Vol. 195, pp.363-401.

2. Afrouz, A. and Harvey, J.M., 1974. "Rheology of Rocks Within the Soft to Medium Strength Range" Int. J. Rock Mech. Min. Sci., Vol.11, pp.281-290.

3. Andrade, E.N. 1914. "The Flow of Metals Under Large Constant Stresses" Proc. Royal Soc., Vol. 90A, pp.328-342.

4. A.S.T.M. C170-50 "Standard Method of Test For Compressive Strength of Natural Building Stone". Reapproved 1970.

5. A.S.T.M. E111-61 "Standard Method of Test For Young's Modulus at Room Temperature". Reapproved 1972.

6. Attewell, P.B., April, 1962. "Composite Model to Simulate Porous Rock" Engineering, Vol.193, No.5010, pp.574-575.

7. Bieniawski, Z.T., 1970. "Time-Dependent Behaviour of Fractured Rock" Rock Mech., Vol.2, No.3, pp.1-16.

8. Boy, G.K.B., 1973. "Strength and Behaviour of Concrete Under Triaxial Stresses Including The Development of A Triaxial Stress Device", Ph.D. Thesis, Univ. of Sheffield.

9. Bridgman, P.W., 1931. "The Physics of High Pressure", G.Bell and Sons Ltd., London, Reprinted in 1952.

10. Buzdar, S.A.R.K., 1968. "A Laboratory Investigation Into the Mechanical Properties of Some Sedimentary Rocks with Special Reference to Potash". Ph.D. Thesis, Univ. of Newcastle upon Tyne.

11. Comte, P.L., 1965. "Creep in Rock Salt" J. Geol., Vol.73, pp.469-484.

12. Considere, A., 1906. "Experimental Researches on Reinforced Concrete", Translation and Introduction by Leon., L. Moisseiff, McGraw-Hill Book Co. Inc., New York.

13. Conway, J.B., 1970. "Numerical Methods for Creep and Rupture Analyses" Gordon and Breach, New York.

14. Cook, R.F., 1974. "Rock Mechanics Investigations Associated with Shaft Excavation in a Deep Evaporite", Ph.D. Thesis, Univ. of Newcastle upon Tyne.

15. Datta, R.N., 1969. "Stress-Strain Characteristics in Bending and Determination of The Tensile Strength of Rocks." Ph.D. Thesis, Univ. of Sheffield.

16. Davis, R.E., Davis, H.E. and Hamilton, J.S., 1934. "Plastic Flow of Concrete Under Sustained Stress", A.S.T.M. Proceedings, Vol.34, Pt.2, pp.354-386.

17. Dekinson, J.H.S., 1922. "Some Experiments on The Flow of Steels at A Low Red Heat, with A Note The Scaling of Heated Steels" J.Iron and Steel Inst., Vol.106, pp.103-140.

18. Denkhas, G., 1958. "The Significance of Some Properties of Rock in Relation to Problem of Rock Bursts in Deep Mining" Int. Strata Control Congress, pp.29-48.

19. Donath, F.A., 1961. "Experimental Study of Shear Failure in Anisotropic Rocks" Bull. Geol. Soc. Am., Vol.72, Pt.1, pp.985-990.

20. Duckworth, W., 1953. "Discussion of Ryshkewitch[76] Work", J.Am.Ceram. Soc., Vol.36, p.68.

21. Durelli, A.J., Philips, E.A. and Tsoa, C.H., 1958. "Introduction to the Theoretical and Experimental Analysis of Stress and Strain", McGraw-Hill Book Co. Inc., London, pp.107-117.

22. Evans, R.H. and Wood, R.H., 1937. "The Elasticity and Plasticity of Rocks and Artificial Stones", Proc. Leeds Phil. Lit. Soc., Vol.3, No.5, pp.540-552.

23. Franklin, J.A., 1971. "Triaxial Strength of Rock Materials", Rock Mech., Vol.3, pp.86-98.

24. Folweirler, R.C., May, 1961. "Creep Behaviour of Pore-Free Polycrystalline Aluminium Oxide", J. Appl. Phys., Vol.32, pp.773-778.

25. Forster, J., 1967. "Stability Investigations Applied to Mining of Evaporites." Ph.D. Thesis, Univ. of Newcastle upon Tyne.

26. Griggs, D.T., 1936. "Deformation of Rocks Under High Confining Pressure", J.Geol., Vol.44, pp.541-577.

27. Griggs, D.T., 1940. "Experimental Flow of Rocks Under Conditions Favouring Recrystallization", Geol. Soc. Am.Bull., Vol.51, pp.1001-1022.

28. Griggs, D.T., 1939. "Creep of Rocks", J. Geol., Vol.74, pp.225-251.

29. Glucklich, J. and Amar, A., 1972. "The Volumetric Creep of Mortars Subjected to Triaxial Compression", Int.Symposium, Rilem, Cannes, Vol.1, pp.79-95.

30. Handin, J.W. and Hager, R.V., 1957. "Experimental Deformation of Sedimentary Rocks Under Confining Pressure: Tests at Room Temperature on Dry Samples." Am.Ass.Petr.Geol. Bull., Vol.41, No.1, pp.1-50.

31. Hardy, H.T., 1959. "Time-Dependent Deformation and Failure of Geologic Materials", Colo.Sch.Min.Quart., Vol.54, No.3, pp.135-175.

32. Hawkes, I. and Mellor, M., 1970. "Uniaxial Testing in Rock Mechanics Laboratories." Eng. Geol., Vol.4, No.3, pp.177-285.

33. Heard, H.C., 1963. "Effect of Large Changes in Strain Rate in The Experimental Deformation of Yule Marble", J.Geol., Vol.71, pp.162-195.

34. Hedley, D.G.F., 1965. "Deformation and Failure Characteristics of Rock Salt and Potash." Ph.D. Thesis, Univ. of Newcastle upon Tyne.

35. Hoek, E. and Franklin, J.A., 1968. "Simple Triaxial Cell for Field or Laboratory Testing of Rock." Trans. Inst. Min. Metall., Vol.77, pp. A22-A26.

36. Hofer, K.H., 1958. "The Principles of Creep in Rock Salt and their Significance to Mining Eng." Int. Strata Control Congress, pp.49-63.

37. Hofer, K.H. and Noll, P., 1971. "Investigation into the Mechanism of Creep Deformation in Carnallitite and Practical Application." Int. J. Rock Mech. Min. Sci., Vol.8, pp.61-73.

38. Honeycombe, R.W.K., 1971. "The Plastic Deformation of Metals". Edward Arnold, London, pp.352-396.

39. Hooper, J.H., 1966. "The Measurements of Stress in Concrete Using Optical Transducers." M.Eng. Thesis, Univ. of Sheffield.

40. Ibrahim, A.B., 1972. "Structural Properties and Behaviour of High Early Strength Lightweight Aggregate (Solite) Concrete." Ph.D. Thesis, Univ. of Sheffield.

41. Jeffreys, H., 1929. "The Earth." 2nd Ed., Macmillan Co., New York, p.265.

42. Jones, I.W., 1968. "The Problems Associated with the Design and Development of Workings in Stratfield Deposits, with particular reference to Gypsum". Ph.D. Thesis, Univ. of Newcastle upon Tyne.

43. Kendall, H.A., 1958. "An Investigation of Creep Phenomena exhibited by Solehofen Limestone, Halite and Cement Under Confining Pressure". M.Sc. Thesis, Agriculture and Mech. College of Texas.

44. Kennedy, A.J., 1962. "Process of Creep and Fatigue in Metals." Oliver and Boyd, London.

45. King, M.S., 1973. "Creep in Model Pillars of Saskatchewan Potash", Int. J. Rock Mech. Min. Sci., Vol.10, pp.363-371.

46. Lomintz, C., 1956. "Creep Measurements in Igneous Rocks." J.Geol., Vol.64, pp.473-479.

47. Love, A.E.H., 1952. "A treatise of the Mathematical Theory of Elasticity." 4th Ed. Cambridge, The Univ. Press.

48. Michelson, A.A., 1917. "The Laws of Elastico-Viscous Flow." J.Geol., Vol.25, pp.405-410.

1920. "The Laws of Elastico-Viscous Flow." Part 2, J.Geol., Vol.28, pp.166-168.

49. Misra, A.K., 1962. "An Investigation of Time-Dependent Deformation or - Creep - in Rocks." Ph.D. Thesis, Univ. of Sheffield.

50. Murrell, S.A.F., 1962. "The Effect of Triaxial Stress System on Strength of Brittle Materials with particular reference to Rocks." Ph.D. Thesis, Univ. of Sheffield.

51. Murrell, S.A.F., and Misra, A.K., 1962. "Time-Dependent Strain or - Creep - in Rocks and Similar Non-Metallic Materials.", Trans. Inst. Min. Met., Vol.71, pp.353-378.

52. Murgatroyd, J.B. and Sykes, R.F.R., 1947. "The Delayed Elastic Effect in Silicate Glasses at Room Temperature." J.Soc. Glass Tech. Trans., Vol.31, pp.17-35.
"The Relation Between The Delayed Elastic Effect and the Decay of Strength of Silicate Glasses at Room Temperature." Ditto, pp.36-49.

53. Nadia, A., 1950. "Theory of Flow and Fracture of Solids." 2nd Ed., McGraw-Hill, New York.

54. Neville, A.M., 1959. "Recovery of Creep and Observation on the Mechanism of Creep of Concrete." Appl. Sci. Res., Vol.9A, No.1, pp.71-84.

55. Newman, K. and Lachance, L., 1964. "The Testing of Brittle Materials Under Uniform Uniaxial Compressive Stress." Proc. A.S.T.M., 64, pp.1044-1067.

56. Obert, L. and Duvall, W.I., 1967. "Rock Mechanics and the Design of Structures in Rocks." John Wiley and Sons, Inc, pp.162-170.

57. Obert, L., Windes, S.L. and Duvall, W.I., 1946. "Standard Test for Determining the Physical Properties of Mine Rock." Bureau of Mines Rept. of Investigation, No.3891, p.67.

58. Passmore, E.A., Duff, R.H. and Vasilos, T., 1966. "Creep of Dense Polycrystalline Magnesium Oxide." J. Am.Ceram. Soc., Vol.49, No.11, pp.594-600.

59. Patchet, S.J., 1970. "Rock Mechanics Studies Associated with the Development of Deep Potash Mine." Ph.D. Thesis, Univ. of Newcastle upon Tyne.

60. Penny, R.K. and Marriott, 1971. "Design for Creep." McGraw-Hill, U.K.

61. Phillips, D.W., 1937. "Physical Properties of Coal Measure Rocks and Experimental Work on the Development of Fracture." Trans. Inst. Ming. Eng., Vol.82, pp.432-450.

1948. "Tectonics of Mining." Colliery Eng., Vol.25, pp.199-202; 278-282 and 349-352.

62. Phillips, P., 1905. "The Slow Strech in India Rubber, Glass and Metal Wires when subjected to a Constant Pull." Phil. Mag. J. Sci. Series 6, Vol.9, pp.513-531.

63. Polakowski, N.H. and Ripling, E.J., 1966. "Strength of Structure of Engineering Materials." Prentice-Hall, Inc., pp.427-438.

64. Potts, E.L.J., 1955. "The Practical Application of Scientific Measurement to Problems in Strata Controls." Iron Coal Trade Rev., Vol.171, pp.1169-1179.

65. Potts, E.L.J., 1956-1957. (a)"A Scientific Approach to Strata Control." Trans.Inst.Min. Engrs., Vol.116,pp.114-127.

1957-1958. (b)"Further Progress in Scientific Approach to Strata Control." Trans.Inst.Min.Engrs., Vol.117, pp.303-318.

66. Potts, E.L.J., 1964. "An Investigation into the Design of Room and Pillar Workings in Rock Salt." Trans.Inst.Min.Engrs., Vol.124, pp.27-44.

67. Potts, E.L.J., 1969. "Production Research and Development - A University Contribution." Min. Eng., Vol.129, pp.139-155.

68. Price, N.J., 1958. "A Study of Rock Properties in Conditions of Triaxial Stress." Proc. Conf. on Mech. Prop. Non-Metallic Brittle Materials, Butterworth, London, pp.106-122.

69. Price, N.J., 1964. "A Study of Time-Strain Behaviour of Coal-Measure Rocks." Int.J. Rock Mech. Min. Sci., Vol.1. pp.277-303.

70. Reiner, M., 1960. "Deformation, Strain and Flow." H.K. Lewis and Co.Ltd., London, pp.127-156.

71. Reynolds, T.D. and Gloyana, E.F., 1961. "Creep Measurements in Salt Mines." 4th Symposium, Rock Mech., Pennsylvania, pp.11-17.

72. Robertson, E.C., 1960. "Creep of Solenhofen Limestone Under Moderate Hydrostatic Pressure." Mem.Geol.Soc.Amer., Vol.79, pp.227-244.

73. Ros, M. and Eichinger, A., 1928. "Federal Materials Testing Laboratory of the E.T.H., Zürich" Report No.28, (Translated in U.S. Bureau of Reclamation, Memo. No.635, 1947).

74. Ross, A.D., 1937. "Concrete Creep Data." The Structural Engineer, Vol.15, pp.314-326.

75. Ross, A.D., 1958. "The Elasticity, Creep and Shrinkage of Concrete." in (Mechanical Properties of Non-Metallic Brittle Materials) Edited by W.H. Walton, London.

76. Ryshkewitch, E., 1953. "Compression Strength of Porous Sintered Alumina and Zirconia." J.Amer.Ceram.Soc., Vol.36, pp.65-68.

77. Schwartz, B., 1961. "Movements of the Roof and Floor in Road-Ways.", 4th Symposium, Rock Mech. Pennsylvania, pp.1-10.

78. Serdengecti, S. and Boozer, D.G., 1961. "The Effect of Strain Rate and Temperature on the Behaviour of Rocks Subjected to Triaxial Compression." Proc. 4th Symp. Rock Mech., Pennsylvania, pp.83-97.

79. Singh, D.P., 1975. "A Study of Creep of Rocks." Int. J. Rock Mech. Sci., Vol.12, pp.271-275.

80. Stravrolakis, J.A. and Norton, F.H., 1950. "Measurements of the Torsion Properties of Alumina and Zirconia at Elevated Temperature." J.Amer. Ceram. Soc., Vol.33, No.9, pp.263-268.

81. Terwilliger, G.R., Bowen, H.K. and Gordon, R.S., 1970. "Creep of Polycrystalline MgO and MgO-Fe_2O_3 Solid Solutions at High Temperatures." J.Amer.Ceram.Soc., Vol.53, No.5, pp.241-251.

82. Vicot, M., 1933. "Note Sur L'Allongement Progressif du fil de fer Soumis a Diverses Tension." Annales de Chemie et de Physique, Vol.54, p.35.

83. Von Karman, T. 1911. "Festigkeitsversuche Unter Allseitigem Druck." Zeits. Ver. Deutsch Ingenieure, Vol.55, pp.1749-1757. cited by J. Handin and R.Hager(30).

84. Vutukuri, V.S., Lama, R.D. and Saluja, S.S., 1974. "Handbook on Mechanical Properties of Rocks." Vol.1, Trans. Tech. Publication, Germany.

85. Washa, G.W., 1947. "Plastic Flow of Thin Reinforced Concrete Slabs." A.C.I. Proc., Vol.44, No.3, pp.237-260.

86. Washa, G.W. and Flunk, P.G., 1952. "Effect of Compressive Reinforcement on the Plastic Flow of Reinforced Concrete Beams." A.C.I. Proc., Vol. 49, No.2, pp.89-108.

87. Washa, G.W. and Flunk, P.G., 1956. "Plastic Flow (creep) of Reinforced Concrete Continuous Beams." A.C.I. Proc., Vol.52, No.5, pp.549-562.

88. Weaver, S.H., 1937. "The Creep Curve and Stability of Steels at Constant Stress and Temperature." Trans. A.S.M.E., Vol.58, pp.745-751.

89. Williams, F.T., 1973-1976. Personal communication.

90. Williams, F.T. and Elizzi, M.A., 1975. "Bending Creep Tests in Gypsum", J. Iraq Engineers Soc., To be published.

91. Williams, F.T. and Elizzi, M.A., "An Apparatus for the Determination of Time-Dependent Behaviour of Rock Under Triaxial Loading." Int.J.Rock Mech.Min.Sci., To be published.

91. Continued. 1975. "The Time-Dependent Behaviour of Rock Under Triaxial Loading." Dept. Civil and Struct.Eng., Univ. of Sheffield, Research Report, No. 66.

92. Williams, F.T. and Elizzi, M.A., 1976. "A Study of the Creep Properties of Gypsum Rock Under Triaxial Loading." Dept. of Civil and Struct. Eng., Univ. of Sheffield, Research Report, No. 72.

93. Winkel, B.V., 1972. "Analysis of Time-Dependent Deformation of Openings in Salt Media." Int. J. Rock Mech. Min. Sci., Vol.9, pp.249-260.

94. Withey, M.O. and Washa, G.W., 1954. "Materials of Construction." John Wiley and Sons, pp.31.9-31.15.

95. Wyatt, O.H., 1953. "Transient Creep in Pure Metals." Proc. Phys. Soc., London, Vol.66, Section B, pp.459-480.

96. Wygant, J.F., 1951. "Elastic and Flow Properties of Dense Pure Oxide Refractories." J.Amer. Ceram. Soc., Vol.34, pp.374-380.

APPENDIX A

Table (A6-1)

Uniaxial compression tests on gypsum*.

Specimen No.	Cross-sectional area mm^2	Load at fracture KN	Stress N/mm^2	Mean Stress N/mm^2	Standard deviation
8G	482.27	27.75	57.54		
12G	488.13	28.37	58.13		
14G	488.91	27.36	55.96		
22G	488.91	30.35	62.08	57.46	2.776
27G	491.66	29.56	60.12		
48G	501.54	27.15	54.13		
63G	497.97	28.55	57.68		
65G	487.74	26.36	54.04		

*The procedure of calculating the mean stress and the standard deviation is given in table (A6-3).

Table (A6-2)

Uniaxial compression tests on anhydrite*

Specimen No.	Cross-sectional area mm^2	Load at fracture KN	Stress N/mm^2	Mean Stress N/mm^2	Standard deviation
2A	488.13	51.28	105.05		
3A	490.87	47.52	96.81		
11A	485.0	44.85	92.47		
12A	488.91	52.91	108.22	101.25	8.491
13A	488.91	47.35	96.85		
14A	486.21	55.27	113.68		
15A	487.74	43.72	89.64		
22A	488.13	52.36	107.27		

*The procedure of calculating the mean stress and the standard deviation is given in table (A6-3).

Table (A6-3)

An example of calculating the mean stress and the standard deviation of gypsum at uniaxial compression*

No.of specimens tested N	Stress σ	Mean stress $\bar{\sigma} = \frac{\Sigma \sigma}{N}$	$\sigma - \bar{\sigma}$	$(\sigma - \bar{\sigma})^2$	$\frac{\Sigma (\sigma - \bar{\sigma})^2}{N-1}$	Standard deviation $S = \sqrt{\frac{\Sigma (\sigma - \bar{\sigma})^2}{N-1}}$
8	57.54	57.46	0.07	0.0049	7.7082	2.776
	58.13		0.67	0.4489		
	55.96		-1.50	2.2500		
	62.08		4.62	21.3444		
	60.12		2.66	7.0756		
	54.13		-3.33	11.0889		
	57.68		0.22	0.0484		
	54.04		-3.42	11.6964		
				53.9575		

* The same procedure was used in calculating all the means and standard deviations of the values given in the other tables.

Table (A6-4)

Experimental data and mean values of triaxial compression tests of gypsum.

σ_3 N/mm^2	Specimen No.	Test results			Mean values		
		σ_1 N/mm^2	Z N/mm^2	Θ deg.	σ_1 N/mm^2	Z N/mm^2	Θ deg.
0	see table (A6-1)				57.46	0	72
5	54G	73.10	43.21	63	73.97	42.20	60
	55G	69.42	38.68	61			
	120G	79.39	44.71	56			
10	66G	79.16	77.31	60	92.07	58.79	58
	46G	87.60	71.78	61			
	128G	96.80	61.10	55			
	121G	98.51	27.28	64			
	83G	98.30	56.48	50			
15	80G	116.92	78.42	55.5	102.51	79.03	55.7
	56G	86.46	78.63	60			
	122G	104.15	80.04	51.5			
20	47G	108.09	107.28	56	114.58	102.57	57.5
	65G	108.81	94.75	59			
	89G	118.40	-	56			
	123G	117.19	105.68	57.5			
	129G	120.40	-	59			
25	99G	128.72	113.12	52	128.37	113.31	53.5
	60G	121.38	113.81	50.5			
	124G	135.01	113.00	58			
30	57G	133.37	132.15	50	136.44	129.20	53
	61G	131.24	120.63	50.5			
	127G	142.80	-	57.5			
	64G	132.92	127.10	50			
	130G	134.60	-	54			
	125G	143.68	136.91	56			
35	67G	143.02	141.00	-	147.80	146.26	-
	126G	145.82	144.91	58.5			
	36G	154.55	152.88	-			

Table (A6-4) cont.

Notations

σ_1 = Axial stress at fracture or yield

σ_3 = Confining pressure

Z = Axial stress immediately after fracture

θ = Measured angle of fracture which is the angle between the plane of failure and the minor principle stress (σ_3).

Table (A6-5)

Experimental data and mean values of triaxial tests of anhydrite*

σ_3 N/mm^2	Specimen No.	Test results σ_1 N/mm^2	Z N/mm^2	θ deg.	Mean values σ_1 N/mm^2	Z N/mm^2	θ deg.
0	see table (A6-2)				101.25	0	75
5	1A	125.30	26.14	62.5			
	4A	137.70	31.56	69.5	131.50	28.85	66
10	16A	164.50	67.29	63.5			
	17A	173.20	69.47	62.5	164.50	65.87	65.5
	25A	156.10	60.85	70.5			
15	5A	181.14	98.18	65			
	6A	191.90	106.04	61	186.52	102.11	63
20	18A	213.88	121.61	55.5			
	19A	202.14	75.78	60.0	200.51	125.10	63
	26A	185.51	177.91	73.5			
25	7A	220.32	168.20	60			
	8A	228.30	160.46	60	224.31	164.33	62.5
30	20A	233.59	125.07	53			
	21A	241.50	235.59	62	236.63	198.16	60
	27A	234.80	233.81	65			
35	9A	248.12	222.10	63	251.11	218.32	60
	10A	254.10	214.54	57			

* For notations see table (A6-4).

APPENDIX B

The creep curves of gypsum in triaxial compression followed, in most of the cases, the power law in the form:

$$\varepsilon = Ct^n \tag{B9-1}$$

In order to be sure that the creep data will fit the above equation well, the data of creep strain against time were plotted on a log-log graph, when a straight line was obtained. The slope of this straight line is n, and C is the creep strain at t = 1 hour. To find n and C the following least square method was applied:

Equation (B9-1) can be written in the form

$$\log \varepsilon = \log C + n \log t \tag{B9-2}$$

let $y = \log \varepsilon$

$x = \log t$

and $k = \log C$

Equation (B9-2) can be rewritten in the form:

$$y = k + nx \tag{B9-3}$$

which is an equation of a straight line of slope n and intercept k on the y-axis. The following equations were used in calculating n and k:

$$n = \frac{\Sigma xy - \frac{(\Sigma x)(\Sigma y)}{N}}{\Sigma x^2 - \frac{(\Sigma x)^2}{N}} \tag{B9-4}$$

$$k = \bar{y} - n\bar{x} \tag{B9-5}$$

where N is the number of readings, $\bar{y}$ is the mean of y-values and $\bar{x}$ is the mean of x-values.

x, y, Σxy, Σx, Σy and Σx^2 are given in table (B9-1). The values of the creep strain ε and the corresponding times are taken from table (9-11) of Chapter 9.

Solving for n and k using the data given in table (B9-1)

$$n = \frac{107.641 - \frac{41.471 \times 66.921}{28}}{92.759 - \frac{(41.471)^2}{28}}$$

$$\therefore n = 0.271$$

$$k = \bar{y} - n\bar{x}$$

$$k = 2.390 - 0.271 \times 1.481$$

$$\therefore k = 1.990$$

Substitute the value of k in k = log C to find C = 97.74 microstrain.

Substitute the values of n and C in equation (B9-1), the following power equation of the creep of gypsum under 50% σu axial stress and at 30 N/mm^2 confining pressure was obtained

$$\varepsilon = 97.74\ t^{0.271} \qquad \text{(B9-6)}$$

TABLE (B9-1)

Creep of gypsum at σ_1 = 50% σu and σ_3 = 30 N/mm^2

Time t	Creep strain ε	log t = x	log ε = y	x.y	x^2	$x-\bar{x}$	$y-\bar{y}$	$(x-\bar{x})^2$	$(y-\bar{y})^2$	$(x-\bar{x})(y-\bar{y})$
0.1	49.3	-1.000	1.693	-1.693	1.000	-2.481	-0.698	6.155	0.487	1.732
0.33	71.5	-0.481	1.854	-0.892	0.232	-1.962	-0.537	3.849	0.288	1.054
0.5	79.7	-0.301	1.901	-0.572	0.091	-1.782	-0.490	3.176	0.240	0.873
1.0	94.1	0	1.974	0	0	-1.481	-0.417	2.193	0.174	0.618
2	118.8	0.301	2.075	0.625	0.091	-1.180	-0.316	1.392	0.100	0.373
3	132.1	0.477	2.121	1.012	0.228	-1.004	-0.270	1.008	0.073	0.271
4	136.8	0.602	2.136	1.286	0.362	-0.879	-0.255	0.773	0.065	0.224
5	145.1	0.699	2.162	1.511	0.489	-0.782	-0.229	0.612	0.052	0.179
6	166.2	0.778	2.221	1.728	0.606	-0.703	-0.170	0.494	0.029	0.120
12	201.5	1.079	2.304	2.486	1.165	-0.402	-0.087	0.162	0.008	0.035
18	212.0	1.252	2.326	2.913	1.576	-0.229	-0.065	0.052	0.004	0.015
24	235.5	1.380	2.372	3.273	1.905	-0.101	-0.019	0.010	0.000	0.002
48	270.5	1.681	2.432	4.088	2.827	0.200	0.041	0.040	0.002	0.008
72	312.1	1.857	2.494	4.632	3.450	0.376	0.103	0.141	0.011	0.039
96	360.9	1.982	2.557	5.068	3.929	0.501	0.166	0.251	0.028	0.083
120	380.2	2.079	2.580	5.364	4.323	0.598	0.190	0.358	0.036	0.114
144	369.1	2.158	2.567	5.540	4.659	0.677	0.177	0.458	0.031	0.120
168	370.7	2.225	2.569	5.716	4.952	0.744	0.179	0.554	0.032	0.133

TABLE (B9-1) cont.

Time t	Creep strain ε	log t = x	log ε = y	x.y	x^2	$x-\bar{x}$	$y-\bar{y}$	$(x-\bar{x})^2$	$(y-\bar{y})^2$	$(x-\bar{x})\times(y-\bar{y})$
192	405.6	2.283	2.608	5.954	5.213	0.802	0.218	0.643	0.048	0.175
216	419.1	2.334	2.622	6.120	5.450	0.853	0.232	0.728	0.054	0.198
240	420.1	2.380	2.623	6.243	5.665	0.899	0.233	0.808	0.054	0.209
264	448.8	2.422	2.652	6.423	5.864	0.941	0.262	0.885	0.069	0.247
288	460.2	2.459	2.663	6.548	6.049	0.978	0.273	0.956	0.075	0.267
312	463.7	2.494	2.666	6.650	6.221	1.013	0.276	1.026	0.076	0.280
336	487.1	2.526	2.688	6.789	6.382	1.045	0.298	1.092	0.089	0.311
360	483.3	2.556	2.684	6.861	6.535	1.075	0.294	1.156	0.086	0.316
384	487.7	2.584	2.688	6.946	6.679	1.103	0.298	1.217	0.089	0.329
408	489.1	2.611	2.689	7.022	6.816	1.130	0.299	1.277	0.089	0.338
		$\Sigma x=41.471$ $\bar{x}=1.481$	$\Sigma y=66.921$ $\bar{y}=2.390$	$\Sigma xy=107.641$	$\Sigma x^2=92.759$			$\Sigma(x-\bar{x})^2=31.466$	$\Sigma(y-\bar{y})^2=2.389$	$\Sigma(x-\bar{x})\times(y-\bar{y})=8.663$

In order to find the degree of correctness of the assumption that the plotted data on the log-log graph represents a straight line, the correlation coefficient (R) was found for each case. The results obtained were extremely satisfactory. In the following pages an example of such calculations is given on a triaxial creep data of gypsum at 30 N/mm^2 confining pressure, subjected to an axial stress of 57.3 N/mm^2 (=50% σu).

$$R = \frac{\Sigma (x-\bar{x})(y-\bar{y})}{(N-1)(Dx.Dy)} \qquad \text{(B9-7)}$$

where R is the correlation factor; x, $\bar{x}$, y, $\bar{y}$ and N as given in table (B9-1) and equation (B9-4); Dx and Dy are the standard deviations of x and y values respectively, where:

$$Dx = \sqrt{\frac{\Sigma (x-\bar{x})^2}{N-1}} \qquad \text{(B9-8)}$$

$$Dy = \sqrt{\frac{\Sigma (y-\bar{y})^2}{N-1}} \qquad \text{(B9-9)}$$

substitute the values of x, $\bar{x}$, N, y and $\bar{y}$ in the above equations:

$$Dx = 1.080$$

$$Dy = 0.300$$

$$R = \frac{\Sigma(x-\bar{x})(y-\bar{y})}{(N-1)(Dx.Dy)}$$

$$= \frac{8.663}{27 \times 1.080 \times 0.300}$$

$\therefore$ R = 0.9902 which gives a good degree of correctness.